Aus der Klinik für Innere Medizin,
Schwerpunkt Hämatologie, Onkologie & Immunologie
Direktor: Prof. Dr. Andreas Neubauer

des Fachbereichs Medizin der Philipps-Universität Marburg

Einfluss der DNA-Bindungskooperativität von p53 auf die Tumorsuppressoraktivität
&
Beobachtung der Entwicklungsdynamik von Tumorklonen *in vitro* & *in vivo* mittels sekretierter Luciferasen

Inaugural-Dissertation zur Erlangung des Doktorgrades
der Naturwissenschaften dem Fachbereich Medizin
der Philipps-Universität Marburg
vorgelegt von

Joël Pierre Alexandre Charles
aus Wiesbaden

Marburg, 2015

Angenommen vom Fachbereich Medizin der Philipps-Universität Marburg am:

Gedruckt mit Genehmigung des Fachbereichs.

Dekan: Herr Prof. Dr. Helmut Schäfer

Referent: Herr Prof. Dr. Thorsten Stiewe

1. Korreferent: Frau Prof. Dr. Uta-Maria Bauer

Für meine Eltern

Inhaltsverzeichnis

Zusammenfassung

Der Tumorsuppressor p53 wird als „Wächter des Genoms“ bezeichnet und spielt eine wichtige Rolle bei der Prävention von Krebserkrankungen. p53 ist ein sequenzspezifischer Transkriptionsfaktor, der durch verschiedene Formen von Zellstress wie DNA-Schäden oder Onkogene aktiviert wird und in Abhängigkeit der Schwere der entstandenen Schäden eine Vielzahl verschiedener Zielgene transaktiviert, die Zellzyklus Arrest, Seneszenz, Differenzierung und Apoptose induzieren. Bei der Entscheidung über Überleben oder Sterben tragen posttranskriptionelle Modifikationen von p53 und Interaktionen mit Kofaktoren dazu bei, dass p53 bestimmte Gruppen von Zielgenen aktiviert. Es ist aber unklar, wie diese Entscheidung über das Zellschicksal auf der Ebene der Promotorbindung von Zielgenen durch p53 getroffen wird. Für die Bindung an die DNA bilden vier p53-Proteine ein Tetramer, wobei die DNA-Bindungsdomänen kooperativ an die DNA binden. Dabei interagieren die H1-Helices der DNA-Bindungsdomänen zweier benachbarter p53-Monomere über eine Salzbrücke.

Um den Einfluss der DNA-Bindungskooperativität für die tumorsuppressive Funktion von p53 zu untersuchen, wurden p53 H1-Helixmutanten generiert, die das komplette Spektrum von niedriger bis starker DNA-Bindungskooperativität aufweisen und bezüglich ihrer genomischen Bindung und Transaktivierung von Zielgenen sowie ihrer Antwort auf Stress untersucht.

Die Ergebnisse zeigen, dass die Kooperativität eine Bindung an degenerierte Motive, wie sie in proapoptotischen Genen vorkommen, ermöglicht und so das Bindungsspektrum von p53 erweitert. Eine niedrige Kooperativität erlaubt die Induktion von Zellzyklus-Arrest, verhindert aber die Induktion von Apoptose. Somit moduliert die DNA-Bindungskooperativität die Entscheidung über das Zellschicksal, bestimmt die Eliminierung von geschädigten Zellen durch Apoptose und trägt zur Tumorsuppressoraktivität von p53 bei.

Tumore sind heterogene Zellpopulationen, die aus genetisch unterschiedlichen Subklonen bestehen, die in einem iterativen Evolutionsprozess aus genetischer Mutation und Selektion entstehen. Die Mehrzahl der Tumorsubklone kann

häufig therapeutisch zerstört werden, doch kann bei einer Therapie der starke Selektionsdruck das Auswachsen und Überleben resistenter Klone fördern. Das Verständnis über die genetischen Veränderungen in der klonalen Tumorentwicklung, die zur Tumorinitiation, Progression, Metastasierung, Therapieresistenz und Rezidiven beitragen, ist von großem Interesse, um Präventionsstrategien und Therapien zu entwickeln. Die Rolle einzelner Gene bei der Tumorentstehung kann spezifisch mittels RNA Interferenz unter Verwendung von short hairpin RNAs (shRNA) untersucht werden, die einen stabilen Funktionsverlust-Phänotyp generieren. Dabei werden in Experimenten shRNA-exprimierende Tumorzellen oft mit Fluoreszenzreportern markiert und verfolgt. Dies funktioniert gut in Zellkulturexperimenten oder Leukämie-Mausmodellen, aber nicht in soliden Tumoren, die 90% aller Tumore im Menschen ausmachen.

Ziel dieser Arbeit war die Entwicklung eines Systems zur konstitutiven und induzierbaren Markierung von Tumorzellen mit sezernierten Luciferasen. Dafür wurde ein dualer Luciferase Assay entwickelt, der es ermöglicht, zwei unterschiedliche shRNA-exprimierende Tumorzellklone kompetitiv zu verfolgen, sowohl *in vitro* als auch *in vivo*. Die Aktivität der sezernierten Gaussia (GLuc) und Cypridina (CLuc) Luciferasen kann verlässlich und spezifisch in Überständen von Zellmischungen oder im Xenograft-Modell ohne größere Eingriffe durch minimalinvasive Methoden im Mausblut gemessen werden und korreliert mit der Tumorzellzahl, bzw. der Tumorgröße. Die Ergebnisse zeigen, dass sich mit diesem dualen Assay die Entwicklungsdynamik von Tumorsubklonen auch in soliden Tumoren zeitlich erfassen lässt, und etablieren die Anwendungsmöglichkeit zur Untersuchung einzelner Gene und deren Beitrag zur Tumorentwicklung, Metastasierung und Tumortherapie. Durch die Verwendung einer der Luciferasen als interne Kontrolle in diesem kompetitiven Ansatz zur Normalisierung der Daten ist die Varianz der Ergebnisse deutlich geringer und die Versuchstierzahlen können somit um bis zu drei Viertel reduziert werden. Durch Verwendung sezernierter Luciferasen konnte so unter Berücksichtigung des 3R-Prinzips eine Methodik etabliert werden, um die Anzahl und die Belastung von Tieren in der Tumorforschung deutlich zu reduzieren.

Summary

p53 is known as the “guardian of the genome” and plays an important role in the prevention of cancer development. In response to different kinds of cellular stress like DNA damage or oncogene activity p53 binds as a sequence specific transcription factor to the DNA and induces the expression of genes involved in cell cycle arrest, senescence, differentiation and apoptosis. It is known that interaction with cofactors and modifying enzymes is involved in the decision between survival and death by p53. Nevertheless it remains unclear how this decision is made at the level of p53 binding to promoters. p53 forms a tetramer and binds to the DNA in a cooperative manner via the DNA binding domain. For this the H1 helices of two adjacent p53 monomers interact by forming a salt bridge.

To determine the role of p53 DNA binding cooperativity for tumour suppression, p53 H1 helix mutants which cover the whole range from low to high cooperativity were generated and analyzed with respect to their genomic binding profiles, transactivation of target genes and response to cellular stress.

The results show that the binding spectrum of p53 is extended by DNA binding cooperativity to include degenerated response elements found in proapoptotic genes. Therefore low cooperativity p53 induces cell cycle arrest but prevents the induction of apoptosis. Hence, DNA binding cooperativity modulates the cell fate decision, determines the elimination of damaged cell through apoptosis and contributes to the tumour suppressor activity of p53.

Tumours are heterogeneous cell populations that consist of genetically distinct subclones. These subclones arise through the reiterative process of genetic mutation and selection. Most of these cancer clones can be eliminated therapeutically but due to a strong selective pressure during therapy resistant variants can expand. The genetic mutations that contribute to tumour initiation, progression, metastasis and therapy resistance are attractive targets for the development of therapeutic treatments. The contribution of single genes to cancer can be analyzed specifically with RNA interference and the use of short hairpin RNAs (shRNA) by generating a loss-of-function phenotype. In such

experiments tumour cells carrying shRNAs can be marked and tracked with fluorescent markers. This works well in in cell culture studies or in leukemia mouse models but not for solid tumours, which comprise 90% of all cancers.
Hence a system was generated to mark tumour cells constitutively or in an inducible manner with secreted luciferases. We developed a dual luciferase assay to track the fate of two different shRNA-expressing tumour cell clones competitively, both *in vitro* and *in vivo*. The activities of the secreted Gaussia (GLuc) and Cypridina (CLuc) luciferases can easily and specifically be measured in the supernatant of cultured cells or minimal-invasively in mouse xenograft models in the blood of mice. The luciferase activities also correlate well with the tumour cell number or the tumour size. We show that this dual assay enables the time-resolved monitoring of clonal tumour evolution in a dynamic manner and its suitability for solid tumours as well as for the analysis of genes and their contribution to tumour development, metastasis and therapy. With one of the secreted luciferases as internal control for normalization the variance of the data is reduced and allows a reduction of animal numbers by approximately 75%. Using secreted luciferases and in consideration of the 3R principle we established a methodology to reduce the burden of animals in tumour research.

1. EINLEITUNG

1.1. Krebs

Der Begriff Krebs steht in der Medizin für eine große Gruppe von Krankheiten, die durch bösartige Gewebeneubildungen (Neoplasien) charakterisiert sind. Es zählen maligne Tumoren mit epithelialem (Karzinome) und mesenchymalem (Sarkome) Ursprung, sowie Leukämien und Lymphome zu Krebserkrankungen. Solchen Neoplasien geht ein unkontrolliertes Zellwachstum voraus, wodurch umliegendes und gesundes Gewebe verdrängt oder infiltriert werden kann und die Tumorzellen über das Blut- und Lymphsystem im Körper metastasieren können.

Die Risiken für eine Krebserkrankung sind u.a. auf karzinogene Noxen, Rauchen, Virusinfektionen, Strahlung, chronische Infektionen aber auch familiäre Dispositionen zurückzuführen. Die Weltgesundheitsorganisation WHO gibt an, dass 30% aller Krebsfälle durch eine allgemein gesunde Lebensweise, wie die Vermeidung von Tabak, Übergewicht und Bewegungsmangel, verhindert werden könnten (World Health Organisation 2007).

Das Zentrum für Krebsregisterdaten (ZfKD) des Robert Koch-Instituts in Berlin hat erhoben, dass aktuell in Deutschland circa 500000 Menschen jährlich an Krebs erkranken und gut 220000 Menschen jährlich daran sterben (Kaatsch et al. 2013). Dabei sind Lunge, Brust, Prostata und Darm die häufigsten Organe, die von Krebs betroffen sind. Auch wenn die Krebsmortalität in Deutschland seit vielen Jahren rückläufig ist, wird aufgrund des demografischen Wandels (Statistisches Bundesamt, 2011) zwischen 2010 und 2030 mit einem Anstieg der Krebsneuerkrankungen um 20% gerechnet (Haberland et al. 2012). Somit macht Krebs in Deutschland nach den Herz- Kreislauferkrankungen immer noch die zweithäufigste Todesursache aus. Dies verdeutlicht, wie wichtig es ist Krebs zu erforschen, weiteres Verständnis über diese Krankheit in Bezug auf Entwicklung, Progression und Verlauf zu gewinnen und damit die Verbesserung von Therapiemöglichkeiten voranzutreiben.

1.2. Tumorentwicklung

Jede Körperzelle ist homöostatischen Mechanismen unterworfen, die Funktion, Wachstum, Proliferation, Differenzierung und den programmierten Zelltod (Apoptose) kontrollieren. DNA-Schäden oder genetische Veränderungen (Mutationen) können dazu beitragen, dass Zellen veränderte Genprodukte exprimieren oder gar nicht mehr bilden. Gewinnt ein Genprodukt durch eine solche Veränderung eine neue Funktion, spricht man von einer Gain-of-function-Mutation, während die Entstehung eines funktionslosen Genprodukts Loss-of-function-Mutation genannt wird. Dadurch können Kontrollmechanismen außer Kraft gesetzt oder verändert werden und unkontrolliertes Wachstum oder invasives Verhalten zur Entwicklung von Tumoren (Karzinogenese) führen.
Nach dem Modell der klonalen Evolution von Nowell (Nowell 1976) erfährt die Ursprungszelle eines Tumors durch eine Mutation einen Wachstumsvorteil. Dies befähigt diese Zelle im Vergleich zu benachbarten Zellen zu vermehrter Zellteilung und geringerer Apoptose, so dass dieser Zellklon andere Zellen langfristig überwächst. Der Prozess aus zufälliger klonaler Diversifizierung durch Mutationen, Expansion und gerichteter Selektion wiederholt sich so oft, bis die Transformation zu einer malignen Tumorzelle vollzogen ist (Cairns 1975; Greaves & Maley 2012; Meacham & Morrison 2013).
Ein weiteres Modell, das im klonalen Evolutionsmodell mit eingeschlossen ist, ist die Mehrschritt-Theorie der Karzinogenese (Barrett, 1987). Darin erfährt eine normale Körperzelle in der Initiationsphase einen irreversiblen DNA-Schaden oder eine epigenetische Veränderung. In der folgenden Promotionsphase, die sich über einen Zeitraum von Jahrzehnten erstrecken kann, erfolgt die klonale Expansion der Zellen mit der Expression veränderter Genprodukte, was zur Entstehung einer präkanzerösen Läsion führen kann. Weitere Mutationen führen in der Progressionsphase dazu, dass eine neoplastische Zelle entsteht, die einen malignen Phänotyp zeigt und die durch klonale Expansion zur Bildung eines Tumors führt (Abb.01). Dabei sind bis zu zehn genetische Alterationen für die maligne Transformation nötig (Barrett, 1993). Letztendlich besteht ein Tumor aus einer heterogenen Zellpopulation, die aus genetisch individuellen Subklonen besteht, die alle zufällig verändert wurden und sich den Kontrollmechanismen des Organismus weitgehend entzogen haben.

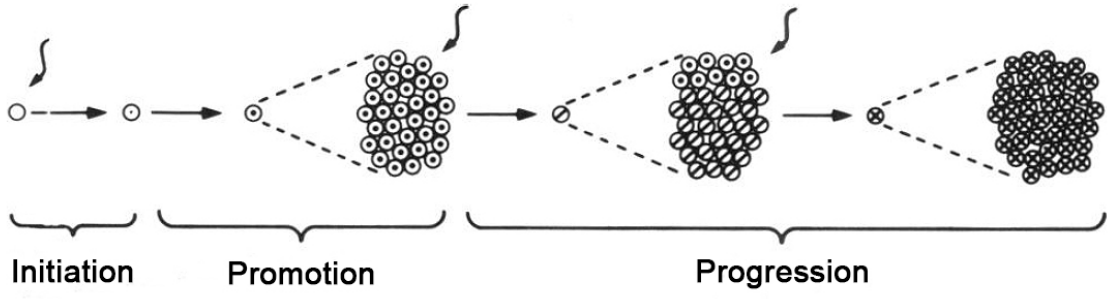

Abb.01: Modell der Mehrschritt-Theorie der Karzinogenese
Aufgrund spontaner Veränderungen oder chemischer Einflüsse können in der Initiationsphase Veränderungen in Genen auftreten, die in der Promotionsphase an Tochterzellen weitergegeben werden. In der Progressionsphase trägt das Ansammeln weiterer Mutationen schließlich zur Karzinogenese bei. Pfeile kennzeichnen genetische Veränderungen einer Zelle. (Barrett, 1987)

Nicht jedes Gen trägt durch Mutationen zur Karzinogenese bei. Dies ist nur bei Genen der Fall, die den Zellzyklus, Wachstum, Invasion oder Metastasierung regulieren, sowie den Phänotyp einer Tumorzelle prägen. Diesbezüglich sind die beiden bedeutendsten Tumorgenklassen die Tumorsuppressoren und die Protoonkogene (Weinberg 1991).

Tumorsuppressoren sind Proteine, die einen repressiven Effekt auf die Regulation des Zellzyklus ausüben können, Apoptose induzieren, Metastasierung inhibieren, DNA-Reparatur initiieren und die genomische Integrität eines Organismus sichern. Mutationen von Tumorsuppressorgenen sind rezessiv, so dass die tumorfördernde Funktion nur dann eintritt, wenn beide Allele eines Chromosomenpaares geschädigt sind (Knudson 1971).

Protoonkogene sind Gene, die meist Zellwachstum, Zellteilung und Differenzierung regulieren. Mutationen im Regulationsbereich dieser Gene führen zur Entstehung von Krebs-Genen, sogenannten Onkogenen und fördern die Karzinogenese. Dabei verhalten sich Onkogene dominant, so dass der Funktionsverlust, bzw. der Funktionsgewinn bei der Veränderung nur eines Allels eintritt und das normale Allel die Veränderung des anderen nicht kompensieren kann.

So komplex und unterschiedlich die Veränderungen und Mechanismen auch sind, die zu einem malignen Phänotyp und der Entstehung von Krebs beitragen, so liegen allen Krebszellen gemeinsame Eigenschaften zugrunde. Zellen müssen Unabhängigkeit von Wachstumssignalen erlangen, ein unbegrenztes Wachstumspotential aufweisen, unempfindlich gegenüber Signalen werden, die das Wachstum hemmen oder den programmierten Zelltod (Apoptose) bewirken,

neue Blutgefäße (Angiogenese) ausbilden, den Energiemetabolismus umprogrammieren und der Eliminierung durch das Immunsystem entgehen, damit letztendlich ein Tumor entstehen, wachsen und metastasieren kann (Hanahan & Weinberg 2000; Hanahan & Weinberg 2011).

1.3. Tumorsuppressor p53

Der Tumorsuppressor p53 wurde erstmals 1979 unabhängig von mehreren Wissenschaftlern beschrieben (Lane & Crawford 1979; Linzer & Lane 1979). Zunächst wurde p53 jedoch für ein Onkogen gehalten, da es im Komplex mit dem großen T-Antigen des Simian-Virus SV40 in transformierten Zellen gefunden wurde (Lane & Crawford 1979; Linzer & Lane 1979; Chang et al. 1979; Kress et al. 1979; DeLeo et al. 1979). Erst zehn Jahre später wurde gezeigt, dass eine mutierte Form von p53 analysiert worden war und es sich beim p53 Wildtyp um einen Tumorsuppressor handelt (Eliyahu & Michalovitz 1989; Finlay et al. 1989). Heute ist p53 der bedeutendste Tumorsuppressor, der als Mittelpunkt einer Vielzahl von Signalwegen Prozesse wie Zellzyklus, Differenzierung, Seneszenz und Apoptose kontrolliert (Vogelstein et al. 2000; Vousden & Prives 2009). Durch die Sicherung der genomischen Integrität des Organismus wirkt p53 als „Wächter des Genoms“ (Lane 1992).

1.3.1. Aufbau und Struktur von TP53 und p53

Das humane *TP53* Gen ist auf Chromosom 17p13.1 lokalisiert und kodiert für ein etwa 53 Kilodalton (kDa) großes Protein. Das *TP53* Gen besteht aus 11 Exonen, wobei durch die Nutzung mehrerer Promotoren (P1, P1´ und P2) und alternatives Spleißen der mRNA bis zu neun verschiedene p53 Isoformen entstehen können (Bourdon et al. 2005; Rohaly et al. 2005). Hauptsächlich wird jedoch konstitutiv das Volllängenprotein vom P1 Promotor ausgehend exprimiert mit Spleißen von Exon 9 mit Exon 10 (Abb.02A).
Das p53-Protein besteht aus 393 Aminosäuren und hat den typischen Aufbau eines Transkriptionsfaktors mit einer N-terminalen Transaktivierungsdomäne (TAD) für die Interaktion mit Proteinen des Transkriptionsapparates, einer

zentralen DNA-Bindungsdomäne (DBD) und einer C-terminalen Oligomerisierungsdomäne (OD) für die Tetramerisierung von p53-Monomeren. Weiterhin verfügt p53 über eine Carboxy-terminale Domäne (CTD), mit der p53 unspezifisch an DNA binden kann (Foord & Bhattacharya 1991; Weinberg, Freund, et al. 2004), eine Prolin-reiche Region (PRR) am N-Terminus, sowie Kernlokalisierungs- (NLS) und Kernexportsignale (NES) (Harms & Chen 2006) (Abb.02B).

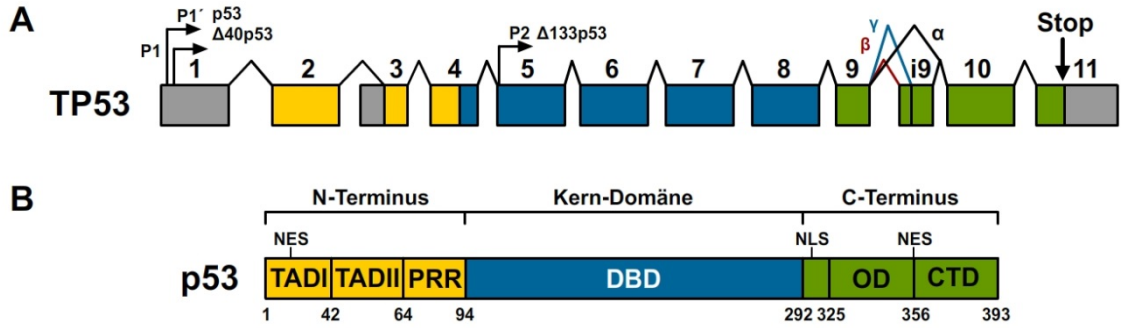

Abb.02: Schematischer Aufbau des humanen *TP53* Gens und des p53 Proteins
(A) Aufbau des *TP53* Gens mit 11 Exonen. Gekennzeichnet sind die alternativen Promotoren P1, P1´und P2, sowie die alternativen Spleißvarianten α, β und γ. **(B)** Übersicht über das p53 Protein mit den Transaktivierungsdomänen I und II (TAD), der Prolin-reichen Region (PRR), der zentralen DNA-Bindungsdomäne (DBD), der Oligomerisierungsdomäne (OD) und der Carboxy-terminalen Domäne (CTD), sowie die Kernlokalisierungs- (NLS) und Kernexportsignale (NES). (Nach Courtois et al. 2004; Bourdon 2007; Joerger & Fersht 2010)

Die N-terminale Domäne des p53-Proteins ist in seiner nativen Konformation intrinsisch nicht gefaltet und nur in einigen Regionen mit wichtigen hydrophoben Aminosäureresten können Sekundärstrukturen ausgebildet werden. Große intrinsisch ungeordnete Regionen finden sich oft als Motiv in der TAD von Transkriptionsfaktoren, da diese Flexibilität eine Vereinfachung der Bindung an verschiedenste Zielproteine mit hoher Spezifität erlaubt (Dunker et al. 2005; Liu et al. 2006). Erst durch die Bindung der p53-TAD mit Partnerproteinen kommt es zur vollständigen Faltung und Stabilisierung helicaler Strukturen.
Die p53-Kerndomäne bildet mit zwei gegenläufigen β-Strängen und einer β-Schleife (β-Sandwich) das Grundgerüst für die DNA-Bindung. Daran schließen sich zwei weitere Elemente an, die für die sequenzspezifische DNA-Bindung wichtig sind. Ein Schleife-Faltblatt-Helix-Motiv beinhaltet die

Schleife L1, die β-Stränge S2 und S2´, sowie Teile des β-Stranges S10 und die C-terminale Helix (H2) und bindet an die große Furche der DNA. Die andere Hälfte der Oberfläche der DNA-Bindung besteht aus zwei großen Schleifen (L2 und L3), die durch ein Zink-Ion stabilisiert sind und an die kleine Furche der DNA-Helix binden (Abb.03A&B). Die L2-Schleife beinhaltet zentral die H1-Helix, die wichtig für Protein-Protein-Interaktionen zwischen den DBDs benachbarter

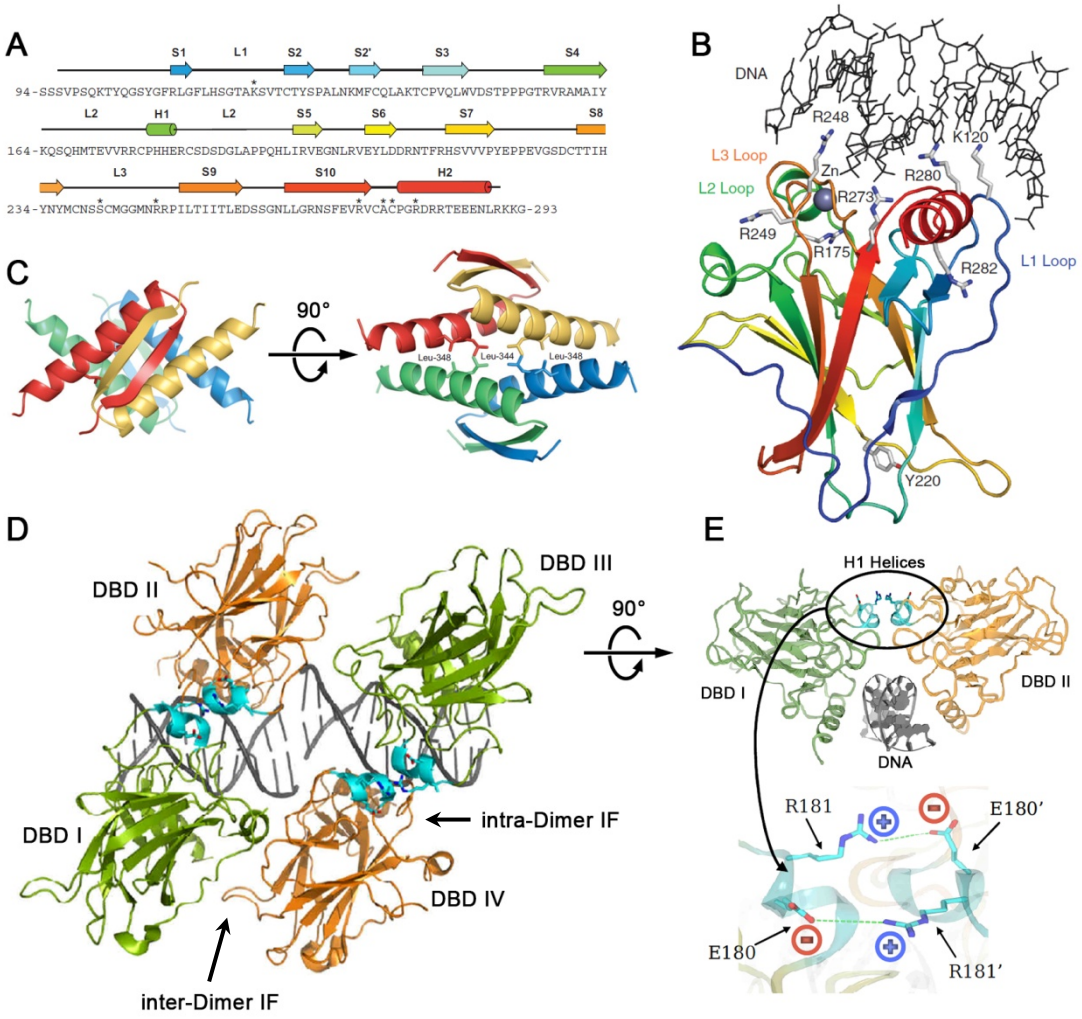

Abb.03: Strukturen der p53-Domänen und die sequenzspezifische DNA-Bindung
(A) Primärstruktur mit eingezeichneten Sekundärstrukturen der humanen p53-DNA-Bindungsdomäne (Cho et al. 1994). Sternchen kennzeichnen Aminosäuren mit Kontakt zur DNA. **(B)** Struktur der DNA-Bindungsdomäne eines p53-Monomers im Bändermodell in Regenbogenfarben vom Amino-Terminus (blau) bis zum Carboxyl-Terminus (rot) mit stabilisierenden Zink-Ion (Zn) in Kontakt zur DNA (Joerger & Fersht 2010). **(C)** Assemblierung der Oligomerisierungsdomäne von p53 als Dimer aus Dimeren, gezeigt in zwei verschiedenen Orientierungen (Jeffrey et al. 1995). **(D)** Quartärstruktur eines p53-DBD-Tetramers in Bindung an DNA (grau) in der Aufsicht (nach Kitayner et al. 2006). Strukturell ergeben sich zwei Interaktionsflächen (IF). **(E)** Innerhalb eines p53-Dimers (DBD I und DBD II) interagieren die DBD-Monomere über die H1-Helix (blau). Eine höhere Auflösung (unten) zeigt die Dimerisierungs-Interaktionsfläche zweier DBDs, die durch doppelte Salzbrücken zwischen Glutamat 180 (E180) und Arginin (R181) entstehen (nach Kitayner et al. 2006).

Monomere ist. Die Kerndomäne des humanen p53 ist von relativ geringer intrinsischer thermodynamischer Stabilität und entfaltet sich bei Körpertemperatur mit einer Halbwertszeit von etwa 9 Minuten (Bullock et al. 1997; Friedler et al. 2003; Ang et al. 2006). Die geringe thermodynamische und kinetische Stabilität erlaubt einen schnellen Wechsel zwischen geordneter und ungeordneter Konformation der DBD und stellt eine zusätzliche Ebene der Funktionsregulation des aktiven zellulären Proteins dar (Joerger & Fersht 2008). Ebenfalls steht diese geringe intrinsische Stabilität in Zusammenhang mit der strukturellen Plastizität, die für die Interaktion mit unterschiedlichen Partnerproteinen erforderlich ist (Joerger & Fersht 2010).

Die DBD ist durch eine flexible Aminosäuresequenz (Linker) mit der OD verbunden. Die OD bildet ein kurzes β-Faltblatt und eine α-Helix, die durch eine scharfe Wende verbunden sind. Die ODs zweier Monomere können sich durch ein intermolekulares anti-paralleles β-Faltblatt, sowie über ein anti-paralleles Helix-Bündel verbinden und kotranslational ein primäres Dimer bilden. Zwei dieser Dimere bilden posttranslational durch ein Helix-Bündel ein Tetramer, das als Dimer aus primären Dimeren bezeichnet werden kann (Abb.03C) (Lee et al. 1994; Clore et al. 1995; Jeffrey et al. 1995).
Der äußerste C-Terminus ist wieder intrinsisch ungeordnet, nimmt aber lokal bei der Interaktion mit Proteinen und der unspezifischen DNA-Bindung eine geordnete Konformation an (Friedler et al. 2005).
Da etwa 40% des p53-Volllängenproteins aus nativen ungeordneten Regionen besteht (Joerger & Fersht 2008), war die Aufklärung der p53-Struktur über lange Zeit schwierig. Die Kombination verschiedener Daten durch Untersuchungen mittels Röntgenstreuung, Elektronenmikroskopie und magnetische Kernspinresonanz (NMR) des Volllängenproteins, sowie Kristallstrukturanalysen isolierter p53-Fragmente trugen schließlich zum besseren Verständnis über die Strukturen der verschiedenen Domänen des p53-Proteins und dessen Bindung an die DNA bei (Cho et al. 1994; Kitayner et al. 2006; Tidow et al. 2007).

1.3.2. p53-Bindung an die DNA

Als sequenzspezifischer Transkriptionsfaktor bindet p53 an ein Bindungsmotiv und aktiviert oder reprimiert so die Transkription seiner Zielgene. Dieses Bindungsmotiv besteht aus zwei palindromischen Dekameren mit der Konsensussequenz 5´-RRRCWWGYYY-3´ (R: Purin-Base; Y: Pyrimidin-Base; W: Adenin oder Thymin), die durch Zwischensequenzen (Spacer) mit der Länge von 0 bis 21 Basenpaaren getrennt sein können (Abb.04) (Funk et al. 1992; El-Deiry et al. 1992; Riley et al. 2008). p53 Bindungsmotive können überall in einem Gen vorkommen, wobei sie verstärkt im Promotorbereich oder in der Nähe des Transkriptionsstartpunkts auftreten (Riley et al. 2008).

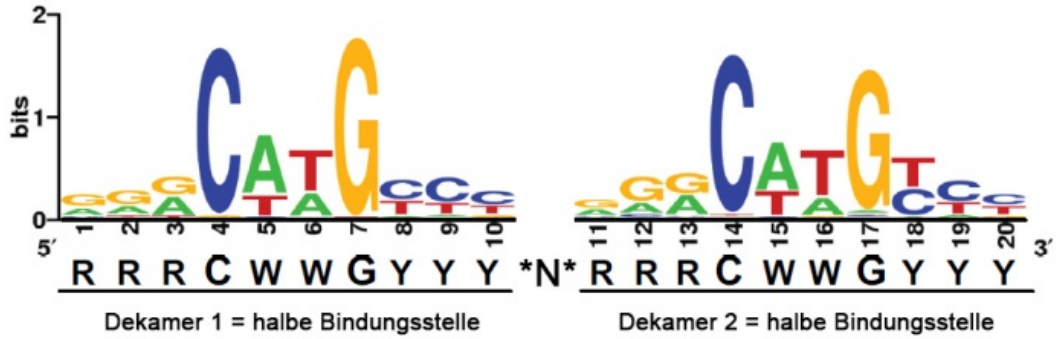

Abb.04: Die p53-Konsensussequenz als DNA-Bindungsmotiv
Genereller Aufbau der p53-Konsensussequenz bestehend aus zwei palindromischen Dekameren, die durch eine Zwischensequenz (*N*) von 0-21 Basenpaaren getrennt sein können. R: Purin-Base; Y: Pyrimidin-Base; W: Adenin oder Thymin. Die Größe der Buchstaben kennzeichnet die Häufigkeit der Base an dieser Position. (Modifiziert nach Wang et al. 2009)

In Lösung bildet das freie p53-Protein mit drei weiteren p53-Monomeren über die ODs einen kreuzförmig gestrecktes Tetramer mit jeweils zwei lose assoziierten DBDs und abstehenden TADs (Tidow et al. 2007). Bei der Bindung an die DNA wickeln sich die p53-Moleküle um die DNA-Helix und binden an diese über ihre DBDs (Abb.03D) (Kitayner et al. 2006). Dies führt zur Stabilisierung und Festigung der Strukturen. Das Tetramer kann als symmetrisches Dimer aus Dimeren bezeichnet werden, da jeweils die DBDs zweier Monomere interagieren und zwei dieser Dimere als Tetramer an die DNA binden (Cho et al. 1994). Dabei besetzt jeweils ein Dimer eine halbe Bindungsstelle der Konsensussequenz, wobei die Bindung an die DNA

kooperativ über Protein-Protein-Interaktionen erfolgt (Balagurumoorthy et al. 1995; Weinberg et al. 2004; Dehner et al. 2005). Eine kooperative Bindung bedeutet dabei, dass die Bindung von vier p53-Molekülen in Form eines Tetramers an die DNA stärker ist als die Bindung vier einzelner Mononere.

Kristallstrukturanalysen des p53-Tetramers in Bindung an DNA zeigen zwei Formen von Protein-Protein-Interaktionsflächen (IF): eine symmetrische intra-Dimer-IF zwischen zwei p53-Monomeren eines Dimers und eine translationale inter-Dimer-IF zwischen p53-Monomeren zweier Dimere (Abb.03D). An der intra-Dimer-Interaktion sind die beiden gegensätzlich geladenen Aminosäuren Glutamat 180 (E180) und Arginin 181 (R181) der H1-Helix beteiligt, die doppelte Salzbrücken ausbilden (Abb.03E). Diese Interaktion zweier p53-Monomere über die H1-Helices scheint entscheidend für die kooperative Form der DBD-Bindung an die DNA zu sein (Dehner et al. 2005). Damit das p53-Tetramer sterisch ungehindert an DNA binden kann, wird die DNA im Bereich des CWWG-Motivs der Konsensussequenz durch p53 verdreht (Kitayner et al. 2010; Beno et al. 2011). Wie flexibel die DNA ist, hängt dabei von der Sequenz der Basen ab. Während das CATG-Motiv eines perfekten p53-Bindungsmotivs sehr flexibel ist, sind CAAG, CTTG und CTAG (CWWG)-Motive starrer und schwerer zu verbiegen (Beno et al. 2011). Diesbezüglich lassen sich Bindungsmotive aufgrund ihrer Affinität unterscheiden. Da p53 für das Verbiegen einer CATG-Sequenz wenig Energie aufbringen muss, ist die Bindungsaffinität und Transaktivierung von Genen, die ein solches Motiv aufweisen, stärker. Bei der Bindung eher starrer CWWG-Sequenzen oder Motiven, die durch Spacer separiert sind, benötigt p53 wesentlich mehr Energie, so dass diese Bindungsstellen eher niedrig-affin sind (Funk et al. 1992; Balagurumoorthy et al. 1995; Weinberg et al. 2005; Beno et al. 2011). Interessanterweise finden sich perfekte Konsensussequenzen mit einem zentralen CATG-Motiv ohne Spacer in Genen, die den Zellzyklus arretieren, während Abweichungen dieser Sequenz mit zentralen CWWG-Motiv, Spacern oder nur halben Bindungsmotiven verstärkt in Apoptosegenen vorkommen (Weinberg et al. 2005; Riley et al. 2008).

1.3.3. Regulation von p53

Unter normalen Bedingungen hat p53 eine Halbwertszeit von ungefähr 20 Minuten. Aktivität und zelluläre Konzentration von p53 werden über das Mouse double minute 2 Protein (Mdm2) negativ reguliert (Oliner et al. 1992). Mdm2 bindet N-terminal an die TAD und verhindert so die transaktivierende Funktion von p53. Zusätzlich katalysiert Mdm2 als E3-Ubiquitin-Ligase die Ubiquitinierung von p53 und fördert so die proteasomale Degradierung des Tumorsuppressors. Da p53 das *Mdm2*-Gen transaktiviert, besteht ein Rückkopplungsmechanismus, der unter normalen Bedingungen die Konzentration von p53 gering hält (Moll & Petrenko 2003; Toledo & Wahl 2006). Verschiedene zelluläre Stressfaktoren wie beispielsweise DNA-Schäden, Hypoxie, Onkogene oder Mangel an Desoxyribonukleosidtriphosphaten (dNTPs) verhindern die Interaktion von p53 mit Mdm2 und führen zur Stabilisierung und Aktivierung von p53 sowie dessen Translokation in den Zellkern und Transkription oder Repression von Zielgenen.

1.3.4. p53-vermittlete Induktion von Zellzyklus-Arrest und Apoptose

Das Schicksal einer geschädigten Zelle wird von p53 durch die sequenzspezifische Bindung an bestimmte Gruppen von Zielgenen beeinflusst, die z.B. einen transienten Zellzyklus-Arrest oder Apoptose induzieren. Das vorübergehende Anhalten des Zellzyklus ermöglicht die Reparatur von Zellschäden und verhindert, dass sich geschädigte Zellen teilen und verändertes Erbmaterial an Tochterzellen weitergeben. Sind die Zellschäden zu stark und können nicht repariert werden, so ist der programmierte Zelltod eine irreversible Möglichkeit solche Zellen zu eliminieren (Lane 1992; Levine & Oren 2009). p53 kann auch einen irreversiblen Zellzyklus-Arrest (Seneszenz) induzieren, wodurch Zellen altern, aber sich nicht mehr teilen können (Rufini et al. 2013) oder zelluläre Differenzierung bewirken, wodurch spezialisierte Zellen entstehen, die ebenfalls nicht mehr proliferieren (Molchadsky et al. 2010).
Um den Zellzyklus anzuhalten aktiviert p53 das Zielgen *CDKN1A*, welches für das p21-Protein kodiert. Als Inhibitor Cyklin-abhängiger Kinasen arretiert p21 den Zellzyklus in der G1-Phase, indem die Cyclin-abhängige Kinase CDK4 gehemmt und die Phosphorylierung des Retinoblastom-Proteins verhindert wird

(Waldman et al. 1995; El-Deiry 1998). *GADD45* (Growth arrest and DNA Damage) und *14-3-3-σ* führen durch p53 zu einem Arrest in der G2/M Phase des Zellzyklus (Hermeking et al. 1997; Kastan et al. 1992).

Apoptose wird durch p53 sowohl über den extrinsischen als auch den intrinsischen Weg induziert. An der extrinsischen Apoptose-Induktion sind *FAS* und *KILLER/DR5* beteiligt, die für sogenannte Todesrezeptoren der Tumornekrosefaktor-Superfamilie kodieren und die Caspase-Kaskade aktivieren (Müller et al. 1998; Ruiz-Ruiz et al. 2003; Tomasetti et al. 2006). Durch Gene der Bcl-Superfamilie, wie *BAX*, *PUMA* und *NOXA* als auch AIP1 oder p53AIP1 wird beim intrinsischen Weg der Apoptose die Mitochondrienmembran zerstört, so dass Cytochrom C freigesetzt wird, was die Aktivierung des Apoptosoms und Caspasen zur Folge hat (Benchimol 2001; Oda et al. 2000; Nakano & Vousden 2001; Miyashita & Reed 1995).

Darüber hinaus kann p53 auch transkriptionsunabhängig Apoptose bewirken. Durch die cytoplasmatische Interaktion mit den Mitgliedern der Bcl-2 (B-cell lymphoma-2) Proteinfamilie Bcl-2 und Bcl-xL verhindert p53 deren antiapoptotische Funktion und bewirkt die Permeabilisierung der äußeren Mitochondrienmembran (Moll et al. 2005; Green & Kroemer 2009).

Bis heute konnte nicht geklärt werden, wie p53 zwischen unterschiedlichen Gruppen von Zielgenen unterscheidet und welche Mechanismen darüber entscheiden, wie p53 als Antwort auf Zellstress entweder das Überleben oder den Tod einer Zelle fördert (Riley et al. 2008; Murray-Zmijewski et al. 2008; Blattner 2008). Weiterführende Erkenntnisse darüber wären für therapeutische Ansätze vorteilhaft, um die p53-Antwort gezielt in Richtung Zelltod zu lenken und Tumorzellen zu eliminieren.

1.3.5. Posttranslationale Modifikationen und Interaktionspartner von p53

Nach dem heutigen Wissensstand ist eine Vielzahl an Faktoren bekannt, die p53 bei der Entscheidung beeinflussen, welches transkriptionelle Programm aktiviert wird. Dabei haben posttranslationale Modifikationen von p53 und Proteine, die als Interaktionspartner fungieren, die größte Bedeutung für die Promotorselektion, von denen auf die Wichtigsten im Folgenden eingegangen wird (Abb.05) (Vogelstein et al. 2000; Levine et al. 2006).

Alle p53-Domänen können temporär posttranslational modifiziert werden. Dies erfolgt z.B. in Form von Phosphorylierung, Acetylierung, Methylierung, Ubiquitinierung, Neddylierung oder Sumoylierung (Toledo & Wahl 2006).
Durch DNA-Schäden wird p53 durch die Proteinkinasen ATM (Ataxia telangiectasia mutated) an Serin 15 und CHK2 (Checkpoint Kinase 2) an Serin 20 phosphoryliert (Chao et al. 2006; Saito et al. 2002). Diese Modifikationen hemmen die Bindung durch Mdm2 und tragen zur Steigerung der zellulären p53-Konzentration bei. Ein weiteres Serin des N-Terminus liegt an Position 46 und wird durch die Kinasen HIPK2 (Homeodomain-interacting protein kinase 2), AMPK (AMP-aktivierte Proteinkinase), oder DYRK2 (Dual-Specificity Tyrosine-(Y)-Phosphorylation Regulated Kinase 2) phosphoryliert. Dies ist bedeutend für die Aktivierung proapoptotischer Zielgene (D'Orazi et al. 2002; Okoshi et al. 2008; Taira et al. 2007).
Durch genotoxischen Stress wird das Lysin 120 (K120) durch hMOF (MYST family acetyltransferase) und TIP60 (Tat interacting protein) acetyliert, wodurch p53 die proapoptotischen Gene *BAX* und *PUMA* aktiviert (Sykes et al. 2006; Tang et al. 2006). p300 (E1A binding protein p300) fördert durch die Acetylierung der Lysine K164, K373 und K382 ebenfalls Apoptose (Liu et al. 1999; Knights et al. 2006).
Acetylierung des Lysins 320 (K320) durch PCAF (P300/CBP-associated factor), K320 Monoubiquitinierung durch E4F1 (E4F Transkriptionsfaktor 1), sowie K320 Neddylierung durch FBXO11 (FBox Protein 11) tragen hingegen zur Induktion eines p21-vermittelten Zellzyklus-Arrests bei (Liu et al. 1999; Le Cam et al. 2006; Abida et al. 2007) .
PRMT5 (Protein Arginin Methyltransferase 5) wiederum überträgt Methylgruppen auf zwei Arginine (R333 und R335) und führt ebenfalls zu einem p53-vermittelten Zellzyklus-Arrest (Jansson et al. 2008).

Neben posttranskriptionalen Modifikationen beeinflussen Kofaktoren das transkriptionelle Programm von p53. Diese Bindungspartner beeinflussen zum einen die Fähigkeit von p53 an spezifische Gruppen von Bindungsmotiven zu binden oder transkriptionelle Koaktivatoren an bestimmte Genorte zu rekrutieren. In speziellen Fällen bedingt der Modifikationsstatus von p53 die selektive Interaktion mit Bindungspartnern.

Die Mitglieder der ASPP Proteinfamilie sind ein Beispiel für Kofaktor-induzierte Promotorselektivität. ASPP1 und ASPP2 (Apoptose stimulierende Proteine von p53 1 & 2) binden an die p53-Kerndomäne und fördern Apoptose durch Transaktivierung von *BAX* (Samuels-Lev et al. 2001). iASPP (inhibitory ASPP) inhibiert hingegen durch seine Bindung an p53 die Transaktivierung proapoptotischer Zielgene (Bergamaschi et al. 2003). Die Regulation der p53-vermittelten Apoptose durch iASPP ist beeinflusst durch einen Polymorphismus im p53 Kodon 72, das entweder für ein Prolin (P72) oder ein Arginin (R72) kodiert. Die P72-Variante ist Teil eines PXXP-Motivs, was die Interaktion mit iASPP über dessen SH3-Domäne verstärkt. Dadurch induziert die P72-Variante weniger Apoptose, als die R72-Variante (Bergamaschi et al. 2006).

Das Zusammenspiel von posttranslationaler Modifikation und selektiver Kofaktorbindung ist durch die Prolyl-Isomerase Pin1 wiedergegeben. Pin1 erkennt Phosphorylierung von p53 an S46 und bewirkt durch Bindung an p53 die Dissoziierung von iASPP, was die Apoptose begünstigt (Mantovani et al. 2007).

Das Protein Hzf (Hematopoietic zinc finger) fördert im Falle von Zellstress durch seine Bindung an die p53-DBD die Aktivierung der Gene *CDKN1A* und *14-3-3-σ* und bewirkt einen Stopp des Zellzyklus (Das et al. 2007).

Die Brn3 Familie von POU-Domänen-Transkriptionsfaktoren interagieren mit p53 über die DBD, haben aber einen gegensätzlichen Effekt. Brn3a beeinflusst p53 hinsichtlich der Transaktivierung von *BAX* und reprimiert p21, wodurch Apoptose eingeleitet wird. Brn3b bewirkt diesbezüglich das Gegenteil und fördert den p21-vermittelten Zellzyklus-Arrest (Budhram-Mahadeo et al. 2006).

Ebenfalls ambivalent verhält sich das Zinkfingerprotein Miz-1 (Myc-interacting zinc finger). Durch Miz1-Bindung an die p53-DBD wird die Expression von p21 induziert. Befindet sich Miz-1 aber im Komplex mit MYC, wird p21 reprimiert, der Zellzyklus nicht mehr angehalten und Apoptose ermöglicht (Miao et al. 2010; Herold et al. 2002).

All diese Modifikationen und Interaktionen sind reversibel und können nach der Reparatur von Schäden und abklingenden Stresssignalen rückgängig gemacht werden. Dadurch kann p53 wieder mit Mdm2 interagieren und degradiert werden.

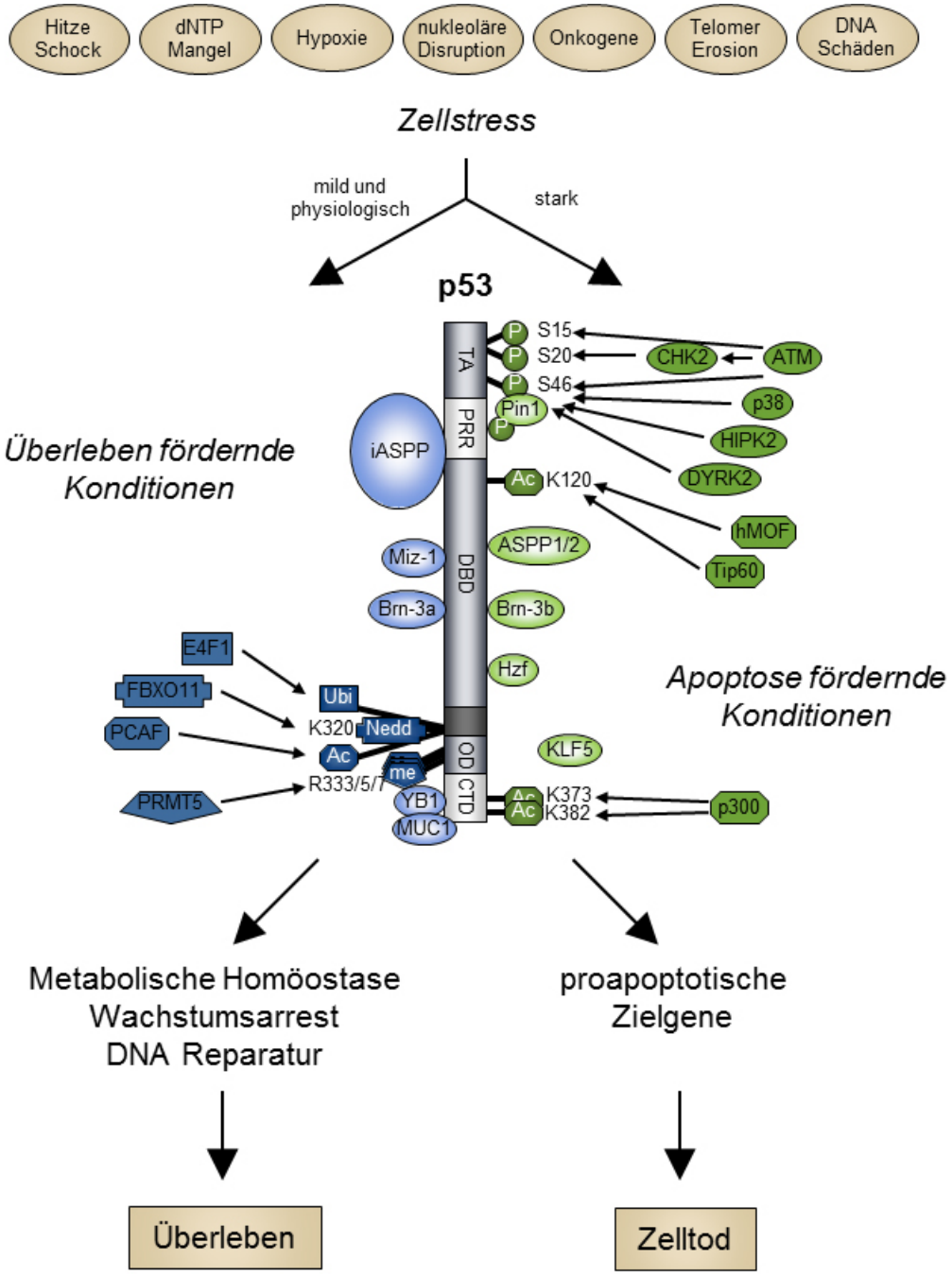

Abb.05: Übersicht über den p53-Signalweg
p53 wird durch verschiedene Formen von Zellstress aktiviert. Abhängig von der Stärke und Dauer des Stresses wird p53 posttranslational modifiziert oder interagiert mit verschiedenen Proteinen. Je nach Modifikation oder Interaktion mit Proteinen wird das Überleben der Zelle gesichert (linke Seite) oder der programmierte Zelltod aktiviert (rechte Seite). P: Phosphorylierung; Ac: Acetylierung; me: Methylierung; Ubi: Ubiquitinierung; Nedd: Neddylierung. (Nach Schlereth et al. 2010)

1.3.6. Mutationen von p53

TP53 ist in etwa 50% aller Tumoren mutiert und damit die häufigste genetische Veränderung bei humanen Krebserkrankungen. Aktuell listet die *TP53* Mutationsdatenbank der Internationalen Agentur für Krebsforschung IARC (http://p53.iarc.fr - Version R17) circa 31000 somatische p53-Mutationen auf, die zu über 1000 unterschiedlichen Tumorproteinen führen (Petitjean et al. 2007). Keimbahnmutationen von p53 sind deutlich seltener und mit dem Li-Fraumeni-Syndrom assoziiert, einer autosomal-dominant vererbbaren Erkrankung, die in einem frühen Lebensalter verschiedene Tumore verursacht (Li & Fraumeni 1969; Malkin 1993).

Etwa 90% aller Mutationen treten innerhalb der DBD in Form von Punktmutationen auf, die den Austausch einer Aminosäure bewirken (Olivier et al. 2002). Dabei treten ein paar wenige Mutationen mit sehr hoher Frequenz auf (Hotspot Mutationen). Strukturell werden p53-Mutationen in zwei Klassen eingeteilt, Kontakt- und Strukturmutanten. Kontaktmutationen betreffen Aminosäuren, die bei der DNA-Bindung direkt in Kontakt mit der DNA stehen, wie z.B. die beiden Arginine 248 und 273, während Strukturmutationen die Gesamtstruktur der DNA-bindenden Proteinoberfläche verändern, wie z.B. Arginine 175, 249 und 282 und das Glycin an Position 245 (Cho et al. 1994). p53-Mutationen verändern die thermodynamische Stabilität, die Proteinhalbwertszeit, die Interaktion mit Partnerproteinen sowie die Bindung an die DNA, was letztendlich den Verlust der Tumorsuppressoraktivität zur Folge hat (Bullock et al. 1997; Friedler et al. 2003; Joerger & Fersht 2007). Mutationen von p53 haben ferner einen dominant-negativen Effekt auf Wildtyp p53, so dass durch die Bildung von Heterotetrameren die tumorsuppressive Funktion von p53 außer Kraft gesetzt wird (de Vries et al. 2002; Dearth et al. 2007). Zusätzlich kann p53 durch Mutationen neue Funktionen und Eigenschaften erhalten, welche die Entstehung von Tumoren begünstigen. Somit wirkt mutiertes p53 wie ein Onkogen und fördert viele Kennzeichen von Krebs, wie beispielsweise Apoptoseresistenz oder einen umprogrammierten Energiemetabolismus (Dearth et al. 2007; Freed-Pastor & Prives 2012; Hanahan & Weinberg 2011).

1.4. RNA-Interferenz

Während man in der „klassischen Genetik“ über den Phänotyp das verantwortliche Gen erforscht, wird in der „reversen Genetik“ gezielt ein Genprodukt verändert oder abgeschaltet (Gen-Silencing), um die Auswirkung dieser Alteration auf den Phänotyp zu analysieren (Hardy et al. 2010). Dies ist u.a. mit Hilfe der RNA Interferenz (RNAi) möglich. Die RNAi ist ein biologischer Mechanismus, der in allen Eukaryoten vorhanden ist, mit dem über doppelsträngige RNA-Moleküle (dsRNA) unter Hilfe diverser Enzymkomplexe Genprodukte herrunterreguliert werden.

Im Nucleus werden von der RNA-Polymerase II oder III sogenannte primary microRNAs (pri-miRNA) mit einer Länge von 500 bis 3000 Nukleotiden transkribiert. Über einen Mikroprozessorkomplex, der u.a. aus dem RNA bindenden Protein Pasha (DGCR8) und der RNase III Drosha besteht, werden pri-miRNAs zu precursor microRNAs (pre-miRNA) prozessiert, welche nur noch eine Länge von etwa 70 Nukleotiden aufweisen. Die pre-miRNA bildet eine Haarnadelstruktur und wird über das Transportprotein Exportin 5 aktiv ins Zytoplasma transportiert (Yi et al. 2003). Im Zytoplasma werden durch das RNAse-III-Enzym Dicer die pre-miRNAs in 19 bis 25 Nukleotid lange microRNAs (miRNAs) geschnitten (Bernstein et al. 2001). Dabei haben alle von Dicer geschnittenen RNA-Moleküle einen 3´-Überhang von 2-3 Nukleotiden, sowie ein phosphoryliertes 5´-Ende. Dies ist nötig, damit die miRNAs von einem Enzymkomplex, dem RNA-induced silencing complex (RISC), aufgenommen werden können. Dort werden die kurzen doppelsträngigen RNA-Moleküle an Argonautenproteine des RISC Komplex übergeben und in einem ATP-abhängigen Prozess durch eine RNA-Helicase entwunden und gespalten (Nykänen et al. 2001). Einer der RNA-Einzelstränge verbleibt im RISC Komplex und wird als Leitstrang bezeichnet. Der andere RNA-Einzelstrang wird aus dem RISC Komplex entlassen und abgebaut. Als nächstes wird eine zum Leitstrang komplementäre mRNA in den RISC Komplex eingebaut, was die Degradierung der mRNA zur Folge hat. Im Zytoplasma kann durch sogenannte Processing-Bodies die degradierte Ziel-mRNA weiter abgebaut werden (Rossi 2005).

Um RNAi zum gezielten Gen-Silencing zu nutzen, können RNA-Moleküle, die eine Haarnadelstruktur ausbilden und short hairpin RNAs (shRNAs) genannt werden, synthetisch erzeugt und durch viralen Gentransfer ins Genom integriert

werden (Brummelkamp et al. 2002). Sie fungieren dann als pre-miRNA Analogon und bewirken das Abschalten eines Genprodukts. Ebenfalls können sogenannte small interfering RNAs (siRNA) transient in Zellen eingebracht werden, die eine perfekte Komplementarität zwischen Leitstrang und Ziel-mRNA aufweisen. Dadurch wird die Ziel-mRNA über Ago2, ein Argonautenprotein mit Endonuklease-Aktivität, gespalten.

Innerhalb kürzester Zeit seit der Aufklärung des RNAi Mechanismus hat sich diese Technologie zu einer wichtigen Methode für Gen-Silencing und Phänotyp-Verluststudien entwickelt. So findet man heute RNAi-basierte Anwendungen in der Grundlagen- und Pharmaforschung oder in der Entwicklung von klinischen Therapien (Jacque et al. 2002; Landen et al. 2005; Pecot et al. 2011).

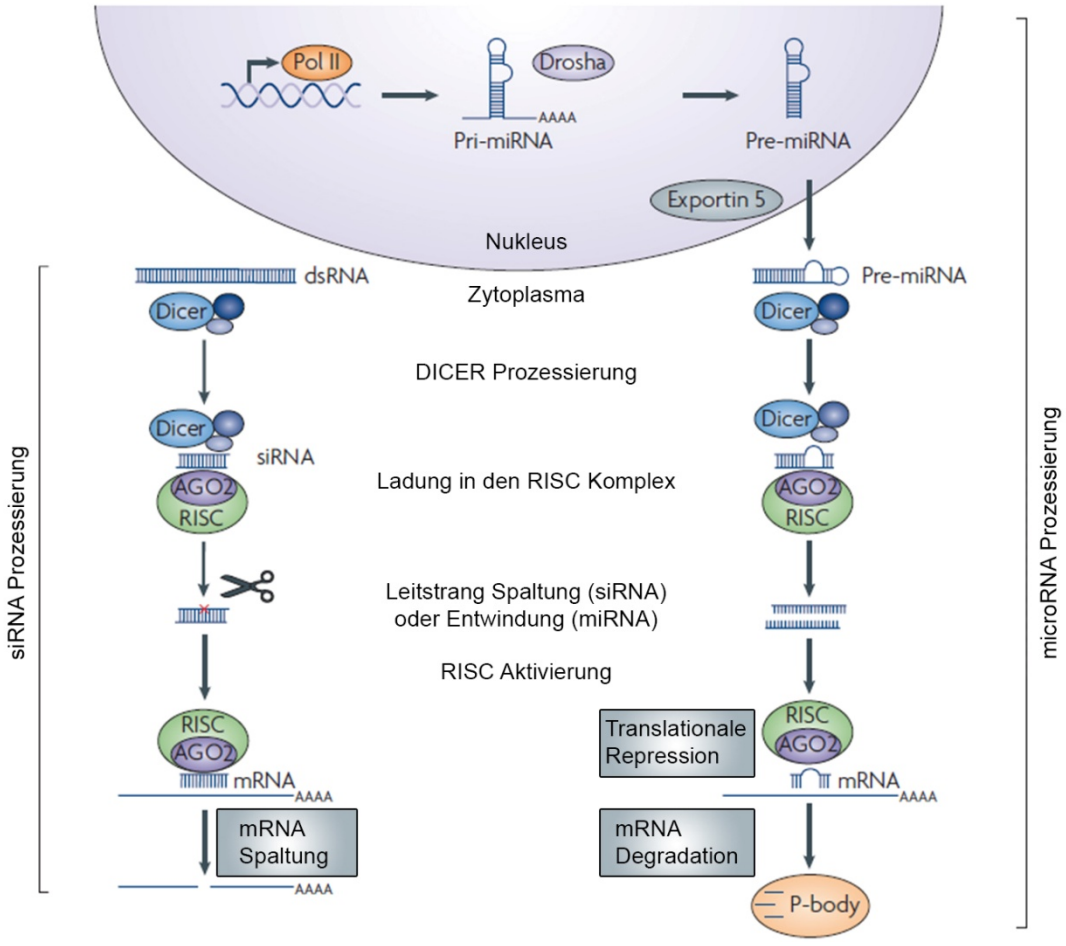

Abb.06: Schema der RNAi vermittelten Genstilllegung
Die pri-miRNA wird nach der Transkription durch die RNA Polymerase II (Pol II) durch Drosha zur pre-miRNA verkürzt und über Exportin 5 ins Zytoplasma transportiert. Durch Dicer entstehen miRNAs und aus eingebrachter dsRNA die siRNAs. Nach Laden der RNA-Duplexe in den RISC Komplex erfolgt eine Spaltung oder Entwindung der doppelsträngigen RNA-Moleküle. Eine dem Leitstrang komplementäre mRNA wird in den RISC Komplex geladen. Im Fall der siRNAs wird die mRNA durch das Argonautenprotein Ago2 gespalten, während miRNAs die Translation der mRNA Ago2-vermittelt reprimieren. Die Degradation der mRNA erfolgt endgültig über die P-bodies. (Modifiziert nach de Fougerolles et al.2007)

1.5. Reportergene

Reportergene werden verwendet, um Zellen zu markieren. Das Produkt des Reportergens kann dabei ein Enzym, ein detektierbares Antigen, ein Fusionsprotein aber auch ein fluoreszierendes oder lumineszentes Reporterprotein sein. Wichtig ist, dass das durch das Reportergen kodierte Protein nicht toxisch ist, sich leicht und sensitiv nachweisen lässt und die Nachweismethode (Assay) kein großes Hintergrundsignal liefert. Reportergene werden in den Biowissenschaften auch für molekulare Bildgebung (Imaging) von Kleintieren wie von Mäusen und Ratten eingesetzt. Dies erlaubt neben der Untersuchung der Genregulation oder Wechselwirkung von Proteinen *in vivo* die gewebespezifische oder entwicklungsabhängige Reportergenexpression am lebenden Objekt.

Als klassische Reportergene werden Gene verwendet, die für die Chloramphenicol Acetyltransferase (CAT), die β-Galactosidase (β-Gal), die Alkalische Phosphatase (AP) oder deren sekretierte Form (SEAP) kodieren (Gorman et al. 1982; Lim & Chae 1989; Yoon et al. 1988; Berger et al. 1988).

Einige der Reportergene kodieren für Enzyme, deren Aktivität in einer chromogenen Reaktion durch das Umsetzen einer bestimmten Indikatorsubstanz photometrisch bestimmt werden kann. Hauptsächlich werden jedoch Gene für autofluoreszierende Proteine oder Luciferasen verwendet, auf die hier näher eingegangen werden soll.

1.5.1 Fluoreszenz-Reporter

Das grün fluoreszierende Protein (GFP) ist das wohl bekannteste Fluoreszenz-Reportergen. GFP wurde zuerst aus der Qualle *Aequorea victoria* isoliert (Shimomura et al. 1962; Shimomura 2005), kommt aber auch in anderen marinen Organismen vor. Das natürliche GFP-Protein besteht aus 238 Aminosäuren mit einer Molekülmasse von 26,9 kDa und fluoresziert grün mit einer Emissionswellenlänge von 508 nm bei der Anregung durch blaues (475 nm) oder ultraviolettes (395 nm) Licht (Prendergast & Mann 1978; Prasher et al. 1992). GFP ist ein sehr stabiles Protein, resistent gegenüber vielen Proteasen, bleibt über einen großen pH-Bereich stabil und denaturiert erst bei Temperaturen über 65°C.

Strukturell bildet GFP ein zylindrisches β-Fass aus 11 β-Faltblättern, die eine α-Helix umschließen, an die das Chromophor 4-(p-Hydroxybenzyliden)-Imidaziolidin-5-on kovalent gebunden ist (Ormö et al. 1996; Yang et al. 1996). Die Chromophor-Gruppe wird in einem autokatalytischen Prozess gebildet, indem bei der Faltung des Proteins die Aminosäuren Ser65, Tyr66 und Gly67 in räumliche Nähe gebracht werden. Dies führt zur Zyklisierung der drei Aminosäuren, gefolgt von einer Dehydrierung und Oxidation zur Fertigstellung des Chromophors (Reid & Flynn 1997). In der angeregten Phenolat-Form fluoresziert GFP unter Abspaltung eines Protons und kehrt dadurch in den Grundzustand zurück (Ormö et al. 1996; Yang et al. 1996).

Durch Mutationen am natürlichen GFP wurden weitere Varianten generiert, die veränderte Fluoreszenzspektren wie BFP (Blue), CFP (Cyan) oder YFP (Yellow) aufweisen, nur noch ein Absorptionsmaximum besitzen oder enhanced-Versionen, wie EGFP, welches vor allem in Säugerzellen verwendet wird (Heim et al. 1995; Cormack et al. 1996). Fluoreszierende Proteine wurden aber auch in anderen Organismen entdeckt (Matz et al. 1999), wie das drFP583 (dsRed) aus der Koralle *Discosoma*, welches rotes Licht emittiert, was vorteilhaft für die Detektion in Geweben ist.

Die große Besonderheit der Fluoreszenz-Reporter ist, dass sie keine Kofaktoren für die Fluoreszenz benötigen. Daher eignen sie sich besonders für den Nachweis von Reportergenprodukten in lebenden Zellen oder wenn Zellen oder Proteine (als Fusionsprotein) markiert werden, um die räumliche oder zeitliche Verteilung zu analysieren. In der Zellbiologie können z.B. Strukturen des Zytoskeletts aber auch Zellorganellen und Zellbestandteile durch Markierung mit GFP sichtbar gemacht und mittels Fluoreszenzmikroskopie analysiert werden (Ludin & Matus 1998; Ballestrem et al. 1998). Ebenso kann damit auch die Regulation und der Transport von Proteinen in Zellen untersucht werden. Mit Hilfe der Durchflusszytometrie lassen sich GFP-markierte Zellen analysieren, quantifizieren und isolieren (Beavis & Kalejta 1999; Sørensen et al. 1999). In der medizinischen Forschung werden Fluoreszenzreporter verwendet, um beispielsweise die Entwicklung von Nervenzellen oder Wachstum und Metastasierung von Tumorzellen zu verfolgen (Hoffman 2002; Kouros-Mehr et al. 2008). Heute gibt es einige gentechnisch veränderte Organismen, wie Pflanzen, Mäuse, Ratten, Katzen oder Affen, in die GFP als Transgen

eingebracht wurde und die in der Forschung eingesetzt werden (Moen et al. 2012; Remy et al. 2010; Wongsrikeao et al. 2011; Sasaki et al. 2009).

1.5.2. Lumineszenz-Reporter

Luciferasen sind Enzyme, die chemische oder biochemische Reaktionen unter Lichtemission (Biolumineszenz) katalysieren. Verschiedene Organismen sind zur Biolumineszenz fähig, von Bakterien über Leuchtkäfer zu marinen Dinoflagellaten, Ruderfußkrebse oder Seefedern, die unterschiedliche Luciferasen und Licht-emittierende Reaktionen nutzen (Bronstein et al. 1994). Die am besten untersuchte Luciferase ist die Firefly Luciferase (FLuc) aus dem Leuchtkäfer *Photinus pyralis* (Gould & Subramani 1988). FLuc besteht aus 550 Aminosäuren mit einer molekularen Masse von 62 kDa und ist als Monomer aktiv (Wood 1995). Für seine Funktion benötigt FLuc zwar keine posttranslationalen Modifikationen, doch ist Luciferin als Substrat erforderlich. FLuc katalysiert die Oxidation des Substrats Luciferin unter Verbrauch von ATP und Sauerstoff zu Oxyluciferin (Abb.07A). In einem nicht-stabilen angeregten Zustand setzt Oxyluciferin ein Lichtphoton frei, wodurch Licht bei 560nm emittiert wird und Oxyluciferin wieder in seinen stabilen Grundzustand zurückkehrt. Dabei ist die Stärke des emittierten Lichtsignals proportional zur Aktivität der Luciferase. Durch verbesserte Reagenzien und Kodon-optimierte Luciferasen können Stabilität und Halbwertszeit des Lichtsignals zeitlich verlängert und lineare Ergebnisse über acht Größenordnungen erzielt werden (Wood 1998; Hawkins et al. 1999). Dies ermöglicht unter anderem den Einsatz der Luciferase in Hochdurchsatz-Formaten zum Analysieren einer großen Probenzahl (Che et al. 2012; Siebring-van Olst et al. 2013). Das Lichtsignal kann am sensitivsten mit einem Luminometer gemessen werden und erfordert im Vergleich zum GFP kein Anregungslicht. In solchen Luciferase Assays kann die geringe Menge von 10^{-20} Mol des Enzyms detektiert werden, was diesen Assay um ein Vielfaches sensitiver gegenüber anderen Reportergenen wie beispielsweise CAT macht (Alam & Cook 1990).

Eine Alternative zur FLuc ist die *Renilla reniformis* Luciferase (RLuc) aus der marinen Seefeder, die keine Sequenzhomologie mit FLuc aufweist (Lorenz 1991). RLuc ist mit der molekularen Masse von 36 kDa als Monomer aktiv

(Matthews et al. 1977) und benötigt Coelenterazin als Substrat für die Biolumineszenz. Enzymatisch katalysiert RLuc die oxidative Decarboxylierung von Coelenterazin zu Coelenteramid, wobei blaues Licht der Wellenlänge 480 nm emittiert wird (Abb.07B). Dieser Vorgang benötigt im Vergleich zu FLuc kein ATP (Hart et al. 1979).

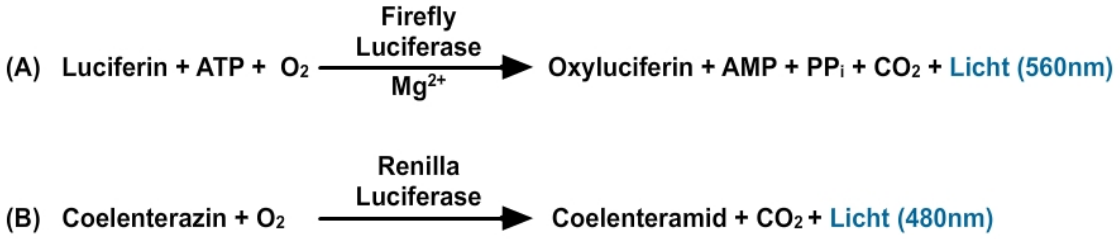

Abb.07: Biolumineszente Reaktionen katalysiert durch Firefly und Renilla Luciferase
A) Die Firefly Luciferase katalysiert unter Verbrauch von ATP die Oxidation von Luciferin zu Oxyluciferin, wobei blaues Licht bei 560nm emittiert wird. B) Blaues Licht bei 480nm entsteht bei der Oxidation von Coelenterazin zu Coelenteramid durch die Renilla Luciferase. ATP: Adenosintriphosphat; O_2: Sauerstoff; Mg^{2+}: Magnesium; AMP: Adenosinmonophosphat; PP_i: Pyrophosphat; CO2: Kohlenstoffdioxid.

Aufgrund ihrer unterschiedlichen Substrate werden FLuc und RLuc oft gemeinsam in sogenannten dualen Luciferase Assays verwendet. Dazu werden beide Reporter zusammen durch Ko-Transfektion in Zellen eingebracht. Dies ermöglicht das unabhängige und zeitgleiche Analysieren beider Luciferasen im selben Zellextrakt (Sherf et al. 1996). Während eine der Luciferasen als experimentelles Reportergen durch die spezifischen experimentellen Konditionen reguliert wird, dient die andere Luciferase als Kontroll-Reportergen und liefert dabei als interne Kontrolle die Basalaktivität. Normalisiert man die Aktivität des experimentellen Reporters auf die Aktivität des Kontroll-Reporters, kann die experimentelle Varianz minimiert werden, die u.a. aus Unterschieden der Zellviabilität oder der Transfektionseffizienz resultieren können. Somit ermöglichen duale Luciferase Assays eine verlässlichere Interpretation der experimentellen Daten, da verschiedene Einflüsse durch Normalisierung reduziert werden. Ebenso ist es möglich, zwei unterschiedliche Luciferase Assays gleichzeitig durchzuführen (Stables 1999). Darüber hinaus können duale Luciferase Assays *in vivo* durchgeführt und die Luciferase-Aktivitäten per Bioimaging analysiert werden (Wang & El-Deiry 2003; Mezzanotte et al. 2011).

Sekretierte Luciferasen sind eine neuere Klasse von Luciferasen. Durch eine Sekretionssequenz werden diese Luciferasen in das endoplasmatische Retikulum eingeschleust und aus der Zelle exportiert, wodurch ihre Aktivitäten in Kulturüberständen von Zellen oder in Körperflüssigkeiten von Tieren gemessen werden können. Die *Gaussia princeps* Luciferase (GLuc) aus dem Ruderfußkrebs ist eine solche sekretierte Luciferase, die als monomeres Protein aus 185 Aminosäuren mit einer molekularen Masse von 19,9 kDa die Oxidation von Coelenterazine katalysiert, wobei Licht bei 480 nm emittiert wird. Es wurde gezeigt, dass GLuc-exprimierende Zellen quantitativ über die Luciferase-Aktivität im Blut von Tieren gemessen oder über bildgebende Verfahren (Imaging) analysiert werden können. Da die Luciferase-Aktivität mit der Zellzahl korreliert kann GLuc indirekt als künstlicher Zellmarker verwendet werden (Tannous 2009; Wurdinger et al. 2008; Chung et al. 2009).

Eine weitere sekretierte Luciferase ist die *Cypridina noctiluca* Luciferase (CLuc) aus einem Muschelkrebs. CLuc oxidiert sein Substrat Vargulin, wobei ebenfalls blaues Licht bei 465 nm emittiert wird (Nakajima et al. 2004). Vorteile der sekretierten Luciferasen sind Stabilität und Sensitivität der Enzyme und eine im Vergleich zu nicht-sekretierten Luciferasen bis zu tausendfach höhere Signalintensität. Da die Lyse der Zellen für die Messung der Luciferase-Aktivität nicht nötig ist, können Luciferase-sekretierende Zellen über einen längeren Zeitraum regelmäßig analysiert und verschiedene Effekte in einer zeitauflösenden Weise untersucht werden. So können sekretierte Luciferasen in dualen Luciferase Assays eingesetzt oder auch mit nicht-sekretierten Luciferasen kombiniert werden (Maguire et al. 2013).

.

2. KUMULATIVER TEIL

2.1. DNA Binding Cooperativity of p53 Modulates the Decision between Cell-Cycle Arrest and Apoptosis

Katharina Schlereth, Rasa Beinoraviciute-Kellner, Marie K. Zeitlinger, Anne C. Bretz, Markus Sauer, Joël P. Charles, Fotini Vogiatzi, Ellen Leich, Martin Eilers, Caroline Kisker, Andreas Rosenwald & Thorsten Stiewe

Molecular Cell 38 (3), 356-368, 2010.

2.1.1. Einleitung

Der Tumorsuppressor p53 wird als „Wächter des Genoms“ bezeichnet, da er die genomische Stabilität eines Organismus überwacht und garantiert (Vousden & Lane 2007). Als Antwort auf verschiedene Formen zellulären Stresses, wie z.B. DNA-Schäden oder Aktivierung von Onkogenen, wird p53 stabilisiert und aktiviert und induziert in Abhängigkeit der Schwere des Stresses und der Zellschäden einen transienten Zellzyklus-Arrest, Seneszenz, Differenzierung oder Apoptose (Vousden & Lu 2002; Stiewe 2007). Die molekularen Details, wie p53 zwischen den Genen von so unterschiedlichen transkriptionellen Programmen unterscheidet, sind unklar. In diesem Projekt wurde die Rolle der DNA-Bindungskooperativität (DBK) von p53 für dessen Tumorsuppressor-Aktivität untersucht.

2.1.2. Zusammenfassung und Diskussion

Um die Rolle der DBK für die Funktion von p53 zu untersuchen, wurden p53 Mutanten mit veränderten Aminosäuren in der H1-Helix generiert, die für die Interaktion innerhalb der Dimere von bedeutend sind. Einerseits wurden im Vergleich zum p53 Wildtyp (E180 und R181 „ER“) Ladungen der Aminosäuren neutralisiert (E180→L „LR“ und R181→L „EL“) und Ladungen umgekehrt (E180→R „RR“ und R181→E „EE“), andererseits wurde eine Doppelmutante erzeugt (E180, R181 →R180, E181 „RE“) oder die beiden komplementären Mutanten „EE“ und „RR“ für funktionale Rettungsexperimente eingesetzt. Die

Nomenklatur der Mutanten kennzeichnet die beiden Aminosäuren der Kodons 180 und 181 wie in Abbildung 08 schematisch aufgeführt.

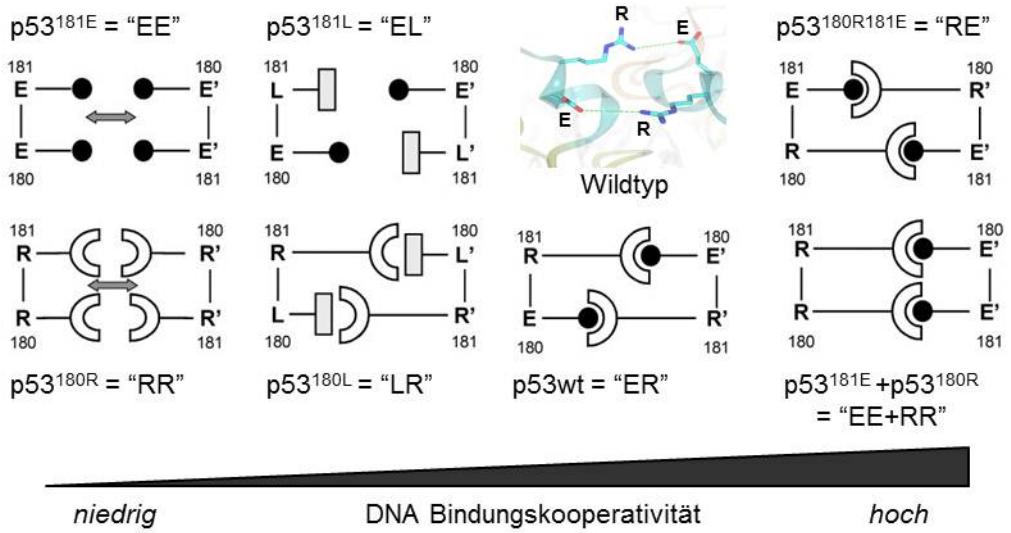

Abb.08: Übersicht über die p53 H1-Helixmutanten
Schematische Übersicht über das Dimerisierungsmuster von Wildtyp p53 „ER" und den H1-Helixmutanten und die wechselseitige Interaktion der Aminosäuren an Stelle 180 und 181. Anordnung nach Stärke der DNA-Bindungskooperativität. (Modifiziert nach Schlereth et.al, 2010)

Alle H1-Helixmutanten bildeten Tetramere unter nativen nicht-denaturierten Bedingungen (Abb.1D). Electrophoretic Mobility Shift Assays (EMSA) zeigten, dass die ladungsinvertierte Mutante EE gar nicht in der Lage ist an DNA zu binden, während RR eine deutlich abgeschwächte DNA-Bindung zeigte. Die ladungsneutralisierten Mutanten EL und RL zeigten eine klar schwächere DANN-Bindung im Vergleich zum Wildtyp. Die Doppelmutanten RE und die Kombination aus EE und RR zeigten dagegen eine starke Interaktion mit der DNA, die sogar stärker als die von Wildtyp p53 war (Abb.1E).

Diese unterschiedlichen Interaktionsstärken mit der DNA konnten durch zeitauflösende Dissoziations-EMSAs bestätigt werden (Abb.1G & H). Dies zeigt, dass die kooperative DNA-Bindung von p53 durch die H1-Helix vermittelt wird und dass die H1-Helixmutanten für die Untersuchung der Rolle der p53 DBK für die Tumorsuppressor-Aktivität verwendet werden können.

Die mit GFP-gekoppelte Expression der H1-Helixmutanten, sowie des p53 Wildtyps in p53-negativen H1299 Zellen zeigte, dass die schwach kooperative Mutanten EE, RR, LR und EL zwar einen Zellzyklus-Arrest induzieren konnten,

aber nicht mehr in der Lage waren, Apoptose einzuleiten. Während der p53 Wildtyp sowohl Zellzyklus-Arrest als auch Apoptose induzierte, waren die stark kooperative Mutante RE und die Kombination aus EE und RR ausschließlich zur Apoptose fähig (Abb.2A). Dies wurde anhand von Zellzyklusprofilen (Abb.2B) und Apoptose Assays (Abb.2D & E) bestätigt. Somit ist eine starke Interaktion der H1-Helix essentiell für die Induktion von Apoptose und Änderungen in der Interaktionsstärke beeinflussen die Entscheidung zwischen Zellzyklus-Arrest und Apoptose.

Um die DNA-Bindungsaktivität der H1-Helixmutanten *in vivo* zu untersuchen, wurden ChIP-on-chip Analysen der schwachen kooperativen Mutante EL und der stark kooperativen Mutante RE durchgeführt und die Bindung an über 25000 humane Promotorregionen untersucht. Dabei zeigte eine Auswahl zufällig ausgesuchter Bindungsstellen (BS) eine über fünffache Anreicherung für RE in ChIP-PCR Validierungsexperimenten (Abb.3A). Insgesamt wurden alle BS stärker von RE als durch EL gebunden und jede EL-BS wurde auch von RE gebunden. Dies weist darauf hin, dass mit einer hohen p53 DBK eine größere Anzahl an BS durch p53 gebunden werden kann. Die Daten konnten ebenfalls genutzt werden, um zu zeigen, dass allen BS, die gemeinsam durch EL und RE gebunden wurden eine p53 Konsensussequenz ähnlich sind, während BS, die ausschließlich durch RE gebunden wurden ein kürzeres Motiv aufwiesen, welches mehr dem Mittelstück eines Dekamers ähnelt (Abb.3B & C). Die Analyse spezifischer p53 Zielgene zeigte, dass die Promotoren von *p21*^{CDKN1A} und *HDM2* von beiden Mutanten gebunden wurden, aber nur RE in der Lage war, an proapoptotische Zielgenpromotoren wie *PUMA*, *NOXA* oder *CASP1* zu binden und diese Promotoren zu besetzen (Abb.3E & F). Eine erhöhte DBK aufgrund einer stärkeren H1-Helix Interaktion ermöglicht p53 somit die Rekrutierung an Promotoren apoptotischer Gene, die mit einer schwachen DBK nicht effizient gebunden werden können.

Weiterführend wurde die Transaktivierungsfunktion der H1-Helixmutanten im Vergleich zu p53 Wildtyp untersucht. Genexpressionsprofile mittels cDNA Microarrays zeigten zwei unterschiedliche Klassen an Genen, die abhängig von der Kooperativitätsstärke aktiviert wurden. Eine Klasse mit antiapoptotischen Genen wurde durch die schwach kooperativen Mutanten aktiviert, die andere Klasse mit apoptotischen Genen durch die stark kooperativen Mutanten

(Abb.4A & B). Dieses unterschiedliche Transaktivierungsmuster von p53 Zielgenen in Abhängigkeit von der p53 DBK konnte ebenfalls in Luciferase Assays mit unterschiedlichen p53-Bindungssequenzen (Abb.4C) und in Zeitverlaufsstudien auf Proteinebene (Abb.4E & F) für die verschiedenen H1-Helixmutanten gezeigt werden.

Wurden Zellen, die unterschiedliche H1-Helixmutanten exprimieren, mit Reagenzien behandelt, die DNA-Schäden verursachen und p53 aktivieren, korrelierte auch hier das Maß der induzierten Apoptose direkt mit der Kooperativität (Abb.5A-G). So bestimmt die p53 DBK ebenfalls das Ausmaß der Apoptose nach Schädigung der DNA.

Nur bei einer sehr geringen Anzahl von Krebspatienten sind somatische p53 Mutationen oder Keimbahnmutationen an den Positionen E180 oder R181 beschrieben. Es war daher ungewiss, ob solche Mutationen kausal für die Entstehung von Tumoren verantwortlich sein können. Daher wurden Untersuchungen an weiteren p53 H1-Helix-Mutanten durchgeführt, die genetisch mit dem Li-Fraumeni-Syndrom (Li & Fraumeni 1969), einer autosomal-dominant vererbbaren Tumorerkrankung, verknüpft sind. All diese Mutanten zeigten eine reduzierte DNA-Protein-Komplexstabilität *in vitro* (Abb.6A & B) sowie Defekte in der Promotorbindung und der Transaktivierung von proapoptotischen p53 Zielgenen (Abb.6C-F). Diese Mutanten induzierten aber $p21^{CDKN1A}$ und führten einen Zellzyklus-Arrest herbei (Abb.6E-H). Somit zeigten die Li-Fraumeni-Mutanten einen selektiven Verlust der Apoptoseaktivität, was für eine reduzierte DBK charakteristisch ist. Da diese Mutationen genetisch mit der Anfälligkeit für Krebs in Patienten verknüpft sind, kann aufgrund der Ergebnisse darauf geschlossen werden, dass die DNA-Bindungskooperativität zu der Tumorsuppressor-Aktivität von p53 beiträgt.

Für die Ausbildung eines Tetramers durch p53-Vollängenproteine ist die starke Interaktion der Oligomerisierungsdomänen wichtig. Die DBK ist dabei zwar nicht für die Assemblierung eines Tetramers von Bedeutung, doch zeigen die hier erhobenen Daten, dass die Interaktion der H1-Helices die Bindungseigenschaften von p53 an die DNA entscheidend steuert. Dabei scheint eine erhöhte DBK p53 energetisch zusätzlich zu stabilisieren, um Bindungsstellen im Genom, die von der perfekten Konsensussequenz abweichen und vermehrt in apoptotischen Zielgenen vorkommen, zu binden.

Interessant dabei ist, dass die DBK nicht nur die Apoptosefunktion von p53 steigert, sondern zeitgleich die Aktivierung von Zellzyklus-Arrestgenen reduziert. Die Daten zeigen, dass die stark kooperativen Mutanten hocheffektiv an die p53 Bindungsstelle des p21^{CDKN1A} Gens rekrutiert werden, das Gen aber nicht transaktivieren. Eine Erklärungsmöglichkeit dafür könnte sein, dass die stark kooperativen Mutanten an so viele Bindestellen im Genom binden, dass einer oder mehrere Koaktivatoren limitierend werden und dadurch die Transaktivierung von Genen, wie beispielsweise von p21^{CDKN1A}, reduziert ist. Somit dirigiert ein Anstieg der Kooperativität die p53-vermittelte Zellstressantwort von Zellzyklus-Arrest in Richtung Apoptose. Weiterführende Arbeiten in Mäusen haben gezeigt, dass die p53 DBK auch *in vivo* essentiell für Apoptose und Tumorsuppression ist (Timofeev et al. 2013). So trägt die DBK zu der Tumorsuppressor-Aktivität von p53 bei und Strategien zur Modulation der Kooperativität und Aktivität von p53 stellen interessante Ansatzpunkte für eine Verbesserung von Krebstherapien über den Tumorsuppressor p53 dar.

2.1.3. Eigenanteil an der Publikation

Für diese Publikation wurden von mir Zellzyklusprofile von HCT 116 Zellen generiert und analysiert, die p53-Wildtyp oder die H1-Helix Kooperativitätsmutanten exprimierten und mit 5-Fluoruracil (5-FU) oder Oxaliplatin behandelt wurden (Abbildung 5). Weiter war ich an den Untersuchungen zur Bedeutung der Serin 46 Phosphorylierung im Kontext der DNA-Bindungskooperativität beteiligt und habe hierfür einen FACS-basierten Apoptose-Assay zur Messung aktiver Caspasen etabliert (Abbildung S4).

2.2. Life or death: p53-induced apoptosis requires DNA binding cooperativity

Katharina Schlereth, Joël P. Charles, Anne C. Bretz, & Thorsten Stiewe
Cell Cycle **9** (20), 4068-4076, 2010.

2.2.1. Einleitung

Jede Zelle eines Organismus ist permanent einer Vielzahl intrinsischer und extrinsischer Gefahren ausgesetzt, die das Genom verändern und schädigen können. Durch die Akkumulation genetischer und epigenetischer Veränderungen können Zellen entstehen, deren Auswachsen zu einem malignen Tumor führen kann, der den gesamten Organismus gefährdet. Der programmierte Zelltod, die Apoptose, ist ein wichtiger Mechanismus zum frühzeitigen Eliminieren solcher Tumor-initiierender Vorläuferzellen. Eine solche Option muss aber gut überlegt sein, da leichte Schäden durch zelleigene Mechanismen repariert werden können und das endgültige Eliminieren von Zellen in der Reduktion von Stammzellen und somit in frühzeitigem Altern des Organismus resultieren kann. In solchen Situationen ist jede Zelle mit der Entscheidung konfrontiert: reparieren und leben oder sterben. Bei dieser wichtigen Entscheidung nimmt der Tumorsuppressor p53 eine bedeutende Rolle ein und veranlasst unter Stress eine gut ausbalancierte Entscheidung über das weitere Zellschicksal (Vogelstein et al. 2000). Daher ist die Frage, wie p53 diese Entscheidung trifft, von beträchtlichem biomedizinischem Interesse. Als sequenzspezifischer DNA-bindender Transkriptionsfaktor reagiert p53 auf das Ausmaß und den Grad an Stress und Schäden und induziert Zielgene, die entweder Zellzyklus-Arrest (Levine & Oren 2009) oder Apoptose einleiten (Aylon & Oren 2007; Murray-Zmijewski et al. 2008). Alle durch p53 transaktivierten Gene haben eine genomische Sequenz gemeinsam, an die p53 mit hoher Spezifität und Affinität bindet. Diese Konsensussequenz besteht aus zwei sich wiederholenden Dekameren mit der Sequenz RRRCWWGYYY (Riley et al. 2008; Funk et al. 1992; El-Deiry, 1992). Es bleibt unklar, wie p53 diese verschiedenen genomischen Bindungsstellen unterscheidet und selektiv aktiviert, um das Zellschicksal in eine bestimmte Richtung zu steuern (Das et al. 2008; Blattner 2008). Bekannt ist, dass p53 durch die Interaktion mit einer

Vielzahl an Partnerproteinen vermittelt an die Promotoren von Zielgenen bindet, wodurch, je nach Kofaktor, entweder Zellzyklus-Arrest oder Apoptose induziert werden. Zusätzlich beeinflussen kovalente posttranslationale Modifikationen von p53 wie z.B. Phosphorylierung, Acetylierung, Methylierung, Ubiquitinierung, Neddylierung oder Sumoylierung die Bindung von p53 an die DNA und modulieren die Entscheidung zwischen Überleben oder Sterben. All dies weist auf eine enorme Komplexität hin, mit der die DNA-Bindungseigenschaften von p53 moduliert und das Zellschicksal unter Stress gesteuert wird.

2.2.2. Zusammenfassung und Diskussion

Um der Hypothese nachzugehen, ob p53 für die Bindung an proapoptotische Zielgene eine stärkere DNA-Bindungskooperativität benötigt, als für die Bindung an antiapoptotische Gene, wurden die genomischen Bindungsprofile der H1-Helixmutante EL mit schwacher p53 DBK und der H1-Helixmutante RE mit starker p53 DBK untersucht. Mit kombinierten Daten aus ChIP-on-chip und ChIP-qPCR Experimenten konnten bioinformatische Analysen etwa 1250 Bindungsstellen für die stark kooperative Mutante RE in Promotorregionen des humanen Genoms bestätigen, von denen etwa 100 Bindungsstellen ebenfalls durch die schwach kooperative Mutante EL gebunden werden (Abb.2B). Untersuchungen der Bindungsstellensequenzen zeigten, dass in der Gruppe, die durch EL und RE gemeinsam gebunden werden, eine vollständige p53 Konsenssequenz mit einer höherer Frequenz auftritt als in der Gruppe, die nur durch RE gebunden wird. Das Motiv einer halben Bindungsstelle trat aber mit gleicher Frequenz in den beiden Gruppen EL/RE und nur-RE Bindungsstellen auf (Abb.2C & 2D). Die Analyse der Bindestellen auf Spacer identifizierte eine höhere Frequenz in den p53 Bindungsstellen, die ausschließlich durch die stark kooperative Mutante gebunden wurden (Abb.2F). Diese Daten zeigen, dass die p53 DBK die Anzahl an Bindungsstellen im Genom erhöht, indem es die Bindung an weniger perfekte Konsensussequenzen ermöglicht, die nur aus einem halben Bindungsmotiv bestehen oder durch Spacer unterbrochen sind.
Dass die Stärke der Kooperativität die Bindung an weniger perfekte p53 Motive bestimmt, wurde experimentell mittels EMSA untersucht. Wurde die zentrale CATG-Sequenz der Konsensussequenz gegen CAAG, CTTG oder CTAG

ausgetauscht oder wurden Spacer eingefügt, so reduzierte sich die Bindung von Wildtyp p53 und den schwach kooperativen Mutanten RR, LR und EL, während die stark kooperativen Mutanten RE und EE+RR weiter eine starke Bindung an alle Motive zeigten und Spacer tolerierten (Abb.3A & 3B). Somit beeinflussen die H1-Helixinteraktionen die Sequenzspezifität des p53 Tetramers, indem eine hohe Kooperativität p53 diese tolerant gegenüber Abweichungen von der Konsensussequenz macht.

Zur Untersuchung des Einflusses der Kooperativität auf die Transaktivierung von Zielgenen wurden Luciferase Assays mit Reporterplasmiden durchgeführt, die die Konsensussequenz des 5´ Transkriptionsverstärkerelements aus dem p21 Promotor oder Varianten mit veränderter CATG-Kernsequenz mit und ohne zusätzlichen Spacern enthielten (Abb.4A). Die Aktivierung dieser Reporter wurde nach der Kotransfektion mit den p53 H1-Helixmutanten in p53 negativen H1299 Zellen gemessen. Der Reporter mit der perfekten p53 Konsensussequenz (CATG) wurde bevorzugt durch Mutanten mit schwacher p53 DBK aktiviert. Dieses Aktivierungsmuster änderte sich aber durch eingefügte Zwischensequenzen, so dass mit einem Spacer aus 14 Basenpaaren die Reporteraktivierung Kooperativitäts-unabhängig wurde und der Reporter durch alle p53 H1-Helixmutanten gleich stark aktiviert wurde (Abb.4B). Mit einer zentralen CTAG-Sequenz wurde der Reporter ebenfalls stärker durch p53 mit schwacher Kooperativität aktiviert, jedoch wurde dieses Muster durch Spacer invertiert, so dass der Reporter durch p53 mit hoher Kooperativität stärker aktiviert wurde. Auffällig war ebenfalls, dass mit den Abweichungen vom perfekten Motiv durch ein zentrales CAAG, CTTG oder CTAG-Motiv in den Bindungsstellen, sowie durch eingefügte Spacer die Maximalaktivierung der Reporter insgesamt abnahm (Abb.4C). Dies zeigt, dass über die Stärke der DNA-Bindungskooperativität nicht nur bestimmt wird, welche Promotorsequenzen durch p53 gebunden, sondern auch welche transaktiviert werden.

Es wurde vielfach postuliert, dass Sequenzen, die nur eine geringe Affinität für die Bindung durch p53 aufweisen und Spacer enthalten, eher in proapototischen und nicht in antiapoptotischen Genen vorkommen. Dies könnte erklären, warum die apoptotische Funktion von p53 mit der Stärke der DBK korreliert. In der Tat bestimmt die Menge an p53 in der Zelle das weitere

Schicksal in dem Sinne, dass eine geringe Menge p53 Zellzyklus-Arrest induziert und hohe p53 Mengen in starken und anhaltenden Stresssituationen Apoptose einleiten (Ko et al. 1996). Für die Untersuchung, ob abweichende p53 Bindungssequenzen in proapoptotischen Genen den Motiven ähneln, die bevorzugt durch stark kooperative p53-Mutanten gebunden werden, wurden 60 p53 Bindungsstellen analysiert, die in 39 experimentell validierten p53 Zielgenen gefunden wurden. Nicht-apoptotische Gene zeigten verstärkt halbe p53 Bindungssequenzen mit zentralem CATG-Kernmotiv. CAAG, CTTG oder CTAG-Sequenzen, sowie Spacer innerhalb der halben Bindungsstellen wurden signifikant vermehrt in apoptotischen Genen gefunden (Abb.5A & B).
Diese Untersuchungen liefern erste experimentelle Hinweise dafür, dass für die Aktivierung des apoptotischen Programms die Bindung von p53 an nicht perfekte Bindungsstellen nötig ist und dies von der kooperativen Bindung des p53 Tetramers an die DNA abhängt. Damit ist die Kooperativität essentiell für die Apoptose- und Tumorsuppressorfunktion von p53. Die Modulation der p53-Interaktionen innerhalb eines Tetramers stellt somit eine neue und vielversprechende Strategie dar, um die p53-vermittelte Entscheidung über das Zellschicksal zu beeinflussen.

2.2.3. Eigenanteil an der Publikation

In dieser Publikation wurde von mir die Frage nach dem Einfluss der DNA-Bindungskooperativität von p53 auf die Transaktivierung von Zielgenen bearbeitet. Dafür habe ich die verschiedenen p53 Bindungsmotive konzipiert und in den Luciferase-Reporter kloniert. Sämtliche Luciferase Assays wurden von mir durchgeführt, ausgewertet und in Abbildung 4 präsentiert.

2.3. Monitoring the dynamics of clonal tumour evolution in vivo using secreted luciferases

Joël P. Charles*, Jeannette Fuchs*, Mirjam Hefter, Jonas B. Vischedyk, Maximilian Kleint, Fotini Vogiatzi, Jonas A. Schäfer, Andrea Nist, Michael Wanzel & Thorsten Stiewe
(* gemeinsame Erstautorenschaft)
Nature Communications **5**, Artikelnummer: 3981, 2014.

3.1. Einleitung

Tumore sind heterogene Zellpopulationen, die aus genetisch individuellen Subklonen bestehen. Die genetischen Veränderungen, die zur Tumorinitiation, Progression, Metastasierung, Therapieresistenz und Rezidiven beitragen, sind interessante Ansatzpunkte für die gezielte Tumortherapie. Bedenkt man die mittlere Mutationsfrequenz von über einer Mutation pro Megabase, ist es schwierig, einzelne genetische Veränderungen zu identifizieren, die vor- oder nachteilhaft für die Selektion bei der klonalen Tumorevolution sind (Alexandrov et al. 2013).

Mit RNA-Interferenz lassen sich Funktionsverlust-Phänotypstudien durchführen, indem gezielt einzelne Gene ausgeschaltet werden und sich so deren Beitrag zur Tumorentstehung aber auch bezüglich anderer Fragestellungen *in vitro* und *in vivo* untersuchen lassen (Hardy et al. 2010). Short hairpin RNAs (shRNAs) können für das Runterregulieren der Expression von Genen verwendet und stabil in das Genom von Zellen integriert werden (Brummelkamp et al. 2002). Mit Hilfe neuartiger Sequenziermethoden (Next Generation Sequencing) von shRNAs konnte bereits die klonale Entwicklung experimentell generierter heterogener Tumorzellpopulationen untersucht werden (Possemato et al. 2011; Zuber et al. 2011). Die klonale Untersuchung mittels Sequenzierung von Tumor-DNA stellt aber letztendlich eine Endpunktanalyse dar, mit der sich nur begrenzt Informationen über die Dynamik der Tumorentstehung gewinnen lassen.

Um die Dynamik der klonalen Evolution in einer zeitaufgelösten Art und Weise zu untersuchen, wurden bisher shRNA-exprimierende Tumorzellen meistens anhand von Fluoreszenzreportersystemen mittels Durchflusszytometrie oder

Fluoreszenzmikroskopie verfolgt. Dabei spiegeln prozentuale Änderungen an fluoreszierenden Zellen innerhalb der Population eines shRNA-exprimierenden Subklons indirekt den Effekt des runterregulierten Gens wieder. Durch die Verwendung eines zweiten Fluoreszenzreporters kann in diesen Versuchen parallel eine nicht-zielgerichtete Kontroll-shRNA mitgeführt werden, um unspezifische shRNA Effekte zu detektieren (Smogorzewska et al. 2007). Mit Fluoreszenzreportern lassen sich in Zellkulturversuchen ebenfalls unterschiedliche shRNA-exprimierende Tumorzellpopulationen kompetitiv verfolgen. *In vivo* funktioniert dies aber nur in Modellen, in denen Tumorzellen für durchflusszytometrische Analysen leicht zugänglich sind, wie es im Fall von Leukämiezellen möglich ist, die im Blutstrom zirkulieren. Weiter sind bildgebende Methoden zur Fluoreszenzquantifizierung zeitaufwendig, benötigen teure Geräte und die wiederholte Anästhesie von Versuchstieren.

Nicht zu vernachlässigen ist die Tatsache, dass es sich bei 90% aller Krebserkrankungen um solide Tumoren handelt. Dies macht es schlichtweg unmöglich, in regelmäßigen Intervallen Tumorbiopsien für Zeitverlaufsstudien zu entnehmen und zu analysieren.

Eine vielversprechende Möglichkeit diese Probleme zu umgehen, scheint die Verwendung von sekretierten Luciferasen als artifizielle Tumormarker. In diesem Zusammenhang wurde eine natürlich sekretierte *Gaussia princeps* Luciferase (GLuc) als hoch sensitiver Reporter für die Lokalisation von Zellen per Biolumineszenz-Bildgebung beschrieben. Zudem können *in vivo* die Zellen über die Konzentrationsmessung der Luciferase-Aktivität im Blut quantitativ erfasst werden (Tannous 2009; Wurdinger et al. 2008; Chung et al. 2009). Es sind weitere sekretierte Luciferasen bekannt, z.B. die *Cypridina noctiluca* Luciferase (CLuc), die eine andere Substratspezifität im Vergleich zu GLuc aufweisen (Nakajima, 2004). Diese beiden sekretierten Luciferasen wurden in diesem Projekt verwendet, um einen dualen Luciferase Assay zu entwickeln, mit dem sich simultan zwei unterschiedlich markierte Zellpopulationen unter kompetitiven Kulturbedingungen beobachten lassen und in Zeitverlaufsstudien die klonale Tumorentwicklung *in vitro* aber auch in soliden Tumoren *in vivo* analysiert werden kann.

3.2. Zusammenfassung und Diskussion

Für die Markierung von Zellen mit GLuc und CLuc wurden die sekretierten Luciferasen in einen lentiviralen Vektor kloniert und damit produzierte Lentiviren für die Markierung der Zellen verwendet. In den Experimenten wurde stets eine zu untersuchende GLuc-markierte Zelllinie mit einer CLuc-markierten Kontrollzelllinie gemischt und für Zellkulturexperimente ausgesät oder für *in vivo* Versuche subkutan oder intravenös in Mäuse injiziert. Die Aktivität beider Luciferasen in Zellkulturüberständen, Mausplasma und Tumorgewebe wurde per Luminometer gemessen. Parallel wurde in isolierter genomischer DNA aus Tumorzellmischungen oder Tumoren mit einem TaqMan Assay die GLuc und CLuc Kopienanzahl bestimmt. Mittels Bioimaging konnten GLuc- und CLuc-sekretierende Tumoren lokalisiert und in Tumoren *ex vivo* quantifiziert werden. Eine Übersicht über die Versuchsdurchführung ist in Abbildung 09 gezeigt.

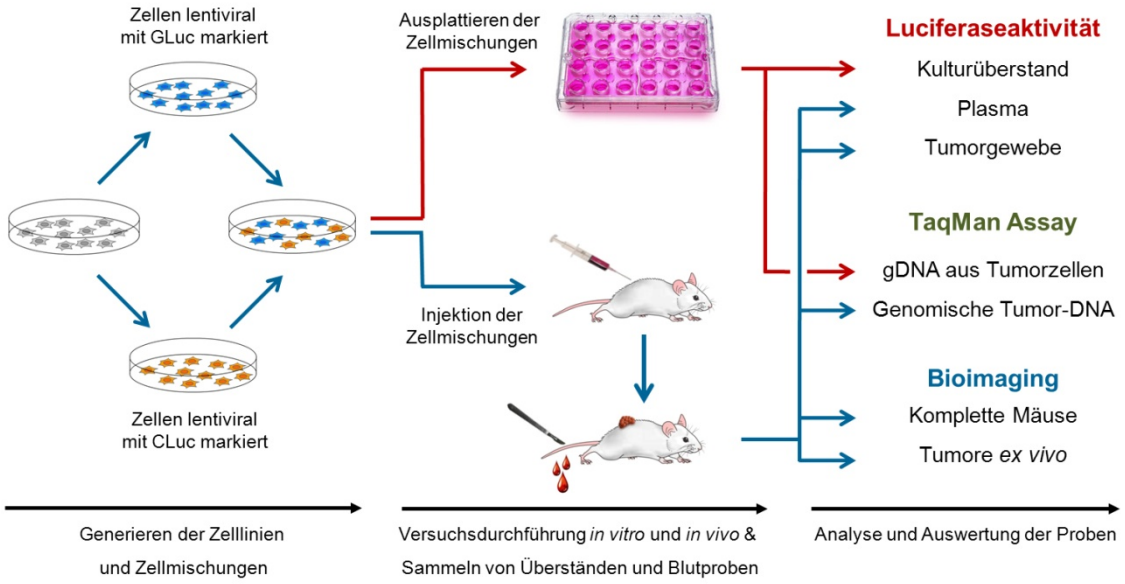

Abb.09: Schematische Durchführung des GLuc/CLuc Assays *in vitro* und *in vivo*

Zellen wurden lentiviral transduziert und mit GLuc oder CLuc markiert. Mischungen von Zellen wurden für Zellkulturexperimente kultiviert oder für Untersuchungen im Tiermodell in Mäuse injiziert. Die Luciferase-Aktivität wurde in Kulturüberständen, Zelllysaten, Mausplasma oder Tumorgewebe gemessen. Genomische DNA aus Zellmischungen oder Tumoren wurde mittels TaqMan Assay analysiert und Mäuse oder Tumore *ex vivo* wurden per Bioimaging untersucht.

Die Eignung der beiden Luciferasen für ein duales Reportersystem wurde in Zellkulturexperimenten untersucht und validiert. Es zeigte sich, dass die Luciferase-Aktivitäten in Kulturüberständen von GLuc und CLuc markierten

Zellen ($GLuc^+$ und $CLuc^+$) mit hoher Spezifität und ohne Kreuzreaktionen zwischen den beiden Substraten Coelenterazin und Vargulin gemessen werden konnten (Abb.1b), die Luciferase-Aktivitäten direkt mit den Zellzahlen korrelierten (Abb.1c) und dass in Zellkulturversuchen mit unterschiedlichen Mischungen an $GLuc^+$ und $CLuc^+$ Zellen (1000:1 bis 1:1000) eine stabile Ratio der beiden Luciferase-Aktivitäten (G/C Ratio) über zwei Wochen gemessen wurde (Abb.1e). Somit konnten auch kleine Zellpopulationen stabil über einen längeren Zeitraum kultiviert und analysiert und ein selektiver Nachteil durch die Expression einer der beiden Luciferasen für die Zellen ausgeschlossen werden. In einem Modell zur Beobachtung der klonalen Evolution im Zellkulturexperiment wurden parentale H460 Lungenkarzinomzellen mit GLuc und ein Cisplatin (CDDP) resistenter Zellklon mit CLuc markiert und in 1:1 Mischung kultiviert. Die G/C Ratio im Kulturüberstand der unbehandelten Zellmischung blieb über den Zeitraum des Experiments unverändert, sank aber in der CDDP behandelten Gruppe um zwei Zehnerpotenzen durch das Verschwinden der sensitiven $GLuc^+$Zellen und das Auswachsen der resistenten $CLuc^+$Zellen (Abb.1f).

Um die beiden sekretierten Luciferasen für *in vivo* Versuche zu etablieren, wurden Mäusen subkutan GLuc oder CLuc-markierte parentale HCT 116 Kolonkarzinomzellen injiziert. Die Luciferase-Aktivitäten im Plasma von Mäusen mit Tumoren waren deutlich über dem Hintergrundsignal und konnten auch dort ohne Kreuzreaktion der beiden Substrate gemessen werden (Abb.2a). Bei der Etablierungsarbeit für bioluminezente Bildgebung von $GLuc^+$ und $CLuc^+$ Tumoren konnten diese unabhängig voneinander und mit hoher Sensitivität visualisiert werden (Abb.2b). Die subkutane Injektion von Mischungen aus $GLuc^+$ und $CLuc^+$ HCT 116 Zellen führte parallel zum Tumorwachstum zu einem linearen und exponentiellen Anstieg der beiden Luciferase-Aktivitäten im Plasma von Mäusen (Abb.2c). Während die Palpation der Tumore erst nach drei Wochen möglich wurde, konnten die Luciferase-Aktivitäten im dualen Luciferase Assay zwei Wochen früher verlässlich gemessen werden und indirekt Auskunft über das Tumorwachstum geben. Dies deutet darauf hin, dass mit diesem dualen Luciferase Assay die Tumorentwicklung zu einem früheren Zeitpunkt des Experiments analysiert werden und ein zu großes Auswachsen der Tumoren und ein damit verbundenes erhöhtes Leiden der Versuchstiere

vermieden werden kann. Die Injektion unterschiedlicher Mischungen von $GLuc^+$ und $CLuc^+$ Zellen (1000:1 bis 1:1000) lieferte auch *in vitro* eine konstante G/C Ratio im Plasma von Versuchstieren mit Tumoren und korrelierte direkt mit der injizierten G/C Zellratio (Abb.2d & 2e). Als Modell für die Beobachtung der klonalen Tumorentwicklung in Mäusen wurden die markierten parentalen sensitiven H460 und CDDP-resistenten H460 Zellen 1:1 subkutan in Mäuse gespritzt und mit CDDP oder Salzlösung (PBS) als Kontrolle behandelt. Während in den PBS-behandelten Kontrollgruppe beide Luciferase-Aktivitäten im Plasma über den Versuchszeitraum parallel anstiegen, sank die GLuc Aktivität der sensitiven Zellen und die G/C Ratio in CDDP behandelten Tieren signifikant im Vergleich zum Signal der resistenten $CLuc^+$ Zellen ab (Abb.2f-h).
Die Etablierungsversuche kennzeichnen GLuc und CLuc als sekretierte Marker mit hoher Sensitivität und ohne Kreuzreaktion, die kompetitiv zur Kontrolle der Proliferation zweier verschiedener Zellpopulationen *in vitro* und *in vivo* eingesetzt werden können.
Um den Einfluss eines einzelnen Gens auf das klonale Tumorwachstum untersuchen zu können, wurden lentivirale Vektoren verwendet, bei denen die Expression von GLuc und CLuc genetisch an die Expression einer shRNA gekoppelt ist (Abb.3a). Zum Testen dieses Systems, wurden shRNAs verwendet, die gegen den Tumorsuppressor p53 gerichtet sind, welcher einen entscheidenden Mediator in der Tumortherapie darstellt (Vousden & Lane 2007). Die Funktionalität zweier unabhängiger shRNAs gegen p53 (shp53) wurde in einem Immunblot bestätigt (Abb.3b). Funktionslose shRNAs wurden an GLuc ($GLuc^+$nsh) und CLuc ($CLuc^+$nsh) gekoppelt und als Kontrollen verwendet. Im Zellkulturexperiment wurden $GLuc^+$shp53 oder $GLuc^+$nsh HCT 116 Zellen mit $CLuc^+$nsh Zellen 1:1 gemischt und diese mit oder ohne Nutlin-3a behandelt. Nutlin-3a inhibiert die Interaktion von Mdm2 mit p53, und führt zur Stabilisierung von p53 (Vassilev et al. 2004). Die G/C Ratios in den Medienüberständen aller unbehandelten Zellmischungen blieb über den Versuchszeitraum konstant, jedoch stieg die G/C Ratio in den Nutlin-3a behandelten Mischungen an, in denen GLuc an eine shp53 gekoppelt war. Die Nutlin-3a Behandlung in Kombination mit dem Herunterregulieren von p53 förderte das Auswachsen der p53 depletierten $GLuc^+$ Zellen im Vergleich zu den $CLuc^+$ Kontrollzellen in den Mischungen (Abb.3c). Unter Kontroll-

bedingungen mit Gabe einer Klucel-Lösung stiegen die Aktivitäten beider Luciferasen im Plasma von Mäusen mit Tumoren parallel über den Versuchszeitraum an. Unter Nutlin-3a Gabe wuchsen die unter diesen Umständen resistenten GLuc^{+}shp53 Zellen weiter, während die sensitiven CLuc^{+}nsh Zellen deutlich langsamer proliferierten, was sich in einem Absinken der CLuc Aktivität zeigte (Abb.3d). Dies wurde weiter durch Ratio-Berechnungen bestätigten (Abb.3e), sowie durch immunhistochemische Analysen von Tumorschnitten (Abb.3f). Aus diesen Ergebnissen kann gefolgert werden, dass mit der gekoppelten Expression von sekretierten Luciferasen und shRNAs der Einfluss eines einzelnen Gens auf die klonale Tumorentwicklung unter Therapie *in vitro* und *in vivo* untersucht werden kann.

Mutationen von p53 können nicht nur zum Verlust der Tumorsuppressor-Aktivität führen, sondern p53 auch mit neuen onkogenen Eigenschaften ausstatten. Dies ist beispielsweise in der Brustkrebszelllinie MDA-MB-231 der Fall, die ein mutiertes p53 exprimiert, welches zur Metastasierung und Kolonisierung der Lunge beiträgt (Adorno et al. 2009). Um den dualen Assay in einem experimentellen Metastasierungsmodell zu untersuchen, wurden die MDA-MB-231 Zellen mit den Konstrukten CLuc-nsh, GLuc-nsh, GLuc-shp53.1 oder GLuc-shp53.5 lentiviral transduziert und Zellmischungen intravenös in Mäuse gespritzt. Bioluminezente Bilderfassung von GLuc in den Lungen der Mäuse zeigte klar eine erhöhte Anreicherung von GLuc^{+}nsh-Kontrollzellen im Vergleich zu p53 depletierten Zellen (Abb.4a). Die Endpunktanalyse von Lungenlysaten zeigte eine reduzierte G/C Ratio für Mischungen mit shRNAs gegen p53 (Abb.4c). Die Untersuchungen der Luciferase-Aktivitäten im Mausplasma wies für die Kontrollgruppe GLuc^{+}nsh/CLuc^{+}nsh eine vergleichbare Kinetik auf, während in den Gruppen mit einer shp53 die GLuc Aktivität signifikant reduziert war (Abb.4f-h), was ebenfalls mit Immunhistochemie in Lungenschnitten bestätigt werden konnte (Abb.4e).

Diese Ergebnisse kennzeichnen den dualen Kompetitionsassay als valides System aus, um Effekte einzelner Gene auf die Tumormetastasierung *in vivo* zu untersuchen.

Essentielle Tumorgene stellen bedeutende Angriffspunkte für die Tumortherapie dar, da das Herunterregulieren solcher Gene die Viabilität der Tumorzelle stark beeinträchtigt. Um solche essentiellen Gene mit sekretierten

Luciferasen als Marker zu untersuchen, wurde ein induzierbares Vektorsystem generiert, in dem erst die Administration von Doxyzyklin (Dox) die Expression von Luciferasen und der shRNA anschaltet (Abb.5a). Zur Validierung des induzierbaren Systems wurden shRNAs gegen den p53-Antagonisten Mdm2 (shMdm2) sowie gegen die Polo-like-Kinase 1 PLK1 (shPLK1) verwendet, deren Herunterregulieren zur Induktion von Zellzyklus-Arrest oder Apoptose führt (de Rozieres et al. 2000; Liu & Erikson 2003). HCT 116 Zellen mit induzierbarer GLuc und CLuc Expression zeigten eine starke und substratspezifische Luciferase-Aktivität im Kulturüberstand nach Behandlung mit Dox gegenüber dem Hintergrundsignal unbehandelter Zellen (Abb.5b). Im Zellkulturexperiment mit 1:1 Mischungen von GLuc$^+$shMdm2 oder GLuc$^+$shPLK1 mit CLuc$^+$nsh HCT 116 Zellen sank die normalisierte G/C Ratio in Abhängigkeit von der Effizienz der shRNAs im Vergleich zu Kontrollmischungen GLuc$^+$nsh/CLuc$^+$nsh über den Versuchszeitraum ab (Abb.5e & 5f). Dieser Effekt war im Falle der shMdm2 p53-abhängig, nicht aber für shPLK1. Zusätzlich war das Herunterregulieren von PLK1 mit steigenden Dox-Konzentrationen titrierbar und resultierte in einem dosisabhängigen Abfall der PLK1 Proteinlevel und der G/C Ratio in Kulturüberständen (Abb.5g-i). Als die Zellmischungen subkutan in Mäuse injiziert wurden, blieben die Luciferase-Aktivitäten ohne Dox zunächst gering. Mit Beginn der Dox-Applikation und der gekoppelte Expression der Luciferasen und der shRNAs, stiegen die Luciferase-Aktivitäten in der Kontrollgruppe mit GLuc$^+$nsh und CLuc$^+$nsh Zellen stark an und kennzeichneten über den weiteren Versuch ein stetes und paralleles Anwachsen beider Zellpopulationen in den Tumoren. Im Plasma der Tiere mit zielgerichteter shRNA stiegen die beiden Luciferase-Aktivitäten nach Anschalten ebenfalls stark an, doch flachte der GLuc-Anstieg in Zellen mit shMdm2 im Vergleich zum CLuc Signal ab und ging in Zellen mit shPLK1 sogar deutlich zurück (Abb.6a). Endpunktanalysen der G/C Ratios in Tumorlysaten zeigten eine reduzierte Ratio in der Gruppe mit GLuc$^+$shMdm2 Zellen im Vergleich zur Mischung aus Kontroll-shRNAs. Dieser Effekt war noch stärker in der Gruppe mit GLuc$^+$shPLK1 Zellen (Abb.6b). Diese Ergebnisse konnten durch die Analyse der G/C Ratio in genomischer Tumor-DNA validiert werden (Abb.6c) und korrelierten auch mit gemessenen Zelllysaten aus diesen Tumoren (Abb.6d). Diese Daten zeigen deutlich eine Negativselektion der

Zellen mit zielgerichteten shRNA gegen Mdm2 und PLK1 in Zellkultur oder in Tumoren. Somit stellt die Dox-induzierbare Variante dieses dualen Luciferase Assays eine sensitive Methode dar, um essentielle Tumorgene *in vitro* und *in vivo* zu untersuchen.

Die Untersuchung und das Identifizieren von Genen, die eine klonale Tumorentwicklung antreiben, sind für das Verständnis solcher Prozesse und zur Entwicklung präventiver Maßnahmen und Therapien von großer Bedeutung. Ebenso ist die Überwachung der Tumorentwicklung und des Tumorwachstums wichtig, um den Krankheitsverlauf zu verfolgen und die Wirkung von Krebstherapien zu analysieren. Im klinischen Alltag erfolgt dies über die Überwachung von tumorspezifischen Tumormarkern im Blut (Sethi et al. 2013; Roses et al. 2009; Teng et al. 2012). Dabei wurde kürzlich gezeigt, dass auch im Blut zirkulierende Tumor-DNA als neuer genetische Biomarker für das Monitoring von Tumorklonen verwendet werden kann (Dawson et al. 2013). Da zirkulierende Tumor-DNA aber nur in geringen Mengen im Plasma vorhanden ist, sind regelmäßige Entnahmen größerer Blutmengen, speziell von kleinen Versuchstieren nicht durchführbar. In der Forschung ist das Monitoring von Tumorentwicklung in Versuchstieren mit minimal-invasiven Methoden über fluoreszierende oder lumineszente Marker an komplizierte, teure und zeitaufwendige Methoden gekoppelt (Weissleder & Ntziachristos 2003). Zudem ist die Quantifizierung dieser Marker durch Absorption des Lichtsignals durch das umliegende Gewebe beeinträchtigt, da die Photonenabsorption von Wellenlänge, Tiefe im Gewebe und Gewebetyp abhängig ist. Daher sind sekretierte Tumormarker, die in kleinen Blutmengen *ex vivo* gemessen werden können, von großem Vorteil. Die Gaussia Luciferase erfüllt dieses Kriterium und wurde als künstlicher Marker für vitale Tumorzellen auch in Kleintiermodellen validiert (Tannous 2009; Wurdinger et al. 2008).

Durch die Verwendung der beiden sekretierten Luciferasen GLuc und CLuc wurde hier ein dualer Luciferase Assay entwickelt und validiert, dessen Luciferasen durch ihre hohe Spezifität und Sensitivität als artifizielle Marker von Tumorzellen verwendet werden können, um zwei unterschiedliche Zellklone im Zellkulturexperiment sowie im Tiermodell kompetitiv zu analysieren. Dabei ist das Sammeln von Proben einfach und erfolgt im Fall von Versuchstieren minimal-invasiv durch Blutentnahme über die Schwanzvene. Da stets ein zu

analysierender Zellklon mit einem Kontrollklon zusammen kompetitiv untersucht wird, kann die Anzahl der Versuchstiere um 50% reduziert werden. Zudem reduziert das parallele Untersuchen zweier Zellklone in einem Tier die experimentelle Varianz, was sicher noch eine weitere Reduktion der Versuchstiere für ausreichend statisch signifikanten Daten erlaubt. Folglich reduziert dieser duale Luciferase Assay im Sinne des 3R-Prinzips von Russel und Burch die benötigte Versuchstierzahl (Russell & Burch 1959). Da das Tumorwachstum mit sekretierten Luciferasen sensitiver als mit anderen Methoden nachweisbar ist, können darüber hinaus die Versuche in für das Tier weniger belastenden Krankheitsstadien durchgeführt werden.
Über das Koppeln von shRNAs an die Luciferaseexpression kann die Funktion eines spezifischen Gens in Bezug auf dessen Beitrag zur Tumorentwicklung, Tumorprogression, Metastasierung und in der Tumortherapie untersucht werden. Somit ist dieser duale Luciferase Assay mit sekretierten Luciferasen als valide Methode für die zeitaufgelöste Untersuchung der Entwicklung solider Tumore geeignet.

3.3. Eigenanteil an der Publikation

Im Rahmen dieses Projekts wurden die beiden Vektorsysteme für die konstitutive und die induzierbare Luciferase-gekoppelt shRNA Expression von mir kloniert. Initiale Experimente zum Testen der Verwendbarkeit der beiden Luciferasen GLuc und CLuc *in vitro*, sowie die Lagerung von Proben, das Messen der Substratspezifität und die Korrelation der Zellzahl mit der Luciferase-Aktivität wurden von mir durchgeführt. Im Rahmen einer von mir betreuten Masterarbeit wurden die Untersuchungen mit den verschiedenen G/C Zellratios gemacht. Die Daten der Zellkulturversuche mit Nutlin-3a und 5-FU wurden im Rahmen einer medizinischen Doktorarbeit erhoben, die ebenfalls durch mich betreut wurde. Sämtliche Arbeiten und Versuche mit dem induzierbaren System zur Untersuchung essentieller Tumorgene wurden von mir etabliert und durchgeführt. Der TaqMan Assay zur Messung der G/C Ratio in genomischer DNA von Tumoren wurde von mir entwickelt und alle gezeigten Versuche dazu vom mir getätigt. Die Abbildungen dieser Publikation wurden von mir zusammengestellt und bearbeitet.

Literaturverzeichnis

Abida WM, Nikolaev A, Zhao W, Zhang W & Gu W (2007): FBXO11 promotes the neddylation of p53 and inhibits its transcriptional activity. *J. Biol. Chem.* 282, 1797–1804.

Adorno M, Cordenonsi M, Montagner M, Dupont S, Wong C, Hann B, Solari A, Bobisse S, Rondina MB, Guzzardo V, Parenti AR, Rosato A, Bicciato S, Balmain A & Piccolo S (2009): A Mutant-p53/Smad Complex Opposes p63 to Empower TGF??-Induced Metastasis. *Cell* 137, 87–98.

Alam J & Cook JL (1990): Reporter genes: Application to the study of mammalian gene transcription. *Anal. Biochem.* 188, 245–254.

Alexandrov LB, Nik-Zainal S, Wedge DC, Aparicio S a JR, Behjati S, Biankin A V, Bignell GR, Bolli N, Borg A, Børresen-Dale A-L, Boyault S, Burkhardt B, Butler AP, Caldas C, Davies HR, Desmedt C, Eils R, Eyfjörd JE, Foekens J a, Greaves M, Hosoda F, Hutter B, Ilicic T, Imbeaud S, Imielinski M, Imielinsk M, Jäger N, Jones DTW, Jones D, Knappskog S, Kool M, Lakhani SR, López-Otín C, Martin S, Munshi NC, Nakamura H, Northcott P a, Pajic M, Papaemmanuil E, Paradiso A, Pearson J V, Puente XS, Raine K, Ramakrishna M, Richardson AL, Richter J, Rosenstiel P, Schlesner M, Schumacher TN, Span PN, Teague JW, Totoki Y, Tutt ANJ, Valdés-Mas R, van Buuren MM, van 't Veer L, Vincent-Salomon A, Waddell N, Yates LR, Zucman-Rossi J, Futreal PA, McDermott U, Lichter P, Meyerson M, Grimmond SM, Siebert R, Campo E, Shibata T, Pfister SM, Campbell PJ & Stratton MR (2013): Signatures of mutational processes in human cancer. *Nature* 500, 415–21.

Ämter S & Länder D (2011): Demografischer Wandel in Deutschland. *Stat. Ämter des Bundes und der Länder*, 1–40.

Ang HC, Joerger AC, Mayer S & Fersht AR (2006): Effects of common cancer mutations on stability and DNA binding of full-length p53 compared with isolated core domains. *J. Biol. Chem.* 281, 21934–21941.

Aylon Y & Oren M (2007): Living with p53, Dying of p53. *Cell* 130, 597–600.

Balagurumoorthy P, Sakamoto H, Lewis MS, Zambrano N, Clore GM, Gronenborn a M, Appella E & Harrington RE (1995): Four p53 DNA-binding domain peptides bind natural p53-response elements and bend the DNA. *PNAS* 92, 8591–8595.

Ballestrem C, Wehrle-Haller B & Imhof B (1998): Actin dynamics in living mammalian cells. *J. Cell Sci.* 1658, 1649–1658.

Beavis AJ & Kalejta RF (1999): Simultaneous analysis of the cyan, yellow and green fluorescent proteins by flow cytometry using single-laser excitation at 458 nm. *Cytometry* 37, 68–73.

Benchimol S (2001): P53-Dependent Pathways of Apoptosis. *Cell Death Differ.* 8, 1049–1051.

Beno I, Rosenthal K, Levitine M, Shaulov L & Haran TE (2011): Sequence-dependent cooperative binding of p53 to DNA targets and its relationship to the structural properties of the DNA targets. *Nucleic Acids Res.* 39, 1919–1932.

Bergamaschi D, Samuels Y, O'Neil NJ, Trigiante G, Crook T, Hsieh J-K, O'Connor DJ, Zhong S, Campargue I, Tomlinson ML, Kuwabara PE & Lu X (2003): iASPP oncoprotein is a key inhibitor of p53 conserved from worm to human. *Nat. Genet.* 33, 162–167.

Bergamaschi D, Samuels Y, Sullivan A, Zvelebil M, Breyssens H, Bisso A, Del Sal G, Syed N, Smith P, Gasco M, Crook T & Lu X (2006): iASPP preferentially binds p53 proline-rich region and modulates apoptotic function of codon 72-polymorphic p53. *Nat. Genet.* 38, 1133–1141.

Berger J, Hauber J, Hauber R, Geiger R & Cullen BR (1988): Secreted placental alkaline phosphatase: a powerful new quantitative indicator of gene expression in eukaryotic cells. *Gene* 66, 1–10.

Bernstein E, Caudy a a, Hammond SM & Hannon GJ (2001): Role for a bidentate ribonuclease in the initiation step of RNA interference. *Nature* 409, 363–366.

Blattner C (2008): Regulation of p53: The next generation. *Cell Cycle* 7, 3149–3153.

Bourdon J-C (2007): P53 and Its Isoforms in Cancer. *Br. J. Cancer* 97, 277–82.

Bourdon J-C, Fernandes K, Murray-Zmijewski F, Liu G, Diot A, Xirodimas DP, Saville MK & Lane DP (2005): P53 Isoforms Can Regulate P53 Transcriptional Activity. *Genes Dev.* 19, 2122–37.

Bronstein I, Fortin J, Stanley PE, Stewart GS & Kricka LJ (1994): Chemiluminescent and bioluminescent reporter gene assays. *Anal. Biochem.* 219, 169–181.

Brummelkamp TR, Bernards R & Agami R (2002): A system for stable expression of short interfering RNAs in mammalian cells. *Science* 296, 550–553.

Budhram-Mahadeo VS, Bowen S, Lee S, Perez-Sanchez C, Ensor E, Morris PJ & Latchman DS (2006): Brn-3b enhances the pro-apoptotic effects of p53 but not its induction of cell cycle arrest by cooperating in trans-activation of bax expression. *Nucleic Acids Res.* 34, 6640–6652.

Bullock a N, Henckel J, DeDecker BS, Johnson CM, Nikolova P V, Proctor MR, Lane DP & Fersht a R (1997): Thermodynamic stability of wild-type and mutant p53 core domain. *PNAS* 94, 14338–14342.

Cairns J (1975): Mutation selection and the natural history of cancer. *Nature* 255, 197–200.

Le Cam L, Linares LK, Paul C, Julien E, Lacroix M, Hatchi E, Triboulet R, Bossis G, Shmueli A, Rodriguez MS, Coux O & Sardet C (2006): E4F1 Is an Atypical Ubiquitin Ligase that Modulates p53 Effector Functions Independently of Degradation. *Cell* 127, 775–788.

Chang C, Simmons D, Martin M & Mora P (1979): Identification and partial characterization of new antigens from simian virus 40-transformed mouse cells. *J. Virol.* 31, 463–471.

Chao C, Herr D, Chun J & Xu Y (2006): Ser18 and 23 phosphorylation is required for p53-dependent apoptosis and tumor suppression. *EMBO J.* 25, 2615–2622.

Che P, Cui L, Kutsch O, Cui L & Li Q (2012): Validating a firefly luciferase-based high-throughput screening assay for antimalarial drug discovery. *Assay Drug Dev. Technol.* 10, 61–8.

Cho Y, Gorina S, Jeffrey PD & Pavletich NP (1994): Crystal structure of a p53 tumor suppressor-DNA complex: understanding tumorigenic mutations. *Science (80-.).* 265, 346–355.

Chung E, Yamashita H, Au P, Tannous B a., Fukumura D & Jain RK (2009): Secreted Gaussia luciferase as a biomarker for monitoring tumor progression and treatment response of systemic metastases. *PLoS One* 4, e8316.

Clore GM, Ernst J, Clubb R, Omichinski JG, Kennedy WM, Sakaguchi K, Appella E & Gronenborn a M (1995): Refined solution structure of the oligomerization domain of the tumour suppressor p53. *Nat. Struct. Biol.* 2, 321–333.

Cormack B, Valdivia R & Falkow S (1996): FACS-optimized mutants of the green fluorescent protein (GFP). *Gene* 173, 33–38.

Courtois S, Caron de Fromentel C & Hainaut P (2004): P53 Protein Variants: Structural and Functional Similarities With P63 and P73 Isoforms. *Oncogene* 23, 631–8.

D'Orazi G, Cecchinelli B, Bruno T, Manni I, Higashimoto Y, Saito S, Gostissa M, Coen S, Marchetti A, Del Sal G, Piaggio G, Fanciulli M, Appella E & Soddu S (2002): Homeodomain-interacting protein kinase-2 phosphorylates p53 at Ser 46 and mediates apoptosis. *Nat. Cell Biol.* 4, 11–19.

Das S, Boswell S a., Aaronson S a. & Lee SW (2008): p53 promoter selection: Choosing between life and death. *Cell Cycle* 7, 154–157.

Das S, Raj L, Zhao B, Kimura Y, Bernstein A, Aaronson S a. & Lee SW (2007): Hzf Determines Cell Survival upon Genotoxic Stress by Modulating p53 Transactivation. *Cell* 130, 624–637.

Dawson S-J, Tsui DWY, Murtaza M, Biggs H, Rueda OM, Chin S-F, Dunning MJ, Gale D, Forshew T, Mahler-Araujo B, Rajan S, Humphray S, Becq J, Halsall D, Wallis M, Bentley D, Caldas C & Rosenfeld N (2013): Analysis of circulating tumor DNA to monitor metastatic breast cancer. *N. Engl. J. Med.* 368, 1199–209.

Dearth LR, Qian H, Wang T, Baroni TE, Zeng J, Chen SW, Yi SY & Brachmann RK (2007): Inactive full-length p53 mutants lacking dominant wild-type p53 inhibition highlight loss of heterozygosity as an important aspect of p53 status in human cancers. *Carcinogenesis* 28, 289–298.

Dehner A, Klein C, Hansen S, Müller L, Buchner J, Schwaiger M & Kessler H (2005): Cooperative binding of p53 to DNA: Regulation by protein-protein interactions through a double salt bridge. *Angew. Chemie - Int. Ed.* 44, 5247–5251.

DeLeo a B, Jay G, Appella E, Dubois GC, Law LW & Old LJ (1979): Detection of a transformation-related antigen in chemically induced sarcomas and other transformed cells of the mouse. *PNAS* 76, 2420–2424.

Dunker a. K, Cortese MS, Romero P, Iakoucheva LM & Uversky VN (2005): Flexible nets: The roles of intrinsic disorder in protein interaction networks. *FEBS J.* 272, 5129–5148.

El-Deiry WS (1998): P21/P53, Cellular Growth Control and Genomic Integrity. *Curr. Top. Microbiol. Immunol.* 227, 121–137.

El-Deiry WS, Kern SE, Pietenpol J a, Kinzler KW & Vogelstein B (1992): Definition of a consensus binding site for p53. *Nat. Genet.* 1, 45–49.

Eliyahu D & Michalovitz D (1989): Wild-type p53 can inhibit oncogene-mediated focus formation. *PNAS* 86, 8763–8767.

Finlay CA, Philip W & Levine AJ (1989): The p53 Proto-Oncogene Can Act as a Suppressor of Transformation. *Cell* 57, 1083–1093.

Foord O & Bhattacharya P (1991): A DNA binding domain is contained in the C-terminus of wild type p53 protein. *Nucleic acids …* 19, 5191–5198.

De Fougerolles A, Vornlocher H-P, Maraganore J & Lieberman J (2007): Interfering with disease: a progress report on siRNA-based therapeutics. *Nat. Rev. Drug Discov.* 6, 443–453.

Freed-Pastor W a. & Prives C (2012): Mutant p53: One name, many proteins. *Genes Dev.* 26, 1268–1286.

Friedler A, Veprintsev DB, Freund SM V, Von Glos KI & Fersht AR (2005): Modulation of binding of DNA to the C-terminal domain of p53 by acetylation. *Structure* 13, 629–636.

Friedler A, Veprintsev DB, Hansson LO & Fersht AR (2003): Kinetic instability of p53 core domain mutants. Implications for rescue by small molecules. *J. Biol. Chem.* 278, 24108–24112.

Funk WD, Pak DT, Karas RH, Wright WE & Shay JW (1992): A transcriptionally active DNA-binding site for human p53 protein complexes. *Mol. Cell. Biol.* 12, 2866–2871.

Gorman C, Moffat L & Howard B (1982): Recombinant genomes which express chloramphenicol acetyltransferase in mammalian cells. *Mol. Cell. Biol.* 2, 1044–1051.

Gould S & Subramani S (1988): Firefly luciferase as a tool in molecular and cell biology. *Anal. Biochem.* 13, 5–13.

Greaves M & Maley CC (2012): Clonal evolution in cancer. *Nature* 481, 306–313.

Green DR & Kroemer G (2009): Cytoplasmic functions of the tumour suppressor p53. *Nature* 458, 1127–30.

Haberland J, Wolf U, Barnes B & Bertz J (2012): Kurzfristige Prognosen der Krebsmortalität in Deutschland bis 2015. *UMID*, 16–23.

Hanahan D & Weinberg R a (2011): Hallmarks of cancer: the next generation. *Cell* 144, 646–74.

Hanahan D & Weinberg RA (2000): The Hallmarks of Cancer. *Cell* 100, 57–70.

Hardy S, Legagneux V, Audic Y & Paillard L (2010): Reverse genetics in eukaryotes. *Biol. Cell* 102, 561–580.

Harms KL & Chen X (2006): The functional domains in p53 family proteins exhibit both common and distinct properties. *Cell Death Differ.* 13, 890–7.

Hart RC, Matthews JC, Hori K & Cormier MJ (1979): Renilla reniformis. *Biochemistry*, 2204–2210.

Hawkins E, Jennens-Clough M & Wood K (1999): Steady-Glo luciferase assay system for high-throughput screening applications. *Promega Notes*, 1–6.

Heim R, Cubitt AB & Tsien RY (1995): Improved Green Fluorescence. *Nature*.

Hermeking H, Lengauer C, Polyak K, He TC, Zhang L, Thiagalingam S, Kinzler KW & Vogelstein B (1997): 14-3-3 sigma is a p53-regulated inhibitor of G2/M progression. *Mol. Cell* 1, 3–11.

Herold S, Wanzel M, Beuger V, Frohme C, Beul D, Hillukkala T, Syvaoja J, Saluz HP, Haenel F & Eilers M (2002): Negative regulation of the mammalian UV response by Myc through association with Miz-1. *Mol. Cell* 10, 509–521.

Hoffman RM (2002): In vivo imaging of metastatic cancer with fluorescent proteins. *Cell Death Differ.* 9, 786–789.

Jacque J-M, Triques K & Stevenson M (2002): Modulation of HIV-1 replication by RNA interference. *Nature* 418, 435–438.

Jansson M, Durant ST, Cho E-C, Sheahan S, Edelmann M, Kessler B & La Thangue NB (2008): Arginine methylation regulates the p53 response. *Nat. Cell Biol.* 10, 1431–1439.

Jeffrey PD, Gorina S & Pavletich NP (1995): Crystal structure of the tetramerization domain of the p53 tumor suppressor at 1.7 angstroms. *Science (80-.).* 267, 1498–1502.

Joerger a C & Fersht a R (2007): Structure-function-rescue: the diverse nature of common p53 cancer mutants. *Oncogene* 26, 2226–42.

Joerger AC & Fersht AR (2008): Structural biology of the tumor suppressor p53. *Annu. Rev. Biochem.* 77, 557–82.

Joerger AC & Fersht AR (2010): The tumor suppressor p53: from structures to drug discovery. *Cold Spring Harb. Perspect. Biol.* 2, a000919.

Kaatsch P, Spix C & Hentschel S (2013): Krebs in Deutschland 2009/2010. *Gesundheitsberichterstattung des Bundes*, 146.

Kastan MB, Zhan Q, el-Deiry WS, Carrier F, Jacks T, Walsh W V, Plunkett BS, Vogelstein B & Fornace a J (1992): A mammalian cell cycle checkpoint pathway utilizing p53 and GADD45 is defective in ataxia-telangiectasia. *Cell* 71, 587–597.

Kitayner M, Rozenberg H, Kessler N, Rabinovich D, Shaulov L, Haran TE & Shakked Z (2006): Structural Basis of DNA Recognition by p53 Tetramers. *Mol. Cell* 22, 741–753.

Kitayner M, Rozenberg H, Rohs R, Suad O, Rabinovich D, Honig B & Shakked Z (2010): Diversity in DNA recognition by p53 revealed by crystal structures with Hoogsteen base pairs. *Nat. Struct. Mol. Biol.* 17, 423–429.

Knights CD, Catania J, Di Giovanni S, Muratoglu S, Perez R, Swartzbeck A, Quong A a., Zhang X, Beerman T, Pestell RG & Avantaggiati ML (2006): Distinct p53 acetylation cassettes differentially influence gene-expression patterns and cell fate. *J. Cell Biol.* 173, 533–544.

Knudson a. G (1971): Mutation and Cancer: Statistical Study of Retinoblastoma. *PNAS* 68, 820–823.

Ko LJ, Jayaraman L & Prives C (1996): Damage Determine the Extent of the Apoptotic Response of Tumor Cells. *Genes Dev.*, 2438–2451.

Kouros-Mehr H, Bechis SK, Slorach EM, Littlepage LE, Egeblad M, Ewald AJ, Pai SY, Ho IC & Werb Z (2008): GATA-3 Links Tumor Differentiation and Dissemination in a Luminal Breast Cancer Model. *Cancer Cell* 13, 141–152.

Kress M, May E, Cassingena R & May P (1979): Simian virus 40-transformed cells express new species of proteins precipitable by anti-simian virus 40 tumor serum. *J. Virol.* 31, 472–483.

Landen CN, Chavez-Reyes A, Bucana C, Schmandt R, Deavers MT, Lopez-Berestein G & Sood AK (2005): Therapeutic EphA2 gene targeting in vivo using neutral liposomal small interfering RNA delivery. *Cancer Res.* 65, 6910–6918.

Lane D & Crawford L (1979): T antigen is bound to a host protein in SY40-transformed cells. *Nature* 278, 261–263.

Lane DP (1992): p53, guardian of the genome. *Nature* 358, 15–16.

Lee W, Harvey TS, Yin Y, Yau P, Litchfield D & Arrowsmith CH (1994): Solution structure of the tetrameric minimum transforming domain of p53. *Nat. Struct. Biol.* 1, 877–890.

Levine a J, Hu W & Feng Z (2006): The P53 pathway: what questions remain to be explored?. *Cell Death Differ.* 13, 1027–1036.

Levine AJ & Oren M (2009): The first 30 years of p53: growing ever more complex. *Nat. Rev. Cancer* 9, 749–758.

Li FP & Fraumeni JF (1969): Soft-tissue sarcomas, breast cancer, and other neoplasms. A familial syndrome?. *Ann. Intern. Med.* 71, 747–752.

Li FP & Fraumeni Joseph F. JR (1969): Soft-Tissue Sarcomas, Breast Cancer, and Other NeoplasmsA Familial Syndrome?. *Ann. Intern. Med.* 71, 747–752.

Lim K & Chae CB (1989): A simple assay for DNA transfection by incubation of the cells in culture dishes with substrates for beta-galactosidase. *Biotechniques* 7, 576–579.

Linzer D & Lane DP (1979): Characterization Tumor Antigen and Uninfected of a 54K Dalton Cellular SV40 Present in SV40-Transformed Cells. *Cell* 17, 43–52.

Liu J, Perumal NB, Oldfield CJ, Su EW, Uversky VN & Dunker a. K (2006): Intrinsic disorder in transcription factors. *Biochemistry* 45, 6873–6888.

Liu L, Scolnick DM, Trievel RC, Zhang HB, Marmorstein R, Halazonetis TD & Berger SL (1999): p53 sites acetylated in vitro by PCAF and p300 are acetylated in vivo in response to DNA damage. *Mol. Cell. Biol.* 19, 1202–1209.

Liu X & Erikson RL (2003): Polo-like kinase (Plk)1 depletion induces apoptosis in cancer cells. *PNAS* 100, 5789–5794.

Lorenz W (1991): Isolation and expression of a cDNA encoding Renilla reniformis luciferase. *PNAS* 88, 4438–4442.

Ludin B & Matus A (1998): GFP illuminates the cytoskeleton. *Trends Cell Biol.* 8, 72–77.

Maguire C a, Bovenberg MS, Crommentuijn MH, Niers JM, Kerami M, Teng J, Sena-Esteves M, Badr CE & Tannous B a (2013): Triple bioluminescence imaging for in vivo monitoring of cellular processes. *Mol. Ther. Nucleic Acids* 2, 1–8.

Malkin D (1993): p53 and the Li-Fraumeni syndrome. *Cancer Genet. Cytogenet.* 66, 83–92.

Mantovani F, Tocco F, Girardini J, Smith P, Gasco M, Lu X, Crook T & Del Sal G (2007): The prolyl isomerase Pin1 orchestrates p53 acetylation and dissociation from the apoptosis inhibitor iASPP. *Nat. Struct. Mol. Biol.* 14, 912–920.

Matthews JC, Hori K & Cormier MJ (1977): Substrate and Substrate Analogue Binding Properties of. *Biochemistry* 16, 5217–5220.

Matz M V, Fradkov a F, Labas Y a, Savitsky a P, Zaraisky a G, Markelov ML & Lukyanov S a (1999): Fluorescent proteins from nonbioluminescent Anthozoa species. *Nat. Biotechnol.* 17, 969–973.

Meacham CE & Morrison SJ (2013): Tumour heterogeneity and cancer cell plasticity. *Nature* 501, 328–37.

Mezzanotte L, Que I, Kaijzel E, Branchini B, Roda A & Löwik C (2011): Sensitive dual color in vivo bioluminescence imaging using a new red codon optimized firefly luciferase and a green click beetle luciferase. *PLoS One* 6, 1–9.

Miao L, Song Z, Jin L, Zhu YM, Wen LP & Wu M (2010): ARF antagonizes the ability of Miz-1 to inhibit p53-mediated transactivation. *Oncogene* 29, 711–722.

Miyashita T & Reed JC (1995): Tumor suppressor p53 is a direct transcriptional activator of the human bax gene. *Cell* 80, 293–299.

Moen I, Jevne C, Wang J, Kalland K-H, Chekenya M, Akslen L a, Sleire L, Enger PO, Reed RK, Oyan AM & Stuhr LE (2012): Gene expression in tumor cells and stroma in dsRed 4T1 tumors in eGFP-expressing mice with and without enhanced oxygenation. *BMC Cancer* 12, 1–10.

Molchadsky A, Rivlin N, Brosh R, Rotter V & Sarig R (2010): P53 is balancing development, differentiation and de-differentiation to assure cancer prevention. *Carcinogenesis* 31, 1501–1508.

Moll UM & Petrenko O (2003): The MDM2-p53 Interaction. *Mol. Cancer Res.* 1, 1001–1008.

Moll UM, Wolff S, Speidel D & Deppert W (2005): Transcription-independent pro-apoptotic functions of p53. *Curr. Opin. Cell Biol.* 17, 631–6.

Müller M, Wilder S, Bannasch D, Israeli D, Lehlbach K, Li-Weber M, Friedman SL, Galle PR, Stremmel W, Oren M & Krammer PH (1998): p53 activates the CD95 (APO-1/Fas) gene in response to DNA damage by anticancer drugs. *J. Exp. Med.* 188, 2033–2045.

Murray-Zmijewski F, Slee E a & Lu X (2008): A complex barcode underlies the heterogeneous response of p53 to stress. *Nat. Rev. Mol. Cell Biol.* 9, 702–712.

Nakajima Y, Kobayashi K, Yamagishi K, Enomoto T & Ohmiya Y (2004): cDNA cloning and characterization of a secreted luciferase from the luminous Japanese ostracod, Cypridina noctiluca. *Biosci. Biotechnol. Biochem.* 68, 565–570.

Nakano K & Vousden KH (2001): PUMA, a novel proapoptotic gene, is induced by p53. *Mol. Cell* 7, 683–694.

Nowell P (1976): The clonal evolution of tumor cell populations. *Science (80-.).* 194, 23–28.

Nykänen A, Haley B & Zamore PD (2001): ATP requirements and small interfering RNA structure in the RNA interference pathway. *Cell* 107, 309–321.

Oda K, Arakawa H, Tanaka T, Matsuda K, Tanikawa C, Mori T, Nishimori H, Tamai K, Tokino T, Nakamura Y & Taya Y (2000): p53AIP1, a potential mediator of p53-dependent apoptosis, and its regulation by Ser-46-phosphorylated p53. *Cell* 102, 849–862.

Okoshi R, Ozaki T, Yamamoto H, Ando K, Koida N, Ono S, Koda T, Kamijo T, Nakagawara A & Kizaki H (2008): Activation of AMP-activated protein kinase induces p53-dependent apoptotic cell death in response to energetic stress. *J. Biol. Chem.* 283, 3979–3987.

Oliner J, Kinzler K & Meltzer P (1992): Amplification of a gene encoding a p53-associated protein in human sarcomas. *Nature* 358, 80–83.

Olivier M, Eeles R, Hollstein M, Khan M a, Harris CC & Hainaut P (2002): The IARC TP53 database: new online mutation analysis and recommendations to users. *Hum. Mutat.* 19, 607–14.

Ormö M, Cubitt AB, Kallio K, Gross LA, Tsien RY & Remington SJ (1996): Crystal structure of the Aequorea victoria green fluorescent protein. *Science* 273, 1392–1395.

Pecot C V, Calin G a, Coleman RL, Lopez-Berestein G & Sood AK (2011): RNA interference in the clinic: challenges and future directions. *Nat. Rev. Cancer* 11, 59–67.

Petitjean A, Mathe E, Kato S, Ishioka C, Tavtigian S V., Hainaut P & Olivier M (2007): Impact of mutant p53 functional properties on TP53 mutation patterns and tumor phenotype: Lessons from recent developments in the IARC TP53 database. *Hum. Mutat.* 28, 622–629.

Possemato R, Marks KM, Shaul YD, Pacold ME, Kim D, Birsoy K, Sethumadhavan S, Woo H-K, Jang HG, Jha AK, Chen WW, Barrett FG, Stransky N, Tsun Z-Y, Cowley GS, Barretina J, Kalaany NY, Hsu PP, Ottina K, Chan AM, Yuan B, Garraway L a, Root DE, Mino-Kenudson M, Brachtel EF, Driggers EM & Sabatini DM (2011): Functional genomics reveal that the serine synthesis pathway is essential in breast cancer. *Nature* 476, 346–350.

Prasher DC, Eckenrode VK, Ward WW, Prendergast FG & Cormier MJ (1992): Aequorea victoria. *Gene* 111, 229–233.

Prendergast FG & Mann KG (1978): Chemical and physical properties of aequorin and the green fluorescent protein isolated from Aequorea forskålea. *Biochemistry* 17, 3448–3453.

Reid BG & Flynn GC (1997): Chromophore Formation in Green Fluorescent Protein Chromophore Formation in Green Fluorescent Protein. *Society* 36, 6786–6791.

Remy S, Tesson L, Usal C, Menoret S, Bonnamain V, Nerriere-Daguin V, Rossignol J, Boyer C, Nguyen TH, Naveilhan P, Lescaudron L & Anegon I (2010): New lines of GFP transgenic rats relevant for regenerative medicine and gene therapy. *Transgenic Res.* 19, 745–763.

Riley T, Sontag E, Chen P & Levine A (2008): Transcriptional control of human p53-regulated genes. *Nat. Rev. Mol. Cell Biol.* 9, 402–412.

Rohaly G, Chemnitz J, Dehde S, Nunez AM, Heukeshoven J, Deppert W & Dornreiter I (2005): A novel human p53 isoform is an essential element of the ATR-intra-S phase checkpoint. *Cell* 122, 21–32.

Roses RE, Paulson EC, Sharma A, Schueller JE, Nisenbaum H, Weinstein S, Fox KR, Zhang PJ & Czerniecki BJ (2009): HER-2/neu overexpression as a predictor for the transition from in situ to invasive breast cancer. *Cancer Epidemiol. Biomarkers Prev.* 18, 1385–1389.

Rossi JJ (2005): RNAi and the P-body connection. *Nat. Cell Biol.* 7, 643–4.

De Rozieres S, Maya R, Oren M & Lozano G (2000): The loss of mdm2 induces p53-mediated apoptosis. *Oncogene* 19, 1691–1697.

Rufini a, Tucci P, Celardo I & Melino G (2013): Senescence and aging: the critical roles of p53. *Oncogene* 32, 5129–43.

Ruiz-Ruiz C, Robledo G, Cano E, Redondo JM & Lopez-Rivas A (2003): Characterization of p53-mediated up-regulation of CD95 gene expression upon genotoxic treatment in human breast tumor cells. *J. Biol. Chem.* 278, 31667–31675.

Russell WMS & Burch RL (1959): The Principles of Humane Experimental Technique by W.M.S. Russell and R.L. Burch.

Saito S, Goodarzi A a., Higashimoto Y, Noda Y, Lees-Miller SP, Appella E & Anderson CW (2002): ATM mediates phosphorylation at multiple p53 sites, including Ser46, in response to ionizing radiation. *J. Biol. Chem.* 277, 12491–12494.

Samuels-Lev Y, O'Connor DJ, Bergamaschi D, Trigiante G, Hsieh JK, Zhong S, Campargue I, Naumovski L, Crook T & Lu X (2001): ASPP proteins specifically stimulate the apoptotic function of p53. *Mol. Cell* 8, 781–794.

Sasaki E, Suemizu H, Shimada A, Hanazawa K, Oiwa R, Kamioka M, Tomioka I, Sotomaru Y, Hirakawa R, Eto T, Shiozawa S, Maeda T, Ito M, Ito R, Kito C, Yagihashi C, Kawai K, Miyoshi H, Tanioka Y, Tamaoki N, Habu S, Okano H & Nomura T (2009): Generation of transgenic non-human primates with germline transmission. *Nature* 459, 523–527.

Schlereth K, Charles JP, Bretz AC & Stiewe T (2010): Life or death: p53-induced apoptosis requires DNA binding cooperativity. *Cell Cycle* 9, 4068–4076.

Sethi S, Ali S, Philip P a. & Sarkar FH (2013): Clinical advances in molecular biomarkers for cancer diagnosis and therapy. *Int. J. Mol. Sci.* 14, 14771–14784.

Sherf B, Navarro S, Hannah R & Wood K (1996): Dual-luciferase reporter assay: an advanced co-reporter technology integrating firefly and Renilla luciferase assays. *Promega Notes* 2.

Shimomura O (2005): The discovery of aequeorin and green fluorescent protein. *J. Microsc.* 217, 3–15.

Shimomura O, Johnson FH & Saiga Y (1962): Extraction, purification and properties of aequorin, a bioluminescent protein from the luminous hydromedusan, Aequorea. *J. Cell. Comp. Physiol.* 59, 223–239.

Siebring-van Olst E, Vermeulen C, de Menezes RX, Howell M, Smit EF & van Beusechem VW (2013): Affordable luciferase reporter assay for cell-based high-throughput screening. *J. Biomol. Screen.* 18, 453–61.

Smogorzewska A, Matsuoka S, Vinciguerra P, McDonald ER, Hurov KE, Luo J, Ballif B a., Gygi SP, Hofmann K, D'Andrea AD & Elledge SJ (2007): Identification of the FANCI Protein, a Monoubiquitinated FANCD2 Paralog Required for DNA Repair. *Cell* 129, 289–301.

Sørensen TU, Gram GJ, Nielsen SD & Hansen JE (1999): Safe sorting of GFP-transduced live cells for subsequent culture using a modified FACS vantage. *Cytometry* 37, 284–290.

Stables (1999): Development of a Dual Glow-Signal Firefly and Renilla Luciferase Assay Reagent for the Analysis of G-Protein coupled Receptor Signalling. *J. Recept. Signal Transduct. Res.* 19, 395–410.

Stiewe T (2007): The p53 family in differentiation and tumorigenesis. *Nat. Rev. Cancer* 7, 165–168.

Sykes SM, Mellert HS, Holbert M a., Li K, Marmorstein R, Lane WS & McMahon SB (2006): Acetylation of the p53 DNA-Binding Domain Regulates Apoptosis Induction. *Mol. Cell* 24, 841–851.

Taira N, Nihira K, Yamaguchi T, Miki Y & Yoshida K (2007): DYRK2 Is Targeted to the Nucleus and Controls p53 via Ser46 Phosphorylation in the Apoptotic Response to DNA Damage. *Mol. Cell* 25, 725–738.

Tang Y, Luo J, Zhang W & Gu W (2006): Tip60-Dependent Acetylation of p53 Modulates the Decision between Cell-Cycle Arrest and Apoptosis. *Mol. Cell* 24, 827–839.

Tannous B a (2009): Gaussia luciferase reporter assay for monitoring biological processes in culture and in vivo. *Nat. Protoc.* 4, 582–591.

Teng HW, Huang YC, Lin JK, Chen WS, Lin TC, Jiang JK, Yen CC, Li AFY, Wang HW, Chang SC, Lan YT, Lin CC, Wang HS & Yang SH (2012): BRAF mutation is a prognostic biomarker for colorectal liver metastasectomy. *J. Surg. Oncol.* 106, 123–129.

Tidow H, Melero R, Mylonas E, Freund SM V, Grossmann JG, Carazo JM, Svergun DI, Valle M & Fersht AR (2007): Quaternary structures of tumor suppressor p53 and a specific p53 DNA complex. *PNAS* 104, 12324–12329.

Timofeev O, Schlereth K, Wanzel M, Braun A, Nieswandt B, Pagenstecher A, Rosenwald A, Elsässer HP & Stiewe T (2013): P53 DNA Binding Cooperativity Is Essential for Apoptosis and Tumor Suppression InVivo. *Cell Rep.* 3, 1512–1525.

Toledo F & Wahl GM (2006): Regulating the p53 pathway: in vitro hypotheses, in vivo veritas. *Nat. Rev. Cancer* 6, 909–923.

Tomasetti M, Andera L, Alleva R, Borghi B, Neuzil J & Procopio A (2006): α-Tocopheryl succinate induces DR4 and DR5 expression by a p53-dependent route: Implication for sensitisation of resistant cancer cells to TRAIL apoptosis. *FEBS Lett.* 580, 1925–1931.

Vassilev L, Vu B, Graves B & Carvajal D (2004): In vivo activation of the p53 pathway by small-molecule antagonists of MDM2. *Science (80-.).* 303, 844–849.

Vogelstein B, Lane D & Levine a J (2000): Surfing the p53 network. *Nature* 408, 307–310.

Vousden KH & Lane DP (2007): P53 in Health and Disease. *Nat. Rev. Mol. Cell Biol.* 8, 275–283.

Vousden KH & Lu X (2002): Live or let die: the cell's response to p53. *Nat. Rev. Cancer* 2, 594–604.

Vousden KH & Prives C (2009): Blinded by the Light: The Growing Complexity of p53. *Cell* 137, 413–431.

De Vries A, Flores ER, Miranda B, Hsieh H-M, van Oostrom CTM, Sage J & Jacks T (2002): Targeted point mutations of p53 lead to dominant-negative inhibition of wild-type p53 function. *PNAS* 99, 2948–53.

Waldman T, Kinzler KW & Vogelstein B (1995): p21 Is Necessary for the p53-mediated G 1 Arrest in Human Cancer Cells. *Cancer Res.* 55, 5187–5190.

Wang B, Xiao Z & Ren EC (2009): Redefining the p53 response element. *PNAS* 106, 14373–14378.

Wang S & El-Deiry WS (2003): Requirement of p53 targets in chemosensitization of colonic carcinoma to death ligand therapy. *PNAS* 100, 15095–100.

Weinberg R (1991): Tumor suppressor genes. *Science (80-.).* 254, 1138–1146.

Weinberg RL, Freund SM V, Veprintsev DB, Bycroft M & Fersht AR (2004): Regulation of DNA binding of p53 by its C-terminal domain. *J. Mol. Biol.* 342, 801–11.

Weinberg RL, Veprintsev DB, Bycroft M & Fersht AR (2005): Comparative binding of p53 to its promoter and DNA recognition elements. *J. Mol. Biol.* 348, 589–596.

Weinberg RL, Veprintsev DB & Fersht AR (2004): Cooperative binding of tetrameric p53 to DNA. *J. Mol. Biol.* 341, 1145–1159.

Weissleder R & Ntziachristos V (2003): Shedding light onto live molecular targets. *Nat. Med.* 9, 123–128.

Wongsrikeao P, Saenz D, Rinkoski T, Otoi T & Poeschla E (2011): Antiviral restriction factor transgenesis in the domestic cat. *Nat. Methods* 8, 853–859.

Wood K (1998): The chemistry of bioluminescent reporter assays. *Promega Notes*, 1–7.

Wood K V. (1995): THE CHEMICAL MECHANISM and EVOLUTIONARY DEVELOPMENT OF BEETLE BIOLUMINESCENCE. *Photochem. Photobiol.* 62, 662–673.

World Health Organisation (2007): *Prevention. (Cancer control : knowledge into action : WHO guide for effective programmes ; module 2.) 1.Neoplasms – prevention and control. 2.Health planning. 3.National health programs – organization and administration. 4.Health policy. 5.Guidelines. I.W*,

Wurdinger T, Badr C, Pike L, de Kleine R, Weissleder R, Breakefield XO & Tannous B a (2008): A secreted luciferase for ex vivo monitoring of in vivo processes. *Nat. Methods* 5, 171–173.

Yang F, Moss LG & George P (1996): The molecular structure of green fluorescent protein. *Nat. Biotechnol.* 14, 1246–1251.

Yi R, Qin Y, Macara IG & Cullen BR (2003): Exportin-5 mediates the nuclear export of pre-microRNAs and short hairpin RNAs. *Genes Dev.* 17, 3011–3016.

Yoon K, Thiede M a & Rodan G a (1988): Alkaline phosphatase as a reporter enzyme. *Gene* 66, 11–17.

Zuber J, Shi J, Wang E, Rappaport AR, Herrmann H, Sison E a., Magoon D, Qi J, Blatt K, Wunderlich M, Taylor MJ, Johns C, Chicas A, Mulloy JC, Kogan SC, Brown P, Valent P, Bradner JE, Lowe SW & Vakoc CR (2011): RNAi screen identifies Brd4 as a therapeutic target in acute myeloid leukaemia. *Nature* 478, 524–528.

Anhänge

Abkürzungsverzeichnis

5-FU	5-Fluoruracil
A	Adenin
Abb.	Abbildung
BS	Bindungsstellen
C	Cytosin
CAT	Chloramphenicol Acetyltransferase
CDDP	Cisplatin bzw. Cis-Diammindichloroplatin (II)
CLuc	Cypridina Luciferase
CTD	C-Terminale Domäne
DBD	DNA Bindungsdomäne
DBK	DNA-Bindungskooperativität
DNA	Desoxyribonukleinsäure
Dox	Doxyzyklin
EMSA	Electrophoretic Mobility Shift Assay
et.al	und andere
FLuc	Firefly Luciferase
G	Guanin
GFP	Grün fluoreszierendes Protein
GLuc	Gaussia Luciferase
IF	Interaktionsfläche
kDa	Kilodalton (Atomare Masseneinheit)
Mdm2	Mouse double minute 2
NMR	Nuclear Magnetic Resonance (deutsch: Kernspinresonanz)
p53	Tumorsuppressor p53
PBS	Phosphate buffered saline (deutsch: Phosphatgepufferte Salzlösung
PLK1	Polo-like-Kinase1
RLuc	Renilla Luciferase
RNA	Ribonukleinsäure
RNAi	RNA Interferenz
shRNA	Small hairpin RNA
T	Thymin
TAD	Transaktivierungsdomäne
u.a.	unter anderem
z.B.	zum Beispiel

Tabellarischer Lebenslauf

Entfernt für den finalen Druck

Verzeichnis der akademischen Lehrer

Meine akademischen Lehrer an der Johannes Gutenberg Universität in Mainz waren die Damen und Herren:

Claßen-Bockhoff, Dräger, Eisenbeis, Hankeln, Kamp, Kardereit, König, Kröger, Luhmann, Markl, Müller-Klieser, Paulsen, Rothe, Schmidt, Unden, Walenta, Wegener, Wernicke, Wolfrum, Zerbe

Mein akademischer Lehrer an der Philipps-Universität in Marburg war Prof. Dr. Thorsten Stiewe

Danksagung

Mein größter Dank geht an Prof. Dr. Thorsten Stiewe, der mich als Doktorand in seiner Arbeitsgruppe aufgenommen hat und mir die Arbeit an interessanten Projekten ermöglichte und anvertraute. Vielen Dank für alles, was ich in dieser Zeit lernen durfte, die gute Betreuung und Hilfe sowie die umfassende Förderung.

Ich bedanke mich herzlich bei Fotini Vogiatzi für das kompetente Korrekturlesen meiner Arbeit und ihre kritischen und konstruktiven Verbesserungsvorschläge.

Meine Promotion wäre ohne die Arbeit und Hilfe einiger Kolleginnen und Kollegen nicht möglich gewesen. Daher bedanke ich mich bei Dr. Katharina Schlereth für ihre Arbeiten zur p53 DNA-Bindungskooperativität. Jeannette Fuchs möchte ich für die gemeinsame Etablierung des GLuc/CLuc-Assays danken sowie für die Einführung in tierexperimentelle Arbeiten. Mirjam Hefter und Maximilian Kleint, die ich beide betreuen durfte, danke ich ebenfalls für ihre Mitarbeit und ihren Beitrag zur Etablierung des GLuc/CLuc-Assays.

Vielen lieben Dank all meinen Kolleginnen und Kollegen, die in der Zeit meiner Promotion in der AG Stiewe tätig waren und mir eine besonders ereignisreiche und lehrreiche Zeit in Marburg beschert haben. Vieles wird für mich unvergessen bleiben. Besonderer Dank geht dabei an Björn Geißert, dessen Freundschaft mir stets eine große Stütze im Laboralltag war.

Besonders herzlich möchte ich mich bei meinen Eltern und meiner Familie bedanken. Ohne eure Unterstützung und euren Glauben an mich, wäre ich heute nicht an dieser Stelle. Ich verdanke euch alles.

Ehrenwörtliche Erklärung

Entfernt für den finalen Druck

Anhang mit den Publikationen 1-3

Molecular Cell
Article

DNA Binding Cooperativity of p53 Modulates the Decision between Cell-Cycle Arrest and Apoptosis

Katharina Schlereth,[1,6] Rasa Beinoraviciute-Kellner,[1,2,6] Marie K. Zeitlinger,[1] Anne C. Bretz,[1] Markus Sauer,[1] Joël P. Charles,[1] Fotini Vogiatzi,[1] Ellen Leich,[3] Birgit Samans,[4] Martin Eilers,[5] Caroline Kisker,[2] Andreas Rosenwald,[3] and Thorsten Stiewe[1,*]

[1]Department of Hematology, Oncology, and Immunology, Molecular Oncology, Philipps-University, 35032 Marburg, Germany
[2]Rudolf Virchow Center, DFG Research Center for Experimental Biomedicine, University of Würzburg, 97078 Würzburg, Germany
[3]Institute of Pathology, University of Würzburg, 97080 Würzburg, Germany
[4]Institute of Molecular Biology and Tumor Research, Philipps-University, 35032 Marburg, Germany
[5]Theodor Boveri Institute, Physiological Chemistry, University of Würzburg, 97074 Würzburg, Germany
[6]These authors contributed equally to this work
*Correspondence: thorsten.stiewe@staff.uni-marburg.de
DOI 10.1016/j.molcel.2010.02.037

SUMMARY

p53 limits the proliferation of precancerous cells by inducing cell-cycle arrest or apoptosis. How the decision between survival and death is made at the level of p53 binding to target promoters remains unclear. Using cancer cell lines, we show that the cooperative nature of DNA binding extends the binding spectrum of p53 to degenerate response elements in proapoptotic genes. Mutational inactivation of cooperativity therefore does not compromise the cell-cycle arrest response but strongly reduces binding of p53 to multiple proapoptotic gene promoters (*BAX*, *PUMA*, *NOXA*, *CASP1*). Vice versa, engineered mutants with increased cooperativity show enhanced binding to proapoptotic genes, which shifts the cellular response to cell death. Furthermore, the cooperativity of DNA binding determines the extent of apoptosis in response to DNA damage. Because mutations, which impair cooperativity, are genetically linked to cancer susceptibility in patients, DNA binding cooperativity contributes to p53's tumor suppressor activity.

INTRODUCTION

The tumor suppressor p53 is known as the "guardian of the genome" owing to its central role in an intricate signaling network controlling life and death (Vousden and Lane, 2007). p53 is activated in response to various types of cellular stress, including DNA damage and oncogene activation. As a transcription factor, p53 initiates transcriptional programs that ultimately arrest proliferation and prevent the generation of genetically altered cells. Not surprisingly, defects in the p53 network lead to tumor development and are encountered in the majority of cancer patients either as missense mutations in p53 itself or, alternatively, in genes encoding other components of the p53 network (Stiewe, 2007; Vousden and Lane, 2007).

p53 possesses the classical features of a sequence-specific transcriptional activator, including a transactivation domain at the N terminus, a DNA-binding "core" domain in the center of the protein, and a tetramerization domain at the C terminus. p53 binds as a tetramer in a sequence-specific manner to DNA-binding sites consisting of two decameric motifs or half-sites of the general form RRRCWWGYYY (R = A, G; W = A, T; Y = C, T) separated by 0–14 base pairs (Riley et al., 2008). Depending on the set of target genes activated under a given condition, the outcome of p53 activation is either a transient cell-cycle arrest enabling damage repair, an irreversible block of proliferation by senescence or differentiation, or cell death via apoptosis (Stiewe, 2007; Vousden and Lu, 2002). Whereas cell-cycle arrest depends on the ability of p53 to induce the transcription of target genes such as the CDK inhibitor $p21^{CDKN1A}$, apoptosis depends on the induction of a distinct class of target genes including *BAX*, *PMAIP1* (*NOXA*), *BBC3* (*PUMA*), *P53AIP1*, *FAS*, *FDXR*, and *TP53I3* (*PIG3*). Together with a direct nonnuclear proapoptotic function of p53 in the cytoplasm and mitochondria, these genes promote mitochondrial outer-membrane permeabilization and cytochrome *c* release, leading to the activation of caspases and apoptotic cell death (Chipuk and Green, 2006). The decision between cell-cycle arrest and apoptosis as the two main biological responses initiated by p53 depends strongly on the cellular context and reflects both the concentration and the posttranslational modification state of p53 (Vousden and Lu, 2002). However, the molecular details of how p53 distinguishes between the genes of the different transcriptional programs still remain unclear.

Recent studies combining small-angle X-ray scattering, electron microscopy, and NMR data of full-length p53 with previously solved solution and crystal structures of isolated p53 fragments demonstrated that the intact p53 protein in complex with DNA forms a tetramer that can be described as a symmetric dimer of dimers (Cho et al., 1994; Kitayner et al., 2006; Tidow et al.,

2007). Isolated p53 core domains, although mostly monomeric in solution, bind to DNA as tetramers, indicating cooperative binding supported by protein-protein interactions (Weinberg et al., 2004). The crystal structure of the p53 core domain tetramer reveals two types of protein-protein interfaces: a symmetrical intradimer and a translational interdimer interface (Kitayner et al., 2006). Based on both biochemical and structural studies, the symmetrical interface within each dimer involves the reciprocal interaction of oppositely charged residues (Glu180, Arg181) in helix H1. These residues are evolutionarily conserved in p53 but absent in the p53 family members p63 and p73 (Figures 1A and 1B; see Table S1 available online) (Dehner et al., 2005; Kitayner et al., 2006; Klein et al., 2001; Veprintsev et al., 2006). This interaction between two p53 monomers was found to be crucial for the cooperative nature of DNA binding by isolated recombinant p53 core domains (Dehner et al., 2005). Similarly, in an alternative structure postulated by molecular dynamics simulations on the basis of the asymmetric dimer of the crystal p53-trimer DNA complex (Cho et al., 1994), the four H1 helices form a bundle which is stabilized by circular E180-R181 salt bridges (Ma and Levine, 2007). On the basis of this biochemical and structural evidence for cooperative DNA binding by p53, we here examine the role of DNA binding cooperativity for p53's tumor suppressor activity.

RESULTS

Role of H1 Helix Interactions for In Vitro DNA Binding

To investigate the role of DNA binding cooperativity for p53 function, we introduced modest charge-neutralizing (E180→L "LR" and R181→L "EL") and more severe charge-inverting (E180→R "RR" and R181→E "EE") mutations into the H1 helix of the full-length p53 molecule (Figure 1C). The short names denote the amino acid sequence at positions 180 and 181 in the mutant proteins, for example "ER" for E180,R181 in the wild-type. These point mutations have previously been demonstrated to compromise p53 interactions and thus DNA binding cooperativity in the context of the isolated core domains in vitro (Dehner et al., 2005). To assure that functional defects are truly due to defective core domain interactions and are not caused by structural misfolding of the core domain or disturbed interaction with other cellular proteins, we also introduced the two most severe mutations E180R and R181E together into a single p53 molecule (double mutant E180,R181→R180,E181 "RE") and used the two complementing mutants "EE" and "RR" in functional rescue studies. All H1 helix but not tetramerization domain mutants formed tetramers under native, nondenaturing conditions, indicating that core domain interactions via the H1 helix are not a prerequisite for tetramerization (Figure 1D).

Next, we investigated the impact of H1 helix mutations on DNA binding in the context of the full-length tetrameric p53 molecule by electrophoretic mobility shift assays (EMSAs). Whereas the charge-neutralizing mutations EL and LR had a weak inhibitory effect, the charge-inverting mutations strongly decreased DNA binding to almost undetectable levels in the case of EE (Figure 1E). Importantly, the double mutation RE and the combination of EE and RR restored DNA binding to levels that even exceeded the binding of the wild-type protein. The mutant EE, which was unable to bind DNA on its own, was efficiently recruited into a DNA-bound complex by the complementing mutant RR, as shown by supershift analysis (Figure 1F). To distinguish a role in inter- and intradimer interactions, we further tested the H1 helix mutations in the context of the dimeric L344A tetramerization domain mutant. L344A formed both dimers and tetramers on full sites (20-mers) but only dimers on half-sites (decamers) (Figure 1G). EE and RR in the context of the L344A backbone were both unable to bind half-site DNA. In combination, however, they efficiently bound single half-sites, indicating that these two proteins can complement each other to form a strongly DNA-bound heterodimer, thus proving a role for helix H1 in intradimer versus interdimer interactions. In addition, time-resolved dissociation EMSAs confirmed decreased DNA-protein complex stabilities for the interaction-impaired mutants LR, RR, and EL and increased stabilities for the double mutant RE and the combination of EE+RR (Figures 1H and 1I). The H1 helix therefore not only mediates cooperative DNA binding of isolated p53 core domains but is also crucial in the context of the tetrameric full-length p53 molecule. This allowed us to use H1 helix mutants to investigate the role of DNA binding cooperativity for p53's tumor suppressor activity.

DNA Binding Cooperativity Modulates the Decision between Cell-Cycle Arrest and Apoptosis

Initial data from the H1 helix mutants indicated that p53's antiproliferative activity directly correlated with the interaction strength and thus DNA binding cooperativity (Figures S1A–S1D). p53 exerts its antiproliferative activity by either arresting the cell cycle or inducing rapid apoptotic cell death. We therefore investigated the ability of the H1 helix mutants to induce cell-cycle arrest and apoptosis in p53 null cell lines using adenoviruses expressing the p53 mutants together with GFP as a marker. All p53 proteins were expressed at equal levels and localized predominantly to the nucleus (data not shown). Compared to the GFP-only control, wild-type p53 expression induced both cell-cycle arrest and cell death, as seen by the reduced number of GFP-positive cells and the increased number of condensed apoptotic cells (Figure 2A). Interestingly, the interaction-impaired mutants EE, RR, EL, and LR also showed reduced numbers of GFP-positive cells, indicative of cell-cycle arrest, but failed to show apoptotic cells. This is consistent with a previous study in which the EL mutation was identified as a partial loss-of-function mutation with a selective apoptosis defect (Ludwig et al., 1996). In contrast, the cell cultures infected with the hyperactive mutant RE or the combination EE+RR displayed strongly elevated numbers of apoptotic cells, suggesting that the core domain interaction strength influences the outcome of p53 activation: weak interactions result in selective cell-cycle arrest and strong interactions in preferential induction of apoptosis.

Detailed cell-cycle profiling by flow cytometry confirmed that the interaction-impaired mutants EE, RR, EL, and LR induced cell-cycle arrest in the absence of apoptosis (Figure 2B; Figure S1E). Whereas RR, EL, and LR evoked an increase in both the G1 and G2/M populations, the EE mutant caused a selective increase in G1 that was sufficient to prevent accumulation in G2/M following nocodazole treatment (Figure 2C). In

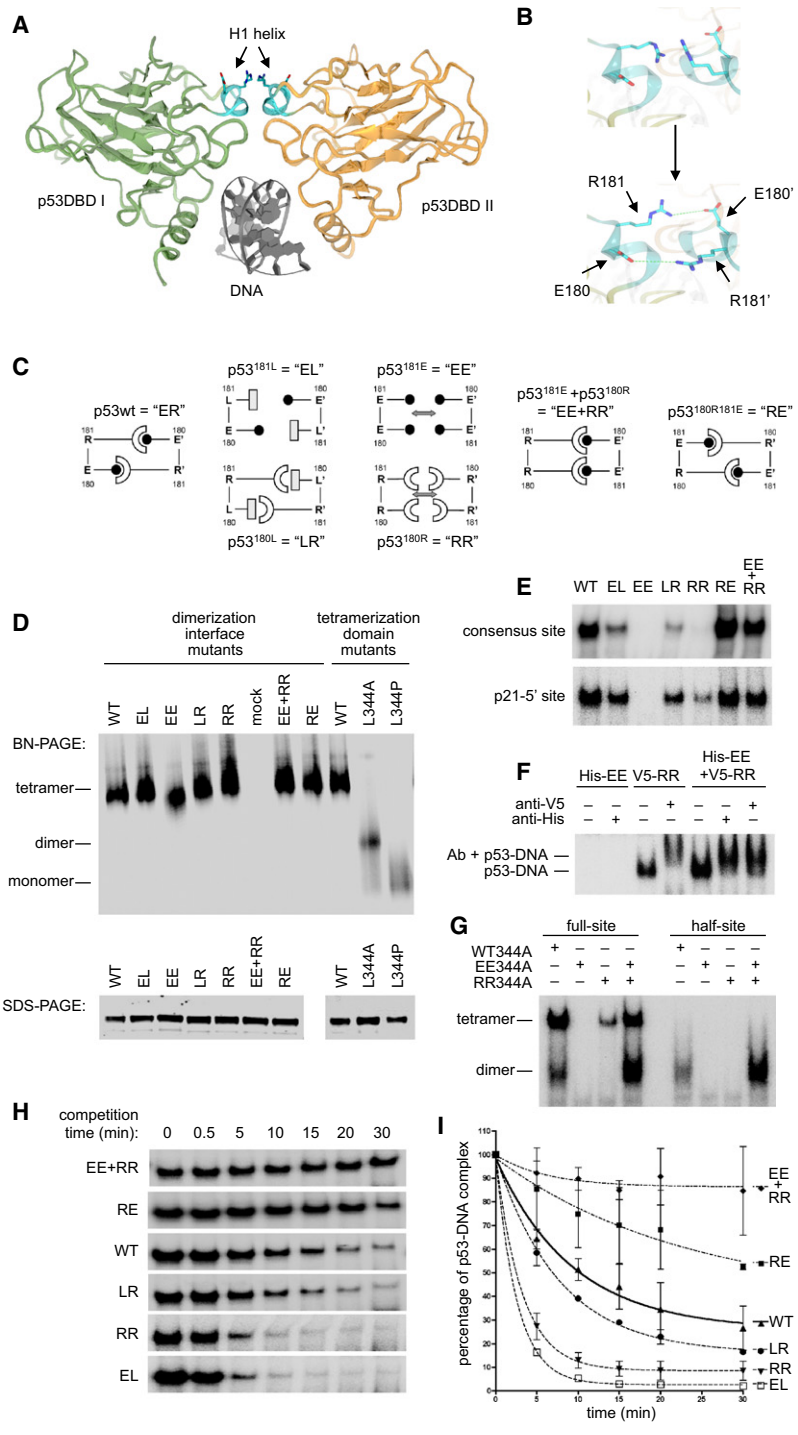

Figure 1. p53 H1 Helix Interactions Influence DNA Binding of Full-Length p53 In Vitro

(A) Structure of two p53 DNA-binding "core" domains (p53DBD I and II) in contact with a consensus binding sequence (Protein Data Bank ID code 2ADY) (Kitayner et al., 2006). The intradimer protein-protein interface involves the short H1 helix (cyan).

(B) View of the dimerization interface. Depicted is the conformation in the crystal (top) and a different Arg rotamer highlighting the stabilization of the dimerization interface by a double intermolecular salt bridge between residues E180 and R181 of each monomer (bottom).

(C) Schematic representation of the dimerization patterns of wild-type p53 "ER" and the H1 helix mutants in this study.

(D) Tetramerization of H1 helix mutants. In vitro translated ^{35}S-labeled p53 full-length proteins containing the indicated H1 helix mutations (EE, EL, RR, LR, RE, and EE+RR) or tetramerization domain mutations (L344A and L344P) were separated by blue native polyacrylamide gel electrophoresis (top panel) or SDS-PAGE (immunoblot, bottom panel).

(E) EMSA of in vitro translated p53 full-length proteins and ^{32}P-labeled dsDNA containing the p53 consensus response element or the 5′ binding site in the p21 promoter.

(F) EMSA of His-tagged EE and V5-tagged RR proteins with the ^{32}P-labeled consensus dsDNA. Anti-His and anti-V5 antibodies were added to the reaction mixture for supershift analysis.

(G) The dimeric L344A tetramerization domain mutant p53 protein was generated without (WT344A) and with H1 helix mutations (EE344A and RR344A) by in vitro translation. EMSA with ^{32}P-labeled dsDNA containing a full consensus response element (20-mer, "full-site") or a decameric "half-site."

(H and I) EMSA showing dissociation of the indicated p53 proteins from ^{32}P-labeled consensus dsDNA upon addition of a 100-fold excess of the same oligonucleotide lacking ^{32}P. Shown is the mean ± SD of two independent experiments.

stark contrast, the hyperactive RE mutant and the combination of the two apoptosis-deficient mutants EE and RR induced earlier caspase activation and higher levels of cell death than wild-type p53 (Figures 2A, 2B, 2D, and 2E). The functional apoptosis rescue was not restricted to the combination EE+RR, but was always observed when an E180 mutant (LR, RR) was combined with an R181 mutant (EL, EE), indicating that H1 helix interactions determine the apoptotic potential (Figure 2F). Furthermore, all H1 helix mutants function in a dominant-negative manner to inhibit apoptosis when coexpressed with wild-type p53 (Figure 2F). Acquisition of an H1 helix mutation in one p53 allele during tumor development could therefore compromise the activity of the remaining wild-type allele in a similar way as it has been reported for other classes of p53 mutations. Combined, these experiments demonstrate that strong H1 helix interactions are essential for apoptosis induction and that changes in interaction strength can alter the decision between cell-cycle arrest and apoptosis.

H1 Helix Interactions Are Essential for Conformational Activation of Bax and Bak

Apoptotic functions of p53 include a nuclear role as a transcription factor that activates expression of target genes and

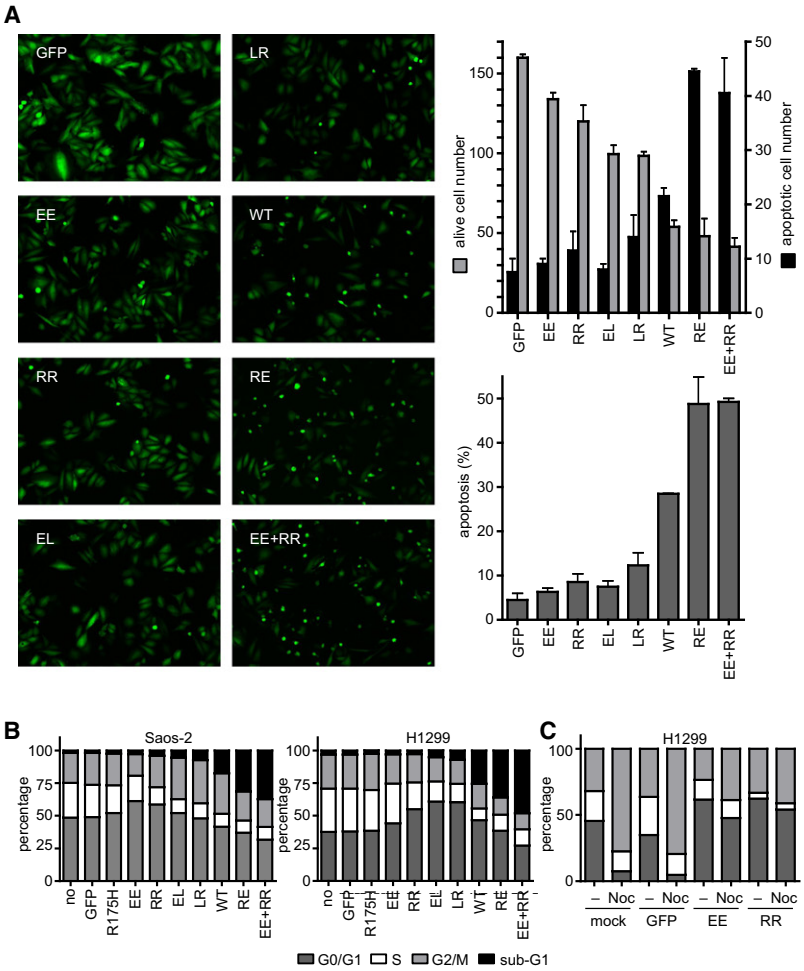

Figure 2. p53 DNA Binding Cooperativity Correlates with Apoptosis Induction

(A) Morphology of Saos-2 cells 30 hr following infection with adenoviruses coexpressing GFP and the indicated p53 proteins. Top right: number alive and apoptotic cells per field of view; lower right: percentage of apoptotic cells (mean ± SD).

(B and C) Cell-cycle profiles of Saos-2 cells 24 hr or H1299 cells 38 hr following infection with adenoviruses expressing the indicated p53 proteins.

(C) The cells were treated as indicated with nocodazole (40 ng/ml) for the last 12 hr to stimulate accumulation of proliferating cells in G2/M.

(D) Caspase-Glo 3/7 activity assay 24 hr following expression of p53 in Saos-2 cells. RLU, relative light units. Results are presented as mean ± SD.

(E) Immunodetection of the caspase-3 cleavage product in Saos-2 cells.

(F) Functional rescue by complementation of apoptosis-defective H1 helix mutants. Saos-2 cells were coinfected with equal amounts of two adenoviruses and apoptosis was quantified by caspase-3/7 activity measurement after 24 hr. The color intensity linearly correlates with caspase-3/7 activity.

(G) Saos-2 cells were infected for 9 hr with adenoviruses expressing the indicated p53 proteins. Mitochondria were purified by subcellular fractionation. Fifteen micrograms of mitochondrial (M), cytosolic (C), and total cellular (L) protein was separated by SDS-PAGE and subjected to immunoblotting.

(H) Total cellular lysates prepared 24 hr after infection as in (G) were immunoprecipitated with antibodies specific for Bak and Bax in their activated conformation. Precipitated proteins and total cellular lysates were separated by SDS-PAGE and subjected to immunoblotting. See also Figure S1.

a nonnuclear role in the cytoplasm and mitochondria involving p53 translocation to the outer mitochondrial membrane (Chipuk and Green, 2006). Despite their apoptosis defect, EE and EL were detected in purified mitochondrial fractions at similar levels as the wild-type protein and the strongly apoptotic RE mutant (Figure 2G). The absence of proliferating cell nuclear antigen (PCNA) in the mitochondrial extracts excluded nuclear contamination as a source of p53 in these fractions.

The endpoint of p53's mitochondrial action is the activation of the BH123 proteins Bax and Bak to allow mitochondrial outer-membrane permeabilization and release of apoptogenic factors triggering the activation of caspases and the apoptotic demise of the cell. The activation of Bax and Bak requires a conformational change that results in the exposure of the hidden BH3 domain as a prerequisite for self-oligomerization. To detect conformational activation, Bax and Bak proteins were immunoprecipitated from mutant p53-transfected Saos-2 cells with conformation-specific antibodies (Figure 2H). Substantial Bax and Bak activation was only induced by wild-type p53 and RE. We concluded that H1 helix mutations do not affect mitochondrial localization but rather the subsequent steps involved in Bax and Bak activation which were recently linked to p53's nuclear function (Chipuk and Green, 2006). In the following, we therefore focused our

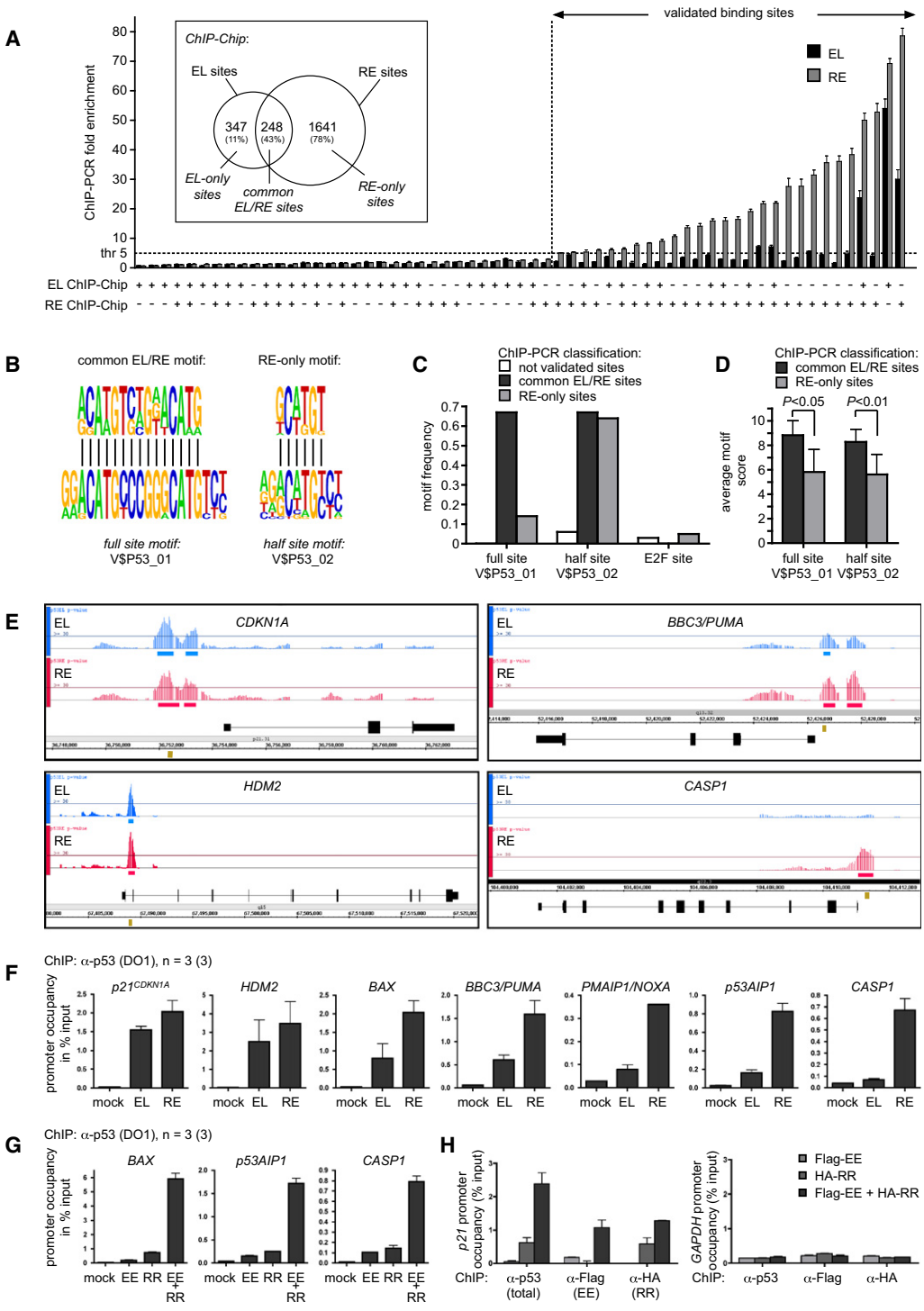

Figure 3. Role of p53 DNA Binding Cooperativity for In Vivo DNA Binding

(A) ChIP-Chip analysis was used to identify p53-binding sites in Saos-2 cells expressing the H1 helix mutant EL or RE compared to mock cells (Table S2). Sixty-one of these BS were randomly chosen for validation by ChIP-PCR. The identification of each site on EL and/or RE arrays is shown on the x axis. Reported is the fold enrichment of p53 (EL or RE) at this genomic position compared to mock as determined by ChIP-PCR. Inset: number and validation rate (in %) of EL and RE sites identified by ChIP-Chip. Results are presented as the mean ± SD.

(B) De novo motif discovery in validated common EL/RE and RE-only binding sequences. Twenty-meric and decameric consensus motifs are shown for comparison.

further analysis on the transcriptional activity of the H1 helix mutants.

In Vivo DNA Binding of H1 Helix Mutants

To measure the in vivo DNA-binding activity of H1 helix mutants in an unbiased manner, we used promoter arrays containing over 4.6 million probes tiled through over 25,500 human promoter regions (Affymetrix GeneChip Human Promoter 1.0R Array; minimum promoter coverage: 7.5 kb upstream through 2.45 kb downstream of the transcriptional start site; TSS). For this purpose, Saos-2 cells were infected with adenoviruses expressing either the H1 helix mutant EL or RE while mock-transfected cells served as internal controls. Cells were harvested 18 hr after infection when apoptosis had not yet occurred (Figure S1E). All ChIP-Chip experiments were done in triplicate, and binding sites (BS) were identified applying a statistical threshold of $p < 0.001$. A total of 595 BS were identified for EL and 1889 for RE (Table S2). A comparable analysis with wild-type p53 yielded 812 BS (data not shown). Twenty-eight of 61 (46%) randomly chosen BS showed a more than 5-fold enrichment for RE in ChIP-PCR validation experiments (Figure 3A; Table S3). The validation rate for EL sites was substantially lower (28%) than for the RE sites (60%) comprising mainly those BS which were also identified on the RE arrays (Table S3). Furthermore, all validated BS were bound stronger by RE than by EL, and not a single BS was identified that recruited EL but not RE. p53 BS can therefore be divided into ''common EL/RE'' sites and ''RE-only'' sites. Based on our experimental validation rate, we predict approximately 100 common and 1250 RE-only BS in the promoter regions of the human genome and concluded that DNA binding cooperativity strongly increases the number of p53 BS.

Functional annotation of common EL/RE sites with GATHER (http://gather.genome.duke.edu) revealed a significant enrichment (p value < 0.01, Bayes factor > 20) for the Gene Ontology (GO) terms ''response to stress'' and ''regulation of cell cycle'' (Table S4). The GO terms ''programmed cell death/apoptosis'' and ''regulation of programmed cell death/apoptosis'' were only significantly enriched among the RE-only sites. In both common and RE-only sites, the p53 consensus sequence (TRANSFAC M00272.p53) was found to be the most significantly enriched transcription factor binding motif. However, whereas 111 hits were found in the list of common sites, 543 hits were found in the list of RE-only sites. Together with the predicted number of true binding sites (~100 common and ~1250 RE-only sites), this implies that most common sites contain a consensus-like p53 binding motif, whereas more than 50% of RE-only sites have a BS that deviates from the consensus.

When using the ChIP-PCR-validated BS (shown in Figure 3A) for de novo motif discovery, we identified a p53 consensus-like binding motif (ACATGTCTGAACATG; Figure 3B; Table S5) in all validated common EL/RE sites. In contrast, in the list of validated RE-only sites, we only discovered a short motif (GCWTGT; Figure 3B; Table S5) resembling the core of a p53 half-site. Similarly, the p53 full-site motif (V$P53_01) was strongly enriched in the set of validated common sites but not in the validated RE-only sites. In contrast, the p53 half-site motif (V$P53_02) was found with equal frequency in all validated binding sites (Figure 3C). In both cases, the average motif score as a measure of similarity to the consensus was significantly lower among the validated RE-only sites (Figure 3D), indicating that RE tolerates mismatches to the consensus binding site better than EL. Another explanation for the absence of 20-meric full sites in RE-only sequences despite the presence of decameric half-sites are spacer elements that separate two half-sites. Applying a spacer-tolerant algorithm, we indeed identified spacer-containing full sites more frequently in RE-only than in common EL/RE sequences (Figures S2B and S2C). Together, these results suggest that the sequence requirements for recruitment of RE are less stringent than for EL. Consistently, in vitro DNA binding data demonstrated specific enhancement of p53 binding to lower-affinity and spacer-containing BS by increased DNA binding cooperativity (Figures S2A and S2D). Interestingly, the response elements in target genes of the apoptotic program are often lower-affinity BS frequently containing mismatches to the consensus (Riley et al., 2008).

When analyzing the binding profiles of H1 helix mutants on individual p53 target genes, it can be clearly seen that both mutants bind similarly to the $p21^{CDKN1A}$ and *HDM2* promoter but that recruitment to the promoters of the proapoptotic genes *BBC3*/*PUMA*, *CASP1*, *PMAIP1*/*NOXA*, and *BAX* exceeds the stringent threshold only in the case of RE (Figure 3E; Figures S2E and S2F). ChIP-PCR analysis of individual p53 target genes confirmed that the promoter occupancy was particularly different on proapoptotic gene promoters (*BAX*, *BBC3*/*PUMA*, *PMAIP1*/*NOXA*, *p53AIP1*, *CASP1*; Figure 3F). To confirm that the differential DNA binding characteristics of H1 helix mutants are truly due to interaction defects, we also analyzed functional complementation of the two most severely affected p53 mutants EE and RR. Both mutants on their own were strongly impaired in binding to p53 target genes, as expected from the overall negative (EE) or positive (RR) charge of the H1 helix and the in vitro DNA binding data. However, EE and RR mutually enhanced their promoter binding activity, strongly suggesting that in vivo DNA binding is determined by the interaction of the H1 helices (Figures 3G and 3H). Increased DNA binding cooperativity due to strong H1 helix interactions therefore enables p53 recruitment to promoters of proapoptotic genes, which are not efficiently bound in the absence of cooperative DNA binding.

(C and D) Frequency and average motif scores of the TRANSFAC motifs V$P53_01 (full site), V$P53_02 (half-site), and V$E2F_01 (E2F site as a control) in the binding sequences of (A). Results are presented as the mean ± SD.

(E) Genome browser view of EL and RE binding to individual p53 target genes as determined by ChIP-Chip analysis. Shown are the transformed p value averages of three array hybridizations. Genomic regions exceeding the statistical threshold p value of 0.001 are shown as horizontal bars. Yellow bars show the regions used for validation by ChIP-PCR.

(F) ChIP-PCR analysis of H1 helix mutant binding to selected p53 target genes. Results are presented as the mean ± SD.

(G and H) ChIP-PCR analysis of Flag-tagged EE and HA-tagged RR binding to the $p21^{CDKN1A}$ and *GAPDH* promoters using α-p53, α-Flag, or α-HA antibody. Shown is the mean ± SD for three independent experiments with three PCR replicates each, n = 3(3). See also Figure S2.

Gene Expression Profiling of H1 Helix Mutants

To characterize the transactivation function of H1 helix mutants in an unbiased manner, we performed gene expression profiling with cDNA microarrays. Saos-2 cells were infected with adenoviruses expressing the p53 proteins EE, EL, WT, and RE, which span the entire spectrum of apoptotic activity. A total of 186 genes were induced by wild-type p53 more than 3-fold 18 hr after infection (Figure 4A; Table S6). As expected from the weak DNA-binding activity of EE, the gene expression profile of EE-expressing cells was most similar to the GFP control sample. Based on our chromatin immunoprecipitation data, we expected RE to transactivate more genes than EL. However, the sets of activated genes appeared mutually exclusive, so two clusters of target genes could be distinguished: class I genes preferentially activated by the EL mutant with impaired DNA binding cooperativity, and class II genes selectively induced by the hyperactive mutant RE. Class I genes include $p21^{CDKN1A}$ and *HDM2* as key players of cell-cycle arrest and apoptosis inhibition, whereas class II genes include the proapoptotic genes *NOXA* (*PMAIP1*) and *CASP1* (validation qRT-PCR in Figure 4B).

Similarly, luciferase reporter assays demonstrated the $p21^{CDKN1A}$ promoter to be preferentially activated by H1 helix mutants with low interaction strength (RR, LR, EL), whereas the proapoptotic *BAX* and *p53AIP1* promoters were activated better by the p53 proteins WT, RE, and EE+RR (Figure 4C). Reduced transactivation of $p21^{CDNK1A}$ and *HDM2* by RE and EE+RR appeared paradoxical, considering efficient binding of these mutants to the promoters. A detailed analysis of the $p21^{CDNK1A}$ gene confirmed efficient binding of RE to the 5′ and 3′ p53 binding sites in the $p21^{CDNK1A}$ promoter, which even exceeded binding of EL (Figure S3A). Histone H3 and H4 panacetylation as well as H3K4 trimethylation were comparable for both p53 mutants. Recruitment of RNA polymerase II to the TSS and throughout the gene was lower in the case of RE. Lower RNA polymerase binding was similarly observed at the TSS of the *HDM2* promoter but not the *CASP1* promoter (Figure S3B). Higher levels of RE binding to the $p21^{CDNK1A}$ promoter but equal histone modification levels and reduced RNA pol II binding indicate an impaired coupling of RE to polymerase, possibly due to insufficient recruitment of coactivators. In addition, expression of transactivation-competent but not transactivation-deficient p53 inhibited the expression of a Gal4-dependent reporter driven by a fusion protein consisting of the Gal4-DNA-binding domain and the transactivation domain of p53 (Figure S3C). Because this effect was much stronger in the presence of RE than of EL, we concluded that RE, presumably because of its binding to many more sites in the genome than EL, causes a relative deficiency of coactivators, which results in a lower transactivation of $p21^{CDNK1A}$.

These data raised the question of whether RE is a stronger inducer of apoptosis than EL because of its ability to better activate proapoptotic genes or because it induces lower levels of antiapoptotic p21. Knockdown of p21 expression, however, did not result in apoptosis in EL-transfected cells, indicating that it is not the high-level induction of p21 but rather the defect in transactivating proapoptotic targets that limits apoptosis induction in the absence of DNA binding cooperativity (Figures S3D and S3E).

Furthermore, time course analysis of p53 target proteins following EL and RE expression indicated that EL primarily induced p21 and Hdm2 expression whereas RE induced strong expression of the proapoptotic Noxa, Bax, and Puma proteins, indicating intrinsically different target gene spectra of the two mutants (Figure 4E). Importantly, this difference was already observed at the earliest time points when p53 levels were lower than in p53 wild-type U2OS cells after DNA damage (Figures 4D and 4E). Similar to EL, the RR mutant also strongly activated p21 and Hdm2 (Figure 4F). However, coexpression of RR with the transcriptionally mostly inactive EE mutant shifted the target selectivity to Noxa and Bax, resulting in caspase-3 and PARP cleavage. Phosphorylation of key serine residues (S15, S20, S46, S392) was comparable for all mutants and could not account for the different apoptotic activities (data not shown). These findings were further confirmed in H1299 cells with inducible p53-ER^{TAM} constructs carrying the EL and RE mutations expressed at physiological levels (Figures S4A–S4H).

DNA Binding Cooperativity Enhances Apoptosis in Response to DNA Damage

Interestingly, in the H1299 p53-ER^{TAM} system, the difference between EL and RE became even more pronounced following additional treatment of these cells with the DNA-damaging agent doxorubicin, suggesting a role for DNA binding cooperativity in the DNA damage response (Figures S4E–S4H). Likewise, in Saos-2 cells transfected with the panel of H1 helix mutants, basal and DNA damage-induced levels of apoptosis directly correlated with cooperativity (Figures 5A–5C). To confirm these findings, we investigated p53 knockout HCT116 colon cancer cells that were reconstituted with our panel of H1 helix mutants. The p53 mutants were expressed at physiological levels and were similarly phosphorylated and stabilized in response to 5-fluorouracil (5-FU) (Figure 5D). Like typical loss-of-function p53 mutants (data not shown), the most inactive mutant EE was expressed at higher levels. Binding of p53 to the proapoptotic target genes *FAS* and *FDXR* was weak in unstressed cells and strongly induced 6 hr after 5-FU treatment in a cooperativity-dependent manner (Figure 5E). Transactivation of *FAS* and *FDXR* (Figure 5F) and apoptosis induction (Figures 5G and 5H) were similarly determined by DNA binding cooperativity. We therefore concluded that DNA binding cooperativity determines the extent of apoptosis in response to DNA damage.

The apoptotic function of p53 is stimulated in response to DNA damage by a number of posttranslational modifications and cofactors. For example, phosphorylation of serine 46 provides a docking site for the prolyl isomerase Pin1, which displaces the apoptosis inhibitor iASPP from p53 to promote cell death (Mantovani et al., 2007). This mechanism can be mimicked by the 46F mutation, which enhances p53's apoptotic function (Nakamura et al., 2006). Whereas the 46F mutation increased the apoptotic function of both p53 WT and EL, *NOXA* expression and basal as well as DNA damage-induced levels of apoptosis remained substantially lower for EL (Figures S4I–S4K). Furthermore, overexpression of ASPP2, which is known to stimulate p53 binding to proapoptotic target promoters (Samuels-Lev et al., 2001), increased the cytotoxicity of the H1 helix mutants, but the absolute amount of apoptosis

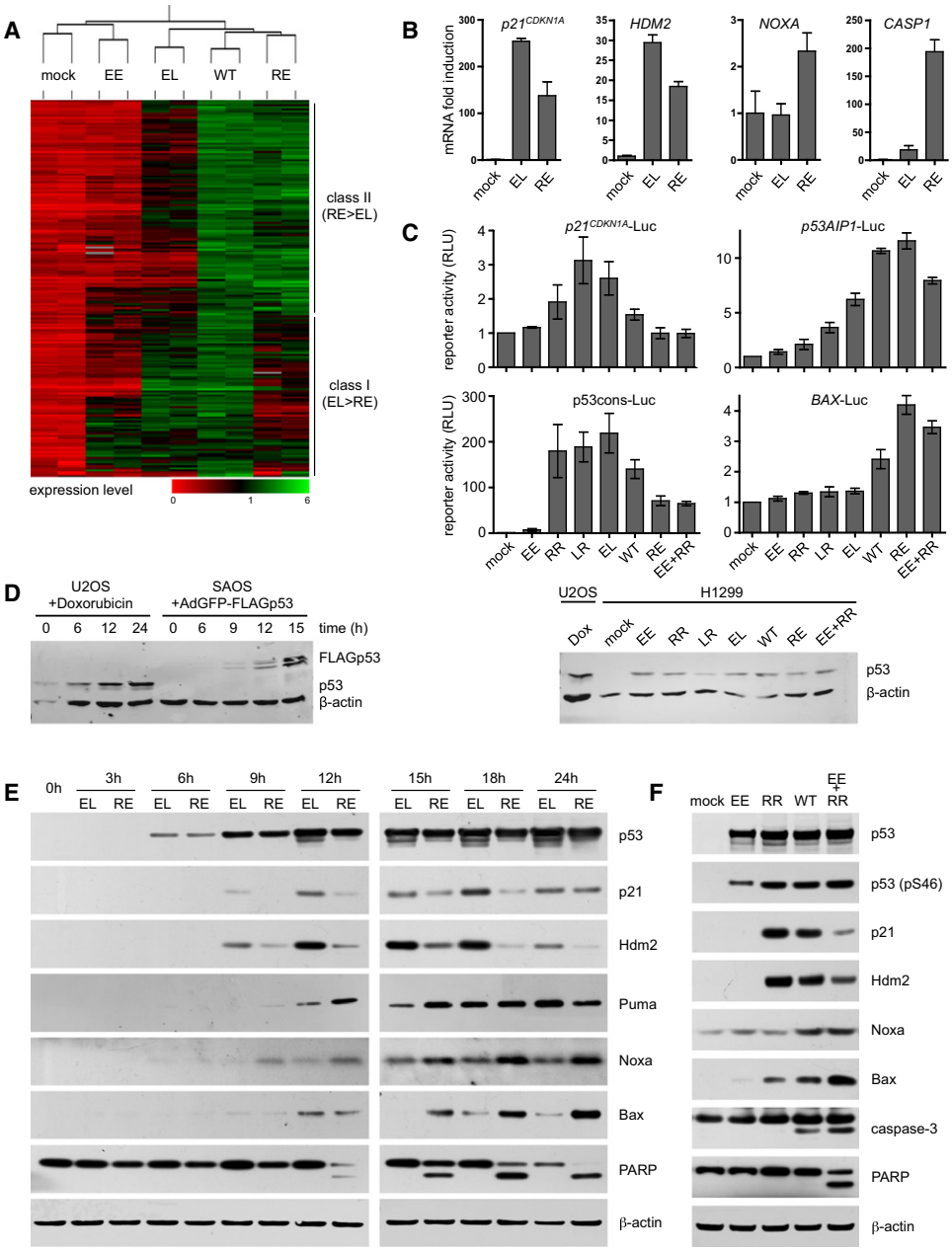

Figure 4. p53 DNA Binding Cooperativity Distinguishes Two Functionally Distinct Classes of p53 Target Genes

(A) Heat map depicting gene expression profiles of Saos-2 cells infected with adenoviruses expressing p53 wild-type and H1 helix mutants. Shown are the 186 genes that were induced by wild-type p53 more than 3-fold (Table S6). Two gene clusters are distinguished based on the relative induction by RE and EL.

(B) Validation by qRT-PCR. Samples as in (A) were analyzed for expression of target genes relative to the GFP-control sample (mock) and *GAPDH* as an internal standard. Shown is the mean ± SD (n = 3).

(C) Luciferase reporter assay of H1299 cells transfected with p53 expression and luciferase reporter plasmids. Luciferase activity was normalized to the mock control. Shown is the mean ± SD of two independent experiments with two replicates each. Immunoblot shows comparable expression of p53 in transfections and doxorubicin-treated U2OS cells.

(D–F) Immunoblots of doxorubicin-treated U2OS cells or Saos-2 cells infected with p53-expressing adenoviruses for the indicated time periods, 18 hr in (F). See also Figure S3.

was limited in the absence of DNA binding cooperativity (Figure S4L). Interestingly, ASPP2 could not further stimulate the apoptotic activity of the most highly cooperative mutant EE+RR, implying that ASPP2 functions by enhancing cooperativity. Together, these data suggest that DNA binding cooperativity is crucial for at least some posttranslational modifications and modulating cofactors to increase p53-mediated apoptosis in response to DNA damage.

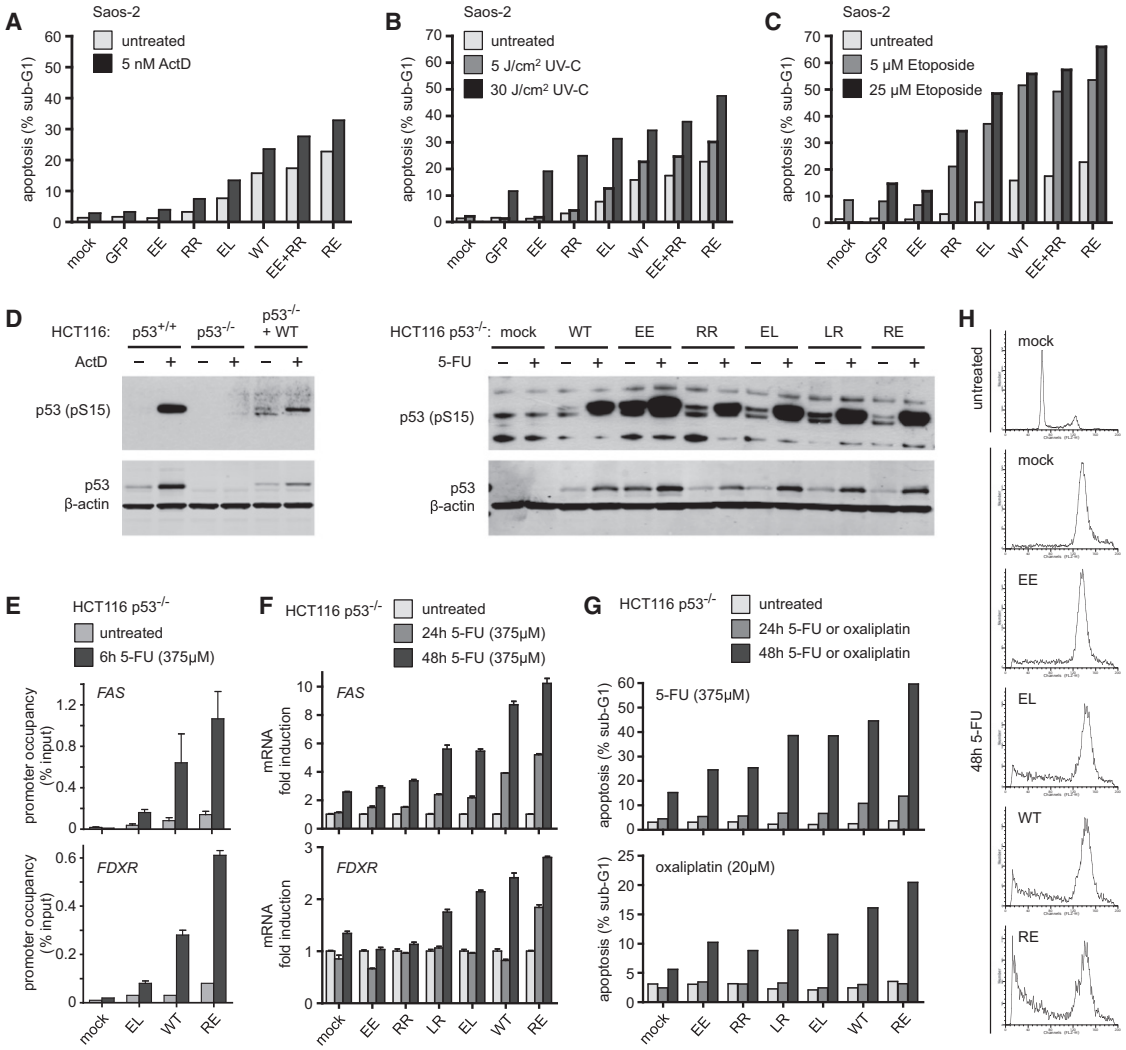

Figure 5. DNA Binding Cooperativity Is Crucial for Apoptosis in Response to DNA Damage

(A–C) Apoptosis of Saos-2 cells 24 hr following infection with indicated p53 adenoviruses in the absence or presence of DNA damage.

(D–H) p53 knockout ($p53^{-/-}$) HCT116 cells were reconstituted with wild-type or H1 helix mutant p53 by stable retroviral transduction.

(D) Immunoblots of parental ($p53^{+/+}$), $p53^{-/-}$, and p53-reconstituted HCT116 cells. For p53 activation, cells were treated for 24 hr with ActD (10 nM), 5-FU (375 μM), or oxaliplatin (20 μM).

(E) ChIP-PCR of p53 binding to *FAS* and *FDXR* promoters.

(F) qRT-PCR for *FAS* and *FDXR* mRNA.

(G and H) Apoptosis (sub-G1 population) (G) and cell-cycle profiles (H) of 5-FU-treated p53-reconstituted HCT116 cell lines. Results are presented as the mean ± SD. See also Figure S4.

DNA Binding Cooperativity Is Essential for p53's Tumor Suppressor Activity

The International Agency for Research on Cancer (IARC) TP53 Mutation Database, release R14, lists 146 tumor patients with somatic and 28 with germline mutations at positions E180 or R181. However, for rare somatic p53 mutations, the causal role for tumorigenesis is often unclear. We therefore focused our further studies on the mutations E180K (= KR), R181L (= EL), R181H (= EH), R181C (= EC), and R181P (= EP), which are genetically linked to tumor development in families with the hereditary Li-Fraumeni or Li-Fraumeni-like cancer susceptibility syndrome. DNA-protein complex stabilities in vitro were reduced for all five mutations in the order WT > EL > EH = EC > KR > EP (Figures 6A and 6B). The EP mutant showed no DNA binding and no significant activity in our further experiments. Considering that proline is known to kink or break helices, we assume that the EP mutation not only disrupts H1 helix interactions but has more profound effects on the folding of the DNA-binding domain. The remaining mutants displayed a defect in promoter binding and transactivation of apoptotic target genes (Figures 6C–6F), and this correlated with a loss of their apoptotic activity (Figures 6G and 6H). Similarly as seen for other low-cooperativity mutants (Figures 4B–4F), luciferase reporter constructs containing consensus-like p53 response elements were efficiently

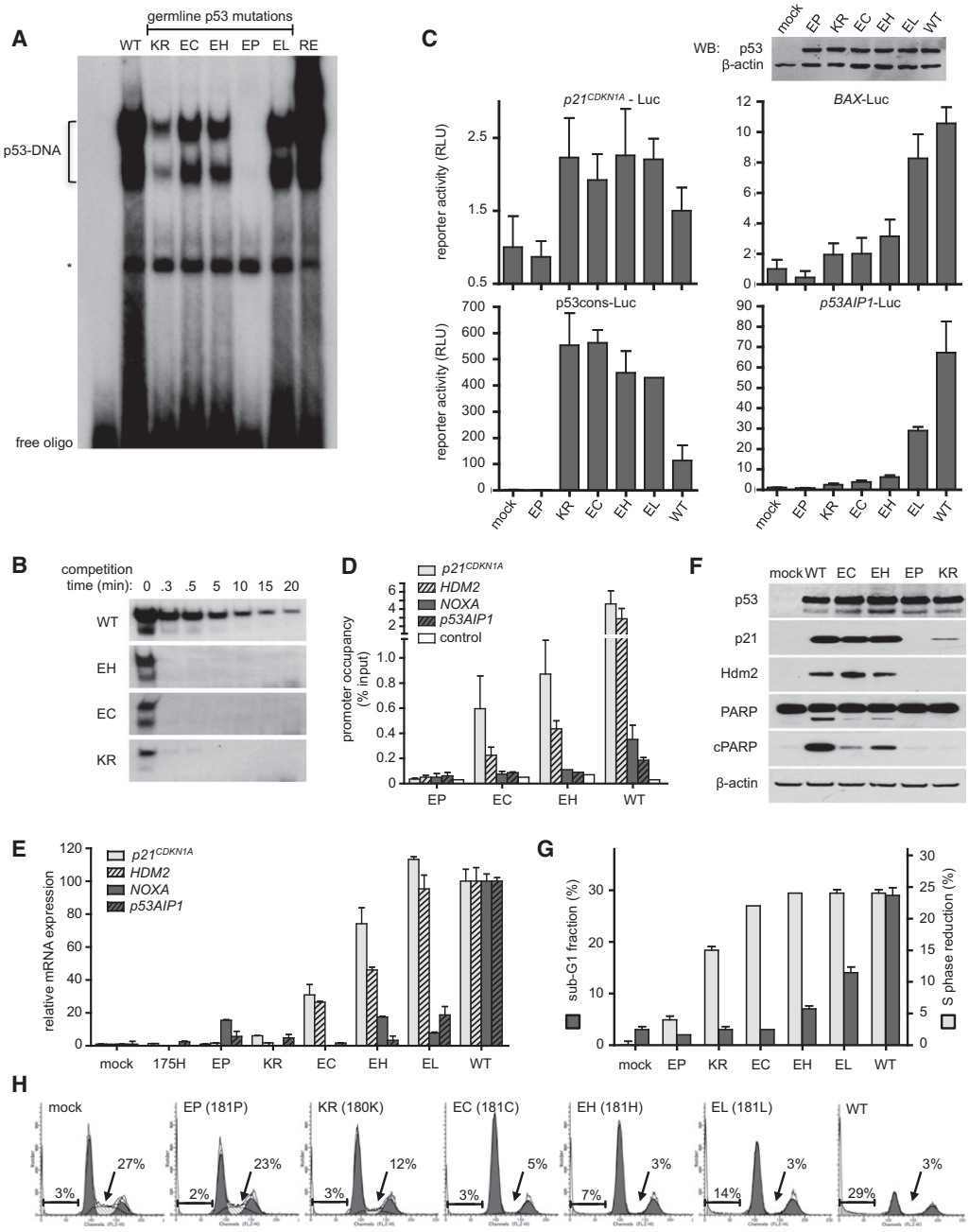

Figure 6. DNA Binding Cooperativity Is Essential for p53's Tumor Suppressor Activity

(A and B) EMSA of in vitro translated full-length p53 proteins and ^{32}P-labeled dsDNA containing the p53 consensus response element showing reduced DNA binding of p53 with germline H1 helix missense mutations.

(B) EMSA displaying dissociation of the indicated p53 proteins from ^{32}P-labeled consensus dsDNA upon addition of a 100-fold excess of the same oligonucleotide lacking ^{32}P.

(C) Luciferase reporter assay of H1299 cells transfected with p53 expression and luciferase reporter plasmids. Luciferase activity was normalized to the mock control. Shown is the mean ± SD of three transfections. Immunoblot shows comparable expression of all p53 constructs.

(D–H) Saos-2 cells were infected for 18 hr (D–F) or 34 hr (G and H) with adenoviruses expressing the indicated p53 proteins.

(D) ChIP-PCR.

(E) qRT-PCR.

(F) Immunoblot.

(G and H) Cell-cycle profiles determined by flow cytometry following propidium iodide staining. Results are presented as mean ± SD.

transactivated by these Li-Fraumeni mutants despite their lower than WT DNA binding affinity (Figures 6B and 6C). Consistently, the Li-Fraumeni mutants induced $p21^{CDKN1A}$ and caused a cell-cycle arrest. In the case of the KR mutant, p21 induction was lower than expected from the reporter activation study, which might reflect an unnatural activatability of the naked reporter plasmid compared to the endogenous gene in its chromatin context. In summary, four of the five Li-Fraumeni mutants showed the selective loss of apoptotic activity characteristic for reduced DNA binding cooperativity. As these mutations are genetically linked to cancer susceptibility in patients, we concluded that DNA binding cooperativity contributes to p53's tumor suppressor activity.

DISCUSSION

The structural basis for the DNA binding cooperativity of p53 is the interaction of H1 helices in the DNA-binding core domains. This interaction forms the symmetrical intradimer interface in the crystal structure of the DNA-bound core domain tetramer (Kitayner et al., 2006) and the solution dimerization interface as revealed by NMR spectroscopy (Klein et al., 2001). Mutational perturbation of this interface strongly impairs the cooperativity of in vitro DNA binding by isolated p53 core domains (Dehner et al., 2005). Considering that full-length p53 is assembled into a tetramer by strong interactions of the oligomerization domains, it remained unknown whether the H1 helix interaction interface plays a similar role in the context of the full-length p53 molecule. Our data demonstrate that the interaction of H1 helices is not required for the assembly of the tetramer. All H1 helix mutants formed tetrameric p53 molecules. Nevertheless, mutational perturbation of the interface strongly affected the DNA binding properties of p53 in vitro and in vivo, indicating that this interface determines DNA binding cooperativity also in the context of the tetrameric full-length p53 molecule.

As the H1 helix does not directly contribute to the DNA-binding surface of the core domain, indirect effects have to be considered to explain the influence of H1 helix mutations on DNA binding. Early attempts to model the tetrameric p53-DNA complex on the basis of the crystal structure by Cho et al. already indicated that the assembly of four core domains on a straight DNA strand with the experimentally predicted C2 symmetry would be accompanied by steric hindrance between the H1 helices (Cho et al., 1994). However, this steric clash is relieved and the H1 helices are optimally aligned for interaction when the DNA is bent toward the major groove away from the p53 core dimer, as has been observed in bending analyses (Balagurumoorthy et al., 1995), in the crystal structure of the DNA-bound tetramer (Kitayner et al., 2006), and by atomic force microscopy (Balagurumoorthy et al., 2002). DNA bending, however, is dependent on the nucleotide sequence. The CATG sequence within the p53 consensus response element is unusually flexible and exhibits extreme bending and kinking in many DNA-protein complexes (Balagurumoorthy et al., 2002; Olson et al., 1998). DNA binding affinity experiments have shown that p53 exhibits higher binding affinity for sites in cell-cycle control target genes than for sites in apoptosis target genes, and that these differences coincide with the prevalence of the highly flexible CATG in the cell-cycle control group (Weinberg et al., 2005). Efficient binding to non-CATG response elements (CAAG, CTTG, CTAG) may therefore require higher bending forces that depend on energetic stabilization provided by strong H1 helix interactions. Based on this model, interaction-impaired H1 helix mutants (EL, LR, RR) would be competent for forming a stable, optimally bent complex with a CATG response element but unable to bind the more rigid non-CATG sequences. In contrast, enhanced interactions (RE, EE+RR) would facilitate bending and binding to non-CATG sites. Indeed, electrophoretic mobility shift assays demonstrated efficient binding of EL, LR, and RR to the CATG sequences but only weak binding to non-CATG sites, in contrast to strong binding of RE and EE+RR to both CATG and non-CATG sites (Figure S2A). Thus, the H1 helix region would regulate DNA binding not by directly influencing the DNA contact surface but rather indirectly by providing additional energetic stabilization, which is required for p53 binding to sequences that are less easily bent, such as non-CATG response elements in many proapoptotic promoters.

In addition to the "dimer of dimers" structure of four DNA-bound core domains (Kitayner et al., 2006), recently an alternative "H14" binding mode of p53 was postulated on the basis of molecular dynamics simulations and the interaction interface in the asymmetric AB dimer of the p53-trimer DNA complex determined by X-ray crystallography (Ma and Levine, 2007). In contrast to the dimer of dimers structure, the H14 binding model nicely fits the recently described cryo-EM image of p53 (Okorokov et al., 2006). Whereas the H1 helices solely determine the intradimer interactions in the dimer of dimers structure, in the H14 binding mode they form a circular salt bridge which holds together all four core domains in the DNA-bound tetramer. Although our data reveal that H1 helix interactions play a role for intradimer interactions when tested in the context of the dimeric L344A mutant p53 molecule, they are also consistent with the proposed H14 structure, which is expected to be significantly stabilized by H1 helix interactions.

Interestingly, our study also indicates that cooperativity not only increases p53's apoptotic functions but also reduces its ability to activate cell-cycle arrest genes. This appears to be an indirect effect, as highly cooperative p53 molecules (RE and EE+RR) are efficiently recruited to the p53 response elements in the $p21^{CDKN1A}$ gene. According to our data, reduced transactivation results from an impaired coupling of promoter-bound p53 to the transcription machinery. One explanation is that highly cooperative p53 binds to so many sites in the genome that one or more, yet to be identified, coactivators become limiting, so that transactivation of genes such as $p21^{CDKN1A}$ is reduced. Hence, an increase in cooperativity shifts the cellular response away from cell-cycle arrest toward apoptosis (Figure 7).

Considering that the apoptotic function of p53 in response to DNA damage is regulated by posttranslational modifications or cofactor binding (Das et al., 2007; D'Orazi et al., 2002; Sykes et al., 2006; Taira et al., 2007; Tang et al., 2006), one question was whether cooperativity is upstream or downstream. First, we did not observe any differences in the basal and DNA damage-induced phosphorylation status of the p53 H1 helix mutants. However, given the multitude of posttranslational modifications that have been described for p53, we cannot

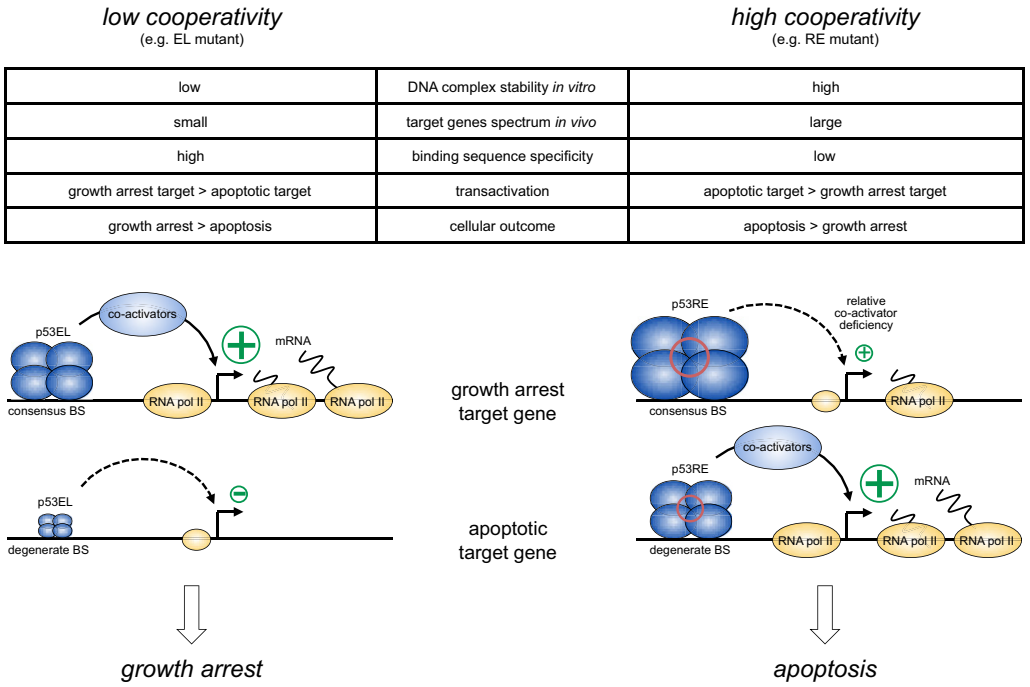

Figure 7. Role of DNA Binding Cooperativity for p53 Function

Model of the role of DNA binding cooperativity for target gene selection. The symbol size represents the amount of p53 and RNA pol II on the promoters as detected by ChIP. A red circle in the p53 tetramer symbolizes strong H1 helix interactions as the structural basis for DNA binding cooperativity.

exclude that other modifications might be affected in the set of mutants. In addition, various DNA-damaging agents, the activating 46F mutation, and expression of ASPP2 stimulated the apoptotic activity of the H1 helix mutants, but the resulting apoptosis level was in all cases determined by the extent of cooperativity. Together, these findings suggest that cooperativity is downstream in the p53 activating pathway. We therefore hypothesize that activating signals such as posttranslational modifications are upstream and translated into changes in DNA binding cooperativity causing p53 to switch from a weakly to a highly cooperative DNA binding factor. However, because DNA binding cooperativity cannot be directly measured in living cells at present, this hypothesis remains to be proven.

In general, tumor-derived point mutations in p53 fall into two classes: contact mutations affect p53 residues that directly interact with the DNA, whereas structural mutations cause local unfolding or global denaturation of the core domain. The H1 helix mutations described here represent a mechanistically distinct class of p53 mutations that affect a protein-protein interface in the quaternary structure of the p53-DNA complex. Mutations in this region have been identified as sporadic mutations in cancer patients (e.g., R181 to His; Leu, Pro, Cys, or E180 to Lys) as well as germline mutations in families with the Li-Fraumeni or Li-Fraumeni-like cancer susceptibility syndrome (IARC TP53 Mutation Database). Segregation of the cancer phenotype with the R181L (EL), R181C (EC), R181H (EH), and E180K (KR) mutations in Li-Fraumeni-like families, which all show a selective apoptotic defect (Figure 6), clearly indicates that impaired DNA binding cooperativity reduces p53's tumor suppressor activity. H1 helix interactions therefore contribute to the tumor suppressor function of p53 and could provide a therapeutic target to direct the outcome of p53 activation to either cell-cycle arrest or apoptosis.

EXPERIMENTAL PROCEDURES

Cell Culture and Viral Transduction

Cell lines were cultured in Dulbecco's modified Eagle's medium (Sigma) supplemented with 10% fetal bovine serum (Sigma) using standard conditions and procedures. Recombinant adenoviruses for p53 H1 helix mutants were generated with the AdEasy System (Stratagene). Cells were transduced with recombinant retro- and adenovirus as previously described (Cam et al., 2006).

Chromatin Immunoprecipitation and Genome-wide Promoter Analysis

Chromatin immunoprecipitations were performed as described (Cam et al., 2006). ChIP-Chip assays were performed with the p53 DO-1 antibody (Santa Cruz Biotechnology) on GeneChip Human Promoter 1.0R Arrays (Affymetrix) according to manufacturer recommendations. Detailed procedures for ChIP-PCR and ChIP-Chip can be found in Supplemental Experimental Procedures. The complete set of ChIP-Chip data has been deposited in EBI ArrayExpress (http://www.ebi.ac.uk/arrayexpress) under accession number E-MEXP-1748.

RT-PCR and Expression Profiling

Quantitative RT-PCR was performed as described (Cam et al., 2006). Primers and expression profiling procedures can be found in Supplemental Experimental Procedures. The complete set of microarray data has been deposited in EBI ArrayExpress (http://www.ebi.ac.uk/arrayexpress) under accession number E-MEXP-1209.

Additional experimental procedures are provided in Supplemental Information.

SUPPLEMENTAL INFORMATION

Supplemental Information includes Supplemental Experimental Procedures, four figures, and six tables and can be found with this article online at doi:10.1016/j.molcel.2010.02.037.

ACKNOWLEDGMENTS

We thank Moshe Oren, Bert Vogelstein, Trevor Littlewood, Yoichi Taya, Michael Schön, and Xin Lu for providing reagents, Michael Krause for assistance with microarrays, Justus Beck for mitochondrial localization experiments, Anna-Maria Maas for luciferase assays, Jochen Kuper for viewing and discussing p53 crystal structures, and Helmut Hänsel for help with bioinformatic data analysis. A.R. is supported by the Interdisciplinary Center for Clinical Research (IZKF), Würzburg, Germany. This work was funded by grants to T.S. of the Deutsche Forschungsgemeinschaft (Transregio TR17 Teilprojekt B2, Klinische Forschergruppe KFO210 STI 182/3-1, Forschungszentrum FZ82), Deutsche Krebshilfe (107904), and von Behring-Röntgen-Stiftung (57-0012).

Received: August 11, 2009
Revised: August 17, 2009
Accepted: February 16, 2010
Published: May 13, 2010

REFERENCES

Balagurumoorthy, P., Sakamoto, H., Lewis, M.S., Zambrano, N., Clore, G.M., Gronenborn, A.M., Appella, E., and Harrington, R.E. (1995). Four p53 DNA-binding domain peptides bind natural p53-response elements and bend the DNA. Proc. Natl. Acad. Sci. USA *92*, 8591–8595.

Balagurumoorthy, P., Lindsay, S.M., and Harrington, R.E. (2002). Atomic force microscopy reveals kinks in the p53 response element DNA. Biophys. Chem. *101-102*, 611–623.

Cam, H., Griesmann, H., Beitzinger, M., Hofmann, L., Beinoraviciute-Kellner, R., Sauer, M., Huttinger-Kirchhof, N., Oswald, C., Friedl, P., Gattenlohner, S., et al. (2006). p53 family members in myogenic differentiation and rhabdomyosarcoma development. Cancer Cell *10*, 281–293.

Chipuk, J.E., and Green, D.R. (2006). Dissecting p53-dependent apoptosis. Cell Death Differ. *13*, 994–1002.

Cho, Y., Gorina, S., Jeffrey, P.D., and Pavletich, N.P. (1994). Crystal structure of a p53 tumor suppressor-DNA complex: understanding tumorigenic mutations. Science *265*, 346–355.

Das, S., Raj, L., Zhao, B., Kimura, Y., Bernstein, A., Aaronson, S.A., and Lee, S.W. (2007). Hzf determines cell survival upon genotoxic stress by modulating p53 transactivation. Cell *130*, 624–637.

Dehner, A., Klein, C., Hansen, S., Muller, L., Buchner, J., Schwaiger, M., and Kessler, H. (2005). Cooperative binding of p53 to DNA: regulation by protein-protein interactions through a double salt bridge. Angew. Chem. Int. Ed. Engl. *44*, 5247–5251.

D'Orazi, G., Cecchinelli, B., Bruno, T., Manni, I., Higashimoto, Y., Saito, S., Gostissa, M., Coen, S., Marchetti, A., Del Sal, G., et al. (2002). Homeodomain-interacting protein kinase-2 phosphorylates p53 at Ser 46 and mediates apoptosis. Nat. Cell Biol. *4*, 11–19.

Kitayner, M., Rozenberg, H., Kessler, N., Rabinovich, D., Shaulov, L., Haran, T.E., and Shakked, Z. (2006). Structural basis of DNA recognition by p53 tetramers. Mol. Cell *22*, 741–753.

Klein, C., Planker, E., Diercks, T., Kessler, H., Kunkele, K.P., Lang, K., Hansen, S., and Schwaiger, M. (2001). NMR spectroscopy reveals the solution dimerization interface of p53 core domains bound to their consensus DNA. J. Biol. Chem. *276*, 49020–49027.

Ludwig, R.L., Bates, S., and Vousden, K.H. (1996). Differential activation of target cellular promoters by p53 mutants with impaired apoptotic function. Mol. Cell. Biol. *16*, 4952–4960.

Ma, B., and Levine, A.J. (2007). Probing potential binding modes of the p53 tetramer to DNA based on the symmetries encoded in p53 response elements. Nucleic Acids Res. *35*, 7733–7747.

Mantovani, F., Tocco, F., Girardini, J., Smith, P., Gasco, M., Lu, X., Crook, T., and Del Sal, G. (2007). The prolyl isomerase Pin1 orchestrates p53 acetylation and dissociation from the apoptosis inhibitor iASPP. Nat. Struct. Mol. Biol. *14*, 912–920.

Nakamura, Y., Futamura, M., Kamino, H., Yoshida, K., Nakamura, Y., and Arakawa, H. (2006). Identification of p53-46F as a super p53 with an enhanced ability to induce p53-dependent apoptosis. Cancer Sci. *97*, 633–641.

Okorokov, A.L., Sherman, M.B., Plisson, C., Grinkevich, V., Sigmundsson, K., Selivanova, G., Milner, J., and Orlova, E.V. (2006). The structure of p53 tumour suppressor protein reveals the basis for its functional plasticity. EMBO J. *25*, 5191–5200.

Olson, W.K., Gorin, A.A., Lu, X.J., Hock, L.M., and Zhurkin, V.B. (1998). DNA sequence-dependent deformability deduced from protein-DNA crystal complexes. Proc. Natl. Acad. Sci. USA *95*, 11163–11168.

Riley, T., Sontag, E., Chen, P., and Levine, A. (2008). Transcriptional control of human p53-regulated genes. Nat. Rev. Mol. Cell Biol. *9*, 402–412.

Samuels-Lev, Y., O'Connor, D.J., Bergamaschi, D., Trigiante, G., Hsieh, J.K., Zhong, S., Campargue, I., Naumovski, L., Crook, T., and Lu, X. (2001). ASPP proteins specifically stimulate the apoptotic function of p53. Mol. Cell *8*, 781–794.

Stiewe, T. (2007). The p53 family in differentiation and tumorigenesis. Nat. Rev. Cancer *7*, 165–168.

Sykes, S.M., Mellert, H.S., Holbert, M.A., Li, K., Marmorstein, R., Lane, W.S., and McMahon, S.B. (2006). Acetylation of the p53 DNA-binding domain regulates apoptosis induction. Mol. Cell *24*, 841–851.

Taira, N., Nihira, K., Yamaguchi, T., Miki, Y., and Yoshida, K. (2007). DYRK2 is targeted to the nucleus and controls p53 via Ser46 phosphorylation in the apoptotic response to DNA damage. Mol. Cell *25*, 725–738.

Tang, Y., Luo, J., Zhang, W., and Gu, W. (2006). Tip60-dependent acetylation of p53 modulates the decision between cell-cycle arrest and apoptosis. Mol. Cell *24*, 827–839.

Tidow, H., Melero, R., Mylonas, E., Freund, S.M., Grossmann, J.G., Carazo, J.M., Svergun, D.I., Valle, M., and Fersht, A.R. (2007). Quaternary structures of tumor suppressor p53 and a specific p53 DNA complex. Proc. Natl. Acad. Sci. USA *104*, 12324–12329.

Veprintsev, D.B., Freund, S.M., Andreeva, A., Rutledge, S.E., Tidow, H., Canadillas, J.M., Blair, C.M., and Fersht, A.R. (2006). Core domain interactions in full-length p53 in solution. Proc. Natl. Acad. Sci. USA *103*, 2115–2119.

Vousden, K.H., and Lane, D.P. (2007). p53 in health and disease. Nat. Rev. Mol. Cell Biol. *8*, 275–283.

Vousden, K.H., and Lu, X. (2002). Live or let die: the cell's response to p53. Nat. Rev. Cancer *2*, 594–604.

Weinberg, R.L., Veprintsev, D.B., and Fersht, A.R. (2004). Cooperative binding of tetrameric p53 to DNA. J. Mol. Biol. *341*, 1145–1159.

Weinberg, R.L., Veprintsev, D.B., Bycroft, M., and Fersht, A.R. (2005). Comparative binding of p53 to its promoter and DNA recognition elements. J. Mol. Biol. *348*, 589–596.

Molecular Cell, *Volume 38*

Supplemental Information

DNA Binding Cooperativity of p53 Modulates the Decision between Cell-Cycle Arrest and Apoptosis

Katharina Schlereth, Rasa Beinoraviciute-Kellner, Marie K. Zeitlinger, Anne C. Bretz, Markus Sauer, Joël P. Charles, Fotini Vogiatzi, Ellen Leich, Birgit Samans, Martin Eilers, Caroline Kisker, Andreas Rosenwald, and Thorsten Stiewe

SUPPLEMENTAL FIGURES AND LEGENDS

Figure S1, related to Figure 2: p53 DNA binding cooperativity correlates with apoptosis induction

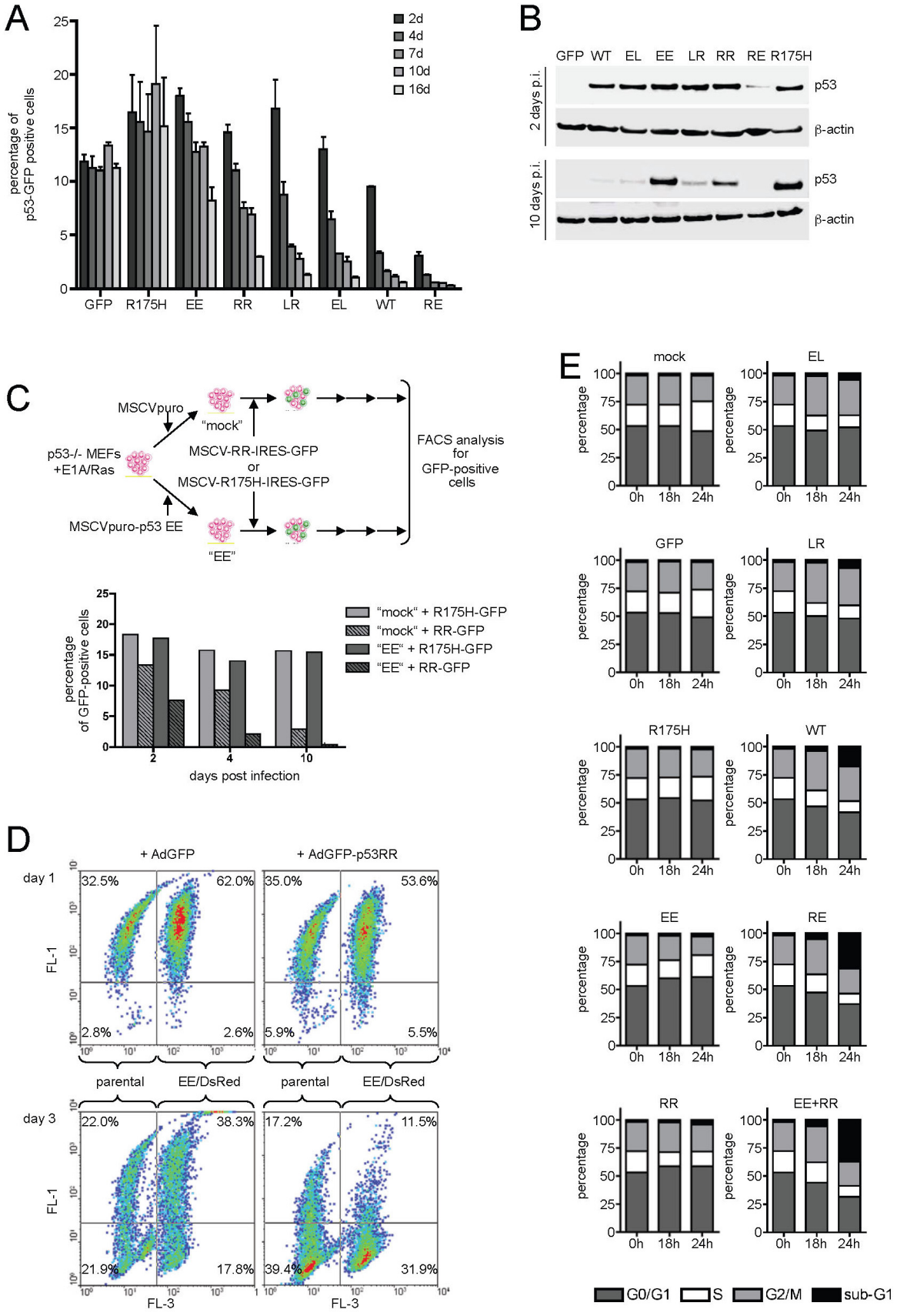

(A, B) *p53 DNA binding cooperativity correlates with anti-proliferative activity.* We first analyzed the role of core domain interactions for the anti-proliferative activity of p53 in the genetically defined model of E1A/H-RasV12 transformed p53-null mouse embryo fibroblasts. These cells were infected with retroviral vectors (pMSCV-p53-IRES-GFP) expressing wild-type or H1 helix mutant p53 linked to GFP with an efficiency of approximately 10-20%. The resulting mixture of p53-expressing and non-expressing cells allowed us to determine the impact of p53 on tumor cell proliferation in a competitive co-culture setting by following the percentage of GFP-positive p53-expressing cells over serial passages by flow cytometry (A) and by determining p53 expression in immunoblots (B). Wild-type p53 expression progressively reduced the percentage of GFP-positive cells, which did not change over time in the case of the GFP control and the structurally inactive p53 mutant R175H. All mutants with decreased interaction strength (EE, RR, LR and EL) reduced the percentage of GFP-positive cells but with lower efficiency than the wild-type protein. In contrast, the double mutant RE was more active than the wild-type p53. On day 2 of the experiment all p53 mutants with the exception of RE were expressed at comparable levels. 10 days after transduction, selection against active p53 mutants had been completed so that only the p53 variant proteins (R175H, EE and RR) with little anti-proliferative activity were clearly detected. The RE mutant already displayed reduced expression after 2 days and was undetectable after 10 days, which can be explained by an extremely rapid anti-proliferative effect of this possibly hyperactive p53 protein.

(C, D) *Functional rescue of anti-proliferative activity by mutant complementation.* (C) E1A/HrasV12-transformed p53-null MEFs were infected with retroviral vectors pMSCVpuro (mock) and pMSCVpuro-EE (EE) and selected with puromycin. EE was largely inactive in this setting and could be stably expressed for several months. Subsequently, these two cell populations were infected with retroviruses expressing GFP together with the H1 helix mutant RR (pMSCV-RR-IRES-GFP) or the inactive p53 mutant R175H (pMSCV-R175H-IRES-GFP) as a control. The cells were serially passaged and the percentage of GFP-positive cells was measured by flow cytometry 2, 4 and 10 days after infection. Whereas R175H had no significant anti-proliferative effect, RR reduced the percentage of GFP-positive mock and EE cells over time. Importantly, the effect was faster and more pronounced in EE cells indicating functional cooperation of EE and RR with respect to anti-proliferative activity. (D) p53-null H1299 cells were transduced to stably co-express the p53 mutant EE and DsRed as a fluorescent marker. The EE/DsRed-expressing cells were mixed with parental H1299 cells and infected with the adenoviruses AdGFP or AdGFP-p53RR. Green (FL-1) and red (FL-3) fluorescence were determined by flow cytometry one and three days after infection. Numbers indicate the percentage of cells in the respective quadrant. The experiment shows that adenoviral expression of RR reduced the proliferation of EE-transfected DsRed-labeled H1299 cells stronger than of parental DsRed-negative H1299 cells indicating functional cooperation of EE and RR with respect to anti-proliferative activity.

(E) *Cell-cycle profiles of Saos-2 cells expressing p53 H1 helix mutants.* Saos-2 cells were infected with adenoviruses expressing the indicated p53 H1 helix mutants. No infection (mock), adenovirus expressing GFP (GFP) or the p53 R175H mutant (R175H) were used as negative controls. Cells were harvested before and 18 or 24 hours after infection and analyzed by flow cytometry after propidium iodide staining. The percentage of cells in G0/G1, S, G2/M and sub-G1 was determined with ModFit LT (Becton Dickinson).

Figure S2, related to Figure 3: Role of p53 DNA binding cooperativity for in vivo DNA binding

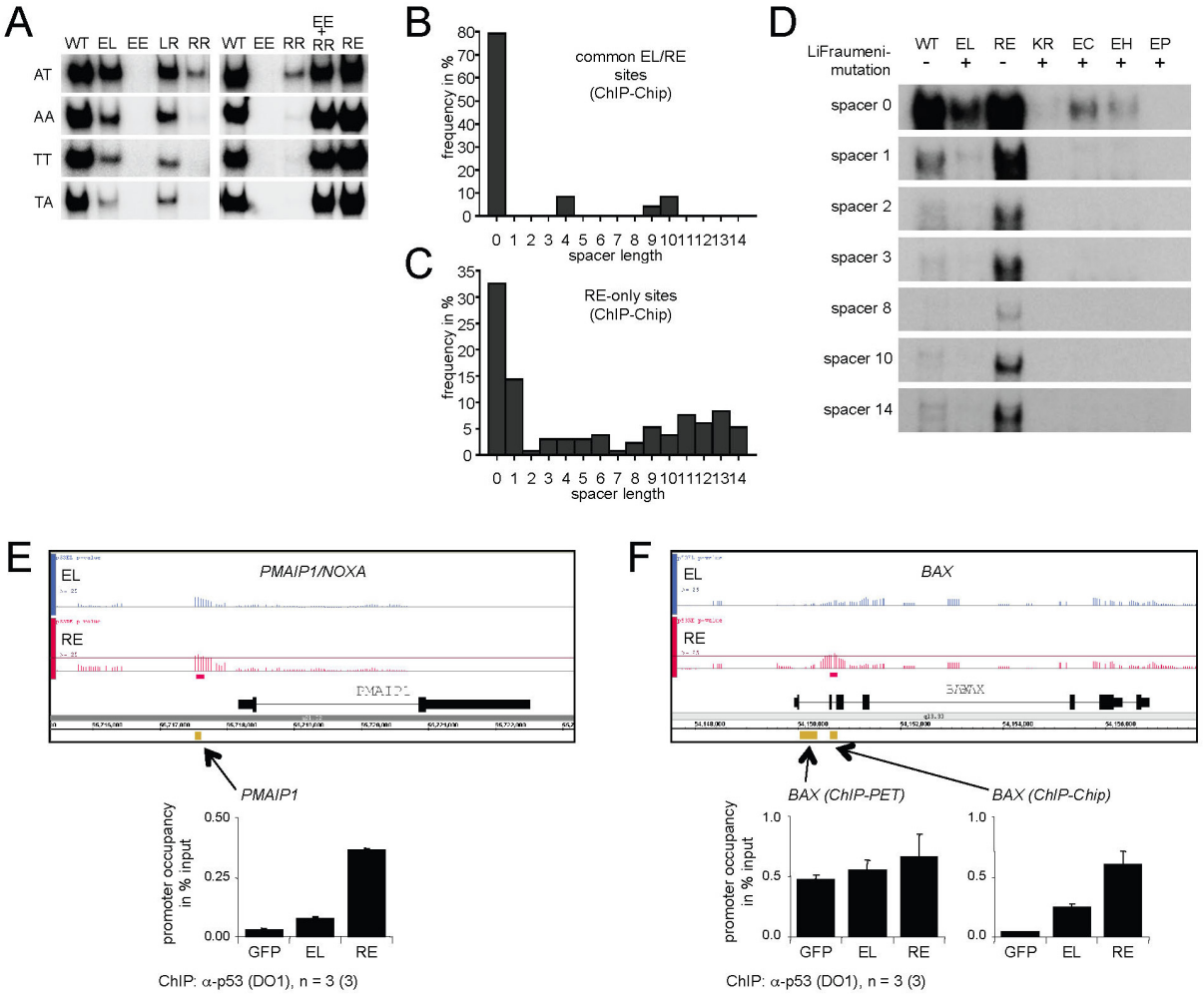

(A) *DNA binding cooperativity enhances binding to low affinity BS.* The consensus DNA binding sequence PuPuPuCWWGPyPyPy allows substantial sequence variation. It has been previously demonstrated that central CATG sequences show a higher affinity for wild-type p53 than non-CATG (CAAG, CTTG, CTAG) sequences (Riley et al., 2008). Furthermore non-CATG sequences are more commonly found in the promoters of proapoptotic than cell cycle arrest genes. Shown are electrophoretic mobility shift assays (EMSA) for DNA binding of *in vitro* translated wild-type p53 and the indicated H1 helix mutants to dsDNA oligonucleotides (5'-GGG AGC TTA GGC WWG TCT AGG CWW GTC TA-3') with AT, AA, TT or TA sequences in the center of each half site. Compared to H1 helix mutants with reduced DNA binding cooperativity (EE, RR, LR, EL), mutants with increased DNA binding cooperativity (RE and EE+RR) revealed an increased ability to bind the lower affinity non-CATG sequences.

(B-D) DNA binding cooperativity increases p53 binding to spacer-containing motifs. (B, C) Distribution of spacer lengths in binding sites determined by the spacer-tolerant p53MH algorithm in ChIP-Chip sequences. (D) Shown are electrophoretic mobility shift assays (EMSA) for DNA binding of *in vitro* translated wild-type p53 and the indicated H1 helix mutants to dsDNA oligonucleotides containing the 5' p53 binding site in the p21 promoter (5'-TCT GGC CGT CAG GAA CATG TCC CAA CATG TTG AAG CTC TGG CAT A -3') with increasing central spacer sequences. The H1 helix mutant with increased DNA binding cooperativity (RE) showed an increased ability to bind the spacer-containing motifs, while the

germline Li-Fraumeni mutants with decreased cooperativity (EL, EH, EC, KR, EP) were largely unable to bind spacer-containing elements.

(E) ChIP-Chip data on BAX and PMAIP1/NOXA. Genome browser view of EL (blue) and RE (red) binding to the (E) *PMAIP1/NOXA* and (F) *BAX* gene as determined by ChIP-Chip and Chip-PCR analysis in Saos-2 cells. For ChIP-Chip the averages of three array hybridizations are shown. The threshold lines represent a p-value of <0.005. For ChIP-PCR validation experiments primers were used that amplify the regions labeled with yellow bars. Shown is the promoter occupancy in percent of input DNA. Shown is the mean ± SD of three chromatin immunoprecipitations each quantified by triplicate qPCR reactions; n=3 (3). In the case of *BAX*, we used the region previously identified by ChIP-PET (Wei et al., 2006) as well as the region identified in this ChIP-Chip study.

Figure S3, related to Figure 4: p53 DNA binding cooperativity distinguishes two functionally distinct classes of p53 target genes

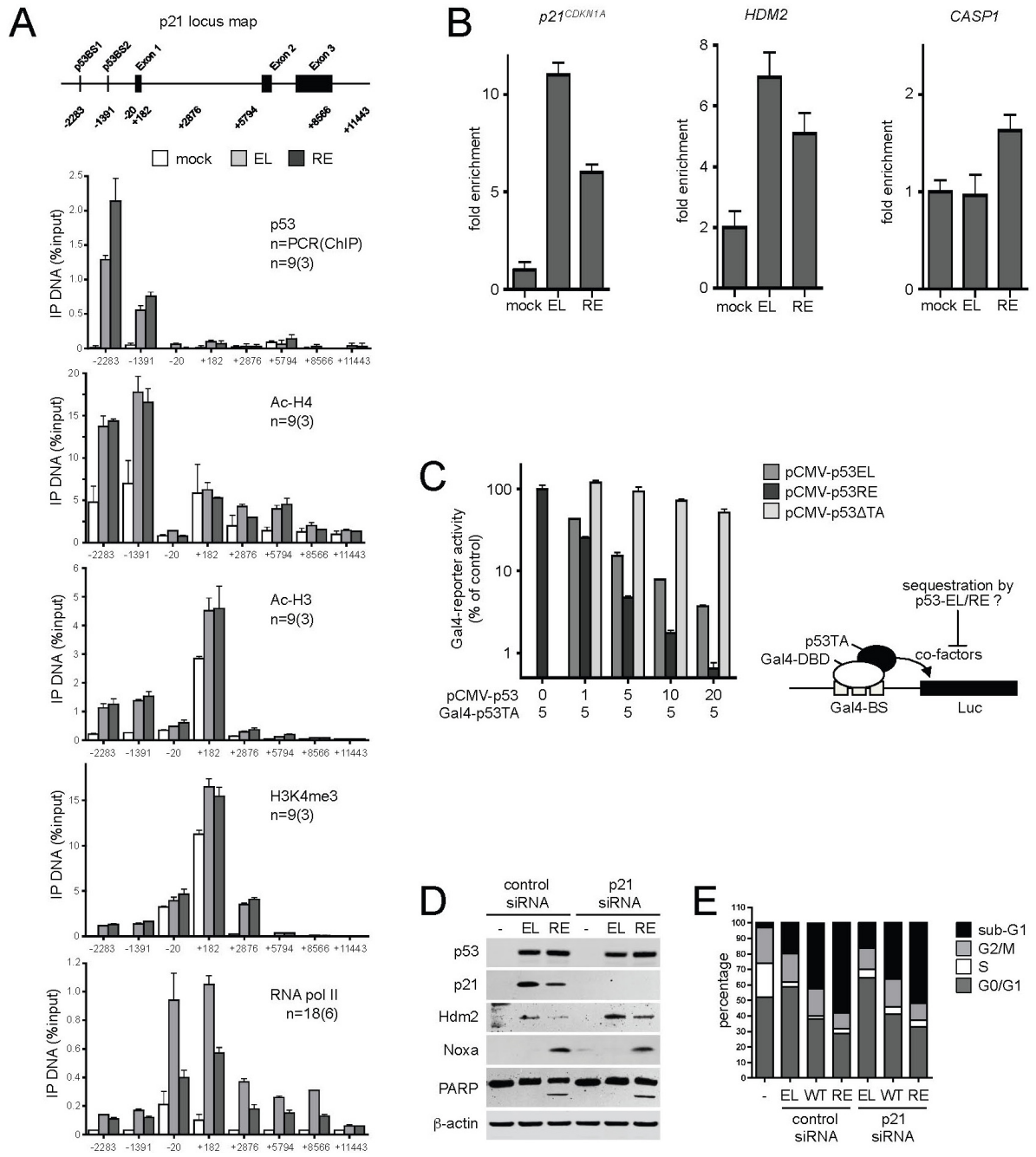

(A, B) *Increased cooperativity leads to reduced p21^{CDKN1A} transcription.* (A) ChIP-PCR analysis of p53 recruitment, histone H4 and H3 pan-acetylation, H3K4 trimethylation and RNA polymerase II binding at the *p21^{CDKN1A}* locus 18 hours following expression of H1 helix mutants EL and RE in Saos-2 cells. Primer binding sites used for ChIP analysis are shown in the schematic view of the *p21^{CDKN1A}* gene locus. Despite higher binding of p53 RE than EL to the 5' and 3' binding sites in the upstream promoter region, p53-induced histone modifications are similar and RNA pol II binding is lower at the transcriptional start site and throughout the transcribed region. Shown is the mean±SD of X chromatin immunoprecipitations each quantified by Y qPCR reactions; n=X (Y). (B) While p53-induced RNA pol II binding at the transcriptional start site is lower for RE at both the *p21^{CDKN1A}* and *HDM2* genes, it is higher at the proapoptotic *CASP1* gene. Data were normalized to RNA pol

II binding in AdGFP infected cells (mock). Shown is the mean ± SD of three ChIPs each quantified by three qPCR reactions; n=3 (3).

(C) *The high cooperativity mutant RE causes a sequestration of co-activators.* H1299 cells were co-transfected with 100 ng Gal4-Luc reporter plasmid, 100 ng pRL-TK Renilla luciferase reporter plasmid for normalization, 5 ng Gal4-p53TA expression plasmid and 0-20 ng pCMV-p53 expression plasmid for EL, RE or p53ΔTA. Gal4-p53TA is a fusion protein consisting of the Gal4 DNA binding domain coupled to the p53 transactivation domain. p53ΔTA is a transactivation-deficient p53 lacking the N-terminal transactivation domain (Stiewe et al., 2003). 48 hours after transfection Firefly luciferase activity was measured and normalized to Renilla luciferase activity. Both transactivation-competent p53 constructs EL and RE, but not the transactivation-deficient p53, reduced Gal4-dependent reporter activity. This inhibitory effect was much stronger for RE than for EL. These data are consistent with our model where highly cooperative p53 (RE) binds to a large number of genomic binding sites and thereby sequesters one or more co-activators. These become limited at other sites and could cause reduced activity of the Gal4-dependent reporter system or reduced expression of for example $p21^{CDKN1A}$.

(D, E) *Role of $p21^{CDKN1A}$ for the apoptotic activity of p53.* Role of p21 induction for (D) the target gene profile and (E) the apoptotic activity of p53 wild-type and H1 helix mutants EL and RE. Saos-2 cells were transfected with p21 or control siRNA and 24 hours later infected with p53 adenoviruses for further 18 hours. Knockdown of p21 did not enhance the apoptotic activity of any p53 protein indicating that high levels of p21 induction are not the cause for the apoptotic defect of the p53 mutant EL.

Figure S4, related to Figure 5: DNA binding cooperativity is crucial for apoptosis in response to DNA damage

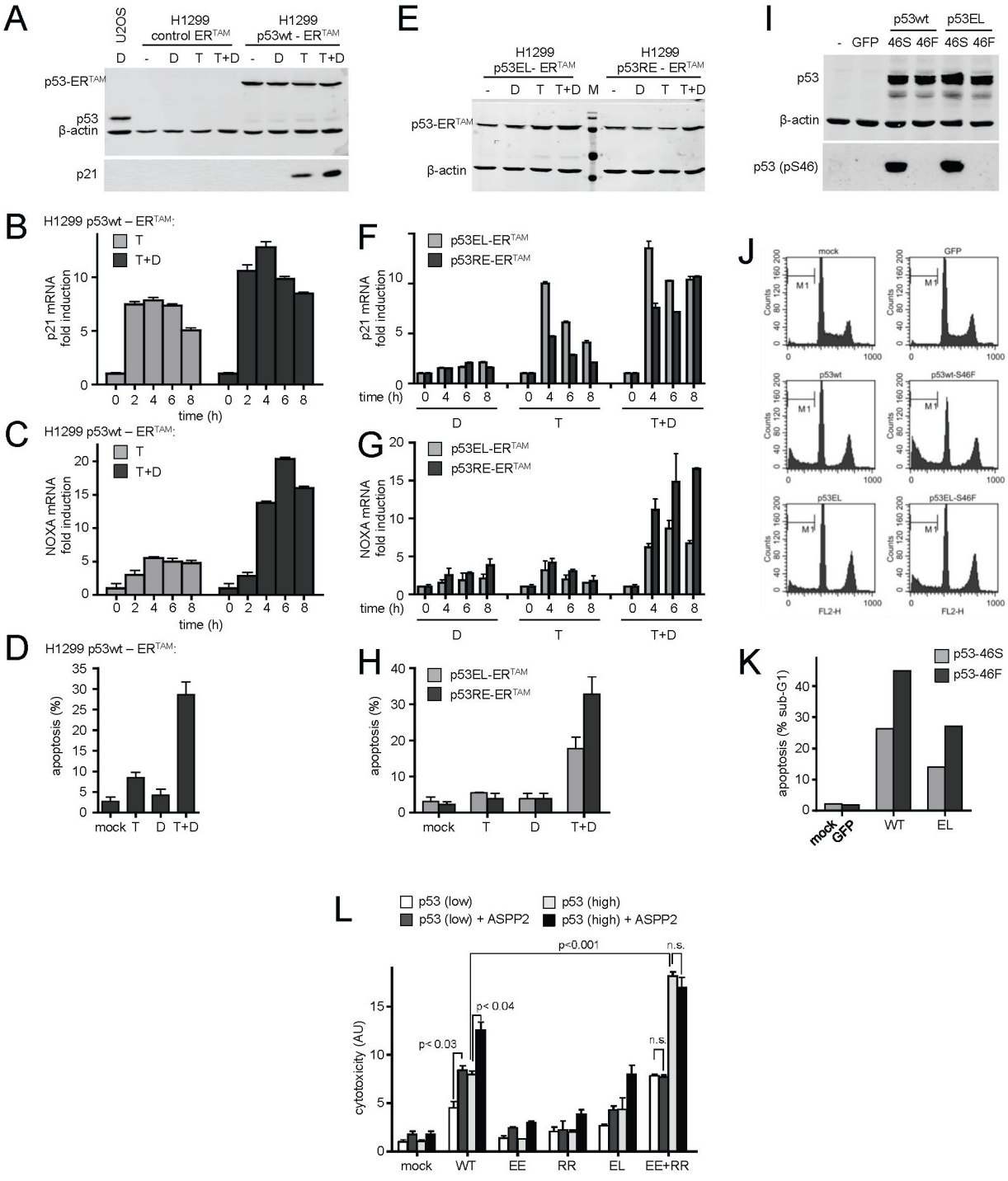

(A-H) *Tamoxifen-inducible p53-ER^{TAM} system.* p53-null H1299 cells were transfected with wild-type (wt) or H1 helix mutant p53 (EL or RE) fused to a modified version of the ligand binding domain of the murine estrogen receptor ER^{TAM} by stable retroviral transduction (pBABEpuro-p53-ER^{TAM}). Expression of the fusion proteins was comparable to expression of endogenous wild-type p53 in U2OS cells after DNA damage. (A-D) Control and p53wt-ER^{TAM} cells or (E-H) p53EL-ER^{TAM} and p53RE-ER^{TAM} cells were treated with either 100 nM 4-hydroxytamoxifen (T) and/or 0.5 µg/ml doxorubicin (D). (A, E) Immunoblot for p53, p21 and β-actin 24 hours after treatment. (B, C, F, G) qRT-PCR for *p21^{CDKN1A}* and *NOXA* mRNA. (D, H) Apoptosis as determined by flow cytometry analysis for active caspase-3 24 hours after

treatment. In this system p53 activation by tamoxifen alone did not induce substantial amounts of apoptosis, which correlated with predominant induction of $p21^{CDKN1A}$. Only upon additional treatment with doxorubicin *NOXA* was induced in a p53-dependent manner and cells entered apoptosis. Both in the absence and presence of DNA damage EL was a stronger activator of $p21^{CDKN1A}$ transcription, while RE was a stronger activator of *NOXA* transcription. Consistently, DNA damage-induced levels of apoptosis were higher when RE (instead of EL) was activated by tamoxifen.

(I-K) *Cooperativity limits the proapoptotic effect of the p53 S46F mutation.* Phosphorylated serine 46 has been shown to be a docking site for the prolyl isomerase Pin1, which displaces the apoptosis inhibitor iASPP from p53 to promote cell death (Mantovani et al., 2007). Mutation of S46 to phenylalanine appears to mimic the effect of phosphorylation and enhances p53's apoptotic function (Nakamura et al., 2006). Here, Saos-2 cells were infected with adenoviruses expressing wild-type (wt) and H1 helix mutant p53 (EL) with either serine (46S) or phenylalanine (46F) at codon 46. (I) Immunoblots for p53 and phospho-p53 (Ser46) demonstrate equal expression levels for all four adenoviruses and confirm the presence of the 46F mutation. (J, K) The 46F mutation increases apoptosis induction by both p53 wild-type and EL. The total amount of apoptosis, however, is reduced in the case of EL. An impaired DNA binding cooperativity therefore reduces both basal and 46F-stimulated apoptosis levels.

(L) *Cooperativity limits the proapoptotic effect of ASPP2.* ASPP2 has been shown to specifically stimulate the proapoptotic function of p53. We therefore analyzed the effect of co-expressing ASPP2 together with p53 H1 helix mutants. For this, Saos-2 cells were co-infected with adenoviruses expressing the indicated p53 mutants and ASPP2 (or AdGFP as a control). Two different doses of p53 adenovirus were used, indicated as *low* or *high*. Cytotoxicity was measured after 26 hours using the CytoTox-Glo Cytotoxicity Assay (Promega). Cytotoxicity was normalized to AdGFP (mock) infected cells. AU, arbitrary units. Results are reported as mean±SD. Statistical significance was calculated by a two-sided unpaired t-test. The data demonstrate that (i) p53-induced cytotoxicity directly correlated with DNA binding cooperativity, (ii) ASPP2 stimulated the cytotoxicity of both p53 wild-type and reduced cooperativity mutants of p53, and (iii) the total level of cytotoxicity was limited by impaired cooperativity. Interestingly, the cytotoxic effect of EE+RR, which displays maximal cooperativity, could not be further enhanced by ASPP2. Together these data indicate that the proapoptotic effect of ASPP2 depends strongly on the DNA binding cooperativity of p53 and suggest that ASPP2 might function by modulating cooperativity.

SUPPLEMENTAL TABLES

Table S1, related to Figure 1: Sequence alignment of the H1 helix region

The amino acid sequence of the H1 helix region of p53, p63 and p73 is shown for several species. Residues that differ from the human p53 sequence are shown in bold, the crucial residues E180 and R181 are shown in white on black background.

	Species	H1 helix region	Identities (BLAST search)
p53	Human	VRRCPHHERCSD-SDGL-AP	bait
p53	Beechey ground squirrel	VRRCPHHERCSD-SDGL-AP	100%
p53	Crab eating macaque	VRRCPHHERCSD-SDGL-AP	100%
p53	Green monkey	VRRCPHHERCSD-SDGL-AP	100%
p53	Guinea pig	VRRCPHHERCSD-SDGL-AP	100%
p53	Japanese macaque	VRRCPHHERCSD-SDGL-AP	100%
p53	Rabbit	VRRCPHHERCSD-SDGL-AP	100%
p53	Rhesus macaque	VRRCPHHERCSD-SDGL-AP	100%
p53	Woodchuck	VRRCPHHERCSD-SDGL-AP	100%
p53	Zea mays (Maize)	VRRCPHHERCSD-SDGL-AP	100%
p53	Blind subterranean mole rat	V**K**RCPHHERCSD-SDGL-AP	94%
p53	Field vole	VRRCPHHERCSD-**G**DGL-AP	94%
p53	Hispid cotton rat	VRRCPHHERCSD-**G**DGL-AP	94%
p53	Mouse	VRRCPHHERCSD-**G**DGL-AP	94%
p53	Rat	VRRCPHHERCSD-**G**DGL-AP	94%
p53	Short-tailed field vole	VRRCPHHERCSD-**G**DGL-AP	94%
p53	Southern vole	VRRCPHHERCSD-**G**DGL-AP	94%
p53	Tundra vole	VRRCPHHERCSD-**G**DGL-AP	94%
p53	Beluga whale	VRRCPHHERCSD**Y**SDGL-AP	94%
p53	Dog	VRRCPHHERCSD**S**SDGL-AP	94%
p53	Donkey	VRRCPHHERCSD**S**SDGL-AP	94%
p53	Horse	VRRCPHHERCSD**S**SDGL-AP	94%
p53	Bovine	VRRCPHHER**S**SD**Y**SDGL-AP	89%
p53	Cat	VRRCPHHERC**P**D**S**SDGL-AP	89%
p53	Pig	VRRCPHHER**S**SD**Y**SDGL-AP	89%
p53	Zebu	VRRCPHHER**S**SD**Y**SDGL-AP	89%
p53	African soft-furred rat	VRRCPHHERC**T**D-**G**DGL-AP	88%
p53	Sheep	VRR**S**PHHER**S**SD**Y**SDGL-AP	84%
p53	Barbel	VRRCPHHER**TP**D-**G**DGL-AP	83%
p53	Golden hamster	VRRCPHHER**S**S**E**-**G**DGL-AP	83%
p53	Channel catfish	VRRCPHHER**SN**D**S**SDG**P**-AP	78%
p53	Chicken	VRRCPHHERC**GGGT**DGL-AP	78%
p53	Chinese hamster	VRRCPHHERSS**E**-**G**D**S**L-AP	77%
p53	Zebrafish	VRRCPHHER**TP**D-**G**D**N**L-AP	77%
p53	Mongolian gerbil	VRRCPHHERCS**ENEA**SD**PR**G**R**AP	69%
p53	Short-tailed gray opossum	V**K**RCPHHEQC**TQHK**DT**L**-AP	63%
p53	Xenopus laevis	V**K**RCPHHERC**VEPGEDA**-AP	58%
p73	Human	V**K**RCP**N**H**E****LGR**D**FNE**G**QS**AP	50%
p73	Green monkey	V**K**RCP**N**H**E****LGR**D**FNE**G**QS**AP	50%
p73	Mouse	V**K**RCP**N**H**E****LGR**D**FNE**G**QS**AP	50%
p73	Barbel	V**K**RCP**N**H**E****LGR**D**FNE**S**QT**AP	45%
p73	Zebrafish	V**K**RCP**N**H**E****LGR**D**FNESQT**AP	45%
p63	Human	V**K**RCP**N**H**E****LSREFNE**G**QI**AP	45%
p63	Chicken	V**K**RCP**N**H**E****LSREFNE**G**QI**AP	45%
p63	Mouse	V**K**RCP**N**H**E****LSREFNE**G**QI**AP	45%
p63	Rat	V**K**RCP**N**H**E****LSREFNE**G**QI**AP	45%
p63	Sheep	V**K**RCP**N**H**E****LSREFNE**G**QI**AP	45%
p63	Xenopus laevis	V**K**RCP**N**H**E****LSREFNE**G**QI**AP	45%

Table S3, related to Figure 3: Validation of ChIP-Chip data by ChIP-PCR

A total of 75 binding sites (25 EL-only, 25 RE-only and 25 common EL/RE sites) were randomly chosen from Table S2 for validation by ChIP-PCR. All validation experiments were performed on independent chromatin immunoprecipitations from Saos-2 cells infected with adenoviruses expressing the p53 H1 helix mutants EL or RE or GFP as a control. Precipitated DNAs were quantified by qPCR in triplicate measurements. Data for 14 binding sites were excluded from further analysis either because of a lack of the expected PCR product or because of non-specific PCR amplification by-products. The results for the remaining 61 binding sites are reported as the fold enrichment (EL- or RE-samples versus GFP-controls) ± SD.

ChIP-Chip region#	chromosome	start	end	Gene symbol	NCBI accession number (mRNA)	site specification by ChIP-Chip		fold enrichment in ChIP-PCR	
						EL	RE	EL	RE
region146	chr16	87523599	87524294	CBFA2T3	NM_175931	+	-	0.81	0.66
region108	chr14	20340849	20340884	RNASE1	NM_002933	+	-	0.94	0.78
region155	chr17	7387032	7387069	TNFSF12	NM_003809	+	-	1.02	1.08
region74	chr13	113650271	113650302	FAM70B	NM_182614	+	+	1.30	1.09
region9	chr1	46412883	46412948	TSPAN1	NM_005727	+	+	1.25	1.30
region227	chr22	29291822	29291994	GAL3ST1	NM_004861	+	-	0.77	1.30
region153	chr3	196937378	196937418	MUC20	NM_152673	+	+	1.19	1.32
region54	chr11	46365238	46365301	CHRM4	NM_000741	+	+	1.15	1.33
region235	chr3	180267932	180268120	ZMAT3	NM_022470	+	-	1.02	1.36
region380	chr11	63360514	63360552	MARK2	NM_001039468	-	+	1.10	1.38
region146	chr22	17226395	17226677	DKFZp434K191	NM_001029950	+	+	1.26	1.40
region308	chr8	86884594	86884745	REXO1L1	NM_172239	+	+	1.45	1.41
region162	chr4	8969381	8969564	DUB3	NM_201402	+	+	1.04	1.49
region290	chr7	104539695	104539793	MLL5	NM_182931	+	-	1.71	1.53
region207	chr7	116379429	116379503	ST7	NM_021908	+	+	1.65	1.55
region9	chr1	31538650	31538684	WDR57	NM_004814	+	-	1.49	1.57
region64	chr12	6587292	6587378	CHD4	NM_001273	+	+	1.57	1.66
region30	chr1	146844664	146844981	NBPF15	NM_173638	+	-	1.34	1.71
region344	chrX	56272637	56272743	KLF8	NM_007250	+	-	2.03	1.81
region222	chr8	86761300	86761411	REXO1L1	NM_172239	+	-	2.14	1.86
region31	chr1	148102059	148102240	HIST2H4A	NM_003548	+	+	1.21	1.88
region56	chr10	42947956	42948127	RET	NM_020975	+	-	1.47	1.91
region137	chr20	23916066	23916313	GGTLA4	NM_178311	+	+	1.60	1.98
region803	chr18	33404236	33404545	BRUNOL4	NM_020180	-	+	1.15	2.05
region470	chr12	109619357	109619396	HVCN1	NM_001040107	-	+	1.30	2.07
region1071	chr22	41743811	41743926	PACSIN2	NM_007229	-	+	1.97	2.15
region207	chr2	106175476	106175551	UXS1	NM_025076	+	-	1.76	2.35
region11	chr1	46372094	46372163	PIK3R3	NM_003629	+	-	1.58	2.37
region185	chr19	39916233	39916420	ZNF181	NM_001029997	+	-	2.05	2.42
region317	chr9	35719717	35719753	TLN1	NM_006289	+	-	3.15	2.52
region220	chr21	25902841	25903091	MRPL39	NM_017446	+	-	2.02	2.69
region126	chr2	37446250	37446710	QPCT	NM_012413	+	+	1.56	2.71
region44	chr1	19409875	19409998	ZUBR1	NM_020765	-	+	1.69	2.93
region1602	chr9	135218731	135218841	SURF4	NM_033161	-	+	2.17	5.12
region1424	chr7	23476976	23477068	IGF2BP3	NM_006547	-	+	4.45	5.36
region75	chr14	22459383	22459420	PRMT5	NM_001039619	+	+	1.77	5.43
region88	chr1	45013188	45013332	RPS8	NM_001012	-	+	2.06	6.03
region258	chr5	43076735	43076927	LOC389289	NM_001014279	+	-	3.73	6.11
region101	chr17	22644402	22644475	WSB1	NM_015626	+	+	2.27	6.38
region1019	chr21	21287071	21287144	NCAM2	NM_004540	-	+	1.76	7.83
region119	chr19	48955614	48955652	KCNN4	NM_002250	+	+	1.30	8.40
region91	chr16	29530443	29530660	BOLA2	NM_001031833	+	+	2.04	9.04
region22	chr1	12214028	12214286	VPS13D	NM_015378	-	+	1.52	10.68
region326	chr10	104470389	104470495	SFXN2	NM_178858	-	+	3.51	13.64
region1613	chrX	48253549	48253766	PORCN	NM_203474	-	+	2.76	14.22
region191	chr6	30965887	30966341	DDR1	NM_013994	+	+	4.25	15.93
region180	chr5	141363905	141364107	GNPDA1	NM_005471	+	+	3.00	16.07
region1352	chr6	31881771	31881962	LSM2	NM_021177	-	+	2.68	16.49
region11	chr1	52607409	52607446	CC2D1B	NM_032449	+	+	2.68	19.16
region1136	chr3	137224218	137224593	PPP2R3A	NM_181897	-	+	7.31	21.76
region247	chrX	72220010	72220874	LOC340529	NM_001012977	+	+	7.19	22.01
region1001	chr20	35588233	35588540	BLCAP	NM_006698	-	+	2.34	27.60
region665	chr16	28455807	28456242	NUPR1	NM_001042483	-	+	3.37	27.73
region1541	chr8	108577354	108577942	ANGPT1	NM_001146	-	+	5.67	31.49
region515	chr13	113007403	113008050	LAMP1	NM_005561	-	+	4.43	35.67
region1307	chr5	175756580	175757251	CLTB	NM_001834	-	+	1.66	36.09
region967	chr2	238808842	238809372	HES6	NM_018645	-	+	4.77	38.41
region233	chr9	28290739	28291140	LRRN6C	NM_152570	+	+	23.86	50.10
region524	chr14	22410320	22410644	LRP10	NM_014045	-	+	4.15	52.83
region270	chr6	82526424	82526606	FAM46A	NM_017633	+	-	54.07	69.23
region1206	chr4	52612677	52613481	SPATA18	NM_145263	-	+	30.13	78.61

Table S4, related to Figure 3: Functional annotation of binding sites by GATHER

The lists of binding sites identified by ChIP-Chip analysis as common EL/RE-sites or RE-only sites were annotated with GATHER (http://gather.genome.duke.edu/) using Gene Ontology terms with the option “infer from network”. Shown are all Gene Ontology terms that met the threshold *P*-value of 0.01 and Bayes Factor ≥20.

common EL/RE-sites	Gene Ontology	#ŹGenes	*P-v*alue	Bayes Factor
1	regulation of cell cycle	65	0.005	37
2	response to stress	97	0.006	32
3	response to stimulus	160	0.009	26
4	cell proliferation	102	0.01	23
5	regulation of cellular physiological process	67	0.01	22

RE-only sites	Gene Ontology	#ŹGenes	*P-v*alue	Bayes Factor
1	response to stress	300	0.001	69
2	organismal physiological process	510	0.003	52
3	immune response	251	0.003	48
4	cell-cell signaling	195	0.004	45
5	response to stimulus	521	0.004	45
6	defense response	266	0.004	42
7	response to pest, pathogen or parasite	172	0.004	40
8	regulation of cellular physiological process	196	0.004	39
9	response to biotic stimulus	291	0.004	39
10	regulation of cellular process	251	0.005	39
11	cell proliferation	311	0.005	37
12	response to external biotic stimulus	176	0.005	36
13	cell communication	817	0.005	36
14	response to abiotic stimulus	142	0.006	34
15	response to chemical substance	99	0.006	33
16	sensory perception of chemical stimulus	7	0.006	32
17	perception of smell	5	0.007	31
18	regulation of cell cycle	139	0.008	27
19	response to wounding	109	0.008	27
20	pos. regulation of cellular physiological process	102	0.009	26
21	humoral immune response	72	0.01	24
22	positive regulation of physiological process	119	0.01	23
23	morphogenesis	308	0.01	23
24	regulation of programmed cell death	96	0.01	23
25	organogenesis	257	0.01	22
26	organ development	257	0.01	22
27	regulation of apoptosis	95	0.01	22
28	programmed cell death	144	0.01	22
29	apoptosis	143	0.01	21
30	DNA repair	75	0.01	21
31	response to DNA damage stimulus	80	0.01	21
32	death	150	0.01	20
33	cell death	149	0.01	20
34	regulation of body fluids	50	0.01	20
35	taxis	55	0.01	20
36	chemotaxis	55	0.01	20
37	inflammatory response	78	0.01	20

Table S5, related to Figure 3: De novo motif discovery

Binding sites from ChIP-Chip analysis that were validated by ChIP-PCR (see Figure 3A and Table S3) as true p53 binding sites were grouped into common EL/RE-sites (n=6) and RE-only sites (n=22). The sequences were analyzed with MEME (http://meme.sdsc.edu/meme/) for *de novo* motif discovery. All MEME results were tested with JASPAR (http://jaspar.genereg.net/) for their similarity to the p53 consensus binding sequence. Shown are the motifs that showed the highest similarity to V$P53_01 and V$P53_02 from the TRANSFAC database.

MEME analysis: common EL/RE-sites validated by ChIP-PCR

NAME	STRAND	START	P-VALUE	MOTIF
region270	+	54	1.12e-08	TATGTCTTCT ACAAGTCTGGACATG TCTTGGAACA
region233	+	137	1.12e-08	CCTACATTGA ACATGTCAGAACATG TCAGCTTTGA
region1206	+	205	1.74e-08	GGAAGGAAGG ACATGTGTGTACATG CCCTTGTCTC
region247	+	448	4.46e-08	CTAAGGCCTT GCATGTCCGAACATG TCCAAACTTC
region1136	+	200	1.21e-07	GGAACCAGCT GCATGTCAGGACAAG CATAGATTGT
region1541	+	365	1.01e-06	AATGAATTGC AGAAGTGTGTTCATA ATTTAATAGG

MEME analysis: RE-only sites validated by ChIP-PCR

NAME	STRAND	START	P-VALUE	MOTIF
region191	+	5	2.43e-04	TAGA GCATGT AAATCAGATA
region11	+	221	2.43e-04	GACTAACTTA GCATGT TCAGGCATGT
region101	-	30	2.43e-04	ATTTGTACAG GCATGT GACACCAAGC
region75	-	315	2.43e-04	TTAGACCCAG GCATGT TCAGATCTGT
region1001	+	171	2.43e-04	GAAATGGAAT GCATGT GTTTCAAAGA
region967	-	213	2.43e-04	GGGCATGTCC GCATGT CAGCTTCACT
region326	-	5	2.43e-04	CTTGATTTCT GCATGT TAAG
region665	-	330	2.43e-04	TTTTGTTCGG GCATGT GTGTGCTTGC
region515	+	264	2.43e-04	ACAAGTGAAA GCATGT CATTTCTGCA
region180	+	142	4.86e-04	TGATTTAGAT GCTTGT TTATTGGCTT
region119	-	347	4.86e-04	ACAAGCCGGT GCTTGT TTGTAGCCCT
region1019	+	45	4.86e-04	CATGTTCTAG GCTTGT TAAGTTTTCT
region91	-	50	7.11e-04	GCACCACCAT GCAGGT CAAAGCCGGG
region1602	-	78	7.11e-04	CAGGGGTGAG GCAGGT TTCTGCTCAT
region1307	+	319	9.74e-04	CAGTGTTCAG TCATGT CCCCACAGCC
region258	-	151	1.20e-03	TCTTAGCCTC GCTGGT ATCAGGTTCC
region524	-	189	1.46e-03	TCAGTACTTT TCTTGT CCCAGGGTCT
region1352	+	167	1.69e-03	GTGGGAAGGA GCATGG TAGGGAGGAG
region88	+	1	2.66e-03	TCTGGT GGCTTTAATT
region1424	+	22	2.66e-03	TAAAGGGTTA TCTGGT CTGGGCGGAT
region1613	-	117	3.37e-03	AACGCTGTAA TCATGG TACTTTGGGA
region22	+	104	3.37e-03	TAGGGCCTGA ACTTGT TTACAAACTG

SUPPLEMENTAL EXPERIMENTAL PROCEDURES

EBI ArrayExpress data

All microarray data have been submitted to EBI Array Express (http://www.ebi.ac.uk/arrayexpress/).
cDNA microarrays: E-MEXP-1209
ChIP-Chip data: E-MEXP-1748

Plasmids, RNAi

p53 (codon 72P) cDNA was amplified and cloned into pENTR-vector using pENTR/D-TOPO Cloning Kit (Invitrogen). p53 point mutants were generated using the QuickChange Multi Site Directed Mutagenesis Kit (Stratagene). Mutant p53 cDNAs were recombined into Gateway-adapted destination vectors pEXP1-DEST (Invitrogen), pcDNA6.2/nLumio-DEST (Invitrogen), pAdTrackCMV (He et al., 1998), pMSCV-IRES-GFP and pMSCVpuro (Clontech) using Gateway LR Clonase II Enzyme Mix (Invitrogen). H1 helix mutations were introduced into pBABEpuro-p53-ER^{TAM} (Littlewood et al., 1995) by site-directed mutagenesis (Stratagene). Luciferase plasmids p21-Luc, BAX-Luc, p53AIP1-Luc, and p53cons-Luc have been described (el-Deiry et al., 1993; Miyashita and Reed, 1995; Oda et al., 2000; Stiewe and Putzer, 2000). Saos-2 cells were transfected with p21 SMARTpool siRNA (Dharmacon) using RNAiMAX (Invitrogen) at a final concentration of 10 nM according to the manufacturer's protocol.

RNA isolation, qRT-PCR, microarray experiments

RNA isolation and cDNA synthesis were performed using the RNeasy Mini Kit (Qiagen) and Omniscript Reverse Transcriptase (Qiagen) as previously described (Cam et al., 2006). Gene expression was quantified by qRT-PCR using SYBR Green Jumpstart Taq ReadyMix (Sigma) on an ABI Prism 7000 (Applied Biosystems) or Mx3005P (Stratagene). Expression data were normalized to GAPDH and the mock sample using the $\Delta\Delta$Ct method.

cDNA microarrays

For microarray analysis, Saos-2 cells were infected with adenoviruses expressing either GFP or GFP together with p53 (WT, EE, EL, RE). Total RNA was purified with RNeasy spin columns (Qiagen). After mRNA amplification with MessageAmp II aRNA Kit (Ambion), Cy3 and Cy5 labeled cDNA probes were generated in a two-step procedure using the CyScribe Post-Labelling Kit (Amersham Biosciences). The first step involved the incorporation of amino allyl-dUTP during cDNA synthesis by CyScript-RT. In the second step, the amino allyl-modified cDNA was chemically labeled with CyDye NHS-esters. The coupling reactions of amino allyl-modified cDNA were performed separately with Cy3 and Cy5. Cy3- and Cy5-labeled probes were purified with Qiagen spin columns, combined and hybridized to microarray slides for 16 h at 55°C and washed at a stringency of 0.1xSSC/0.1% SDS and 0.1xSSC. The microarrays contained 11,551 DNA spots from the human cDNA library 'Human Sequence-Verified cDNA UniGene Gene Sets gf200, gf201 and gf202' (ResGen/Invitrogen/Cat.No. 97001.V). The microarrays were scanned and quantitated using Scan Array Express (Perkin Elmer). Each experiment was performed as a sandwich hybridization, i.e., instead of a coverslip, a second microarray slide was used. This provides a replicated measurement for each hybridization that can be used for quality control and to reduce technical variability. For each spot, median signal and background intensities for both channels were obtained. To account for spot differences, the background-corrected ratio of the two channels was calculated and log2 transformed. To balance the fluorescence intensities for the two dyes, as well as to allow for comparison of expression levels across

experiments, the raw data were standardized. We used the printtip-lowess normalization to correct for inherent bias on each chip (Yang et al., 2001). The R environment (http://www.r-project.org) was used for gene filtering and normalization of the data. Data were processed with GeneSpring 7.0 (Silicon Genetics) to extract a list of 186 genes that were changed > 3-fold following expression of wild-type p53 (Table S6) and for generation of the heatmap (Figure 4A). The complete set of microarray data has been deposited to EBI Array Express (http://www.ebi.ac.uk/arrayexpress) under accession number E-MEXP-1209.

ChIP-PCR

The ChIP assay was essentially performed as described (Cam et al., 2006). Each ChIP was repeated at least three times for each sample. The precipitated DNA fragments were amplified by qPCR (three replicates) with primers for p53 target gene promoters and GAPDH or an intragenic region in the *p21*^{CDKN1A} locus as a control.

ChIP-Chip

Chromatin immunoprecipitation
Saos-2 cells were infected with adenovirus encoding GFP or GFP together with the p53 H1 helix mutants EL or RE. The amount of p53 protein was confirmed by Western Blot to be equal in all EL and RE samples. Cells were fixed 18 hours after infection in fresh 1% paraformaldehyde (PFA) for 10 min at room temperature (RT). To quench unreacted PFA, glycine was added to 125 mM end concentration and the cells were incubated further for 5 min at RT. Cells were washed with ice-cold PBS twice and scraped from the dishes in ice-cold phosphate buffered saline supplemented with proteinase inhibitor (Complete, Roche). Cells were pelleted at 700 g for 5 min at 4°C and lysed at a concentration of $1x10^7$ cells/ml in SDS lysis buffer (1% SDS, 10 mM EDTA, 50 mM Tris pH 8.1) supplemented with proteinase inhibitor. Cells were sonicated on ice in 700 µl aliquots six times at 30% power for 10 s followed by a 50 s pause on a SONOPLUS sonifier (BANDELIN electronic, Germany) with sonotrode MS72 followed by centrifugation at 10,000 g for 10 min at RT. Supernatants were stored in 1 ml aliquots at -80°C. Agarose gel electrophoresis confirmed shearing of crosslinked DNA into a smear in the range of 200-800 bp. For one chromatin IP, sheared chromatin from $1x10^7$ cells was diluted 1:10 with Dilution Buffer (0.01% SDS, 1.1% Triton X-100, 1.2 mM EDTA, 16.7 mM Tris-HCl pH 8.1, 167 mM NaCl) and after 1 h of pre-clearing p53 was precipitated with 10 µg monoclonal p53-antibody (clone DO-1) over night at 4°C. Mock-chromatin was immunoprecipitated in the absence of antibody. 1% input was removed from each sample. Complexes were bound to Protein G agarose beads (Fast Flow, Millipore) for 1 h at 4°C and washed once with Low Salt Immune Complex Wash Buffer (0.1% SDS, 1% Triton X-100, 2 mM EDTA, 20 mM Tris-HCl pH 8.1, 150 mM NaCl), once with High Salt Immune Complex Wash Buffer (0.1% SDS, 1% Triton X-100, 2 mM EDTA, 20 mM Tris-HCl pH 8.1, 500 mM NaCl), once with LiCl Immune Complex Wash Buffer (0.25 M LiCl, 1% IGEPAL-CA630, 1% deoxycholic acid (sodium salt), 1 mM EDTA, 10 mM Tris-HCl pH 8.1), and twice with TE (10 mM Tris-HCl, 1 mM EDTA, pH 8.0) for at least 30 min at 4°C. Complexes were eluted with Elution buffer (1% SDS, 0.1 M $NaHCO_3$) for 20 min at RT. Crosslinks were reversed at 65°C in 200 mM NaCl over night followed by RNase A (37°C, 30 min) and Proteinase K digestion (45°C, 2 h). DNA was precipitated in the presence of glycogen as a carrier with 0.1 Vol. 3 M sodium acetate pH 5.0 and 2.5 Vol. ethanol at -80°C over night. The DNA pellet was washed with 70% ethanol, dried and dissolved in TE. For purification the GeneChip® Sample Cleanup Module (Affymetrix) was used. DNA concentration was measured with PicoGreen (PicoGreen dsDNA Quantitation reagent, Molecular Probes).

Promoter array hybridization
The ChIP DNA was amplified, fragmented, labeled, and hybridized to GeneChip® Human Promoter 1.0R Arrays exactly according to the manufacturer's protocol. For the initial Sequenase Reaction 9 ng DNA were used. The DNA was amplified for 15 cycles. The

number of cycles was optimized to avoid saturation and to ensure that the IP enrichment was maintained. Enrichment was verified by qPCR using primers for the 5' p53 binding site in the p21 promoter. 3-4 µg of the amplified DNA were fragmented, labeled and finally hybridized to the arrays. Each ChIP-Chip experiment was repeated three times for each sample yielding three arrays each for EL, RE and control.

Data analysis
The Affymetrix CEL-files were first analyzed with TAS (Tiling Analysis Software, Affymetrix) for normalization and computation of genomic intervals bound by either p53EL or p53RE. In detail, arrays were quantile-normalized within treatment/control replicate groups and then all were scaled to have a median feature intensity of 500. Using the Affymetrix BPMAP file each perfect match (PM) probe was mapped to its position in the genome (NCBIv36). For each genomic position to which a probe mapped, a data set was generated consisting of all probes mapping within a window of ±250 bp. A Wilcoxon Rank Sum test was applied to the $\log_2$-transformed PM signal intensities from the treatment (three EL or three RE) and control arrays within the local data set, testing the null hypothesis of equality of the two population distribution functions against the alternative of a positive difference in location between the probability distribution of the treatment and that of the control. The Wilcoxon test was applied in a sliding window across the genome. The *P*-values were $-10\log_{10}$ transformed. Genomic positions belonging to p53 binding sites were defined by applying a *P*-value cutoff of 0.001 ($-10\log_{10}=30$). Resultant positions separated by <150 bp were merged and regions with a length of less than 30 bp were rejected (Table S2).
Binding data for individual genes were visualized with IGB (Integrated Genome Browser, Affymetrix). The two lists of EL- and RE-binding sites were intersected with Galaxy (http://main.g2.bx.psu.edu) to obtain lists of EL-only, common EL/RE, and RE-only sites (inset Figure 3A).

Functional annotation
The frequency of transcription factor binding motifs enriched in the identified genomic regions was determined with Cisgenome (http://www.biostat.jhsph.edu/~hji/cisgenome) applying a Likelihood ratio of 500 and Order of Background Markov Chain of 3. The same software was used to annotate the detected genomic regions with the closest genes (10,000 bp from TSS, Genome hg18). A functional annotation of the resulting gene lists with Gene Ontology terms was performed with GATHER (http://gather.genome.duke.edu) using as a significance cutoff a *P*-value of 0.01 and a Bayes Factor of 20. *De novo* motif discovery was done with MEME (Multiple Em for Motif Elicitation; http://meme.nbcr.net/meme) using the sequences of genomic regions confirmed by ChIP-PCR to contain p53 binding elements. All MEME results were tested with JASPAR (http://jaspar.genereg.net) for their similarity to the p53 consensus sequence. The MEME motifs, which showed the highest similarity to the p53 consensus, were used to generate sequence logos using WebLogo V2.8.2 (http://weblogo.berkeley.edu). Binding sites for which ChIP-PCR data were available, were screened for 20-meric p53 (V$P53_01), decameric p53 (V$P53_02) and E2F (V$E2F_01) motifs using MAPPER (http://mapper.chip.org) with a threshold motif score of 3. In addition, all ChIP-Chip sequences identified on RE arrays only (RE-only sites) or on both EL and RE arrays (common EL/RE sites) were screened with the spacer-tolerant p53MH algorithm for the top scoring p53 full site in each sequence without applying filtering and gap weights (Hoh et al., 2002). Sites yielding a threshold score of at least 80 were analyzed for the length of a central spacer. The spacer length distribution is shown in Figure S7A-B.

In vitro translation, BN-PAGE, SDS-PAGE, immunoblotting

p53 proteins were expressed *in vitro* using the TNT T7 Quick Coupled Transcription/Translation System (Promega). 40 µl TNT master mix were added to 1.2 µg DNA and 1 µl [^{35}S] labeled or unlabeled methionine and incubated at 30°C for 1.5 h. 2 µl of the TNT reaction were separated under non-denaturing conditions on NativePAGE Novex 3-12% Bis-Tris gels and under reducing, denaturing conditions on NuPAGE Novex 4-12%

Bis-Tris gels (Invitrogen) and visualized by autoradiography or immunoblotting. For western blot analysis, cells were lysed in RIPA buffer (50 mM Tris-Cl, pH 7.4, 150 mM NaCl, 1% NP-40, 0.5% sodium deoxycholate, 0.1% SDS) and 50-100 µg of total cellular protein were separated by SDS-PAGE and transferred to nitrocellulose membranes. Enhanced chemiluminescence (Thermo Scientific) or fluorescence (Odyssey Infrared Imaging System, LI-COR) was used for detection.

Electrophoretic mobility shift assays

Electrophoretic mobility shift assays (EMSAs) were performed in 20 µl mixtures containing 20 mM HEPES (pH 7.8), 0.5 mM EDTA (pH 8.0), 6 mM $MgCl_2$, 60 mM KCl, 1 mM DTT, 120 ng salmon sperm DNA, 50 ng α-p53 antibody (Pab421), 2.5-5.0 nM of [^{32}P] oligonucleotide, and 1-2 µl of *in vitro* translated protein. After 40 min incubation at room temperature reaction mixtures were subjected to electrophoresis on a 3.5% native polyacrylamide gel (37.5:1 acrylamide/bisacrylamide) containing 0.5× Tris-borate-EDTA buffer at 150 V for 120 min at room temperature. For supershift analysis 0.5 µg α-V5 and/or 0.4 µg α-His antibody were added. When time-resolved dissociation experiments were performed, 100-fold self-competitor (oligonucleotide with the same sequence as the labeled probe without the [^{32}P] labels) was used and the samples were loaded onto the running gel to minimize the time before the samples entered the gel. DNA-protein complexes were quantified by phosphorimaging (FLA-3000, Fujifilm).

Immunoprecipitation

Mitochondria were isolated using the Qproteome Mitochondria Isolation Kit (QIAGEN). For analysis of Bak and Bax activation, cells were harvested, washed in ice-cold PBS, lysed in CHAPS buffer (150 mM NaCl, 10 mM HEPES, pH 7.4, 1% CHAPS, protease inhibitors), and pre-cleared with protein G agarose. 500 µg of pre-cleared protein extract were incubated in the presence of 1 µg of the primary antibody (Bax, clone 3, BD; Bak, TC-100, Calbiochem) at 4°C over night and protein G agarose at 4°C for 1 h. The immune complex was sedimented at 3000 g and 4°C for 2 min and washed twice in CHAPS buffer. Precipitated proteins were eluted in LDS sample buffer (Invitrogen) and analyzed by western blot.

Cell cycle and apoptosis analysis, GFP tracking

For cell cycle analysis cells were fixed in 70% ethanol and stained with 10 µg/ml propidium iodide in the presence of 100 µg/ml RNaseA. The samples were measured on a FACSCalibur (BD Biosciences) and analyzed with CellQuest and ModFit LT (BD Biosciences). Apoptotic H1299 cells were measured using staining for active caspase-3 with FITC-DEVD-FMK according to the manufacturer's protocol (CaspGLOW Caspase-3 Staining Kit, Biovision). For GFP tracking the percentage of GFP-positive (FL-1) and/or DsRed-positive (FL-3) cells was analyzed with WinMDI.

Luciferase assay, Caspase activity and Cytotoxicity assay

Plasmid transfections for luciferase assay were performed with 1 µg total DNA (200 ng reporter plasmid, 50-200 ng p53 expression vector) per 10^4 cells in a 24-well plate using the Escort V Transfection Reagent (Sigma). Luciferase activity was measured 48 h later using a luciferase assay system (Promega). Apoptosis was quantified using the Caspase-Glo 3/7 Assay (Promega). Cytotoxicity was quantified using the CytoTox-Glo Cytotoxicity Assay (Promega).

Primer sequences

Gene/Sequence	Application	Sense primer	Antisense primer
14-3-3σ	ChIP	CTTGGAAACCCTGTAGCATTAGC	GGGACCAAAGACGAGATCCTT
BAX	ChIP	AGATCATGAAGACAGGGGCCCTTT	TGGAGTGAGGGTGCAGAATCAGAA
BAX ChIP-PET site	ChIP	GGGTGAGGCGGGAGGCAGAC	AGGAAGGATCCCGGACGGGC
BBC3	ChIP	GCGAGACTGTGGCCTTGTGT	CGTTCCAGGGTCCACAAAGT
BTG2	ChIP	AGACGAGGCAAAGCGGTAAA	TCCAACCATTCACGGTCAGA
CASP1	ChIP	GGCCTGTACATGTATTGG	GATCTATCCAAGGGCTGGTG
CASP1 TSS	ChIP	CAAAAAGGAAGGCGAAGCAT	TAAAAGACTCACCGGCCATG
FAS	ChIP	AGCCTGCAGCCTTCAGAACAGATA	CTGCTTCGGTGCTGACTTATTTCC
FDXR	ChIP	AGATCCCGGTGGTGTACG	TCCGTATCATCCTCCATTCA
GADD45	ChIP	AGCGGAAGAGATCCCTGTGA	CGGGAGGCAGGCAGATG
GAPDH	ChIP	GTATTCCCCCAGGTTTACAT	TTCTGTCTTCCACTCACTCC
HDM2	ChIP	GTTCAGTGGGCAGGTTGAC	CAGCTGGAGACAAGTCAGGA
HDM2 TSS	ChIP	CTGTGTGTCGGAAAGATGGAGCAA	CGAAAGCAGCAGGATCTCGGT
NOXA	ChIP	CAGCGTTTGCAGATGGTCAA	CCCCGAAATTACTTCCTTACAAAA
p21-2283 (5' BS)	ChIP	AGCAGGCTGTGGCTCTGATT	CAAAATAGCCACCAGCCTCTTCT
p21-1391 (3' BS)	ChIP	CTGTCCTCCCCGAGGTCA	ACATCTCAGGCTGCTCAGAGTCT
p21-20	ChIP	TATATCAGGGCCGCGCTG	GGCTCCACAAGGAACTGACTTC
p21+182	ChIP	CGTGTTCGCGGGTGTGT	CATTCACCTGCCGCAGAAA
p21+2786	ChIP	GCACCATCCTGGACTCAAGTAGT	CGGTTACTTGGGAGGCTGAA
p21+5794	ChIP	CTGGAGACTCTCAGGGTCGAA	CACATGTCCGCACCTGTCAT
p21+8566	ChIP	CCTCCCACAATGCTGAATATACAG	AGTCACTAAGAATCATTTATTGAGCACC
p21+11443	ChIP	TCTGTCTCGGCAGCTGACAT	ACCACAAAAGATCAAGGTGAGTGA
p53AIP1	ChIP	GCTGCCCTCCCTTCTCCTAG	CCCCGACTTTGGAGTAGTCTGA
PMAIP1/NOXA	ChIP	TTTTGCTAAACATCCACAATGGGC	CGTGTTTGAGTTGGGAAGGGATTT
from EL only list			
region9	ChIP	CAACGGATCCACCTTAGCAT	CTTCTGTGGCACCCAAGATT
region11	ChIP	GGGAAACAGAATAGAGCCCTT	GCTCGAGTGCTCAAACCAAT
region30	ChIP	CCATATAAGATCCTGCAGACAAA	CCAAGTTTCCCTCAGAGTCAC
region56	ChIP	GCTTGCGGTCTGAAACTACC	TCATCTGAGAGGATGCAGGTC
region108	ChIP	TCCTTCCTCACGTCCTTGAT	GTTTGGCTTCCAAGAGGAAA
region146	ChIP	AGCTGCATGGTCCACGTAA	TGCAGCTGTGGGTATTGGTA
region155	ChIP	GCGAGTTGTGAGAAATGCAA	ACAACATTCTGCCTCACGTC
region185	ChIP	CTCCCAGGATGAGGGTCTGT	CCCTGGAAGGACTTGGAAAT
region207	ChIP	CTGGGAGCAGGAGCTAGAAC	TCTAAACCCTTGCAGCGACT
region220	ChIP	GGAGGGCGGGTGTATCTT	AAGGTTAAATGGGTACAGGCTCT
region227	ChIP	CAGGTGTCACCATTTAGGGA	TGCTTAGTGTGGGATGAATGA
region235	ChIP	TCTCCCTTTACCTGATAATGAGC	GCCCTGGAGGAGCTATGTAA
region258	ChIP	ACTGGCAAACGTGCTGATAC	TCCGGGTTCTGTCTGGAG
region270	ChIP	GTCTGGACATGTCTTGGAACA	AGGTGCCTGTCTCATGTCTG
region290	ChIP	TTCATCTGAGCAACTTTCACAA	TGAGGTGATGGAGGACAGTG
region308	ChIP	CGATGAGGATGGTTTGGG	CAAGACGAGCATCACGTTG
region317	ChIP	TAACCACAGCCTCATCCTCA	TCATCAGCAGCCACTTTAGC
region344	ChIP	TCCTAGACGGACAGGGAAAT	ATCAGCATGTGGTTGGTGTT
from EL and RE list			
region9	ChIP	TCCCAGCGACTAAGACACAA	TGGATTTCTGAGTGTGTGCTC
region11	ChIP	CACTGTCAAACAAGAGCTCCA	ATTGCCTCTCCAAGATCTGC
region31	ChIP	AAACTCCCAGAGGGTGAGTG	CCCTGACCTAGAAATCTACATGC
region54	ChIP	TTGTCCCAGTGTCTTCTACAGG	CTGGAGGGAGGTGTTCTGTT
region64	ChIP	GGGTGATGAATTATTATGGGATG	TTTGCAACTAACCCTCTTAGACA
region74	ChIP	GTATAAAGCATTGGTGTGTCTGG	AAAGCAGAAAGACCATAATCCAC
region75	ChIP	AGCCTATCCAAGACCCAAAG	GGTTCTAATGGACAAGAGCTCAC
region91	ChIP	TCAGAGCCTCAGAGAAACCA	TTCTTCATAAATGTGAGAATGCC
region101	ChIP	TTTGCAATGTTTAGGGTCCA	TGCTAGATGCCAGCTTGGT
region119	ChIP	CACCCTCTTCCAGAACCACT	AAACAGTGCTGGTTGCTGTG
region126	ChIP	TTAAGCAAGGCCAGACAGTG	GCATACACCCTCAACTCCCT
region137	ChIP	GGATGGTCAGGAGCTTGATT	AGCAGCCACTCAATGTCAAT
region146	ChIP	ACATCCGACGAATGAATGAA	CACTTAGCATCGCAGGACTT
region153	ChIP	GGGAGCCAAGAGAATTTCC	CACCATGAAGTTGGGAGATG
region162	ChIP	AGGGAGAAGCTTCCTCTGAGT	CACGTAGCAGGTATTTCCCA
region180	ChIP	TGATTGAAGATTACCCAACAGAA	CTTTGCCCAAGCCAATAAAC
region191	ChIP	CTTTCCACTCTGCCAGAACA	GAGGCGCCAAGAAACAAG
region207	ChIP	AAACGCCAAGAACCTGGA	GCAGCACATGACCAAATGAT
region222	ChIP	CCTGGTGTTGTAGTCCACGA	GACATGCGAGTGGTGTACG
region233	ChIP	TGGAAGAAGAGTAGAGGTGCAA	TGTTTGTGAGTTCTAAGTTGACCAG
region247	ChIP	CACCAGCCTCAATATCCTCA	CAAAGCCAAGCACACAAAGT
from RE only list			
region22	ChIP	TGTTTCCCTTGATTTGGAGA	CAAATTTGAGCAAGAAGCCA
region44	ChIP	TTGGATTGCCCTCATTAACA	CGTAAGCATACGTGGCAAAT
region88	ChIP	ATAAGCCAACGATTCCCAAA	GGGACTAACAGATAGGAAGCTGA
region326	ChIP	TTCTCCCTCAAAGCCAATTT	CCTAGGGTTTCTGACTTGGG
region380	ChIP	GGAAGTGAGAGAGACTGGCA	AAAGCCTTTAGCCTGCATTT
region470	ChIP	AATACCAGTTGTGCACTGATGA	ACCTGGGCAGTAGGATCTGA
region515	ChIP	GGCATGCACGAACTTGTAGT	ACACCTATCTGCCACCACTG
region524	ChIP	CCCAAAGGAAAGACATCACA	GGGTGTAACACGTTTGTCGT
region665	ChIP	GCCCACAGAAATGTATGCAC	CAGGGAGTGTTCCTGCTCTT
region803	ChIP	AAGCAGGGATTACTCCAAGG	GCAGTCGCTCCATAGAGATG
region967	ChIP	GTTGGGAAACATGCTCGTTA	GCATCCCATTCCTCTTCATT
region1001	ChIP	GGATCCAGATTCCTGAGCAT	ATTCCATTTCAAGCCTGTCC
region1019	ChIP	TTTGTCAACATGTTCTAGGCTTG	TTTCTTCACCAAGACATCCCT
region1071	ChIP	CTTGCACCTAGCAGCTTGAC	GCTGCCAGGACAGAAGGTAT
region1136	ChIP	GCTACCAACAAGGAGCAACA	GTCTGTGGCTCCCAATACCT
region1206	ChIP	ATGCCCTTGTCTCAGAGCTT	GGAAGCACTCTCCAGTCTCC
region1307	ChIP	TGCAGCAGTTCCCTAGACAG	TCACGGTACAAGGTCTTCCA
region1352	ChIP	TTCTTTAGTTCCACGACCACA	CTCCTTCCCACATGATGGTT
region1424	ChIP	GCCCAGACCAGATAACCCT	GATTGGGAGAGGGACTCTGA
region1541	ChIP	CAAGTGAATCCATTAACAAGGG	TGCAATTCATTCTGTCTTTGC
region1602	ChIP	ACAGCCGAACTAGTCCCAAC	TCACAGGAGAAGAGAACCCA
p53 half-site	EMSA	GGGAGCTTAGGCATGTCTAGGGATCTCTA	GGGTAGAGATCCCTAGACATGCCTAAGCT
p21-5'	EMSA	GGGAGCTTGAACATGTCCCAACATGTTGA	GGGTCAACATGTTGGGACATGTTCAAGCT

p53cons-CAAG	EMSA	GGGAGCTTAGGCAAGTCTAGGCAAGTCTA	GGGTAGACTTGCCTAGACTTGCCTAAGCT
p53cons-CATG	EMSA	GGGAGCTTAGGCATGTCTAGGCATGTCTA	GGGTAGACATGCCTAGACATGCCTAAGCT
p53cons-CTAG	EMSA	GGGAGCTTAGGCTAGTCTAGGCTAGTCTA	GGGTAGACTAGCCTAGACTAGCCTAAGCT
p53cons-CTTG	EMSA	GGGAGCTTAGGCTTGTCTAGGCTTGTCTA	GGGTAGACAAGCCTAGACAAGCCTAAGCT
p21BS-spacer0	EMSA	TCTGGCCGTCAGGAACATGTCCCAACATGTTGAAGC TCTGGCATA	TATGCCAGAGCTCAACATGTTGGGACATGTTCCTGA CGGCCAGA
p21BS-spacer1	EMSA	TCTGGCGTCAGGAACATGTCC**C**CAACATGTTGAGCT CTGGCATA	TATGCCAGAGCTCAACATGTTGGGACATGTTCCTGA CGCCAGA
p21BS-spacer2	EMSA	TCTGGCGTCAGGAACATGTCC**CG**CAACATGTTGAGC TCTGCATA	TATGCAGAGCTCAACATGTTGCGGGACATGTTCCTG ACGCCACA
p21BS-spacer3	EMSA	TCTGGGTCAGGAACATGTCC**CCG**CAACATGTTGAGC TCTGCATA	TATGCAGAGCTCAACATGTTGCGGGGACATGTTCCT GACCCAGA
p21BS-spacer8	EMSA	TCTGGCAGGAACATGTCC**CCGTTCTG**CAACATGTTG AGCGCATA	TATGCGCTCAACATGTTGCAGAACGGGGACATGTTC CTGCCAGA
p21BS-spacer10	EMSA	TCTGGAGGAACATGTCC**CCGTCCTCTG**CAACATGTT GAGGCATA	TATGCCTCAACATGTTGCAGAGGACGGGGACATGTT CCTCCAGA
p21BS-spacer14	EMSA	TCTGGGAACATGTCC**CCGTCAGAGCTCTG**CAACATG TTGGCATA	TATGCCAACATGTTGCAGAGCTCTGACGGGGACATG TTCCCAGA
p53-E180L	Mutagenesis	GTGAGGCGCTGCCCCCACCATCTGCGCTGCTCAGAT AGCGATGGTCTGG	
p53-E180R	Mutagenesis	GTGAGGCGCTGCCCCCACCATCGCCGCTGCTCAGA TAGCGATGGTCTGG	
p53-E180R-R181E	Mutagenesis	GTGAGGCGCTGCCCCCACCATCGCGAGTGCTCAGA TAGCGATGGTCTGG	
p53-L344A	Mutagenesis	TTCGAGATGTTCCGAGAGGCGAATGAGGCCTTGGAA CTC	
p53-L344P	Mutagenesis	GAGATGTTCCGAGAGCCGAATGAGGCCTTGGAA	
p53-R175H	Mutagenesis	GACGGAGGTTGTGAGGCACTGCCCCCACCATGA	
p53-R181E	Mutagenesis	GTGAGGCGCTGCCCCCACCATGAGGAGTGCTCAGA TAGCGATGGTCTGG	
p53-R181L	Mutagenesis	GCGCTGCCCCCACCATGAGCTCTGCTCAGATAGCGA TGGTC	
GAPDH	qRT-PCR	AATGGAAATCCCATCACCATCT	CGCCCCACTTGATTTTGG
P53AIP1	qRT-PCR	AGCTAATTGACACCCACTGAACTTT	CTGCTCATTCCAAATCTGTCCTATT
CASP1	qRT-PCR	CTTTCTGCTCTTCCACACCA	TTTCCTCCACATCACAGGAA
FAS	qRT-PCR	ATGGTGTCAATGAAGCCAAA	TCCATGAAGTTGATGCCAAT
FDXR	qRT-PCR	Quantitect Primer Assay QT 00012124 (QIAgen)	
HDM2	qRT-PCR	GGGACGCCATCGAATCC	ATCCAACCAATCACCTGAATGTT
NOXA	qRT-PCR	CACGAGGAACAAGTGCAAGT	CAGTCAGGTTCCTGAGCAGA
p21	qRT-PCR	TGGAGACTCTCAGGGTCGAAA	CCGGCGTTTGGAGTGGTA
p53	Cloning	CACCATGGAGGAGCCGCAGTCA	TCAGTCTGAGTCAGGCCCTTC

Antibodies

Name (application)	**Clone (source)**
Acetyl-H4 (ChIP)	#06-866 (Upstate)
Acetyl-H3 (ChIP)	#06-599 (Upstate)
β-actin (WB)	AC-15 (ab2676, Abcam, Cambridge, UK)
Bak (IP)	TC-100 (Ab-1, Calbiochem)
Bak (WB)	NT (Upstate)
Bax (IP)	clone 3 (BD Biosciences)
Bax (WB)	2D2 (SouthernBiotech)
cleaved caspase-3 (Asp175) (WB)	5A1 (Cell Signaling)
Flag-tag (ChIP)	M2 (Sigma)
HA-tag (ChIP)	3F10 (Roche)
His-tag (EMSA)	Penta-His (QIAGEN)
MDM2 (WB)	SMP14 (sc-965, Santa Cruz Biotechnology)
mtHSP70 (WB)	JG1 (Affinity BioReagents)
NOXA (WB)	114C307.1 (Imgenex)
p21 (WB)	C-19 (sc-397, Santa Cruz Biotechnology)
p53 (EMSA)	Pab421 (Ab-1, Calbiochem)
p53 (WB, IP, IF, ChIP)	DO1 (Ab-6, Santa Cruz Biotechnology)
PARP (WB)	C2-10 (BD Biosciences)
Cleaved PARP (WB)	#9541 (Cell Signaling)
PCNA (WB)	PC10 (sc-56, Santa Cruz Biotechnology)
Phospho-p53 (Ser15) (WB)	#9284 (Cell Signaling)
Phospho-p53 (Ser20) (WB)	#9287 (Cell Signaling)
Phospho-p53 (Ser46) (WB)	#2521 (Cell Signaling)
Phospho-p53 (Ser392) (WB)	#9281 (Cell Signaling)
Puma (WB)	ab9645 (Abcam, Cambridge, UK)
RNA Pol II (ChIP)	H-224 (sc-9001, Santa Cruz Biotechnology)
trimethyl-histone H3 Lys4 (ChIP)	MC315 (#04-745, Upstate)
V5-tag (EMSA)	SV5-Pk1 (AbD Serotec)
Alexa Fluor® 546 goat anti-mouse IgG (H+L) (WB)	(Molecular Probes)
Alexa Fluor® 680 goat anti-mouse IgG (H+L) (WB)	(Molecular Probes)
Alexa Fluor® 680 goat anti-rabbit IgG (H+L) (WB)	(Molecular Probes)
anti-mouse IgG, HRP-linked (WB)	(GE Healthcare)
anti-rabbit IgG, HRP-linked (WB)	(GE Healthcare)

SUPPLEMENTAL REFERENCES

El-Deiry, W.S., Tokino, T., Velculescu, V.E., Levy, D.B., Parsons, R., Trent, J.M., Lin, D., Mercer, W.E., Kinzler, K.W., and Vogelstein, B. (1993). WAF1, a potential mediator of p53 tumor suppression. Cell *75*, 817-825.

He, T.C., Zhou, S., da Costa, L.T., Yu, J., Kinzler, K.W., and Vogelstein, B. (1998). A simplified system for generating recombinant adenoviruses. Proc Natl Acad Sci U S A *95*, 2509-2514.

Hoh, J., Jin, S., Parrado, T., Edington, J., Levine, A.J., and Ott, J. (2002). The p53MH algorithm and its application in detecting p53-responsive genes. Proc Natl Acad Sci USA *99*, 8467-8472.

Littlewood, T.D., Hancock, D.C., Danielian, P.S., Parker, M.G., and Evan, G.I. (1995). A modified oestrogen receptor ligand-binding domain as an improved switch for the regulation of heterologous proteins. Nucleic Acids Res 23, 1686-1690.

Miyashita, T., and Reed, J.C. (1995). Tumor suppressor p53 is a direct transcriptional activator of the human bax gene. Cell 80, 293-299.

Oda, K., Arakawa, H., Tanaka, T., Matsuda, K., Tanikawa, C., Mori, T., Nishimori, H., Tamai, K., Tokino, T., Nakamura, Y., and Taya, Y. (2000). p53AIP1, a potential mediator of p53-dependent apoptosis, and its regulation by Ser-46-phosphorylated p53. Cell 102, 849-862.

Stiewe, T., and Pützer, B.M. (2000). Role of the p53-homologue p73 in E2F1-induced apoptosis. Nat Genet 26, 464-469.

Wei, C.L., Wu, Q., Vega, V.B., Chiu, K.P., Ng, P., Zhang ,T., Shahab, A., Yong, H.C., Fu, Y., Weng, Z., Liu, J., Zhao, X.D., Chew, J.L., Lee, Y.L., Kuznetsov, V.A., Sung, W.K., Miller, L.D., Lim, B., Liu, E.T., Yu, Q., Ng, H.H., Ruan, Y. (2006). A global map of p53 transcription-factor binding sites in the human genome. Cell 124, 207-219.

Yang, Y. H., Dudoit, S., Luu, P., and Speed, T. P. (2001). Normalization for cDNA microarray data. In M. L. Bittner, Y. Chen, A. N. Dorsel, and E. R. Dougherty (eds.). Microarrays: Optical Technologies and Informatics, Volume 4266 of Proceedings of SPIE.

Cell Cycle 9:20, 4068-4076; October 15, 2010; © 2010 Landes Bioscience

Life or death

p53-induced apoptosis requires DNA binding cooperativity

Katharina Schlereth, Joël P. Charles, Anne C. Bretz and Thorsten Stiewe*
Molecular Oncology; Philipps-University Marburg; Marburg, Germany

The tumor suppressor p53 provides exquisite protection from cancer by balancing cell survival and death in response to stress. Sustained stress or irreparable damage trigger p53's killer functions to permanently eliminate genetically-altered cells as a potential source of cancer. To prevent the unnecessary loss of cells that could cause premature aging as a result of stem cell attrition, the killer functions of p53 are tightly regulated and balanced against protector functions that promote damage repair and support survival in response to low stress or mild damage. In molecular terms these p53-based cell fate decisions involve protein interactions with cofactors and modifying enzymes, which modulate the activation of distinct sets of p53 target genes. In addition, we demonstrate that part of this regulation occurs at the level of DNA binding. We show that the killer function of p53 requires the four DNA binding domains within the p53 tetramer to interact with one another. These intermolecular interactions enable cooperative binding of p53 to less perfect response elements in the genome, which are present in many target genes essential for apoptosis. Modulating p53 interactions within the tetramer could therefore present a novel promising strategy to fine-tune p53-based cell fate decisions.

Key words: p53, tumor supressor, transcription factor, DNA binding, cell cycle arrest apoptosis

Submitted: 09/08/10

Accepted: 09/11/10

Previously published online: www.landesbioscience.com/journals/cc/article/13595

DOI: 10.4161/cc.9.20.13595

*Correspondence to: Thorsten Stiewe; Email: thorsten.stiewe@staff.uni-marburg.de

Throughout lifetime the cells of our body are continuously exposed to a large variety of environmental and intrinsic hazards that cause damage to the genome. In case these genetic or epigenetic aberrations are replicated and passed on during cell division danger exists that proliferation and survival promoting mutations accumulate so that sooner or later malignant progeny arises posing a threat to the organism as a whole. Early eradication of aspiring cancer cells through activation of an apoptotic cell death program is therefore an efficient means to protect the organism from a full-blown tumor disease. However, considering that moderate damage resulting from mild stress is often reparable, the decision to kill a stressed cell needs to be well-thought-out. Unreflected killing of valuable cells could eventually result in a depletion of stem cell pools and premature aging as a consequence. Every single cell is therefore continuously confronted with the choice: repair and live or die. Too much death poses the risk of aging, too little death the risk of cancer. Balancing these risks for the benefit of the organism is a central task of the tumor suppressor protein p53. Summoned under conditions of stress, p53 functions like a hub in a highly-connected intracellular signaling network to integrate a plethora of inputs from the inside and outside of the cell to trigger a well-balanced cell fate decision.[1]

The Choice of Targets

How p53 executes this cell fate decision is therefore a question of considerable biomedical interest (**Fig. 1**). Since it is known that p53 functions as a sequence-specific DNA binding transcription factor, tremendous efforts have been made in the last decade to identify the p53-regulated targets in the genome that execute the appropriate cell fate responses.[2] The induction

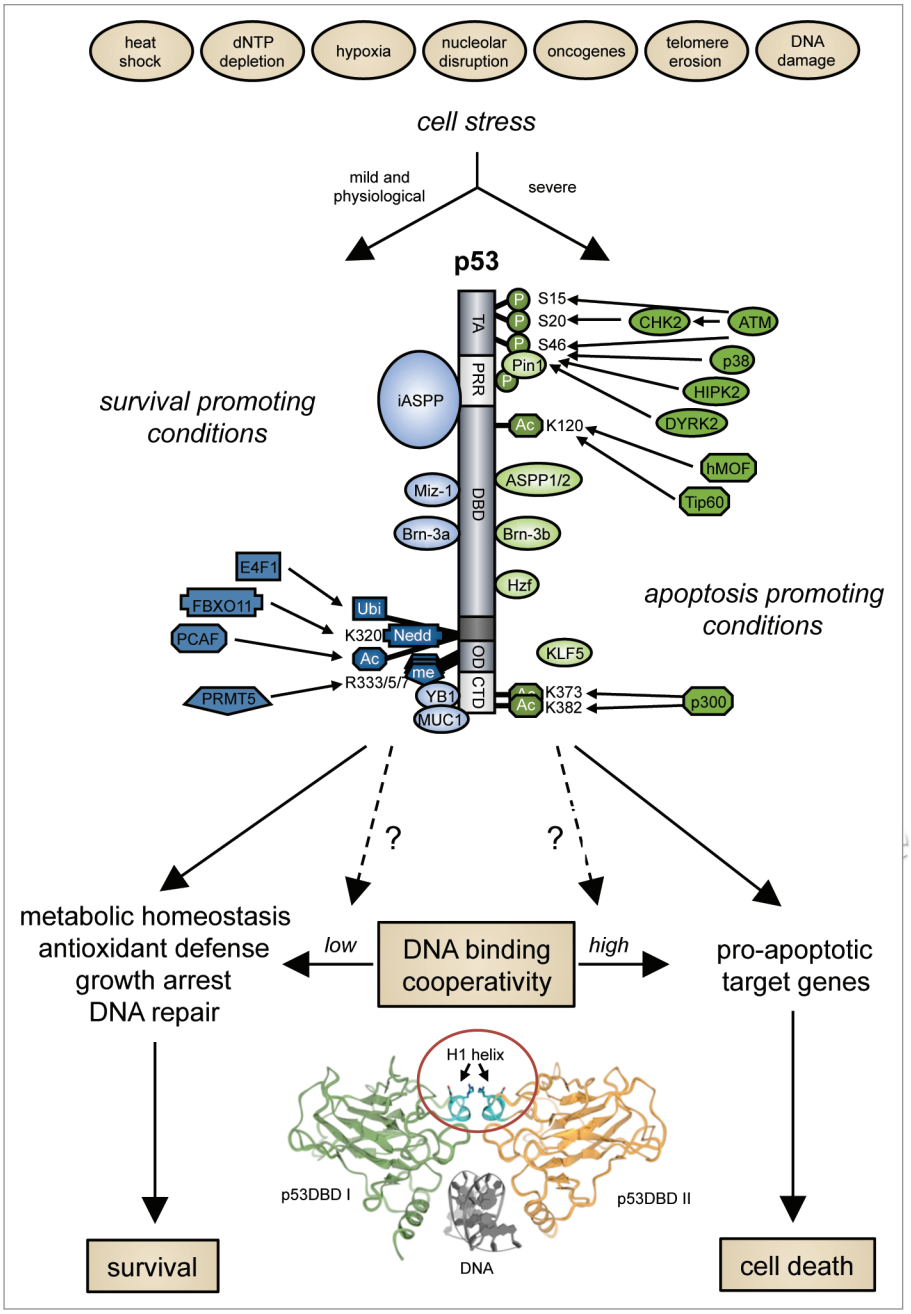

Figure 1. DNA binding cooperativity—a new variable in the p53-based cell fate decision. Post-translational modifications of p53: P, phosphorylation; Ac, acetylation; me, methylation; Ubi, ubiquitylation; Nedd, neddylation.

of a transient cell cycle arrest that allows for damage repair depends critically on the genes *p21* (*CDKN1A*), *14-3-3σ* (*SFN*) and *GADD45A*, with the first being crucial for cell cycle arrest in the G_1 phase and the latter two for arrest in G_2.[3] In the case of prolonged damage p53-mediated transactivation of the sestrins (*SESN1* and *SESN2*) causes inhibition of mTOR signaling and helps to maintain the arrest reversible, while activation of mTOR under these conditions triggers a shift to cell cycle exit termed senescence.[4-8] Another way for p53 to permanently stop cell proliferation without compromising cell viability is induction of differentiation.[9] For example, differentiation follows experimental reactivation of p53 in a murine model of Ras-dependent liver cancer or genotoxic stress induced-p53 activation in acute myeloid leukemia cells bearing an activated Ras oncogene.[10,11]

Only when cells have encountered sustained and irreparable damage that is incompatible with further survival, p53 shifts to the most extreme and irrevocable antiproliferative response—apoptotic cell death.[12,13] In line with the importance of this activity numerous studies have identified many different proapoptotic p53 target genes including *BAX*, *FAS*, *TP53I3* (*PIG3*), *TNFRSF10B* (*KILLER/DR5*), *LRDD* (*PIDD*), *P53AIP1*, *APAF1*, *PERP*, *PMAIP1* (*NOXA*) and *BBC3* (*PUMA*)—to name just the most commonly cited. Of note, accumulating evidence shows that p53-induced apoptosis does not only require activation of these proapoptotic target genes but also involves transcription-independent functions of p53 in the cytoplasm.[14-16]

Not enough, a recent review lists a total of 129 transcriptional targets of p53 with experimentally validated binding sites and global approaches using chromatin-immunoprecipitation in conjunction with microarrays (ChIP-chip) or massively parallel sequencing reveal increasingly more sites within the genome that are bound by p53.[2,17-20] The majority of these genomic sequences contain a common consensus motif to which p53 binds with high affinity and specificity. This motif is composed of two decameric half-sites RRR CWW GYY Y, where R is a purine, Y a pyrimidine and W is either adenine (A) or thymine (T), separated by a spacer, usually composed of 0–21 base pairs.[2,21,22] Considering that most of the p53-regulated genes contain response elements that more or less concur with the consensus motif, it remains a mystery how p53 can distinguish between the various genomic binding sites with their associated target genes and selectively activate a subset of them to drive cell fate into the desired direction.[2,12,13,23-25]

The Role of Cofactor Recruitment

One way to target p53 to the promoters of specific target genes is through interaction with partner proteins. Considering the vast amount of p53 binding proteins described so far we will focus on a small

fraction with a clear role in redirecting p53 towards a specific cellular outcome.

For example, the proteins of the ASPP family have turned out to be potent regulators of p53's apoptotic function.[26] The apoptosis promoting members, ASPP1 and ASPP2, specifically stimulate p53 binding to the promoters of the proapoptotic target genes *BAX* and *PIG3* but not to the promoters of *p21* or *MDM2*.[27] On the other hand, the inhibitory ASPP family member, iASPP, competes with the other ASPP proteins and blocks p53-mediated apoptosis.[28] Interestingly, iASPP discriminates between two common polymorphic variants of p53 that differ at codon 72.[29] iASPP preferentially binds the proline 72 (P72) variant and inhibits its activity, providing an intriguing explanation for why the arginine 72 (R72) variant is a more potent inducer of apoptosis than the P72 variant.

Another family of proteins that regulates p53 is the Brn3 family of POU domain transcription factors that interact with the p53 DNA binding domain (DBD). While Brn3a stimulates p53-dependent transcription of *p21* and inhibits its ability to activate the *BAX* and *NOXA* promoters, Brn3b functions in the opposite manner by assisting p53 to activate *BAX* but not *p21* expression.[30-32]

The zinc-finger protein Hzf is a target gene of p53 and by interacting with the p53 DBD regulates its target selectivity.[33,34] Hzf promotes p53 binding to the *p21* and *14-3-3*σ promoters early after DNA damage. Inactivation of Hzf—experimentally or by degradation in response to sustained DNA damage—prevents p53 binding to these promoters and allows relocalization to the response elements in the proapoptotic target genes *BAX*, *PUMA*, *NOXA* and *PERP*.[35] A notable exception to the regulation of target selectivity is *MDM2* which appears to be unaffected by Hzf.

Similarly, Miz1 also interacts with the DNA binding domain of p53 to prevent the activation of the proapoptotic targets *BAX* and *PUMA*.[36] Together with Miz1 being a potent transactivator of *p21* expression this results in promotion of cell survival. c-Myc via interaction with Miz1 suppresses *p21* induction by p53 and thus switches the p53-response from cytostatic to apoptotic.[36,37]

The Role of Post-Translational Modifications

Discriminatory effects on target selectivity can also be exerted by interacting proteins that modulate p53's DNA binding properties via covalent post-translational modifications including phosphorylation, acetylation, methylation, ubiquitylation, neddylation, sumoylation and even addition of N-acetyl glucosamine. Here we will highlight those modifications that most prominently influence p53's promoter selectivity.

Among the phosphorylation sites, serine 46 (S46) has clear discriminatory function for p53 as a transcriptional activator. p53 is phosphorylated at this residue by homeodomain interacting protein kinase 2 (HIPK2), dual-specificity tyrosine-phosphorylation-regulated kinase 2 (DYRK2), AMPK, protein kinase C delta or p38 mitogen activated protein kinase in response to severe cellular damage.[38-44] S46-phosphorylated p53 is recognized by the peptidyl-prolyl cis/trans isomerase Pin1 leading to dissociation of the apoptosis-inhibiting protein iASPP from p53 and induction of apoptosis via, for example, transactivation of *p53AIP1*, a proapoptotic factor that promotes the release of mitochondrial cytochrome *c* during apoptosis.[45,46]

While numerous studies have implicated acetylation of lysine residues in the C-terminus of p53 as being important for p53's transcriptional activity in general, acetylation of lysine 120 (K120) in the DNA binding domain by the MYST family histone acetyl transferases hMOF and Tip60 specifically results in increased binding to proapoptotic targets like *BAX* and *PUMA* while the nonapoptotic targets *p21* and *MDM2* remain unaffected.[47,48] On the other hand, acetylation of lysine 320 (K320) by the transcriptional coactivator p300/CBP-associated factor (PCAF) predisposes p53 to activate *p21* and decreases its ability to induce proapoptotic target genes. Cells ectopically expressing a mutant p53 where K320 is mutated to glutamine (K320Q) to mimic acetylation, display reduced apoptosis after some forms of DNA damage.[49] Vice versa K317R (corresponding to human K320R) knockin mice, where K317 acetylation is missing, consistently display increased apoptosis and higher expression of relevant target genes in several cell types.[50] However, K320 is not only a target for acetylation but it is also ubiquitylated by the zinc-finger protein E4F1.[51] This modification facilitates p53-dependent activation of *p21* and *Cyclin G1* expression without affecting the expression of the proapoptotic gene *NOXA*, overall resulting in reduced p53-mediated cell death in response to UV.

p53-mediated cell cycle arrest is also favored following methylation of at least two arginine residues (R333 and R335) by the arginine methyltransferase PRMT5.[52,53] Consistently, depletion of PRMT5 by siRNA in cancer cell lines leads to increased apoptosis following p53 activation.

The Role of DNA Binding Cooperativity

Together these data highlight the complexity of how p53 binding proteins modulate—in a covalent or non-covalent manner—the DNA binding properties of p53 to influence the cell fate decision in favor of survival or death. Despite this substantial body of knowledge, very little is known about the molecular details. Even a structurally simple modification such as the acetylation of K120 does not directly explain why p53's specificity for certain promoter sequences changes and p53 is redirected to proapoptotic target genes. The recent progress in solving the 3D structures of p53 in contact to DNA, however, promises that it will be possible to gain a clearer view of how p53's sequence specificity is regulated by either modifications or through association with interaction partners.

One striking result of the recent structural studies was that the p53 molecules within the tetramer, which assembles as a dimer of dimers on two cognate half sites in the DNA, do not only interact through their oligomerization domains but also tightly and specifically via their DBDs. Nuclear magnetic resonance (NMR) spectroscopy, X-ray crystallography and computational studies indicate that the oppositely charged glutamate (E180) and arginine (R181) residues in the short helix

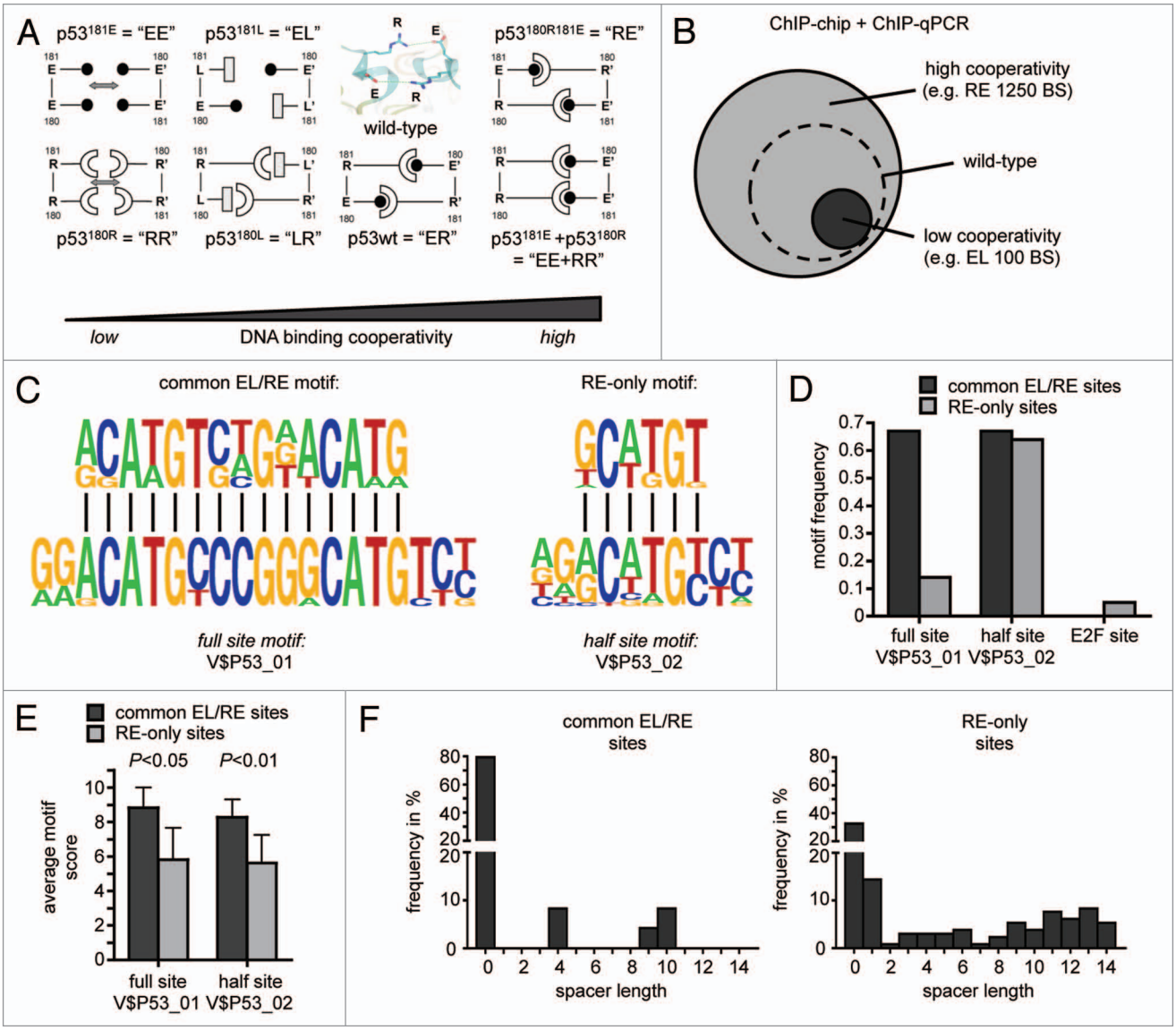

Figure 2. Role of cooperativity for DNA binding of p53 in the human genome. (A) Schematic representation of the dimerization patterns of wild-type p53 and the H1 helix mutants used in this study. The small insert shows the 3D structure of the double salt bridge in the wild-type molecule. To disrupt the intradimer interface we introduced modest charge-neutralizing (E180→L "LR" and R181→L "EL") and more severe charge-inverting (E180→R "RR" and R181→E "EE") mutations into the H1 helix of the full-length p53 molecule. The short names denote the amino acid sequence at positions 180 and 181 in the mutant proteins, e.g., "ER" for E180, R181 in the wild-type. To assure that functional defects are truly due to defective core domain interactions and are not caused by structural misfolding of the core domain or disturbed interaction with other cellular proteins, we also introduced the two most severe mutations E180R and R181E together into a single p53 molecule (double mutant E180R, R181E "RE") and used the two complementing mutants "EE" and "RR" in functional rescue studies. (B) p53 DNA binding cooperativity determines the number of binding sites in the genome. The number of binding sites was estimated by bioinformatic analysis combining ChIP-chip results with experimental validation rates determined by ChIP-qPCR.[9] (C) De novo motif discovery in validated common EL/RE and RE-only binding sequences. Twenty-meric and decameric consensus motifs are shown for comparison. (D and E) Frequency and average motif scores of the TRANSFAC motifs V$P53_01 (full site), V$P53_02 (half-site) and V$E2F_01 (E2F site as a control) in validated common EL/RE and RE-only binding sequences. Results are presented as the mean ± SD. (F) Distribution of spacer lengths in validated common EL/RE and RE-only binding sequences as determined by the spacer-tolerant p53MH algorithm.

H1 of the DBDs engage in intermolecular interactions to form a so-called double salt bridge as part of the DBD dimer interface.[54-58] This dimer interface was further confirmed when Fersht and colleagues succeeded in obtaining a structure of full-length p53 bound to DNA by using a combination of small angle X-ray scattering, NMR and electron microscopy.[59] In vitro studies with recombinant p53 DBDs carrying targeted mutations in the critical residues highlighted that the dimer interface is crucial for a long-known property of p53, called DNA binding cooperativity, which simply means that four interacting p53 subunits cooperate to bind DNA better than four non-interacting subunits.[54]

To better understand the relevance of this dimer interface and the resulting DNA binding cooperativity for the biology of p53, we analyzed the consequences

of expressing dimer interface mutants of full-length p53 in cells.[9] For this, we generated a panel of p53 expression constructs with mutations in the H1 helix residues E180 and R181 that reduced or increased interactions between neighboring p53 subunits (**Fig. 2A**). This mutant panel covers the whole cooperativity range from barely detectable to super-physiological DNA binding cooperativity.

The expression of these mutants in p53-null cell lines resulted in distinct biological outcomes. Low cooperativity mutants induced *p21* and *MDM2* expression leading to a selective cell cycle arrest while high cooperativity mutants activated *BAX*, *NOXA* and other proapoptotic target genes causing cell death. Likewise, when p53 function in $p53^{-/-}$ HCT116 cells was restored with the panel of cooperativity mutants at physiological expression levels the extent of apoptosis induced by genotoxic stress correlated directly with DNA binding cooperativity, indicating that p53's killing function strongly depends on its ability to bind DNA in a cooperative manner.

DNA Binding Cooperativity Enables Binding to Imperfect Binding Elements

One hypothesis was that the binding of p53 to apoptotic target genes requires higher levels of cooperativity than binding to survival genes. To test this we compared the genomic binding profiles of a low (EL) and high (RE) cooperativity mutant by chromatin immunoprecipitation coupled to the unbiased detection of binding sites (BS) with genome-wide promoter tiling microarrays (ChIP-chip). Bioinformatic analysis combining ChIP-chip results with experimental validation rates determined by ChIP-qPCR revealed approximately 1,250 BS for the high cooperativity mutant RE in the promoter regions of the human genome (**Fig. 2B**). Interestingly, the low cooperativity mutant EL showed only approximately 100 BS, which represent a subset of the RE BS. This led us to the conclusion that the DNA binding cooperativity serves to increase the number of BS in the genome.

To understand the differences between BS that are strongly dependent on cooperativity (RE-only BS) and those, which are bound independently of cooperativity (common BS of EL and RE), we performed motif analysis on experimentally validated "common EL/RE" and "RE-only" BS. De novo motif discovery as well as screening the bound sequences for p53 binding motifs of the TRANSFAC database revealed that common EL/RE but not RE-only BS were strongly enriched for the 20-meric p53 full-site motif (V$P53_01) (**Fig. 2C and D**). In contrast, the decameric p53 half-site motif (V$P53_02) was identified with equal frequency in both sets of BS. Nevertheless, in both cases, the average motif score as a measure of similarity to the consensus was significantly lower among the validated RE-only sites (**Fig. 2E**), suggesting that RE tolerates mismatches to the consensus binding site better than EL. Another explanation for the absence of 20-meric full sites in RE-only sequences—despite the presence of decameric half-sites—are spacer elements that separate two half-sites. Applying a spacer-tolerant algorithm, we indeed identified spacer-containing full sites much more frequently in RE-only than in common EL/RE sequences (**Fig. 2F**). Together, these results indicate that the sequence requirements for recruitment of RE are less stringent than for EL and that DNA binding cooperativity increases the number of binding sites in the genome by enabling binding to imperfect, i.e., mismatch- and spacer-containing, response elements.

A Role for Cooperativity in Binding and Activating Imperfect Binding Sites

To experimentally confirm that the extent of DNA binding cooperativity determines binding to imperfect response elements, we performed electrophoretic mobility shift assays. It has been previously shown that even subtle changes in the core CWWG sequence of a RRR CWWG YYY half-site can dramatically reduce DNA binding affinity, which is known to be maximal for CATG.[2] Mutation of the invariable C or G nucleotides typically results in a complete loss of binding activity, whereas changing of the central AT to AA, TT or TA reduces binding only.[2] Consistently, binding of wild-type p53 and even more pronounced of low cooperativity mutants (RR, LR and EL) was reduced when the core CATG sequence was mutated to CAAG, CTTG or CTAG (**Fig. 3A**). In contrast, the high cooperativity mutants RE and EE + RR bound these non-CATG sequences even better than wild-type p53. Similarly, spacer elements in between the two half-sites completely abolished the binding of low cooperativity mutants whereas high cooperativity mutants were still bound (**Fig. 3B**). H1 helix interactions therefore strongly influence the sequence specificity of the p53 tetramer in the way that high cooperativity renders p53 tolerant to deviations from the consensus sequence.

To investigate whether cooperativity also affects transactivation of target genes in a way predicted by the DNA binding experiments, we analyzed luciferase reporter plasmids containing the consensus-like 5' p53 binding site of the *p21* promoter in comparison to derivative constructs containing central CTAG sequences and/or variable spacers (**Fig. 4A**). Activation of these reporters by our panel of cooperativity mutants was measured following transfection into p53-null H1299 cells. The parental promoter construct—with central CATG sequence and without any spacer—yielded high levels of reporter activity and was preferentially activated by low cooperativity mutants (**Fig. 4B**). Mutation of the central CATG to CTAG in both half-sites as well as the insertion of a 5 or 14 bp spacer reduced the maximal activity of the reporter (**Fig. 4C**). However, this decrease primarily affected the transactivation by low cooperativity mutants so that the difference between low and high cooperativity mutants became less apparent (**Fig. 4D**). In fact, insertion of a 14 bp spacer rendered the promoter with a CATG core independent of cooperativity so that all p53 H1 helix mutants induced equal reporter activity levels (**Fig. 4B**). By combining a central CTAG sequence with a spacer insertion we even obtained reporters that were preferentially induced by high cooperativity mutants (**Fig. 4B and D**). Together these experiments illustrate that the level of DNA binding cooperativity determines which promoter sequences are activated by p53.

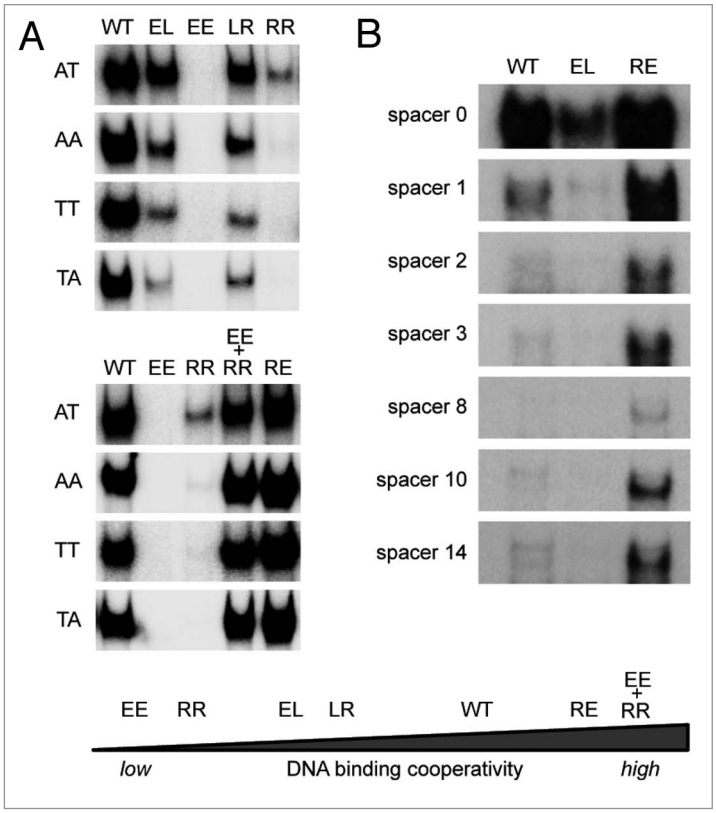

Figure 3. Impact of DNA binding cooperativity on sequence selectivity of p53. (A) Shown are electrophoretic mobility shift assays (EMSA) for DNA binding of in vitro translated wild-type p53 and the indicated H1 helix mutants to dsDNA oligonucleotides (5'-GGG AGC TTA GGC WWG TCT AGG CWW GTC TA-3') with WW denoting AT, AA, TT or TA sequences in the center of each half site. EMSAs were performed as previously described.[9,72] Compared to H1 helix mutants with reduced DNA binding cooperativity (EE, RR, LR, EL), mutants with increased DNA binding cooperativity (RE and EE+RR) revealed an increased ability to bind the lower affinity non-CATG sequences. (B) Same as in (A) using dsDNA oligonucleotides containing the 5' p53 binding site in the *p21* promoter (5'-TCT GGC CGT CAG GAA CATG TCC $(N)_{1-14}$ CAA CATG TTG AAG CTC TGG CAT A-3') with increasing central spacer sequences $(N)_{1-14}$. The high cooperativity mutant (RE) showed an increased ability to bind the spacer-containing motifs, while the low cooperativity mutant (EL) was largely unable to bind these spacer-containing elements.

The Consensus Sequence Binding-Transactivation Paradox

Curiously, high cooperativity mutants often bound perfect consensus-like response elements at least equally well if not even stronger than low cooperativity mutants, but failed to efficiently transactivate reporter constructs made up of these binding sites. Although not fully understood at present, we can envision two possible mechanisms. First, because high cooperativity mutants bind to many more sites in the genome than low cooperativity mutants, essential cofactors that might be present in limiting amounts could be sequestered, so that the local availability of these factors on a given promoter might be insufficient to support high expression levels of the target gene. This idea is experimentally supported by our data showing that coexpression of a high cooperativity mutant also limits transactivation in a heterologous reporter system, which depends on the transactivation domain but not the DNA binding domain of p53.[9] Second, it still remains unclear how p53 and other transcription factors (TF) efficiently drive a promoter to maturation.[60-62] Many different chromatin-modifying enzymes and chromatin remodellers have been identified as essential players involved in this transactivation process.[63,64] In one scenario, TFs stably associate with a binding site in the promoter and serve as a docking site for the various cofactors that one after the other are recruited to the promoter for its activation. In a contrasting model, various different preformed TF-cofactor complexes exist in the nucleoplasm and the TF functions as a shuttling factor to transport these factors to the target gene promoters.[65-67] In the latter model, stable association of p53 with the promoter DNA (as in the case of high cooperativity mutants on consensus binding sites) could compromise the hypothetical shuttling function and be detrimental to the transactivation process. Therefore, an efficient shuttling of highly cooperative p53 would only be possible on imperfect, low-affinity binding sites. No matter which model applies, excessively high levels of cooperativity prevent efficient transactivation of genes with perfect p53 binding elements so that high cooperativity contributes to shifting the expression profile to target genes with imperfect binding sites.

Imperfect binding sites are enriched in proapoptotic target genes. Importantly, there is evidence that low-affinity and spacer-containing sequences are more common in proapoptotic than in non-apoptotic genes, which could explain that the apoptotic potential of p53 correlates with the level of DNA binding cooperativity. It has been known for a while that the cellular level of p53 can dictate the response of the cell such that lower levels of p53 result in arrest whereas higher levels result in apoptosis.[68] It has therefore been hypothesized that only high levels of p53 protein, for example following stabilization in response to massive DNA damage, allow for sufficient binding to proapoptotic target genes, which in many cases contain p53 binding elements that only poorly resemble the consensus binding sequence and which—compared to response elements in cell cycle arrest targets—show very little evolutionary conservation.[69] To investigate whether the imperfect response elements in proapoptotic target genes resemble the binding sequences that we found to be preferentially bound by high cooperativity mutants, we analyzed 60 p53 binding sites found in 39 experimentally validated bona fide p53 target genes (**Supp. Table 1**).[70] The p53 response elements in non-apoptotic genes were indeed significantly enriched for the half-site RRR CATG YYY, whereas central CAAG,

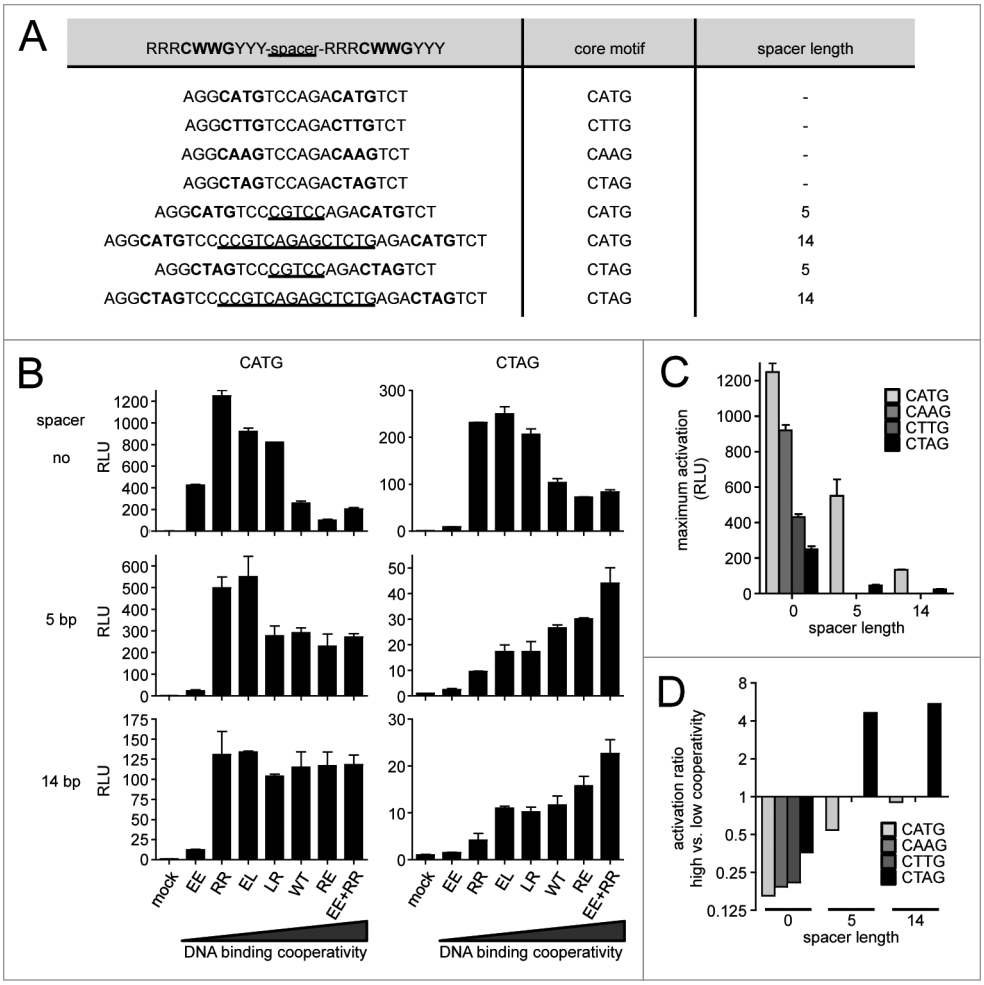

Figure 4. Impact of DNA binding cooperativity on sequence selectivity of transactivation. (A) Shown are p53 binding sequences that differ from the consensus sequence with respect to the CATG in the core of a half-site (bold) and with respect to spacer length (underlined). (B) Luciferase reporter assays. Single copies of the sequences in (A) were cloned into pGL4.23[luc2/minP] and tested for transactivation by the indicated p53 cooperativity mutants. Firefly luciferase activity was measured 48 hours following co-transfection of 100 ng reporter plasmid and 5 ng p53 expression plasmid (pCMVneo-BamHI) into p53-null H1299 cells. The p53 mutants are shown in the order of increasing DNA binding cooperativity. Mean ± SD. (C) Shown is the maximum p53-induced reporter activation for the different promoter sequences. (D) Shown is the ratio of the reporter activities induced by "EE + RR" (high cooperativity) and "RR" (low cooperativity) for the different promoter sequences.

CTTG or CTAG sequences as well as spacers between the two half-sites were significantly more common in the pro-apoptotic genes (**Fig. 5**). Our study therefore provides the first direct experimental evidence that the activation of the apoptosis program indeed requires p53 binding to imperfect binding sites, which are overrepresented in the promoters of many known proapoptotic target genes, and that this depends on the cooperative nature of DNA binding by the p53 tetramer.

Open Questions

Considering the relevance of DNA binding cooperativity for binding and activation of proapoptotic target genes, it can be hypothesized that known p53 binding proteins or post-translational modifications that affect p53-based cell fate decisions act via modulating this cooperativity. For example, chromatin-associated factors only present on proapoptotic promoters could be envisioned to attach to p53 and stimulate DBD interactions to allow a more stable binding to the imperfect binding sequences in these promoters. So far, direct evidence for this is missing and will be difficult to obtain, because the cooperativity status of p53, i.e., the interaction strength of neighboring p53 subunits in a p53 tetramer, cannot be easily measured in living cells. However, there is some indirect evidence that at least a few of the known apoptosis-promoting factors might function via modulation of cooperativity.[9] First of all, known apoptosis-promoting conditions such as ectopic expression of ASPP2 or the apoptosis-enhancing mutation of serine 46 to phenylalanine appear to be less effective when cooperativity is impaired. Second, ASPP2 was able to increase apoptosis induced by low cooperativity mutants but could not further increase the apoptotic function of the engineered high cooperativity p53 "EE+RR", suggesting that ASPP2 binding to the p53 DBD—possibly in a hit-and-run mechanism—enhances cooperativity to enable p53 to bind to proapoptotic target genes.

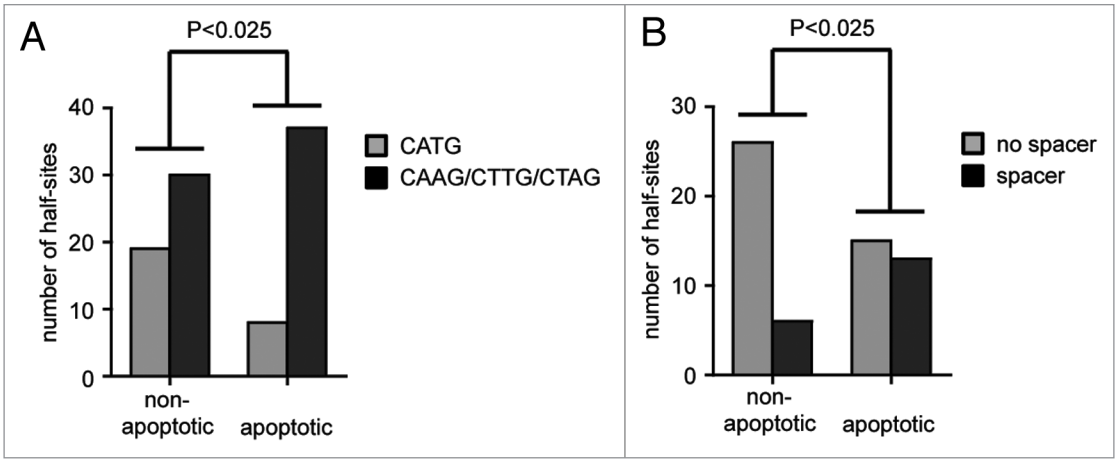

Figure 5. Proapoptotic target genes in a list of experimentally validated p53 target genes (Supp. Table 1) are enriched for p53 response elements with spacers and non-CATG core sequences. Statistical significance was calculated by Pearson's Chi-square test. (A) Number of half-sites with a central CATG versus CAAG, CTTG or CTAG sequence in non-versus proapoptotic target genes. (B) Presence of spacer containing response elements in non-versus proapoptotic target genes.

While it is clear that cooperativity is essential for high-level induction of apoptosis by p53, it remains to be elucidated, whether an increase in cooperativity mediates the proapoptotic activity of p53-stimulating cofactors or modifying enzymes.

Importantly, mutations that reduce cooperativity by interfering with H1 helix interactions are found in human tumors. Apart from many somatic mutations affecting residues E180 and R181, even families with Li Fraumeni-like syndrome carrying germline mutations in the H1 helix have been described. Interestingly, the R181H mutation (EH) has been identified very early in a family with familial breast carcinoma, but was excluded as a cancer-promoting mutation in part because the mutant protein retained the ability to suppress proliferation of p53-null Saos-2 cells in culture.[71] Nevertheless, similar germline mutations (R181C and R181L) have been found in other families. We confirmed that these p53 mutant proteins were indeed able to induce cell arrest, but showed strongly impaired apoptotic activity.[9] This implies that H1 helix mutations cause a loss of DNA binding cooperativity resulting in an increased cancer risk. However, formal confirmation, which could be provided by the analysis of cooperativity mutant mice, remains to be obtained. In summary, cooperativity appears to be essential for both p53's apoptotic activity and its tumor suppressor function.

Acknowledgements

We thank Andreas Rosenwald, Caroline Kisker and Martin Eilers for their cooperation and all members of the laboratory—in particular Rasa Beinoraviciute-Kellner, Markus Sauer and Marie Zeitlinger—for their contribution to this study. This work was funded by grants to T.S. from the Deutsche Forschungsgemeinschaft (Transregio TR17 Teilprojekt B2, Klinische Forschergruppe KFO210 STI 182/3-1), Deutsche Krebshilfe (107904), LOEWE research program, "Tumor & Inflammation" and von Behring-Röntgen-Stiftung (57-0012).

Note

Supplementary materials can be found at: www.landesbioscience.com/supplement/SchlerethCC9-20-sup.pdf

References

1. Vogelstein B, Lane D, Levine AJ. Surfing the p53 network. Nature 2000; 408:38-44.
2. Riley T, Sontag E, Chen P, Levine A. Transcriptional control of human p53-regulated genes. Nat Rev Mol Cell Biol 2008; 9:402-12.
3. Levine AJ, Oren M. The first 30 years of p53: growing ever more complex. Nat Rev Cancer 2009; 9:749-58.
4. Budanov AV, Karin M. p53 target genes sestrin1 and sestrin2 connect genotoxic stress and mTOR signaling. Cell 2008; 134:451-60.
5. Korotchkina LG, Demidenko ZN, Gudkov AV, Blagosklonny MV. Cellular quiescence caused by the Mdm2 inhibitor nutlin-3A. Cell Cycle 2009; 8:3777-81.
6. Steelman LS, McCubrey JA. Intriguing novel abilities of Nutlin-3A: induction of cellular quiescence as opposed to cellular senescence—implications for chemotherapy. Cell Cycle 2009; 8:3634-5.
7. Demidenko ZN, Korotchkina LG, Gudkov AV, Blagosklonny MV. Paradoxical suppression of cellular senescence by p53. Proc Natl Acad Sci USA 2010; 107:9660-4.
8. Korotchkina LG, Leontieva OV, Bukreeva EI, Demidenko ZN, Gudkov AV, Blagosklonny MV. The choice between p53-induced senescence and quiescence is determined in part by the mTOR pathway. Aging (Albany NY) 2010; 2:344-52.
9. Schlereth K, Beinoraviciute-Kellner R, Zeitlinger MK, Bretz AC, Sauer M, Charles JP, et al. DNA binding cooperativity of p53 modulates the decision between cell cycle arrest and apoptosis. Mol Cell 2010; 38:356-68.
10. Xue W, Zender L, Miething C, Dickins RA, Hernando E, Krizhanovsky V, et al. Senescence and tumour clearance is triggered by p53 restoration in murine liver carcinomas. Nature 2007; 445:656-60.
11. Meyer M, Rubsamen D, Slany R, Illmer T, Stabla K, Roth P, et al. Oncogenic RAS enables DNA damage- and p53-dependent differentiation of acute myeloid leukemia cells in response to chemotherapy. PLoS One 2009; 4:7768.
12. Aylon Y, Oren M. Living with p53, dying of p53. Cell 2007; 130:597-600.
13. Murray-Zmijewski F, Slee EA, Lu X. A complex barcode underlies the heterogeneous response of p53 to stress. Nat Rev Mol Cell Biol 2008; 9:702-12.
14. Green DR, Kroemer G. Cytoplasmic functions of the tumour suppressor p53. Nature 2009; 458:1127-30.
15. Morselli E, Galluzzi L, Kepp O, Kroemer G. Nutlin kills cancer cells via mitochondrial p53. Cell Cycle 2009; 8:1647-8.
16. Vaseva AV, Marchenko ND, Moll UM. The transcription-independent mitochondrial p53 program is a major contributor to nutlin-induced apoptosis in tumor cells. Cell Cycle 2009; 8:1711-9.
17. Cawley S, Bekiranov S, Ng HH, Kapranov P, Sekinger EA, Kampa D, et al. Unbiased mapping of transcription factor binding sites along human chromosomes 21 and 22 points to widespread regulation of noncoding RNAs. Cell 2004; 116:499-509.
18. Hearnes JM, Mays DJ, Schavolt KL, Tang L, Jiang X, Pietenpol JA. Chromatin immunoprecipitation-based screen to identify functional genomic binding sites for sequence-specific transactivators. Mol Cell Biol 2005; 25:10148-58.

19. Smeenk L, van Heeringen SJ, Koeppel M, van Driel MA, Bartels SJ, Akkers RC, et al. Characterization of genome-wide p53-binding sites upon stress response. Nucleic Acids Res 2008; 36:3639-54.
20. Wei CL, Wu Q, Vega VB, Chiu KP, Ng P, Zhang T, et al. A global map of p53 transcription-factor binding sites in the human genome. Cell 2006; 124:207-19.
21. Funk WD, Pak DT, Karas RH, Wright WE, Shay JW. A transcriptionally active DNA-binding site for human p53 protein complexes. Mol Cell Biol 1992; 12:2866-71.
22. el-Deiry WS, Kern SE, Pietenpol JA, Kinzler KW, Vogelstein B. Definition of a consensus binding site for p53. Nat Genet 1992; 1:45-9.
23. Das S, Boswell SA, Aaronson SA, Lee SW. p53 promoter selection: choosing between life and death. Cell Cycle 2008; 7:154-7.
24. Blattner C. Regulation of p53: the next generation. Cell Cycle 2008; 7:3149-53.
25. Georges SA, Chau BN, Braun CJ, Zhang X, Dobbelstein M. Cell cycle arrest or apoptosis by p53: are microRNAs-192/215 and -34 making the decision? Cell Cycle 2009; 8:680-1.
26. Trigiante G, Lu X. ASPP [corrected] and cancer. Nat Rev Cancer 2006; 6:217-26.
27. Samuels-Lev Y, O'Connor DJ, Bergamaschi D, Trigiante G, Hsieh JK, Zhong S, et al. ASPP proteins specifically stimulate the apoptotic function of p53. Mol Cell 2001; 8:781-94.
28. Bergamaschi D, Samuels Y, O'Neil NJ, Trigiante G, Crook T, Hsieh JK, et al. iASPP oncoprotein is a key inhibitor of p53 conserved from worm to human. Nat Genet 2003; 33:162-7.
29. Bergamaschi D, Samuels Y, Sullivan A, Zvelebil M, Breyssens H, Bisso A, et al. iASPP preferentially binds p53 proline-rich region and modulates apoptotic function of codon 72-polymorphic p53. Nat Genet 2006; 38:1133-41.
30. Perez-Sanchez C, Budhram-Mahadeo VS, Latchman DS. Distinct promoter elements mediate the co-operative effect of Brn-3a and p53 on the p21 promoter and their antagonism on the Bax promoter. Nucleic Acids Res 2002; 30:4872-80.
31. Budhram-Mahadeo VS, Bowen S, Lee S, Perez-Sanchez C, Ensor E, Morris PJ, et al. Brn-3b enhances the proapoptotic effects of p53 but not its induction of cell cycle arrest by cooperating in trans-activation of bax expression. Nucleic Acids Res 2006; 34:6640-52.
32. Hudson CD, Morris PJ, Latchman DS, Budhram-Mahadeo VS. Brn-3a transcription factor blocks p53-mediated activation of proapoptotic target genes Noxa and Bax in vitro and in vivo to determine cell fate. J Biol Chem 2005; 280:11851-8.
33. Sugimoto M, Gromley A, Sherr CJ. Hzf, a p53-responsive gene, regulates maintenance of the G_2 phase checkpoint induced by DNA damage. Mol Cell Biol 2006; 26:502-12.
34. Sharma S, Dimasi D, Higginson K, Della NG. RZF, a zinc-finger protein in the photoreceptors of human retina. Gene 2004; 342:219-29.
35. Das S, Raj L, Zhao B, Kimura Y, Bernstein A, Aaronson SA, et al. Hzf Determines cell survival upon genotoxic stress by modulating p53 transactivation. Cell 2007; 130:624-37.
36. Miao L, Song Z, Jin L, Zhu YM, Wen LP, Wu M. ARF antagonizes the ability of Miz-1 to inhibit p53-mediated transactivation. Oncogene 2010; 29:711-22.
37. Herold S, Wanzel M, Beuger V, Frohme C, Beul D, Hillukkala T, et al. Negative regulation of the mammalian UV response by Myc through association with Miz-1. Mol Cell 2002; 10:509-21.
38. D'Orazi G, Cecchinelli B, Bruno T, Manni I, Higashimoto Y, Saito S, et al. Homeodomain-interacting protein kinase-2 phosphorylates p53 at Ser 46 and mediates apoptosis. Nat Cell Biol 2002; 4:11-9.
39. Rinaldo C, Prodosmo A, Mancini F, Iacovelli S, Sacchi A, Moretti F, et al. MDM2-regulated degradation of HIPK2 prevents p53Ser46 phosphorylation and DNA damage-induced apoptosis. Mol Cell 2007; 25:739-50.
40. Taira N, Nihira K, Yamaguchi T, Miki Y, Yoshida K. DYRK2 is targeted to the nucleus and controls p53 via Ser46 phosphorylation in the apoptotic response to DNA damage. Mol Cell 2007; 25:725-38.
41. Hofmann TG, Moller A, Sirma H, Zentgraf H, Taya Y, Droge W, et al. Regulation of p53 activity by its interaction with homeodomain-interacting protein kinase-2. Nat Cell Biol 2002; 4:1-10.
42. Perfettini JL, Castedo M, Nardacci R, Ciccosanti F, Boya P, Roumier T, et al. Essential role of p53 phosphorylation by p38 MAPK in apoptosis induction by the HIV-1 envelope. J Exp Med 2005; 201:279-89.
43. Yoshida K, Liu H, Miki Y. Protein kinase C delta regulates Ser46 phosphorylation of p53 tumor suppressor in the apoptotic response to DNA damage. J Biol Chem 2006; 281:5734-40.
44. Okoshi R, Ozaki T, Yamamoto H, Ando K, Koida N, Ono S, et al. Activation of AMP-activated protein kinase induces p53-dependent apoptotic cell death in response to energetic stress. J Biol Chem 2008; 283:3979-87.
45. Oda K, Arakawa H, Tanaka T, Matsuda K, Tanikawa C, Mori T, et al. p53AIP1, a potential mediator of p53-dependent apoptosis and its regulation by Ser-46-phosphorylated p53. Cell 2000; 102:849-62.
46. Mantovani F, Tocco F, Girardini J, Smith P, Gasco M, Lu X, et al. The prolyl isomerase Pin1 orchestrates p53 acetylation and dissociation from the apoptosis inhibitor iASPP. Nat Struct Mol Biol 2007; 14:912-20.
47. Sykes SM, Mellert HS, Holbert MA, Li K, Marmorstein R, Lane WS, et al. Acetylation of the p53 DNA-binding domain regulates apoptosis induction. Mol Cell 2006; 24:841-51.
48. Tang Y, Luo J, Zhang W, Gu W. Tip60-dependent acetylation of p53 modulates the decision between cell cycle arrest and apoptosis. Mol Cell 2006; 24:827-39.
49. Knights CD, Catania J, Di Giovanni S, Muratoglu S, Perez R, Swartzbeck A, et al. Distinct p53 acetylation cassettes differentially influence gene-expression patterns and cell fate. J Cell Biol 2006; 173:533-44.
50. Chao C, Wu Z, Mazur SJ, Borges H, Rossi M, Lin T, et al. Acetylation of mouse p53 at lysine 317 negatively regulates p53 apoptotic activities after DNA damage. Mol Cell Biol 2006; 26:6859-69.
51. Le Cam L, Linares LK, Paul C, Julien E, Lacroix M, Hatchi E, et al. E4F1 is an atypical ubiquitin ligase that modulates p53 effector functions independently of degradation. Cell 2006; 127:775-88.
52. Jansson M, Durant ST, Cho EC, Sheahan S, Edelmann M, Kessler B, et al. Arginine methylation regulates the p53 response. Nat Cell Biol 2008; 10:1431-9.
53. Durant ST, Cho EC, La Thangue NB. p53 methylation—the Argument is clear. Cell Cycle 2009; 8:801-2.
54. Dehner A, Klein C, Hansen S, Muller L, Buchner J, Schwaiger M, et al. Cooperative binding of p53 to DNA: regulation by protein-protein interactions through a double salt bridge. Angew Chem Int Ed Engl 2005; 44:5247-51.
55. Madhumalar A, Jun LH, Lane DP, Verma CS. Dimerization of the core domain of the p53 family: a computational study. Cell Cycle 2009; 8:137-48.
56. Klein C, Planker E, Diercks T, Kessler H, Kunkele KP, Lang K, et al. NMR spectroscopy reveals the solution dimerization interface of p53 core domains bound to their consensus DNA. J Biol Chem 2001; 276:49020-7.
57. Kitayner M, Rozenberg H, Kessler N, Rabinovich D, Shaulov L, Haran TE, et al. Structural basis of DNA recognition by p53 tetramers. Mol Cell 2006; 22:741-53.
58. Ho WC, Fitzgerald MX, Marmorstein R. Structure of the p53 core domain dimer bound to DNA. J Biol Chem 2006; 281:20494-502.
59. Tidow H, Melero R, Mylonas E, Freund SM, Grossmann JG, Carazo JM, et al. Quaternary structures of tumor suppressor p53 and a specific p53 DNA complex. Proc Natl Acad Sci USA 2007; 104:12324-9.
60. Hager GL, McNally JG, Misteli T. Transcription dynamics. Mol Cell 2009; 35:741-53.
61. Perissi V, Rosenfeld MG. Controlling nuclear receptors: the circular logic of cofactor cycles. Nat Rev Mol Cell Biol 2005; 6:542-54.
62. Misteli T. Beyond the sequence: cellular organization of genome function. Cell 2007; 128:787-800.
63. Beckerman R, Prives C. Transcriptional regulation by p53. Cold Spring Harb Perspect Biol 2010; 2:935.
64. An W, Kim J, Roeder RG. Ordered cooperative functions of PRMT1, p300 and CARM1 in transcriptional activation by p53. Cell 2004; 117:735-48.
65. Karpova TS, Kim MJ, Spriet C, Nalley K, Stasevich TJ, Kherrouche Z, et al. Concurrent fast and slow cycling of a transcriptional activator at an endogenous promoter. Science 2008; 319:466-9.
66. McNally JG, Muller WG, Walker D, Wolford R, Hager GL. The glucocorticoid receptor: rapid exchange with regulatory sites in living cells. Science 2000; 287:1262-5.
67. Metivier R, Penot G, Hubner MR, Reid G, Brand H, Kos M, et al. Estrogen receptor-alpha directs ordered, cyclical and combinatorial recruitment of cofactors on a natural target promoter. Cell 2003; 115:751-63.
68. Chen X, Ko LJ, Jayaraman L, Prives C. p53 levels, functional domains and DNA damage determine the extent of the apoptotic response of tumor cells. Genes Dev 1996; 10:2438-51.
69. Horvath MM, Wang X, Resnick MA, Bell DA. Divergent evolution of human p53 binding sites: cell cycle versus apoptosis. PLoS Genet 2007; 3:127.
70. Ma B, Pan Y, Zheng J, Levine AJ, Nussinov R. Sequence analysis of p53 response-elements suggests multiple binding modes of the p53 tetramer to DNA targets. Nucleic Acids Res 2007; 35:2986-3001.
71. Frebourg T, Kassel J, Lam KT, Gryka MA, Barbier N, Andersen TI, et al. Germ-line mutations of the p53 tumor suppressor gene in patients with high risk for cancer inactivate the p53 protein. Proc Natl Acad Sci USA 1992; 89:6413-7.
72. Sauer M, Bretz AC, Beinoraviciute-Kellner R, Beitzinger M, Burek C, Rosenwald A, et al. C-terminal diversity within the p53 family accounts for differences in DNA binding and transcriptional activity. Nucleic Acids Res 2008; 36:1900-12.

Gene	***Classification***	***p53 response element***				
		half-site 1		*spacer*	*half-site 2*	
14-3-3s #1	non-apoptotic	AGGCA		TGTGC	CACCA	TGCCC
14-3-3s #2	non-apoptotic	GtAGCA	tt	AGCCC	AGACA	TGTCC
B99	non-apoptotic	GAGCA		AGTTG	GGGCT	TGCCT
BTG2	non-apoptotic	AGTCC		GGGCA	g	AGCCC	GAGCA
CCNG1	non-apoptotic	GCACA		AGCCC	AGGCT	AGTCC
Cyclin G	non-apoptotic	AGACC		TGCCC	GGGCA	AGCCT
Cyclin G,C	non-apoptotic	AGGCT		TGCCC	GGGCA	GGTCT
GADD45A	non-apoptotic	GAACA		TGTCT	AAGCA	TGCTG
GDF	non-apoptotic	CATCT		TGCCC	AGACT	TGTCT
GDF	non-apoptotic	AGCCA		TGCCC	GGGCA	AGAAC
gml	non-apoptotic	ATGCT		TGCCC	AGGCA	TGTCC
mdm2	non-apoptotic	AGTTA		AGTCC	TGACT	TGTCT
mdm2	non-apoptotic	GGTCA		AGTTG	GGACA	CGTTC
MDM2-RE2	non-apoptotic	GAGCT	a	AGTCC	TGACA	TGTCT
mdr1b	non-apoptotic	GAACA		TGTAG	AGACA	TGTCT
mmP2	non-apoptotic	AGACA		AGCCT	GAACT	TGTCT
p21-3'	non-apoptotic	GAAGA		AGACT	GGGCA	TGTCT
p21-5'	non-apoptotic	GAACA		TGTCC	CAACA	TGTTG
p53R2	non-apoptotic	TGACA		TGCCC	AGGCA	TGTCT
PCBP4	non-apoptotic	GGTCT		TGGCC	ca	GACTT	AGCAC
PCNA	non-apoptotic	ACATA		TGCCC	GGACT	TGTTC
Pcna	non-apoptotic	GAACA		AGTCC	GGGCA	TATGT
PLK2	non-apoptotic	GGTCA		TGATT	cct	TAACT	TGCCT
PLK2	non-apoptotic	AAACA		TGCCT	GGACT	TGCCC
PLK2	non-apoptotic	AGACA		TGGTG	tgt	AAACT	AGCTT
RB	non-apoptotic	GGGCG		TGCCC	cgc	GTGCG	CGCGC
RGC	non-apoptotic	TGCCT		TGCCT	ggact	TGCCT	GGCCT
RGC, O	non-apoptotic	GGACT		TGCCT	GGCCT	TGCCT
S100A2	non-apoptotic	GGGCA		TGTGT	GGGCA	CGTTC
SCARA	non-apoptotic	GGGCA		AGCCC	AGACA	AGTTG
TGFA	non-apoptotic	AGCCA		AGTCT	TGGCA	AGCGG
TGFA	non-apoptotic	GGGCA		GGCCC	TGCCT	AGTCT
APAF1	apoptotic	AGGCA		CGTCC	ccagcga	CAGCA	GGCTC
APAF1	apoptotic	AGACA		TGTCT	ggagaccctagga	CGACA	AGCCC
Bax-A	apoptotic	TCACA		AGTTA	g	AGACA	AGCCT
BAX-B,A	apoptotic	AGACA		AGCCT	GGGCG	TGGGC
BAX-human	apoptotic	GGGCA		GGCCC	GGGCT	TGTCG
BAX-mouse	apoptotic	AGGCA		AGCTT	t	GAACT	TGCGG
cFOS,O	apoptotic	AGGCT		TGCCC	CGGCA	AGTTG
Ctsd	apoptotic	AACCT		TGGTT	tg	CAAGA	GGCTT
fas	apoptotic	GGACA		AGCCC	TGACA	AGCCA
H-FAS,A	apoptotic	TGGCT		TGTCA	GGGCT	TGTCC
IGFBP3 A,A	apoptotic	AAACA		AGCCA	c	CAACA	TGCTT
IGFBP3 B,A	apoptotic	GGGCA		AGACC	TGCCA	AGCCT
IRDD	apoptotic	AACCT		TGGTT	tg	CAAGA	GGCTT
IRDD	apoptotic	AAGCT		GGGCC	GGGCT	GACCC
MCG10	apoptotic	GAACT		TAAGA	ccgaggctct	GGACA	AGTTG
m-FAS	apoptotic	GGGCA		TGTAC	AAACA	TGTCA
NOXA	apoptotic	AGGCT		TGCCC	CGGCA	AGTTG
P2XM	apoptotic	GAACA		AGGGC	at	GAGCT	TGTCT
p53aip1	apoptotic	TCTCT		TGCCC	GGGCT	TGTCG
pDINP1	apoptotic	GAACT		TGGGG	GAACA	TGTTT
PERP, 2097	apoptotic	GCGCT		AGTCC	acac	AGACT	AGATT
PERP, 218	apoptotic	GCTCA		AGTGT	agcctt	AGCCA	TGCTC
PIDD	apoptotic	AGGCC		TGCCT	gcgtgctg	GGACA	AGTCT
PIG8	apoptotic	TGGCA		GGCCG	GAGCT	AGTTC
PUMA-BS1	apoptotic	CTCCT		TGCCT	t	GGGCT	AGGCC
PUMA-BS2	apoptotic	CTGCA		AGTCC	TGACT	TGTCC
TNFRSF	apoptotic	GGGCA		TGTCC	GGGCA	AGACG
TP53i3 (PIG3)	apoptotic	CAGCT		TGCCC	ACCCA	TGCTC

nature COMMUNICATIONS

ARTICLE

Received 4 Mar 2014 | Accepted 29 Apr 2014 | Published 3 Jun 2014

DOI: 10.1038/ncomms4981 OPEN

Monitoring the dynamics of clonal tumour evolution *in vivo* using secreted luciferases

Joël P. Charles[1,*], Jeannette Fuchs[1,*], Mirjam Hefter[1], Jonas B. Vischedyk[1], Maximilian Kleint[1], Fotini Vogiatzi[1], Jonas A. Schäfer[1], Andrea Nist[1], Oleg Timofeev[1], Michael Wanzel[1] & Thorsten Stiewe[1]

Tumours are heterogeneous cell populations that undergo clonal evolution during tumour progression, metastasis and response to therapy. Short hairpin RNAs (shRNAs) generate stable loss-of-function phenotypes and are versatile experimental tools to explore the contribution of individual genetic alterations to clonal evolution. In these experiments tumour cells carrying shRNAs are commonly tracked with fluorescent reporters. While this works well for cell culture studies and leukaemia mouse models, fluorescent reporters are poorly suited for animals with solid tumours—the most common tumour types in cancer patients. Here we develop a toolkit that uses secreted luciferases to track the fate of two different shRNA-expressing tumour cell clones competitively, both *in vitro* and *in vivo*. We demonstrate that secreted luciferase activities can be measured robustly in the blood stream of tumour-bearing mice to accurately quantify, in a minimally invasive manner, the dynamic evolution of two genetically distinct tumour subclones in preclinical mouse models of tumour development, metastasis and therapy.

[1] Molecular Oncology, Philipps-University, 35043 Marburg, Germany. * These authors contributed equally to this work. Correspondence and requests for materials should be addressed to T.S. (email: thorsten.stiewe@uni-marburg.de).

Tumours are heterogeneous cell populations composed of genetically distinct subclones. They arise through the reiterative process of clonal expansion, genetic diversification and selective outgrowth of clones that have a phenotypic advantage within a given microenvironmental context[1–6]. Fluctuations in clonal architecture can occur, for example, in the context of disease progression such as metastasis or drug treatment[4,7]. Therapeutic intervention may destroy cancer clones and erode their habitats, but it can also inadvertently provide a potent selective pressure for the expansion of resistant variants[3]. Importantly, genetic alterations that drive metastatic progression or relapse following cancer therapy are attractive targets for therapeutic intervention. However, given an average mutation frequency in tumours of more than one mutation per Mb[8,9], pinpointing the individual genetic alterations that drive positive or negative selection in clonal evolution is far from trivial.

Recently, reverse genetic engineering of loss-of-function phenotypes by RNAi technologies has provided a valuable tool to probe specifically the contribution of individual genes to cancer phenotypes in cell culture and animal models. Short hairpin RNAs (shRNAs) can be expressed from DNA-based vectors integrated into the genome and highly complex shRNA vector libraries can introduce experimental heterogeneity into previously clonal tumour cell lines that covers in principle the whole transcribed genome[10,11]. Clonal evolution of such experimentally engineered heterogeneous tumour cell populations *in vitro* and also *in vivo* has been profiled quantitatively by next generation sequencing of shRNAs that are positively or negatively selected over time[12–14]. Clonal analysis by sequencing of tumour DNA, however, is an endpoint assay and therefore provides only limited information about the dynamics of tumour evolution.

To monitor clonal evolution in a time-resolved manner, shRNA expression has been coupled to fluorescent reporters, which can be tracked over time by fluorescence microscopy or flow cytometry. Changes in the percentage of fluorescent cells in the population inform about the disappearance or expansion of an shRNA-expressing subclone, respectively[15]. By adding a second fluorescent marker, a non-targeting shRNA can be monitored in parallel to control for non target-specific shRNA effects[16]. Fluorescent reporters have been used extensively to track different shRNA-bearing tumour cell populations competitively in cell cultures. In animals, this is limited to models where tumour cells are readily accessible for sampling and flow cytometry, for example, in the case of circulating leukaemia cells, since quantification of fluorescence by imaging techniques requires expensive instrumentation, is time consuming, involves frequent anaesthesia and is biased because of photon absorption as a function of wavelength, tissue and depth[13,17,18].

More than 90% of all tumours in cancer patients, however, are solid tumours. Representative samples from these tumours are not accessible in regular intervals for time course studies precluding the monitoring of their clonal architecture by direct analysis of tumour samples or fluorescence-based methods. In patients, it is routine clinical practice to monitor tumour growth using tumour-specific biomarkers detectable in the blood. Recently, the analysis of circulating tumour DNA in the plasma has been established as a novel genetic biomarker to monitor the evolution of distinct tumour subclones[19]. However, circulating tumour DNA is present in only low concentration and requires plasma sample volumes that cannot be obtained repeatedly from small animal models for time course studies[19–21]. We therefore predicted that artificial reporters secreted from the tumour cells into the circulation could serve as suitable surrogate markers. In this respect, a naturally secreted *Gaussia princeps* luciferase (GLuc) has been described as a highly sensitive reporter for localization of cells by bioluminescence imaging and for quantitative assessment of cells *in vivo* by measuring its concentration in blood[22–24]. Another naturally secreted *Cypridina noctiluca* luciferase (CLuc)[25] has similar properties but different substrate specificity allowing us to develop a dual-secreted luciferase assay for simultaneous monitoring of two differently labelled cell populations in a competitive culture setting. In this study, using lentiviral vectors for constitutive and doxycycline (dox)-regulated, luciferase-coupled expression of shRNAs we validate secreted luciferases for monitoring the clonal evolution of heterogeneous tumour cell populations during tumour progression, metastasis and therapy response both in cell culture and mouse models.

Results

Monitoring clonal evolution in cell culture. To monitor clonal evolution of heterogeneous cell populations, we explored the use of secreted luciferases from GLuc and CLuc as bioluminescence markers. GLuc and CLuc have comparable emission spectra with peaks at $\lambda_{max} = 480$ nm and 465 nm, respectively[24,25]. We labelled HCT116 cells with GLuc or CLuc by lentiviral transduction (Fig. 1a). GLuc and CLuc activities in the cell culture supernatant were measured with high specificity and no detectable crosstalk using coelenterazine or vargulin as substrates, respectively, and correlated directly with cell number (Fig. 1b,c). GLuc and CLuc activities in the cell culture medium remained stable at $-20\,^{\circ}C$ allowing for combined analysis of collected samples at the end of a time course experiment (Supplementary Fig. 1). When $GLuc^+$ and $CLuc^+$ cells were mixed, the ratio of luciferase activities (G/C ratio) measured in the medium correlated with the mixing ratio of the cells and the cell ratio quantified independently by GLuc/CLuc-quantitative PCR (qPCR) at the level of genomic DNA isolated from the mixed cultures (Fig. 1d, Supplementary Fig. 2). G/C ratios measured in the supernatant of long-term cultures remained constant over six orders of magnitude for more than 2 weeks of passaging indicating that expression of neither luciferase confers a selective disadvantage as a confounding source of experimental bias (Fig. 1e). As a model for monitoring clonal evolution in cell cultures, we labelled parental H460 cells with GLuc ($H460^{par}$) and a cisplatin (CDDP)-resistant subclone with CLuc ($H460^{res}$) by lentiviral transduction before mixing at a 1:1 ratio. G/C ratios in the culture medium remained constant in the vehicle control, but dropped by two orders of magnitude following CDDP treatment consistent with disappearance of $GLuc^+$ parental cells and overgrowth of the CDDP-resistant $CLuc^+$ subclone (Fig. 1f).

Monitoring clonal evolution in mice. To explore the suitability of the two secreted luciferases for monitoring tumours *in vivo*, tumours were induced in mice by subcutaneous injection of HCT116 cells labelled with either GLuc or CLuc. Luciferase activities in blood samples of tumour-bearing mice yielded signals at least four orders of magnitude above background without detectable crosstalk (Fig. 2a). A single drop of $\sim 10\,\mu l$ blood was sufficient for reliable quantification of both luciferases. *Ex vivo*, there was negligible background activity and both luciferase activities were stable in whole blood and plasma samples for at least 1 h (Supplementary Fig. 3). Luciferase activity in plasma samples was approximately 10-fold higher than in whole blood, likely because of light absorption by haemoglobin (Supplementary Fig. 3). *In vivo* half-lifes of GLuc and CLuc were 10 and 90 min, respectively, suggesting only a minor contribution of luciferase accumulation over time to the total signal measured in blood samples (Supplementary Fig. 4). $GLuc^+$ and $CLuc^+$ tumours were visualized independently with high sensitivity by

bioluminescence imaging following sequential intravenous (i.v.) injection of the respective substrate (Fig. 2b). Subcutaneous injection of 1:1 mixtures of GLuc$^+$ and CLuc$^+$ HCT116 cells resulted in a parallel, exponential increase of both luciferase activities in the plasma that correlated well with tumour volume measured with calipers (Fig. 2c). However, while tumours became measurable after approximately 3 weeks, dual luciferase assays on plasma samples reliably detected tumour growth 1–2 weeks earlier. When mice were injected with different ratios of GLuc$^+$ and CLuc$^+$ cells, the luciferase ratio measured in the plasma of tumour-bearing mice directly correlated with the ratio of initially injected cells and the ratio measured by GLuc/CLuc-qPCR in the genomic DNA of explanted tumours (Fig. 2d,e). As a model for monitoring clonal tumour evolution in mice, GLuc$^+$H460^{par} and CLuc$^+$H460^{res} cells (see Fig. 1f) were injected in a 1:1 mixture into mice and the developing tumours were treated with CDDP. Whereas both luciferase activities increased in parallel in the untreated control group, the increase in GLuc activity was strongly diminished by CDDP treatment resulting in a significant drop of the G/C ratio in plasma samples and lysates of explanted tumours (Fig. 2f–h). Together these experiments validate GLuc and CLuc as secreted markers that can be measured with high sensitivity and no crosstalk for monitoring competitively the proliferation of two distinct cell populations in mice.

Monitoring shRNA-induced tumour heterogeneity under therapy. Tumour relapse after therapy can be caused by resistance-mediating genetic alterations in preexisting or therapy-induced subclones that overgrow the majority of sensitive clones[3]. To explore the impact of a single gene on clonal tumour evolution, we designed lentiviral vectors that genetically couple expression of GLuc or CLuc to the expression of a target-specific shRNA in the miR30 backbone (Fig. 3a)[26]. To test the system, we used shRNAs targeting the tumour suppressor p53 as a critical mediator of tumour therapy[27]. GLuc-coupled expression of two independent p53-targeting shRNAs (GLuc$^+$shp53) reduced induction of p53 and its target gene p21/CDKN1A by the MDM2 inhibitor nutlin-3a in p53 wild-type HCT116 cells (Fig. 3b). Cells expressing non-targeting control shRNAs (nsh) coupled to either GLuc (GLuc$^+$nsh) or CLuc (CLuc$^+$nsh) served as controls. We mixed GLuc$^+$shp53 or GLuc$^+$nsh cells 1:1 with CLuc$^+$nsh cells as reference. The G/C ratio in the cell culture supernatant of all these mixtures remained stable over 10 days in untreated cells (Fig. 3c). In contrast, in GLuc$^+$shp53 mixtures that were exposed to nutlin-3a the G/C ratio increased progressively consistent with resistance of GLuc$^+$shp53 cells (Fig. 3c). No change in the G/C ratio was observed in a parallel control experiment with p53-knockout HCT116 cells that fail to respond to nutlin-3a treatment (Supplementary Fig. 5).

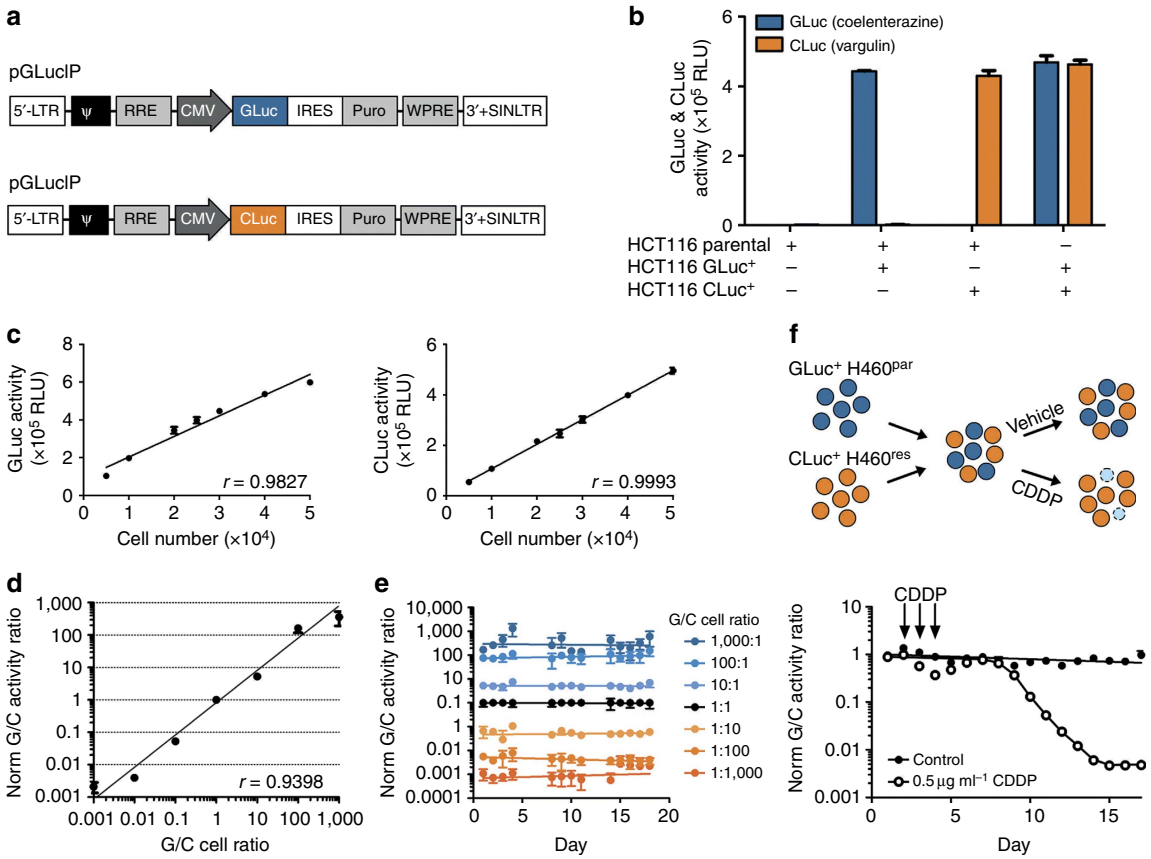

Figure 1 | Dynamic monitoring of clonal evolution in cell culture with secreted luciferases. (**a**) Lentiviral vectors for constitutive, puromycin-selectable cell labelling with GLuc and CLuc. (**b**) GLuc and CLuc activity measured in the supernatant of cultures containing parental, GLuc$^+$ and/or CLuc$^+$ HCT116 cells as indicated ($n=3$). (**c**) Correlation of GLuc and CLuc activity in the cell culture supernatant with cell number ($n=3$). (**d**) Correlation of GLuc/CLuc activity ratio (G/C ratio) in the cell culture supernatant with mixing ratio of GLuc$^+$ and CLuc$^+$ cells. G/C ratio was normalized to the 1:1 mixture ($n=5$). (**e**) Stability of the normalized G/C ratio in the supernatant of long-term cultures ($n=3$). (**f**) Parental cisplatin (CDDP)-sensitive (H460^{par}) and resistant (H460^{res}) H460 cell clones were labelled with either GLuc (GLuc$^+$H460^{par}) or CLuc (CLuc$^+$H460^{res}), mixed in a 1:1 ratio, cultured 3 days in the presence or absence of CDDP (arrows) and monitored daily for GLuc/CLuc activity in the culture supernatant ($n=3$). Shown is the G/C ratio normalized to day 1. All data are presented as mean ± s.d. unless indicated otherwise. Correlation is indicated by the Pearson's correlation coefficient *r*.

A 'flip-color' design, labelling nsh HCT116 p53$^{+/+}$ reference cells with GLuc and shp53 cells with CLuc, yielded the expected inverse result—a progressive decrease in the G/C ratio when cell mixtures were treated with the DNA damaging drug 5-fluorouracil—indicating that both luciferases can be used interchangeably (Supplementary Fig. 6). When 1:1 mixtures of GLuc$^+$shp53 and CLuc$^+$nsh cells were used to generate tumours in mice, both GLuc and CLuc activities increased in vehicle-treated animals with similar kinetics (Fig. 3d). Consistent with resistance of GLuc$^+$shp53 cells to nutlin-3a, GLuc—but not

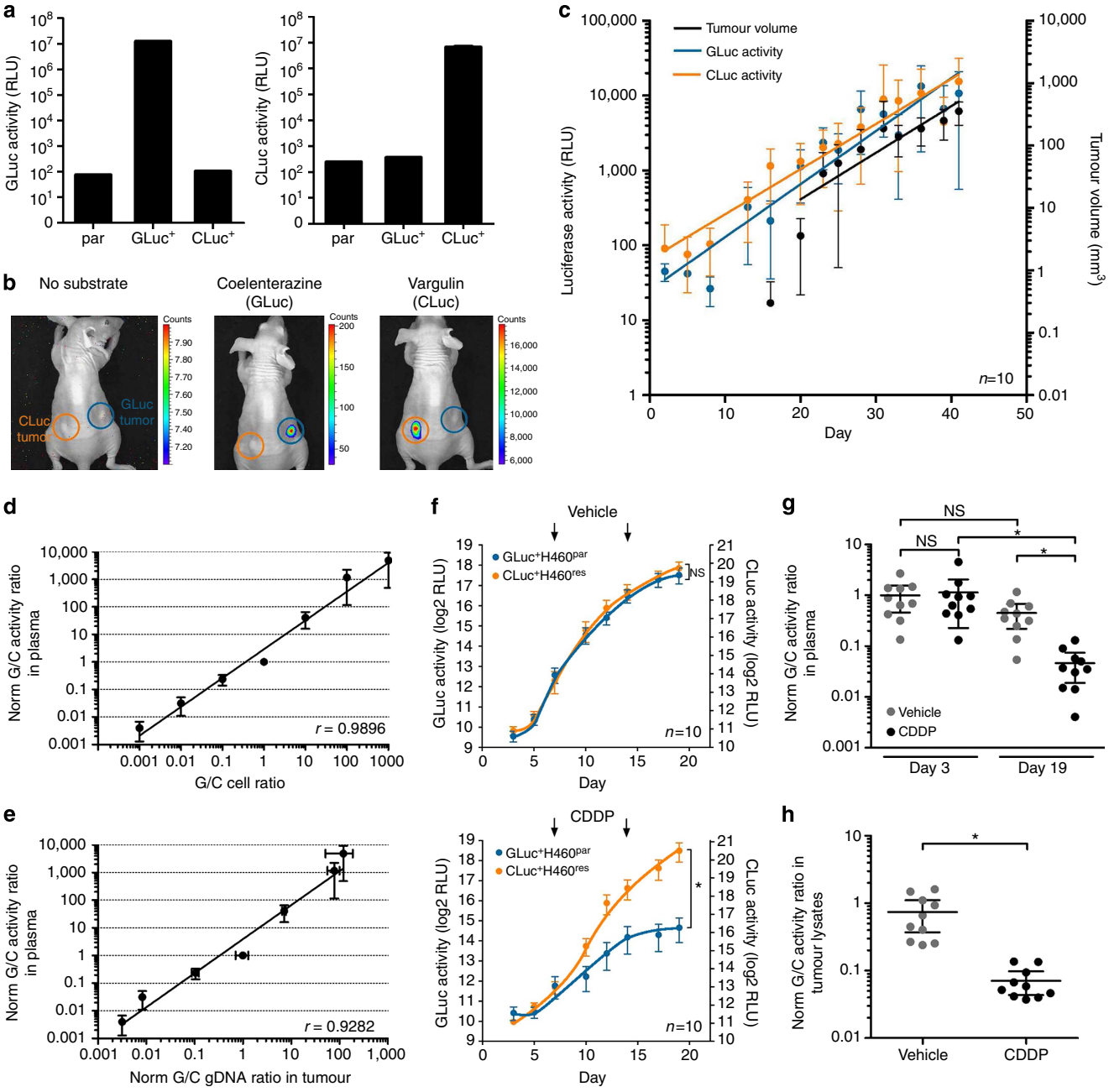

Figure 2 | Monitoring the dynamics of clonal evolution *in vivo* with secreted luciferases. (**a**) Measurement of GLuc and CLuc in the plasma of mice bearing tumours arising from parental (par), GLuc$^+$ or CLuc$^+$ HCT116 cells. (**b**) Bioluminescence images of a single mouse with tumours of GLuc$^+$ (right flank) and CLuc$^+$ HCT116 cells (left flank) following administration of either coelenterazine (GLuc substrate) or vargulin (CLuc substrate). (**c**) Mice were subcutaneously injected with 1:1 mixtures of GLuc$^+$ and CLuc$^+$ HCT116 cells. GLuc and CLuc activity measured in blood plasma and tumour volume measured with calipers are shown. (**d**,**e**) Mice were subcutaneously injected with indicated mixtures of GLuc$^+$ and CLuc$^+$ HCT116 cells ($n=10$ mice per cell mixture). GLuc/CLuc activity ratio in the plasma of tumour-bearing mice correlates with injected cell ratio (**d**) and cell ratio determined by GLuc/CLuc-qPCR on genomic DNA isolated from explanted tumours (**e**). (**f**–**h**) Mice were subcutaneously injected with a 1:1 mixture of GLuc$^+$H460^{par} and CLuc$^+$H460^{res} cells and treated with CDDP on day 7 and day 14. (**f**) GLuc and CLuc activity in the plasma (mean ± s.e.m.). Tumour growth curves were analysed by two-way analysis of variance (*$P<0.001$). (**g**) GLuc/CLuc activity ratio in plasma (mean ± 95% confidence interval; *, $P<0.01$, nonparametric Kruskal–Wallis test and Dunn's post test for multiple comparisons). (**h**) GLuc/CLuc activity ratio in tumour lysate (mean ± 95% confidence interval; *$P<0.0001$, nonparametric Kolmogorov–Smirnov test). Data are presented as mean ± s.d. unless indicated otherwise. Correlation is indicated by the Pearson's correlation coefficient *r*.

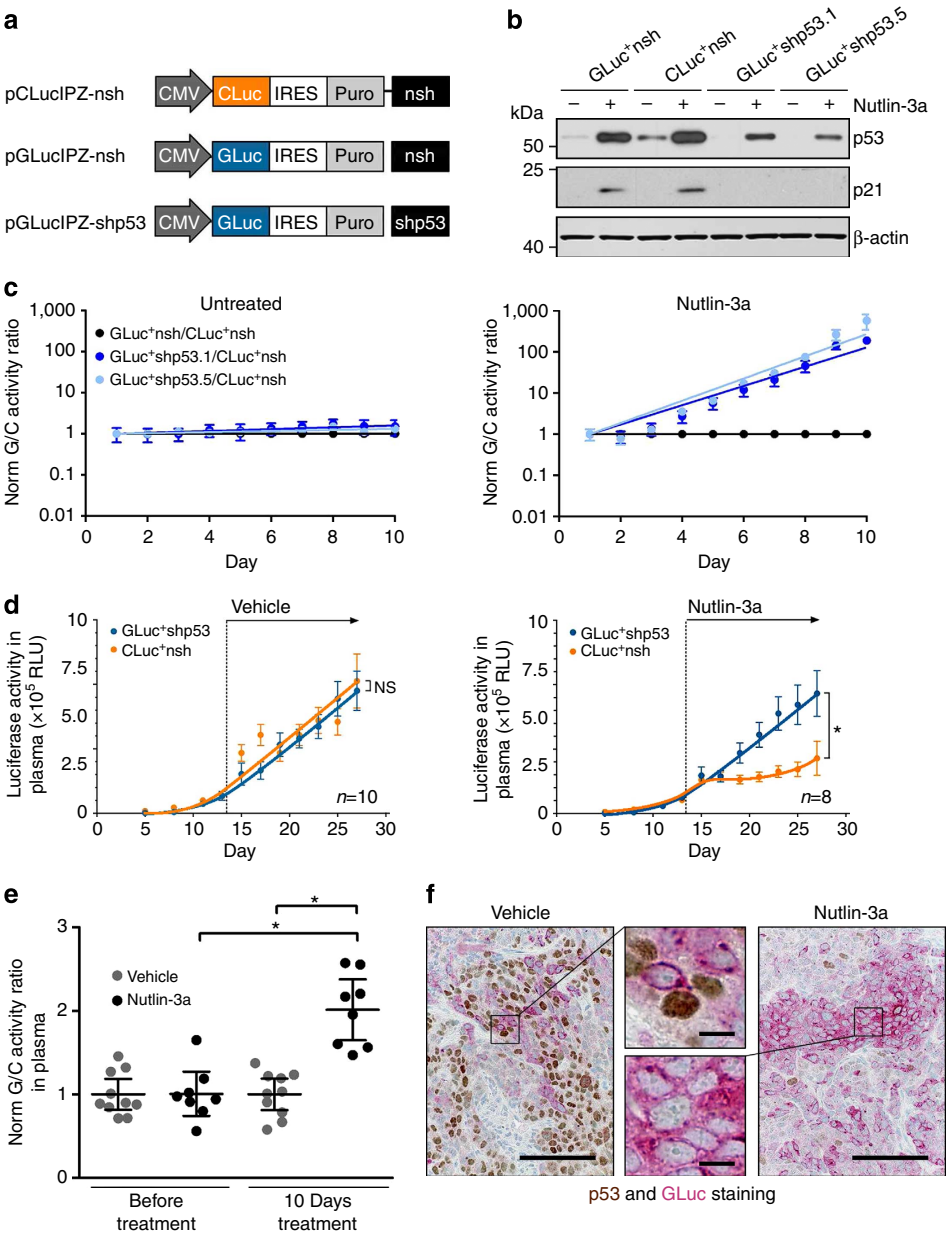

Figure 3 | Monitoring evolution of shRNA-induced tumour heterogeneity under therapy. (**a**) Lentiviral vectors for constitutive, coupled expression of shRNAs with GLuc or CLuc. (**b**) Western blot for p53, p21 (Cdkn1a) and β-actin (control) in HCT116 cells transduced with the indicated shRNA luciferase vectors following treatment with nutlin-3a. (**c**) GLuc/CLuc activity ratio in the supernatant of the indicated mixed cell cultures in the absence (left) and presence (right) of nutlin-3a. G/C ratios were normalized to the GLuc$^+$nsh/CLuc$^+$nsh control mixture ($n=3$). (**d**) Mice were injected subcutaneously with a 1:1 mixture of GLuc$^+$shp53/CLuc$^+$nsh HCT116 cells and treated with vehicle (left) or nutlin-3a (right) starting on day 13. Shown is the mean GLuc and CLuc activity in the plasma (± s.e.m.). Tumour growth curves were analysed by two-way analysis of variance (*$P<0.005$). (**e**) GLuc/CLuc plasma ratio (mean ± 95% confidence interval; *$P<0.01$, nonparametric Kruskal–Wallis test and Dunn's post test for multiple comparisons). (**f**) Immunohistochemistry for p53 (brown) and GLuc (red) in representative tumours explanted from vehicle or nutlin-3a-treated mice. Large scale bars, 100 μm; small scale bars, 10 μm. All data are presented as mean ± s.d. unless indicated otherwise.

CLuc—activity increased progressively in nutlin-3a-treated mice resulting in a significantly elevated G/C plasma ratio in the end (Fig. 3d,e). Immunohistochemistry for p53 and GLuc on tumour sections confirmed the enrichment of GLuc$^+$shp53 cells in nutlin-3a-treated tumours relative to the mixture of GLuc$^+$shp53 and p53-positive CLuc$^+$nsh cells in vehicle-treated tumours (Fig. 3f). We conclude that coupled expression of shRNAs and secreted luciferases can be used to monitor the effects of a gene on clonal tumour evolution under therapy in both cell culture and mouse models.

Monitoring clonal evolution during metastasis. In contrast to the tumour suppressive activity of wild-type p53, mutant p53 (p53mut) exhibits an oncogenic gain-of-function leading to enhanced metastatic potential of tumour cells[28]. We therefore used the same constructs as before to explore whether the dual-secreted luciferase system can also be used to analyse clonal evolution during metastasis. For this, p53-mutated MDA-MB-231 cells were labelled with GLuc or CLuc in combination with control or p53-targeting shRNAs. GLuc$^+$shp53 or GLuc$^+$nsh cells were mixed with CLuc$^+$nsh reference cells and i.v. injected

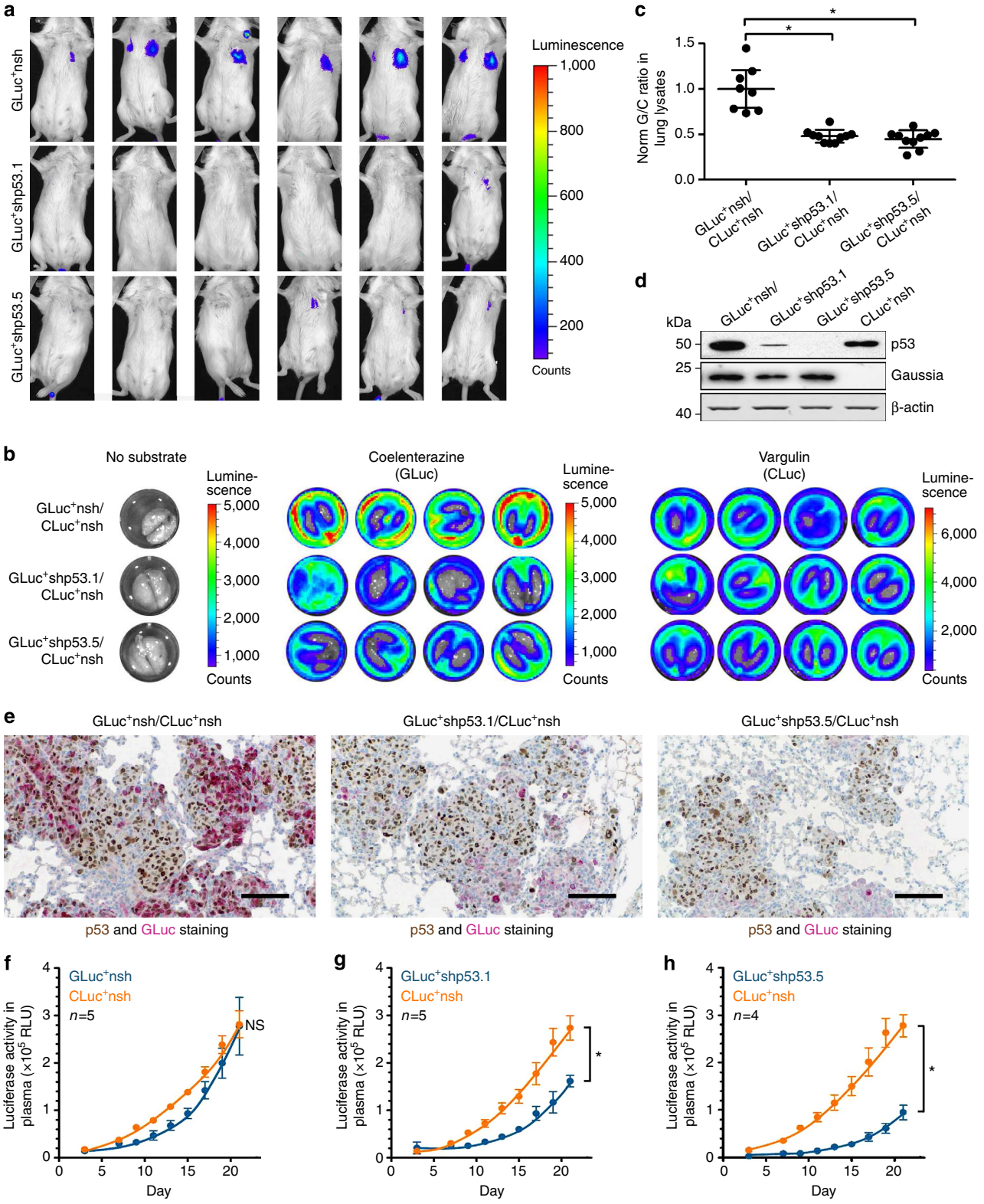

Figure 4 | Monitoring clonal evolution during metastasis. (**a**–**h**) Mice were injected i.v. with the MDA-MB-231 cell mixtures GLuc$^+$nsh/CLuc$^+$nsh, GLuc$^+$shp53.1/CLuc$^+$nsh or GLuc$^+$shp53.5/CLuc$^+$nsh. (**a**) Bioluminescence *in vivo* imaging of GLuc activity with coelenterazine. (**b**) GLuc (coelenterazine) and CLuc (vargulin) imaging of explanted lungs. (**c**) GLuc/CLuc activity ratios in lung lysates (mean ± 95% confidence interval; *$P<0.01$, nonparametric Kruskal–Wallis test and Dunn's post test for multiple comparisons). (**d**) Western blot for knockdown efficiency of experimental shRNAs. (**e**) Immunohistochemical double staining for p53 (brown) and GLuc (red) in lungs explanted from mice injected with (left) GLuc$^+$nsh/CLuc$^+$nsh, (middle) GLuc$^+$shp53.1/CLuc$^+$nsh, and (right) GLuc$^+$shp53.5/CLuc$^+$nsh cell mixtures. Scale bars, 100 μm. (**f**–**h**) GLuc/CLuc plasma activity (mean ± s.e.m.). Tumour growth curves were analysed by two-way analysis of variance (*$P<0.005$).

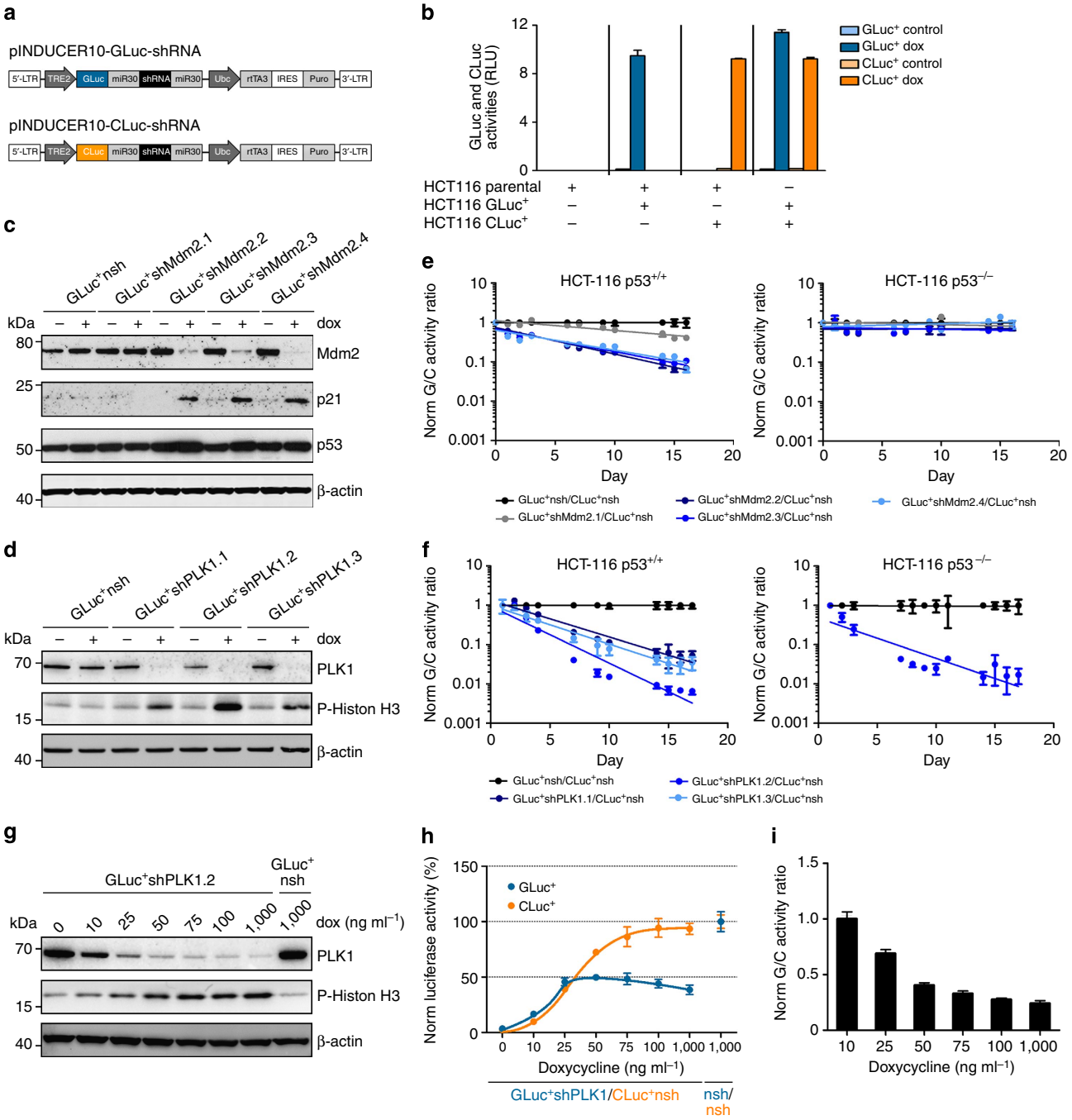

Figure 5 | Validating essential tumour genes in cell culture. (**a**) Lentiviral vectors for dox-inducible, coupled expression of shRNAs with GLuc or CLuc. (**b**) GLuc and CLuc activity measured in the supernatant of uninduced (control) and induced (dox) mixtures of parental, GLuc$^+$ and/or CLuc$^+$ HCT116 cells. (**c**,**d**) Western blot of HCT116 cells transduced with the indicated shRNA-coupled luciferase vectors in the absence and presence of dox. (**e**,**f**) GLuc/CLuc activity ratio in the supernatant of the indicated dox-treated mixtures of shRNA + luciferase expressing HCT116 p53$^{+/+}$ (left) and p53$^{-/-}$ (right) cells ($n=3$). (**g**) Western blot demonstrating dox titration of PLK1 knockdown. (**h**) Dox-dependent luciferase activities in supernatant of GLuc$^+$shPLK1/CLuc$^+$nsh cell mixture ($n=3$). Data were normalized to the dox-induced GLuc$^+$nsh/CLuc$^+$nsh reference mixture set as 100%. (**i**) Dox-dependency of the GLuc/CLuc activity ratio in the supernatant of the GLuc$^+$shPLK1/CLuc$^+$nsh cell mixture ($n=3$). All data are presented as mean ± s.d. unless indicated otherwise.

into mice to model metastatic lung colonization. Consistent with the known role of p53mut in this model[28], bioluminescence GLuc imaging demonstrated extensive colonization of the lungs by GLuc$^+$nsh cells but poorly by p53mut-depleted (GLuc$^+$shp53) cells (Fig. 4a). As *in vivo* bioimaging of the CLuc$^+$nsh reference cells was precluded by high luciferase signals from the blood and attenuation of the blue light emitted from GLuc$^+$ and CLuc$^+$ labelled lung metastases (Supplementary Fig. 7), we measured GLuc and CLuc activities also *ex vivo* in lung lysates and by bioluminescence imaging of explanted lungs (Fig. 4b–d). While all three cell mixtures generated comparable CLuc signals, GLuc activity was lower in the lungs containing GLuc$^+$shp53 cells resulting in a significantly reduced G/C ratio. Reduced lung colonization by GLuc$^+$shp53 cells was independently confirmed

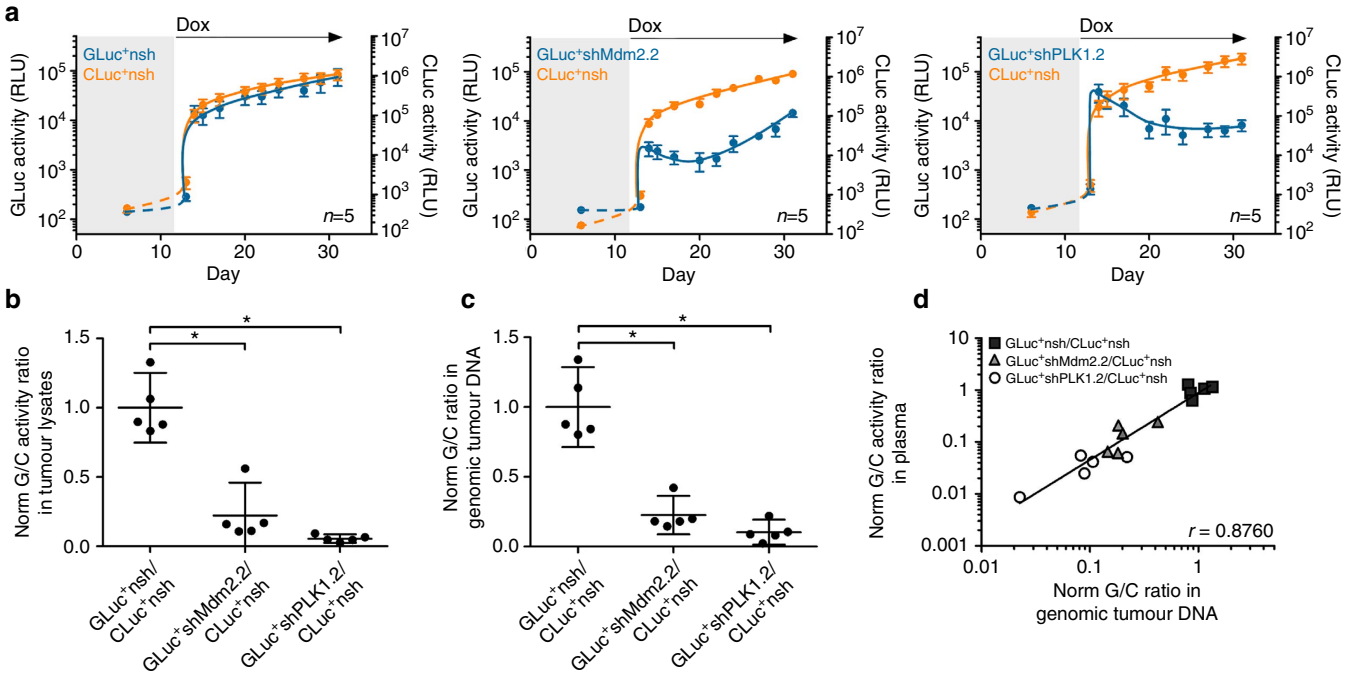

Figure 6 | Validating essential tumor genes *in vivo*. (**a**) Mice were injected subcutaneously with HCT116 cell mixtures (GLuc$^+$nsh/CLuc$^+$nsh, GLuc$^+$shMDM2.2/CLuc$^+$nsh or GLuc$^+$shPLK1.2/CLuc$^+$nsh) and treated with dox starting on day 13. Shown are luciferase activities in blood plasma (mean ± s.e.m.). (**b**) GLuc/CLuc activity ratio in tumour lysates (mean ± 95% confidence interval; *$P<0.01$, nonparametric Kolmogorov–Smirnov test). (**c**) GLuc/CLuc copy number ratio in genomic tumour DNA (mean ± 95% confidence interval; *$P<0.01$, nonparametric Kolmogorov–Smirnov test). (**d**) Correlation of G/C luciferase activity ratio in plasma with G/C copy number ratio in genomic tumor DNA. Correlation is indicated by the Pearson's correlation coefficient *r*.

by immunohistochemistry for p53 and GLuc (Fig. 4e). In addition to these endpoint assays, monitoring of GLuc and CLuc activities in the plasma revealed a parallel increase of GLuc and CLuc activity in mixtures of GLuc$^+$nsh and CLuc$^+$nsh cells (Fig. 4f). In contrast, mice injected with mixtures containing GLuc$^+$shp53 cells showed a weaker increase in GLuc than CLuc activity (Fig. 4g,h). We conclude that the dual-secreted luciferase assay can be used to investigate the effects of a gene on tumour metastasis in both endpoint and time course experiments *in vivo*.

Validating essential tumour genes. Essential tumour genes are attractive targets for tumour therapy. Knockdown of these genes often compromises tumour cell viability so rapidly that constitutive expression of shRNAs coupled to GLuc/CLuc is prevented. For example, knockdown of cancer proliferation genes like polo-like kinase 1 (PLK1) or Mdm2 results in rapid apoptosis or cell cycle arrest and thus impedes selection and expansion of stable knockdown cells for further analysis[29]. We therefore employed the pINDUCER vector system for dox-regulated shRNA expression and adapted it to the GLuc/CLuc secreted luciferase system (Fig. 5a)[30]. HCT116 cells transduced with dox-inducible GLuc- or CLuc-expressing shRNA vectors showed high-level induction of luciferase activities upon dox treatment with negligible background activity in the absence of doxycyclin (Fig. 5b). This enabled transduction, selection and expansion of cells with inducible expression of various Mdm2 or PLK1 shRNAs coupled to GLuc. Addition of dox resulted in Mdm2-knockdown followed by p53 stabilization and p21 induction (Fig. 5c). PLK1 knockdown resulted in histone H3S10 phosphorylation, indicative of mitotic arrest, and apoptosis (Fig. 5d, Supplementary Fig. 8). In competitive co-cultures of GLuc$^+$shMdm2 or GLuc$^+$shPLK1 with CLuc$^+$nsh cells as reference, the G/C ratio in the supernatant progressively dropped in correlation with knockdown efficiency, indicating depletion of GLuc$^+$shMdm2 and GLuc$^+$PLK1sh cells from the culture (Fig. 5e,f). As a proof of specificity, the decrease in the G/C ratio was p53-dependent for Mdm2 but not for PLK1. Furthermore, the PLK1 knockdown could be titrated with increasing dox concentrations, resulting in a dose-dependent decrease in the G/C ratio (Fig. 5g–i).

When mixtures of GLuc$^+$shMdm2, GLuc$^+$shPLK1 or GLuc$^+$nsh with CLuc$^+$nsh cells were subcutaneously injected into mice, GLuc and CLuc activities in the plasma remained low until coupled expression of luciferases and shRNAs was induced by dox administration (Fig. 6a). Under dox, CLuc activity increased further in all mice. GLuc activity was also induced by dox in all mice initially, indicating that GLuc$^+$ cells had expanded and contributed to tumour growth in the absence of dox just as CLuc$^+$ cells. While GLuc activity in blood plasma increased even further in mice with GLuc$^+$nsh tumours, it dropped in mice with GLuc$^+$shMdm2 or GLuc$^+$shPLK1 tumours, consistent with a negative selection of Mdm2- or PLK1-knockdown cells during tumour growth *in vivo*. At the end of the experiment, the tumours were explanted. By measuring luciferase activities in tumour lysates (Fig. 6b) and by qPCR-based quantification of GLuc and CLuc copy numbers in tumour DNA (Fig. 6c), we confirmed a strongly reduced abundance of the GLuc$^+$MDM2sh and GLuc$^+$PLK1sh tumour subclones relative to the CLuc$^+$nsh reference clone. Importantly, G/C luciferase activity ratios measured in plasma samples correlated well with subclone ratios quantified by qPCR (Fig. 6d). We conclude that dox-inducible expression of shRNAs coupled to secreted luciferases provides a sensitive tool to validate a gene as an essential tumour gene *in vivo*.

Discussion

Non-invasive monitoring of tumour development in mice usually requires sophisticated imaging techniques for detection of fluorescent or bioluminescent markers[18]. However, quantification of these markers as a measure of tumour mass is hampered by absorption of light in the surrounding tissues. As photon absorption is a function of wavelength, depth and tissue type, quantitative *in vivo* tracing of cell populations labelled with different markers is therefore, in spite of considerable technical advances, inherently biased[18,31]. Furthermore, emission imaging requires expensive instrumentation, is time consuming, involves frequent anaesthesia and repeated systemic substrate injections[18].

Markers that are secreted from tumour cells and measurable in small volumes of blood *ex vivo* provide considerable advantage. Factors naturally secreted selectively from tumour cells, the so-called 'tumour markers', are therefore routinely used in a clinical setting for tumour screening, monitoring of tumour therapy and detection of relapse. It has been reported previously that a secreted luciferase from GLuc can be used as an artificial marker to label tumour cells and monitor tumour growth and therapy response experimentally in small animal models[22,23]. Importantly, as GLuc secretion is an active energy-consuming process and the half-life of GLuc in circulation is only approximately 10 min, GLuc activity in the blood is a measure of the total number of viable tumour cells in the organism[22].

Here, we describe and validate the use of GLuc together with CLuc, a second secreted luciferase from Cypridina noctiluca, as a dual reporter system to monitor two distinct cell populations in cell culture and small animals. Competitive tracking of two distinct cell populations reduces the number of required animals by at least 50% and possibly even further as analysing test and control cells in a single animal is expected to reduce experimental variance. In addition, compared with immobilization of animals by anaesthesia for bioimaging, tail vein puncture for blood sampling is less invasive and therefore better suited to monitor processes that require repeated analysis at short time intervals. Furthermore, GLuc and CLuc plasma levels rise earlier than tumours become visible or palpable, allowing tumour therapy studies at less advanced and burdening tumour stages. We therefore believe that the dual reporter system contributes to an improved humane animal experimentation as defined by Russell and Burch[32].

Of note, quantitative measurement of total tumour burden occurs at the expense of bioimaging performance. Tumour localization in the living animal with GLuc and CLuc is limited to near surface detection (such as subcutaneous tumours) or sizeable tumour masses in the interior as the blue light emitted from small tumour nodules in internal organs is attenuated by surrounding tissues and masked by luciferases circulating in the blood stream[33]. The use of secreted variants of red-shifted luciferases is expected to improve bioimaging quality.

By expressing GLuc and CLuc together with shRNAs, we can couple cell labelling to genetic manipulation enabling us to interrogate the function of specific genes in tumour development, tumour progression, metastasis and therapy response. By generating genetic heterogeneity, the system is therefore suitable for exploring the dynamic process of clonal tumour evolution as a central cause of phenotypic tumour plasticity and therapy resistance[3].

Methods

Plasmids. Lentiviral vectors for stable, constitutive expression of GLuc, CLuc and shRNAs were derived from the lentiviral vector pGIPZ (Open Biosystems). To create a unique EcoRI restriction site, the EcoRI site in the pGIPZ plasmid backbone was destroyed. GLuc/CLuc were transferred from pGLuc-Basic (NEB N8082S) and pCLuc-Basic2 (NEB N0317S), respectively, via SbfI/NotI into pPRIME-CMV-dsRed-recipient (Stephen Elledge, Addgene plasmid 11658) generating pPRIME-CMV-GLuc/CLuc. In a second step, CMV-GFP in pGIPZ was substituted by CMV-GLuc/CLuc from pPRIME-CMV-GLuc/CLuc via NotI/XbaI digestion and ligation. The resulting constructs, pGLucIPZ-nsh or pCLucIPZ-nsh, contain sequences for production of lentiviral constructs for stable expression of either GLuc or CLuc and non-silencing control shRNAs, and additionally conferring puromycin resistance to transduced cells. For knockdown of p53, non-silencing shRNAs from pGLucIPZ-nsh or pCLucIPZ-nsh were replaced by p53-targeting shRNAs (shp53.1(V2LHS_217), shp53.5(V3LHS_333920), Open Biosystems) via EcoRI/XhoI restriction sites.

To obtain lentiviral vectors for inducible expression of luciferases and shRNAs, the pINDUCER10 vector containing PheS stuffer sequence in the EcoRI/XhoI site[30] was modified: tRFP was replaced by GLuc or CLuc from pCR-Blunt II-TOPO-GLuc or pCR-Blunt II-TOPO-CLuc via restriction digest with AgeI/NotI and ligation. For pCR-Blunt II-TOPO-GLuc or pCR-Blunt II-TOPO-CLuc, luciferases were amplified by PCR (primer sequences 5′-ACCGGTCAAGCTTGG TACC-3′ and 5′-GCATCTTACTTGGCATGACAGTAAG-3′) from pGLuc-Basic (NEB N8082S) and pCLuc-Basic2 (NEB N0317S). For cloning shRNAs, PheS was replaced by shRNAmirs from pGIPZ vectors (Open Biosystems) by EcoRI/XhoI restriction and ligation: shMdm2.1(V2LHS_251529), shMdm2.2(V2LHS_151656), shMdm2.3(V2LHS_379468), shMdm2.4(V2LHS_379469), shPLK1.1(V2LHS_19708), shPLK1.2(V2LHS_19709), shPLK1.3(V2LHS_19711).

Lentiviral vector plasmids for constitutive and inducible expression of GLuc or CLuc coupled to shRNAs are available upon request or through Addgene: pCLucIPZ constitutive expression (ID 53222), and pIND-CLucZ tet-inducible expression (ID 53224).

Lentiviruses. 293T cells were transfected using Arrest-In (Thermo Scientific) with lentiviral vector plasmids and packaging plasmids pMD2.G and psPAX2 (Didier Trono, Addgene plasmids 12259 and 12260). Supernatants containing lentiviruses were collected on the second and third day after transfection and concentrated by polyethylene glycol precipitation[34]. For lentiviral transduction, HCT116, H460 or MDA-MB-231 cells were seeded on six-well plates and infected with concentrated lentivirus in the presence of polybrene (8 μg ml^{-1}) and spin infection (1 h, 1,500 r.p.m., 37 °C). Cells were selected with puromycin (1 μg ml^{-1}) for 5 days.

Cell culture. All cell lines were obtained from the American Tissue Collection Center (ATCC) and cultured in high-glucose Dulbecco's Modified Eagle's Medium (HCT116, MDA-MB-231) or Roswell Park Memorial Institute medium 1640 medium (H460) supplemented with 10% fetal bovine serum, 100 IU ml^{-1} penicillin, 100 μg ml^{-1} streptomycin and 0.25 μg ml^{-1} amphotericin B (Life Technologies) at 37 °C with 5% CO_2. Transduced cell lines were maintained in 0.5–2.0 μg ml^{-1} puromycin after selection was completed. For induction of dox-regulated vectors, cell culture medium was supplemented with 1–2 μg ml^{-1} doxycycline (Sigma). HCT116 cells were treated with 10 μM nutlin-3a (Merck). CDDP was used at 0.5 μg ml^{-1}, 5-fluorouracil at 375 μM.

Luciferase assays with cell culture media. Cell mixtures were seeded in triplicates on 24-well plates. Supernatant was collected every 24 h and replaced with fresh medium. Supernatants were stored in a 96-well plate at − 20 °C until the end of the experiment. At the end of the experiment, all supernatants were thawed and shaken on a Thermomixer (Eppendorf) for 5 min at room temperature. After a short centrifugation, supernatants were further diluted 1:10–1:200 for luciferase activity measurements. Coelenterazine (PJK, Germany), the substrate for GLuc, was prepared as a 10 mM stock in acidified ethanol (10 ml EtOH + 200 μl 6 M HCl). CLuc substrate vargulin (NEB) was prepared according to the manufacturer's protocol. 5 μl of each diluted supernatant was measured in triplicates on white polypropylene 96-well plates with V-bottom (Greiner) using the Orion II luminometer (Berthold) with automated substrate injection of either 50 μl coelenterazine solution (stock diluted 1:500 in phosphate-buffered saline (PBS)) or 25 μl vargulin solution (stock diluted 1:500 in Biolux Cypridina Luciferase Assay Buffer (NEB) prediluted 1:5 in PBS). In time course experiments, all collected samples were stored at − 20 °C and measured together at the end of the experiment with a single batch of reagents without background correction. GLuc/CLuc ratios were normalized to the start of the experiment and the GLuc^{+}nsh/CLuc^{+}nsh reference mixture.

qPCR. Genomic DNA was isolated and purified from cell cultures or tumour samples with the QIAamp DNA Blood Mini Kit (Qiagen) according to the manufacturer's protocol. gDNA (100 ng) was used as template for qPCR. GLuc and CLuc were quantified in a multiplex qPCR reaction on a LightCycler 480 (Roche) with Maxima Probe qPCR Master Mix (Thermo). Primers and probes were used at a final concentration of 300 nM and 250 nM, respectively. Amplification protocol: initial activation of the Hot Start Taq Polymerase for 10 min at 95 °C, followed by 40 cycles of 15 s at 95 °C and 60 s at 60 °C. Primer/probe sequences: GLuc_TaqMan_for 5′-GATCGTCGACATTCCTGAGATT-3′; GLuc_TaqMan_rev 5′-GATCGACCTGTGCGATGAA-3′; GLuc_TaqMan_probe [6FAM]TCCATGGGCTCCAAGTCCTTGAAC[BHQ1]; CLuc_TaqMan_for 5′-AGCTGAACGACTCTGCAATAG-3′; CLuc_ TaqMan_rev 5′-CTTGTGGCACACGTTACATTTC-3′; CLuc_TaqMan_probe [JOE]TCGCCGGTCAAAGTGATCTTGATCA[BHQ1].

Western blots. Cells were lysed in NP-40 Lysis Buffer (50 mM Tris-HCl, 150 mM NaCl, 5 mM EDTA, 2% NP-40, pH 8.0) supplemented with protease inhibitor

(complete ULTRA tablets EASYpack, Roche) and phosphatase inhibitor (PhosSTOP, Roche). Protein yield was determined by Bradford assay (Biorad). Total protein (30–50 µg) was separated on NuPAGE SDS Gels (Life Technologies) and tank-blotted to nitrocellulose membranes. Following blocking in Tris Buffered Saline with Tween 20 (TBST; 5 mM Tris, 15 mM NaCl, 0.1% Tween 20, pH 7.5) with 10% nonfat dry milk or 5% bovine serum albumin for 1 h, membranes were incubated with primary antibodies diluted in TBST/5% nonfat dry milk or TBST/5% bovine serum albumin and incubated overnight at 4 °C. Antibodies: α-p53 (SantaCruz DO-1, 1:10,000); α-PLK1 (SantaCruz F-8, sc-17783, 1:200); α-Mdm2 (Hybridoma supernatant (4B2), 1:2); α-p21 (SantaCruz C-19, sc-397, 1:200); α-Phospho-Histone H3 (Ser10) (Cell Signalling #9701, 1:200); α-GLuc (Nanolight 401P, 1:1000); α-actin (Abcam AC-15, 1:5,000). Proteins were detected with secondary antibody (α-mouse IgG-HRP, α-rabbit IgG-HRP from GE Healthcare, 1:3,000) and ECL kit (SuperSignal West Dura Chemiluminescent Substrate, Thermo Scientific). Uncropped scans of representative Western blots are shown in Supplementary Fig. 9.

Animals. All animal experiments were performed according to regulations and guidelines of the German Protection of Animals Act and were approved by the Regional Board Giessen. For all xenograft experiments, we used immunocompromised 6–12 week-old $Rag2^{tm1.1Flv};Il2rg^{tm1.1Flv}$ male and female mice kept under SPF conditions. Required sample sizes were calculated by an *a priori* power analysis. 1×10^6 HCT116, MDA-MB-231, or H460 cells were injected subcutaneously or i.v. into the tail vein. For induction of dox-regulated vectors, dox was freshly prepared and given in drinking water in darkened bottles at a concentration of 1 mg ml^{-1} in H_2O/2% sucrose. Drinking water was changed every 2nd–3rd day. Nutlin-3a (APAC) was orally administered twice a day at 200 mg kg^{-1} body weight in 2% Klucel, 0.2% Tween-80 (Fagron). Control mice received 2% Klucel, 0.2% Tween-80 as vehicle control. CDDP was administered intraperitoneally at 7 mg kg^{-1} body weight in 0.9% NaCl.

Luciferase assays with blood plasma. 10 µl of blood was obtained by tail vein puncture and mixed directly with 2 µl of 0.125 IE µl^{-1} heparin. Plasma was collected by centrifugation (15 min, 3,600 g, 4 °C). For luciferase activity measurements in the Orion II luminometer (Berthold), plasma was diluted 1:10–1:1,000 with PBS. Each diluted sample (5 µl) was measured by injection of 100 µl coelenterazine (stock diluted 1:200 dilution in PBS) or 25 µl vargulin reagent (stock diluted 1:200 in Biolux Cypridina Luciferase Assay Buffer (NEB) prediluted 1:5 in PBS). All plasma samples were measured in duplicates without background correction. In time course experiments, collected plasma samples were stored at − 20 °C and measured together at the end of the experiment with a single batch of reagents.

Luciferase assays with tumour lysates. Tumours were excised from dead mice and minced. Tumour (10–20 mg) was lysed in 100 µl passive lysis buffer (Promega) with the TissueLyser LT (Qiagen). Tumour lysate (5 µl) was measured in duplicate measurements for GLuc and CLuc activity without background correction as described for blood plasma.

Bioluminescence imaging. Mice were anesthetized with Forane (Baxter). Coelenterazine (50 µg) dissolved in 100 µl PBS was injected i.v. and mice were imaged immediately for 5 min using the IVIS 50 imaging platform (Caliper). Afterwards, mice were i.v. injected with 100 µl of a 1:500 dilution of vargulin (Targeting Systems) and imaged likewise. For *ex vivo* imaging, lungs were excised, placed in 24-well plates, bathed in 1 ml of coelenterazine reagent (stock diluted 1:1,000 in PBS) and imaged immediately for 1 s. After GLuc imaging, tumours were washed for 1 h in fresh PBS on ice to remove residual coelenterazine. CLuc was detected by adding 1 ml of vargulin solution (stock diluted 1:1,000 in Biolux Cypridina Luciferase Assay Buffer (NEB) prediluted 1:5 in PBS) and imaging for 1 s.

Immunohistochemistry. Formalin-fixed tumour tissue was embedded in paraffin, cut and fixed on glass slides overnight at 37 °C. Upon antigen retrieval with Tris-EDTA pH 9.0, sections for double staining were blocked in Dual Endogenous Enzyme Blocking Reagent (Dako) and incubated with α-p53 antibody (DO-1, 1:1,000) in Antibody Diluent (Dako REAL) overnight at 4 °C. Biotinylated rabbit-anti-mouse antibody (Dako, E0464, 1:500) served as secondary antibody and was incubated with Streptavidin-labelled Peroxidase (KPL) followed by detection with DAB Plus Reagent Set (Life Technologies). For subsequent GLuc staining, sections were incubated with α-GLuc antibody (Nanolight Technologies 401 P, 1:1,000) at 4 °C overnight. Biotinylated goat-anti-rabbit antibody (Dako, E0432, 1:500) was used as secondary antibody and was detected with Phosphatase-labelled Streptavidin (KPL) and Liquid Permanent Red (Dako). Nuclei were counterstained with Mayersches Haemalaun (Merck) for 15 s before fixation in Mowiol.

Statistical analysis. All data are presented as mean ± s.d. unless indicated otherwise. Correlation is indicated by the Pearson's correlation coefficient *r*. Statistical significance of single-time-point experiments was tested using nonparametric tests (Kolmogorov–Smirnov test for two group comparisons; Kruskal–Wallis test and Dunn's post test for multiple comparisons). Tumour growth curves were analysed by two-way analysis of variance. All statistics were calculated by GraphPad Prism. $P < 0.05$ was considered statistically significant.

References

1. Cairns, J. Mutation selection and the natural history of cancer. *Nature* **255,** 197–200 (1975).
2. Nowell, P. C. The clonal evolution of tumor cell populations. *Science* **194,** 23–28 (1976).
3. Greaves, M. & Maley, C. C. Clonal evolution in cancer. *Nature* **481,** 306–313 (2012).
4. Burrell, R. A., McGranahan, N., Bartek, J. & Swanton, C. The causes and consequences of genetic heterogeneity in cancer evolution. *Nature* **501,** 338–345 (2013).
5. Meacham, C. E. & Morrison, S. J. Tumour heterogeneity and cancer cell plasticity. *Nature* **501,** 328–337 (2013).
6. Bedard, P. L., Hansen, A. R., Ratain, M. J. & Siu, L. L. Tumour heterogeneity in the clinic. *Nature* **501,** 355–364 (2013).
7. Klein, C. A. Selection and adaptation during metastatic cancer progression. *Nature* **501,** 365–372 (2013).
8. Alexandrov, L. B. *et al.* Signatures of mutational processes in human cancer. *Nature* **500,** 415–421 (2013).
9. Kandoth, C. *et al.* Mutational landscape and significance across 12 major cancer types. *Nature* **502,** 333–339 (2014).
10. Brummelkamp, T. R., Bernards, R. & Agami, R. A system for stable expression of short interfering RNAs in mammalian cells. *Science* **296,** 550–553 (2002).
11. Bernards, R., Brummelkamp, T. R. & Beijersbergen, R. L. shRNA libraries and their use in cancer genetics. *Nat Meth* **3,** 701–706 (2006).
12. Possemato, R. *et al.* Functional genomics reveal that the serine synthesis pathway is essential in breast cancer. *Nature* **476,** 346–350 (2011).
13. Zuber, J. *et al.* Toolkit for evaluating genes required for proliferation and survival using tetracycline-regulated RNAi. *Nat. Biotechnol.* **29,** 79–83 (2011).
14. Zuber, J. *et al.* RNAi screen identifies Brd4 as a therapeutic target in acute myeloid leukaemia. *Nature* **478,** 524–528 (2011).
15. Beitzinger, M. *et al.* p73 poses a barrier to malignant transformation by limiting anchorage-independent growth. *EMBO J.* **27,** 792–803 (2008).
16. Smogorzewska, A. *et al.* Identification of the FANCI protein, a monoubiquitinated FANCD2 paralog required for DNA repair. *Cell* **129,** 289–301 (2007).
17. Dickins, R. A. *et al.* Probing tumor phenotypes using stable and regulated synthetic microRNA precursors. *Nat. Genet.* **37,** 1289–1295 (2005).
18. Weissleder, R. & Ntziachristos, V. Shedding light onto live molecular targets. *Nat. Med.* **9,** 123–128 (2003).
19. Dawson, S.-J. *et al.* Analysis of circulating tumor dna to monitor metastatic breast cancer. *N. Engl. J. Med.* **368,** 1199–1209 (2013).
20. Mouliere, F. *et al.* Circulating cell-free DNA from colorectal cancer patients may reveal high KRAS or BRAF mutation load. *Transl. Oncol.* **6,** 319–328 (2013).
21. Thierry, A. R. *et al.* Origin and quantification of circulating DNA in mice with human colorectal cancer xenografts. *Nucleic. Acids. Res.* **38,** 6159–6175 (2010).
22. Tannous, B. A. Gaussia luciferase reporter assay for monitoring biological processes in culture and *in vivo*. *Nat. Protoc.* **4,** 582–591 (2009).
23. Wurdinger, T. *et al.* A secreted luciferase for ex vivo monitoring of *in vivo* processes. *Nat. Methods* **5,** 171–173 (2008).
24. Chung, E. *et al.* Secreted Gaussia luciferase as a biomarker for monitoring tumor progression and treatment response of systemic metastases. *PLoS ONE* **4,** e8316 (2009).
25. Nakajima, Y., Kobayashi, K., Yamagishi, K., Enomoto, T. & Ohmiya, Y. cDNA cloning and characterization of a secreted luciferase from the luminous Japanese ostracod, Cypridina noctiluca. *Biosci. Biotechnol. Biochem.* **68,** 565–570 (2004).
26. Stegmeier, F., Hu, G., Rickles, R. J., Hannon, G. J. & Elledge, S. J. A lentiviral microRNA-based system for single-copy polymerase II-regulated RNA interference in mammalian cells. *Proc. Natl Acad. Sci. USA* **102,** 13212–13217 (2005).
27. Vousden, K. H. & Lane, D. P. p53 in health and disease. *Nat. Rev. Mol. Cell Biol.* **8,** 275–283 (2007).
28. Adorno, M. *et al.* A mutant-p53/Smad complex opposes p63 to empower TGFbeta-induced metastasis. *Cell* **137,** 87–98 (2009).
29. Schlabach, M. R. *et al.* Cancer proliferation gene discovery through functional genomics. *Science* **319,** 620–624 (2008).
30. Meerbrey, K. L. *et al.* The pINDUCER lentiviral toolkit for inducible RNA interference *in vitro* and *in vivo*. *Proc. Natl Acad. Sci. USA* **108,** 3665–3670 (2011).
31. Darne, C., Lu, Y. & Sevick-Muraca, E. M. Small animal fluorescence and bioluminescence tomography: a review of approaches, algorithms and technology update. *Phys. Med. Biol.* **59,** R1–R64 (2013).

32. Russell, W. M. S. & Burch, R. L. *The Principles of Humane Experimental Technique* (Methuen & Co., 1959).
33. Close, D. M., Xu, T., Sayler, G. S. & Ripp, S. *In vivo* bioluminescent imaging (BLI): noninvasive visualization and interrogation of biological processes in living animals. *Sensors (Basel)* **11,** 180–206 (2011).
34. Kutner, R. H., Zhang, X.-Y. & Reiser, J. Production, concentration and titration of pseudotyped HIV-1-based lentiviral vectors. *Nat. Protoc.* **4,** 495–505 (2009).

Acknowledgements

We thank Sigrid Bischofsberger, Antje Grzeschiczek and Björn Geißert for technical assistance with histopathology and mouse breeding, Uta-Maria Bauer and all lab members for helpful discussions and critical reading of the manuscript. pINDUCER plasmids were kindly provided by Stephen Elledge (Harvard Medical School); pMD2.G and psPAX2 plasmids by Didier Trono (Ecole Polytechnique Fédérale de Lausanne); Mdm2 antibody by Christine Blattner (Karlsruhe Institute of Technology). Rag2$^{-/-}$; IL2R$\gamma^{-/-}$ mice were provided by Cornelia Brendel (Philipps-University Marburg). We acknowledge support from DFG (TRR17, TRR81, KFO210), European Research Council, Deutsche Krebshilfe, Deutsche José Carreras Leukämie Stiftung, Behring|Röntgen| Stiftung, and the Universities of Giessen and Marburg Lung Center (LOEWE).

Author contributions

T.S. conceived the dual-secreted luciferase assay for monitoring clonal tumour evolution. J.P.C., J.F., A.N., M.W., O.T. and T.S. designed experiments. J.P.C., J.F., M.H., J.B.V., M.K., F.V, J.A.S. and M.W. performed experiments and analysed data. J.P.C. cloned constructs for coupled constitutive and inducible expression of luciferases and shRNAs. J.P.C. and J.F. compiled the figures. T.S. wrote the manuscript with contributions from all authors.

Additional information

Supplementary Information accompanies this paper at http://www.nature.com/naturecommunications

Competing financial interests: The authors declare no competing financial interests.

Reprints and permission information is available online at http://npg.nature.com/reprintsandpermissions/

How to cite this article: Charles, J. P. *et al.* Monitoring the dynamics of clonal tumour evolution *in vivo* using secreted luciferases. *Nat. Commun.* 5:3981 doi: 10.1038/ncomms4981 (2014).

SUPPLEMENTARY INFORMATION

Supplementary Figure 1

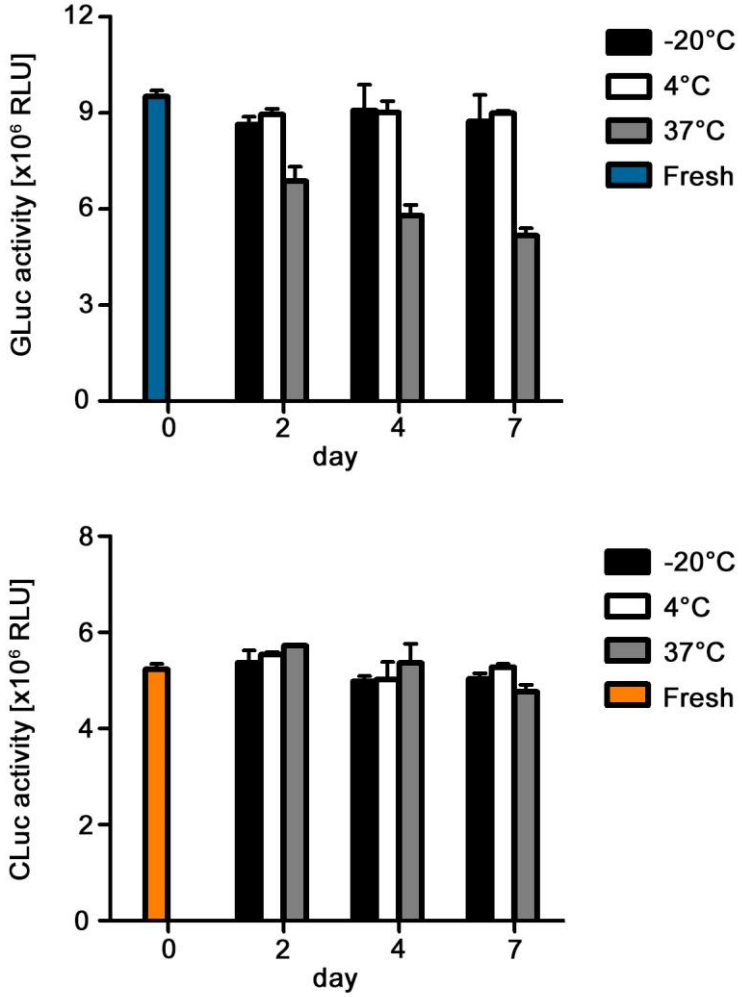

Supplementary Figure 1. Stability of luciferases in cell culture supernatant. Cell culture supernatant of GLuc^{+} or CLuc^{+} HCT116 cells was collected and measured for luciferase activity immediately or after the indicated time of storage at -20°C, 4°C or 37°C. All data are presented as mean ± SD.

Supplementary Figure 2

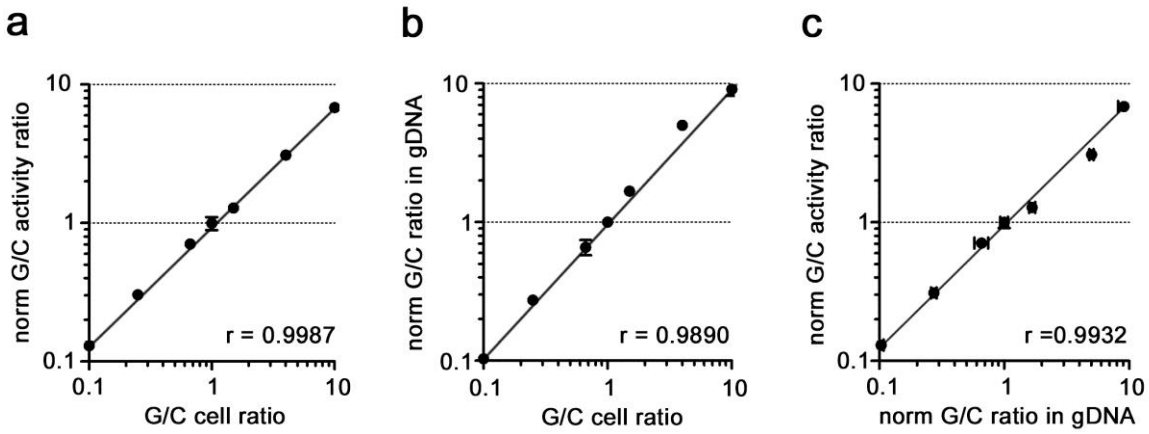

Supplementary Figure 2. Correlation of GLuc/CLuc activity ratio in cell culture supernatant with ratio of $GLuc^+/CLuc^+$ cells. $GLuc^+$ and $CLuc^+$ HCT116 cells were mixed at the indicated ratios of 1:10 to 10:1 and luciferase activity in the cell culture supernatant was measured after 1 day. In addition, the ratio of GLuc and CLuc copy numbers in the cell mixtures was measured by qPCR on genomic DNA (gDNA). (**a**) Correlation of GLuc/CLuc luciferase activity ratio in cell culture supernatant with cell mixing ratio. (**b**) Correlation of GLuc/CLuc copy number ratio in gDNA with cell mixing ratio. (**c**) Correlation of GLuc/CLuc luciferase activity ratio in cell culture supernatant with GLuc/CLuc copy number ratio in gDNA. Shown are mean ± SD, regression line and Pearson's correlation coefficient r.

Supplementary Figure 3

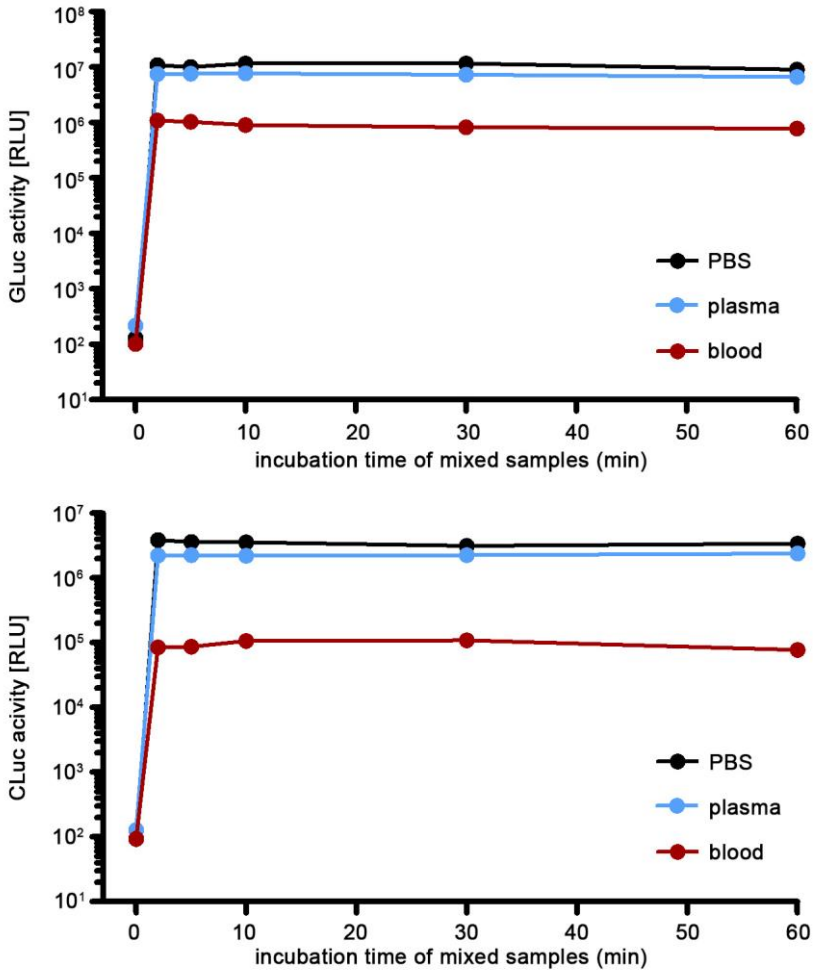

Supplementary Figure 3. Stability of GLuc/CLuc activities in blood samples *ex vivo*. Cell culture supernatant from GLuc^{+} or CLuc^{+} HCT116 cells was mixed 1:10 with PBS, total mouse blood or blood plasma. GLuc (*top*) and CLuc (*bottom*) activity was measured after incubation of the mixed samples for the indicated time period.

Supplementary Figure 4

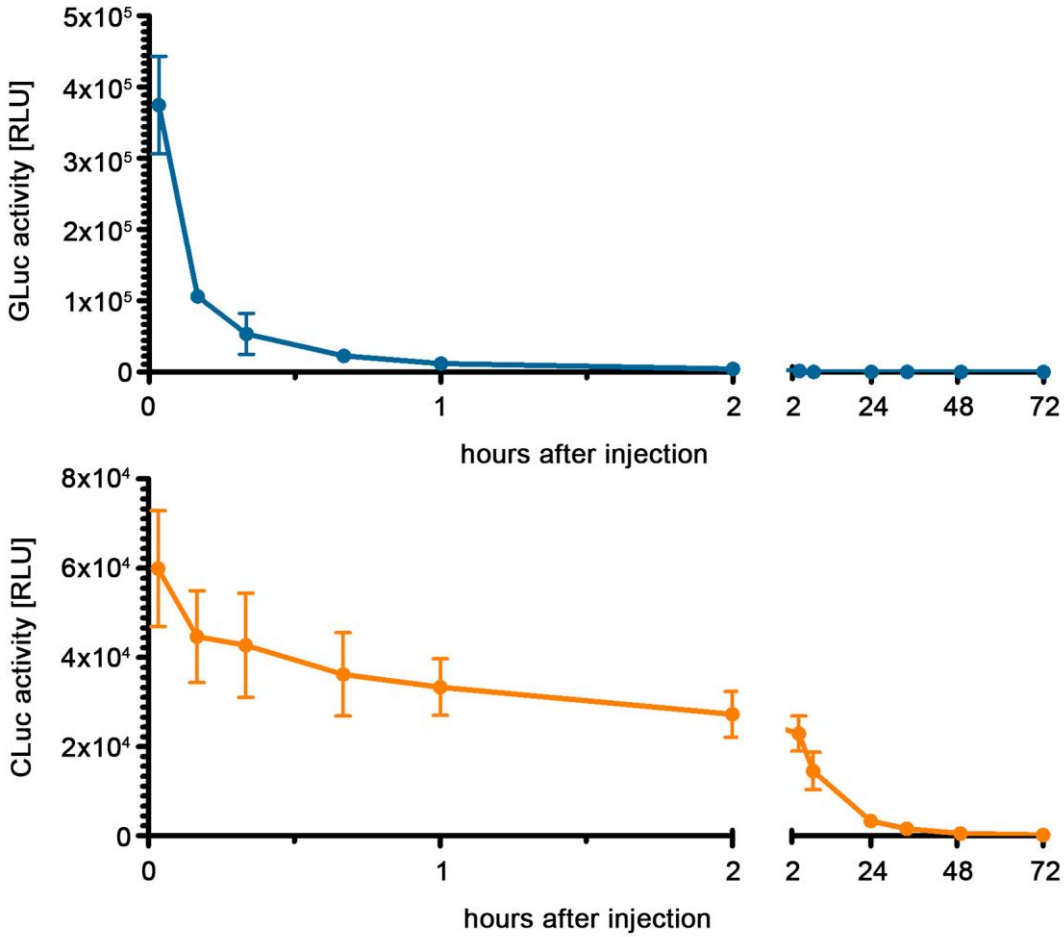

Supplementary Figure 4. Stability of GLuc/CLuc *in vivo*. 100 µl cell culture supernatant of GLuc$^+$ (*top*) and CLuc$^+$ (*bottom*) HCT116 cells was injected intravenously into mice. At the indicated time points blood samples were taken and measured for GLuc and CLuc activity. GLuc half-life: 10 min, CLuc half-life: 90 min. Shown is the mean±SD (n=3).

Supplementary Figure 5

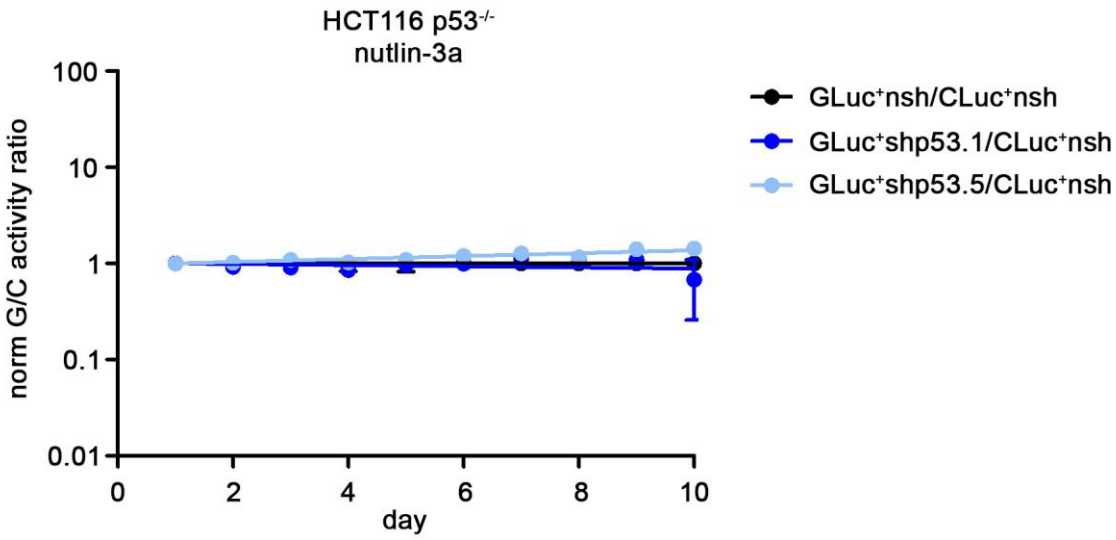

Supplementary Figure 5. Specificity of the dual luciferase assay for monitoring clonal evolution under therapy. HCT116 $p53^{-/-}$ cells were transduced with GLuc and CLuc coupled to p53-targeting (shp53.1 and shp53.5) or non-targeting control (nsh) shRNAs (Fig. 3a). The indicated cell mixtures were monitored by measurement of GLuc and CLuc activity in the cell culture supernatant. Shown is the change in the normalized GLuc/CLuc (G/C) activity ratio in the supernatant over time (mean±SD and regression line).

Supplementary Figure 6

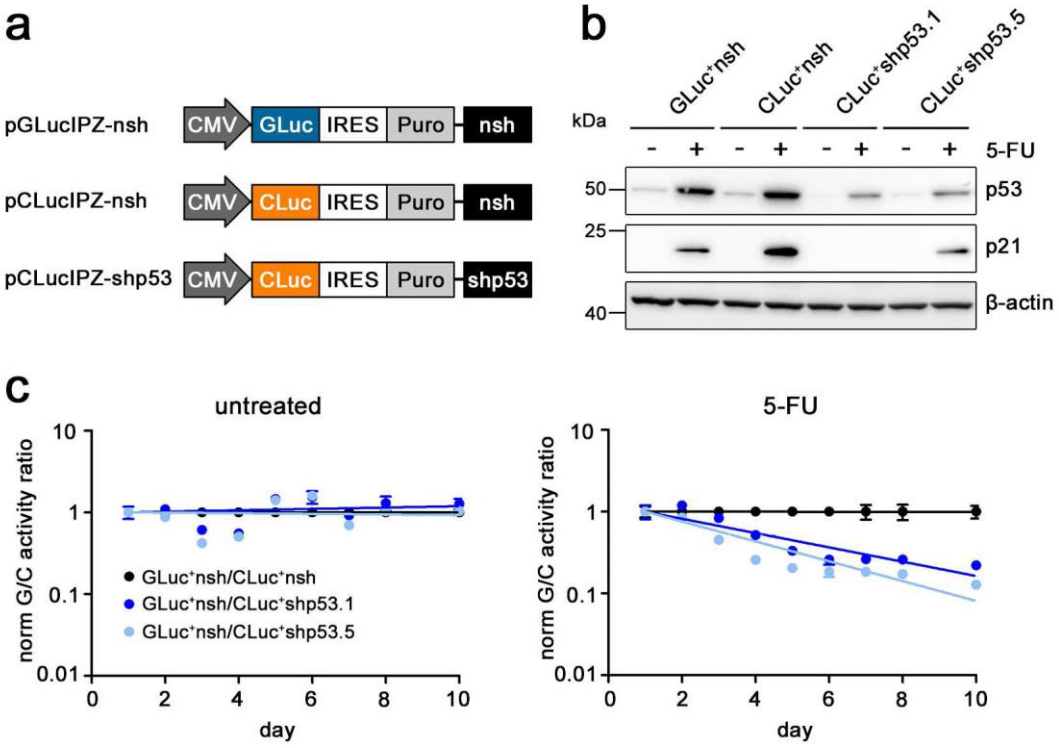

Supplementary Figure 6. Validation of the dual luciferase assay for monitoring clonal evolution under chemotherapy. (**a**) HCT116 $p53^{+/+}$ cells were transduced with GLuc and CLuc coupled to p53-targeting (shp53.1 and shp53.5) or non-targeting control (nsh) shRNAs using the indicated lentiviral vectors. (**b**) Western blot for p53 and the p53 target gene p21(CDKN1A) in vehicle and 5-fluoruracil (5-FU, 375 µM) treated cells validates the knockdown efficiency of the lentiviral constructs. (**c**) The indicated cell mixtures were monitored by measurement of GLuc and CLuc activity in the cell culture supernatant. Shown is the change in the normalized GLuc/CLuc (G/C) activity ratio in the supernatant over time (mean±SD and regression line).

Supplementary Figure 7

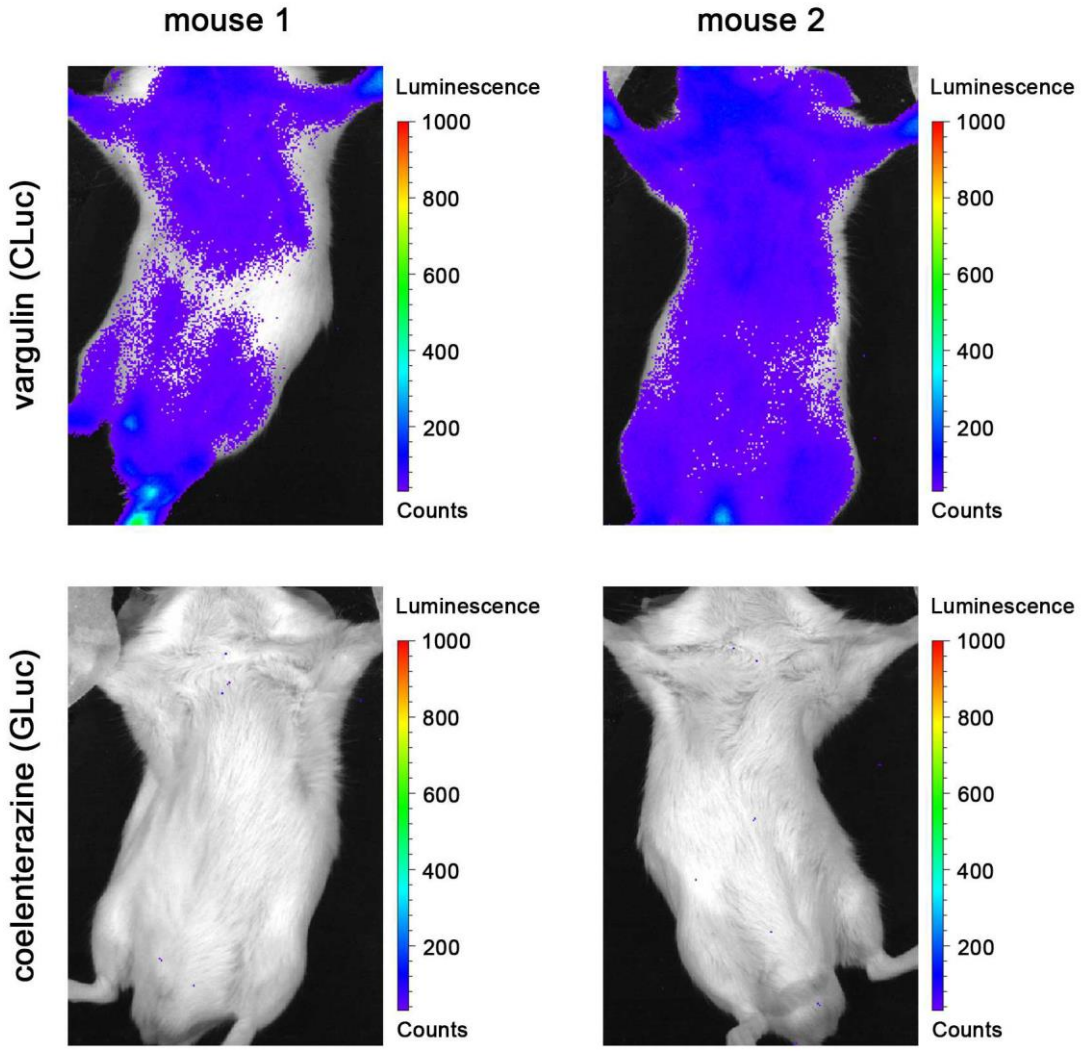

Supplementary Figure 7. Bioluminescence imaging of lung colonization. A mouse was intravenously injected with a mixture of GLuc^{+}nsh and CLuc^{+}nsh MDA-MB-231 cells. 7 days after injection lung colonization was analyzed by sequential bioluminescence imaging with the GLuc substrate coelenterazine and CLuc substrate vargulin.

Supplementary Figure 8

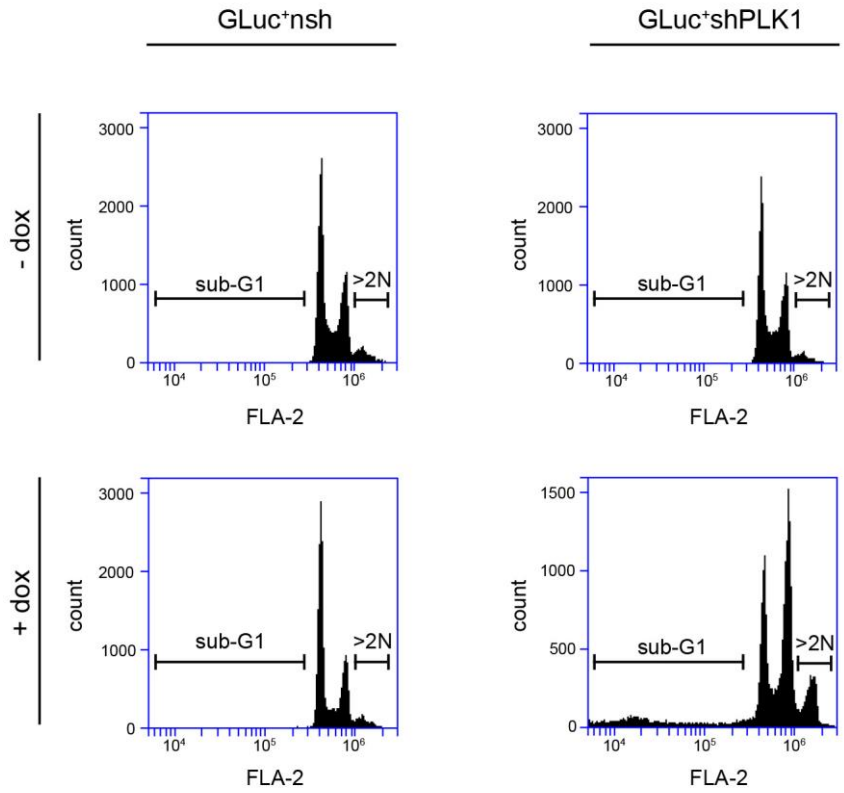

Supplementary Figure 8. Cell cycle profiles of GLuc^{+}nsh and GLuc^{+}shPLK1 HCT116 cells cultured 48 hours in the absence or presence of doxycycline. Indicated are the of apoptotic (sub-G1) and polyploid (>2N) fractions.

Supplementary Figure 9

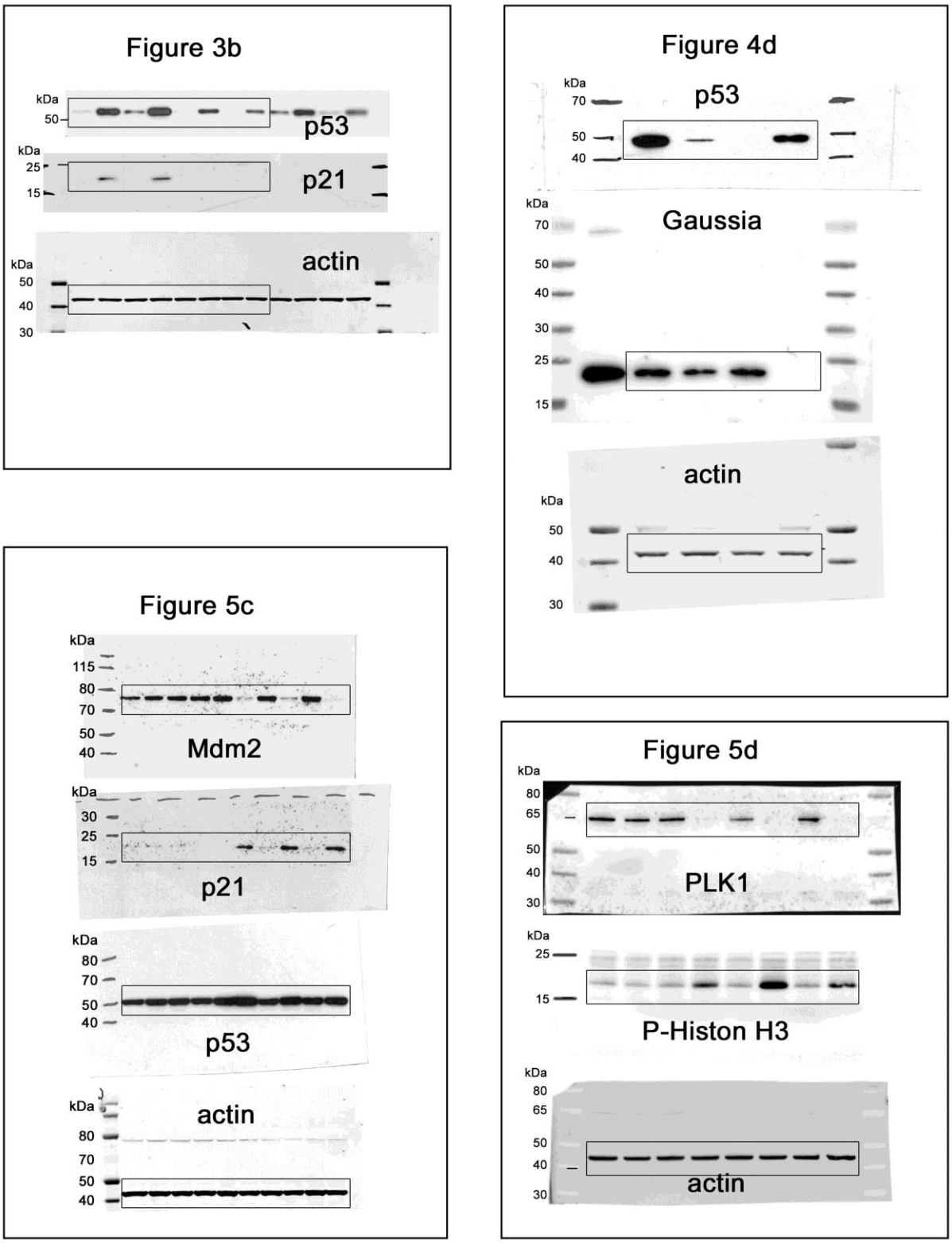

Supplementary Figure 9. Full scans of immunoblots used in main and supplementary figures. Boxes highlight lanes used in figures.

Supplementary Figure 9 (continued)

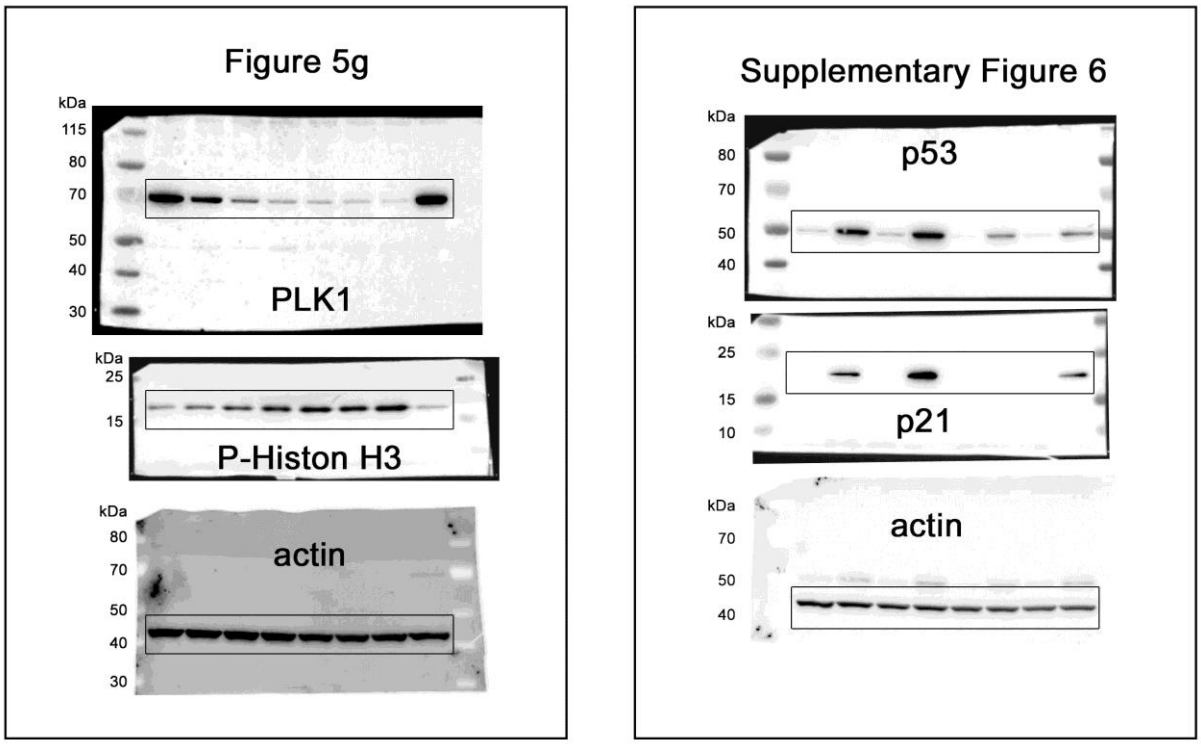

Supplementary Figure 9. Full scans of immunoblots used in main and supplementary figures. Boxes highlight lanes used in figures.